INDUCED PLURIPOTENT STEM CELLS AND GENOME ENGINEERING IN THE STUDY OF THE HUMAN 343DELT HSPB5 CHAPERONE ASSOCIATED WITH EARLY-ONSET SKELETAL MYOPATHY

by

Katie Ann Mitzelfelt

A dissertation submitted to the faculty of
The University of Utah
in partial fulfillment of the requirements for the degree of

Doctor of Philosophy

Department of Biochemistry

The University of Utah

December 2016

The University of Utah Graduate School

STATEMENT OF DISSERTATION APPROVAL

The dissertation of **Katie Ann Mitzelfelt**

has been approved by the following supervisory committee members:

Ivor J. Benjamin	, Chair	**08/25/2016** Date Approved
Dennis R. Winge	, Member	**08/25/2016** Date Approved
Brenda L. Bass	, Member	**08/25/2016** Date Approved
Gabrielle Kardon	, Member	**08/30/2016** Date Approved
Jared P. Rutter	, Member	**08/25/2016** Date Approved

and by **Christopher Peter Hill** , Chair/Dean of

the Department/College/School of **Biochemistry**

and by David B. Kieda, Dean of The Graduate School.

ABSTRACT

HSPB5 (aka αB-crystallin or CRYAB) is a small molecular weight heat shock protein that functions as a key chaperone in striated muscle. Mutations in *HSPB5* are linked with human disease including cardiomyopathy, skeletal myopathy, and cataracts. Abnormal accumulation or protein aggregation including the mutant form of HSPB5 in muscle is a hallmark of the majority of known disease-associated HSPB5 variants, though it is yet unclear mechanistically how this mutant chaperone contributes to myopathy (reviewed in Chapter 1). This dissertation focuses on molecular studies of one such mutation, 343delT, which is associated with severe early-onset skeletal myopathy requiring ventilation to sustain life. Induced pluripotent stem cells (iPSCs) derived from the patient harboring the 343delT mutation along with genome edited isogenic control cell lines are utilized in this work as a mechanism to study the endogenous form of the protein in cell types of interest (i.e., skeletal and cardiac muscle). Molecular studies of 343delT HSPB5 demonstrate extreme insolubility of the mutant protein and suggest a loss of function mechanism for disease, though gain-of-toxic function cannot be excluded (Chapter 3). Chapter 2 is included as an addendum to the Introduction on HSPB5 (Chapter 1) to provide relevant background information on iPSCs and genome editing. The fast-paced genome editing field is currently hampered by inefficient means of isolating cells containing modifications of interest. Previously published approaches employed in Chapter 3 were highly efficient, though required a two-step editing process and were not readily scalable. Chapter 4 presents a strategy for genome editing, termed cotargeting with selection (CTS) that involves simultaneous targeting of two loci, where selection for incorporation of a selection cassette into a safe-harbor locus enriches many fold for a separate modification at a gene of interest. CTS streamlines the genome editing process

compared with previous techniques. Chapter 5 of this dissertation includes a combined discussion and Chapter 6 presents future experiments planned for the study of 343delT HSPB5. Altogether, this dissertation affords molecular insights into myopathy causing 343delT HSPB5 using cutting edge technology of iPSCs and genome editing, as well as providing technical advancement to the field of genome editing.

TABLE OF CONTENTS

LIST OF FIGURES

Figures

LIST OF TABLES

Tables

ACKNOWLEDGEMENTS

Firstly, I would like to express my sincere gratitude to my advisor and mentor, Dr. Ivor Benjamin, for his overwhelming support of my PhD studies over the last six years. He has provided me immense knowledge and guidance while allowing me independence to learn and grow. His unwavering commitment to me was demonstrated when he invited me to accompany him to the Medical College of Wisconsin to complete my PhD research. I am truly fortunate to have had the opportunity to be mentored by him.

In addition to my advisor, I would like to thank the other members of my thesis committee: Drs. Dennis Winge, Brenda Bass, Gabrielle Kardon, and Jared Rutter, as well as former members Drs. Gerald Spangrude and Alana Welm for their insightful comments, encouragement, and suggested direction for my work. My sincere thanks also goes to Drs. Aron Geurts, Alex Minella, and Allison Ebert for their important collaborative efforts in teaching me essential techniques for the advancement of my research.

I thank my fellow lab mates (my "lab family") from beginning to end; though members have come and gone, we have never ceased to have stimulating discussion, unconditional support, and friendship. A special thank you to Dr. Michael Riedel, who was here with me from the beginning and always willing to teach, advise, and support me as a colleague and friend. I thank my friends and peers, fellow graduate students with whom I have shared this experience. Thank you to the Medical College of Wisconsin and Department of Biochemistry at the University of Utah for administrative support in my transition and off-site work following the move of my advisor.

Last but not least, I would like to thank my family. My husband, Donnie, who has made

substantial sacrifices following me across the country to fulfill my requirements, always providing unconditional love and support, and keeping me a grounded, sane human being. My parents, siblings, in-laws, and close friends and family for their continued love, support, and motivation.

CHAPTER 1

INTRODUCTION: MULTIFUNCTIONAL ROLES OF αB-CRYSTALLIN IN SKELETAL AND CARDIAC MUSCLE HOMEOSTASIS AND DISEASE

The Big Book on Small Heat Shock Proteins

Volume 8 of the series Heat Shock Proteins pp 269-299

Multifunctional Roles of αB-Crystallin in Skeletal and Cardiac Muscle Homeostasis and Disease

Katie A. Mitzelfelt, Ivor J. Benjamin

DOI 10.1007/978-3-319-16077-1_11

Print ISBN 978-3-319-16076-4

Online ISBN 978-3-319-16077-1

With permission of Springer

Chapter 11
Multifunctional Roles of αB-Crystallin in Skeletal and Cardiac Muscle Homeostasis and Disease

Katie A. Mitzelfelt and Ivor J. Benjamin

Abstract αB-Crystallin, or HspB5, is a small molecular-weight heat shock protein expressed highly in cardiac and skeletal muscle with multifaceted cellular roles including, chaperone function towards essential myofibrillar components. Insights into protective roles played by αB-crystallin, as well as mutations in the gene encoding αB-crystallin, *CRYAB*, which resulted in human pathologies, have highlighted the critical functions of αB-crystallin in both skeletal and cardiac muscle, *inter alia*. Various human mutations in *CRYAB* appear to have tissue-specific effects, with loss of αB-crystallin only impacting skeletal muscle under basal conditions. This review aims to highlight the roles of αB-crystallin in skeletal and cardiac muscle homeostasis as well as under conditions of stress and disease, drawing insights from human pathologies resulting from *CRYAB* mutations, and to discuss the potential of using induced pluripotent stem cells to model αB-crystallin-opathies in vitro.

Keywords Cardiac muscle • Skeletal muscle • Myopathy • *CRYAB*, HspB5 • Induced pluripotent stem cells (iPSCs) • Protein aggregation

11.1 Introduction

αB-Crystallin, also known as HspB5, is a member of the small molecular-weight heat shock family (sHSPs) of molecular chaperones, a diverse family of proteins that are characterized by the presence of a conserved α-crystallin domain (Ignolia and Craig 1982; Kappé et al. 2002). The α-crystallin domain in αB-crystallin interacts with an adjacent monomer to form a dimeric building block, and further assembles into higher order oligomers (Bagneris et al. 2009; Jehle et al. 2010;

K.A. Mitzelfelt
Department of Biochemistry, University of Utah, Salt Lake City, UT, USA

I.J. Benjamin, M.D. (✉)
Cardiovascular Center, The Medical College of Wisconsin, Milwaukee, WI, USA
e-mail: ibenjamin@mcw.edu

R.M. Tanguay, L.E. Hightower (eds.), *The Big Book on Small Heat Shock Proteins*, Heat Shock Proteins 8, DOI 10.1007/978-3-319-16077-1_11

Laganowsky et al. 2010). The *CRYAB* gene encodes αB-crystallin expression and primarily functions as a molecular chaperone (Horwitz 1992), among other things. Though its expression was originally thought to be confined to the lens, it was later realized that αB-crystallin is relatively ubiquitously and abundantly expressed in cardiac and skeletal muscle (Dubin et al. 1989). Enhancer elements modulating the *CRYAB* promoter account for its tissue specificity (Gopal-Srivastava et al. 1995; Gopal-Srivastava and Piatigorsky 1993). As described in this review, αB-crystallin plays essential functions in tissue maintenance during homeostasis and in stressed or pathological states of cardiac and skeletal muscle. Additionally, mutations in human *CRYAB* result in cardiac and/or skeletal myopathies, with causal mechanisms of the apparent tissue-specific effects of the mutations remaining unresolved. This review discusses the implications and requirements for αB-crystallin in both cardiac and skeletal muscle during homeostasis as well as under stressed or pathological conditions. We also invoke studies involving mutant forms of *CRYAB* present in patients to make inferences into tissue-specific requirements.

11.2 Structure and Function of αB-Crystallin

11.2.1 Constitutive and Inducible Expression

αB-Crystallin is classified as a Class I sHSP due to its ubiquitous expression (Taylor and Benjamin 2005). First discovered in 1894, it was originally thought to be a lens-specific protein (Morner 1894), until murine *CRYAB* was cloned and found to be expressed at high levels in the heart, skeletal muscle, kidney, and lung and low levels in the brain and spleen (Dubin et al. 1989). Muscle-specific expression of *CRYAB* is conferred by upstream enhancer elements that regulate promoter activity. Murine *CRYAB* cis-acting enhancer elements, identified by reporter expression driven by the *CRYAB* promoter, show regions required for expression in skeletal muscle, termed αBE-1, αBE-2, αBE-3, and MRF (Gopal-Srivastava and Piatigorsky 1993), which are also required for cardiac muscle expression along with an additional, unique element, αBE-4 (Gopal-Srivastava et al. 1995). The MRF site contains an E-box that in skeletal muscle is bound and activated by the bHLH myogenic regulatory factors (MRFs), including MyoD and myogenin (Gopal-Srivastava and Piatigorsky 1993). In cardiac muscle, the E-box of the MRF site may be bound by upstream stimulatory factor (USF) or an antigenically similar factor (Gopal-Srivastava et al. 1995). The cardiac-specific element, αBE-4, contains a reverse CArG box, which may be bound by serum response factor (SRF) or an alternate, antigenically similar protein (Gopal-Srivastava et al. 1995).

In addition to its constitutive expression, *CRYAB* is also inducible in response to multiple forms of stress including heat, oxidative stress, and inflammation, which are sensed by heat shock factor 1 (HSF1), a transcriptional activator that

homo-trimerizes to interact with heat shock elements in the promoters of stress-response genes, including *CRYAB* (reviewed in (Morimoto 1998; Christians et al. 2002)). HSF1 deficient mice exhibit decreased basal levels of αB-crystallin in the normal heart, indicating HSF1 may be involved in regulation of *CRYAB* expression under non-stress conditions as well (Yan et al. 2002).

Continuous motor nerve stimulation of rabbit tibialis anterior muscle increases αB-crystallin levels, and this upregulation may involve interaction of the MRFs with the E-box in the *CRYAB* enhancer region (Neufer and Benjamin 1996). Eccentric contraction (lengthening contraction) in skeletal muscle also increases the levels of *CRYAB* along with other HSPs (Kostek et al. 2007; Thompson et al. 2001) resulting from mechanical and/or oxidative stress (Koh 2002). Mechanical load and nerve innervation of skeletal muscle also regulate the level of *CRYAB* expression as shown in experiments where suspension of the rat hindlimb decreases *CRYAB* mRNA levels, and denervation has differential effects on *CRYAB* mRNA levels in different types of skeletal muscle (Atomi et al. 1991). Passive stretch increases *CRYAB* mRNA levels in skeletal muscle (Atomi et al. 1991).

αB-Crystallin is the most abundant sHSP in the heart, making up 3 % of cardiac homogenates and its expression in the heart is limited to cardiomyocytes (Lutsch et al. 1997). Stress including ischemia/reperfusion (I/R) injury upregulates αB-crystallin in the heart (Martin et al. 1997; Ray et al. 2001).

11.2.2 Structure and Oligomerization

sHSPs such as αB-crystallin contain an 80–100 residue, conserved α-crystallin domain (de Jong et al. 1998) comprised of an immunoglobulin-like β-sandwich, including strands β2−β9, which is critical for dimer formation through interaction of the extended β6+7 strand on adjacent monomers (Bagneris et al. 2009). Homo- or hetero-dimers assemble into large, oligomeric structures in the inactive state (Mymrikov et al. 2011) with an average of 40 subunits and a molecular mass of 800 kDa (Bloemendal 1981). Heat stimulates the rapid exchange of subunits, as determined by fluorescence resonance energy transfer experiments, and binding to large, denatured substrates greatly reduced the rate of subunit exchange (Bova et al. 1997). The variable c-terminal region of αB-crystallin contains a conserved I/V/L-X-I/V/L motif that binds the β4/8 groove of the adjacent monomer (Delbecq et al. 2012), contributing to dimer formation, and may also modulate chaperone activity (Bagneris et al. 2009; Laganowsky et al. 2010; Ghosh et al. 2006). The hydrophobic groove at the dimer interface is essential for substrate binding (Clark et al. 2011). The function of the variable N-terminus is less well-defined, though it is thought to impact oligomerization, containing three phosphorylation sites that can modulate the polydispersity of oligomers (Ecroyd et al. 2007) and reduce their size (Peschek et al. 2013).

11.2.3 Subcellular Localization

11.2.3.1 Cytoplasm

αB-Crystallin has disperse cytoplasmic localization and can bind to the intermediate filament protein desmin (Bennardini et al. 1992), as well as contractile proteins, including actin (Bennardini et al. 1992) and titin (Golenhofen et al. 2002; Bullard et al. 2004; Kotter et al. 2014). These interactions are stimulated in response to stress including I/R stress (Golenhofen et al. 1999, 2002) and stretch caused by eccentric contraction in skeletal muscle (Koh and Escobedo 2004; Kotter et al. 2014). Transgenic mice expressing the R120G mutant form of αB-crystallin in cardiomyocytes exhibit defects in mitochondrial organization, architecture, and respiration (Maloyan et al. 2005), which is attributable to breakdown of the desmin network (Wang et al. 2001). Specific mitochondrial alignment along adjacent sarcomeres is critical for maximal respiratory function in striated muscle, dependent upon cytoskeletal components, with cardiac and different types of skeletal muscle having differential arrangements and amounts of mitochondria (Milner et al. 2000; Reipert et al. 1999; Rambourg and Segretain 1980; Rappaport et al. 1998; Ogata and Yamaksak 1997). These data indicate that αB-crystallin, through interactions with cytoskeletal elements including desmin, among other things, may be crucial for maintaining organization and proper function of mitochondria.

11.2.3.2 Mitochondrial Interaction

Mitochondria are vital for both cardiac and skeletal muscle function, and as mentioned previously, the organization of mitochondria along myofibrils, which varies based on muscle type and is maintained through cytoskeletal interactions, is essential for maintaining maximal functional capacity (Milner et al. 2000; Reipert et al. 1999; Rambourg and Segretain 1980; Rappaport et al. 1998; Ogata and Yamaksak 1997). Maintaining mitochondrial integrity is crucial for inhibiting apoptosis and αB-crystallin has been shown to play a key role in this process during stress. αB-Crystallin associates with mitochondria, and this association increases with I/R stress, shown in rats (Mitra et al. 2013), and after exposure to hydrogen peroxide, shown in culture of mouse neonatal cardiomyocytes (Chis et al. 2012). Both phosphorylated and unphosphorylated αB-crystallin interact with the voltage-dependent anion channel (VDAC) and translocase of outer mitochondrial membrane 20 kDa (TOM 20) at the mitochondrial membrane as well as with caspase 3 and caspase 12 (Chis et al. 2012). It is thought that the interaction with VDAC is critical for preventing apoptosis through the mitochondrial pathway during I/R injury (Mitra et al. 2013). Temporal studies with I/R performed ex vivo in mouse hearts demonstrated that αB-crystallin translocates to the mitochondria during ischemia, becomes phosphorylated at Ser-59, and aids in maintaining mitochondrial membrane potential, thereby preventing apoptosis (Whittaker et al. 2009).

11.2.3.3 Nuclear Speckles

Nuclear speckles, located within the interchromatin space of the nucleoplasm, are proposed to be storage sites for splicing components and are associated with transcriptional activity (Spector and Lamond 2011). αB-Crystallin and other sHSPs, including Hsp27 (HspB1) localize to nuclear speckles in a variety of unstressed, transcriptionally active cell lines and primary cells (Vandenijssel et al. 2003). Overexpression of the R120G mutant form of αB-crystallin inhibited localization to nuclear speckles (Vandenijssel et al. 2003). These data suggest a nuclear role for αB-crystallin in modulating transcript processing, which may be important in R120G αB-crystallin-opathy (Vandenijssel et al. 2003).

A study utilizing mouse C2C12 myoblasts and differentiated myotubes showed differential nuclear speckle localization of αB-crystallin in response to heat shock (Adhikari et al. 2004). In the basal state, myoblasts showed expression of αB-crystallin in the cytoplasm and nucleus, with co-localization with lamin A/C and splicing factor SC-35, indicating nuclear speckle localization, and upon heat stress, myoblasts exhibited almost complete re-localization of αB-crystallin to the nucleus in nuclear speckles, returning to basal state following 3 h recovery. Interestingly, myotubes have αB-crystallin expression exclusively in the cytoplasm under basal and heat stressed conditions. This data may speak for a differential role of αB-crystallin in transcriptional modulation or cytoskeletal protection during differentiation and myogenesis.

11.2.3.4 Posttranslational Modifications

αB-Crystallin contains three phosphorylation sites (Ser-19, Ser-45, Ser-59), identified through experiments exposing cultured cells to various forms of stress (Kato et al. 1998; Ito et al. 1997). These sites are located within the n-terminal region, which can impact both structural and functional aspects of the sHSP, though the impact of phosphorylation on protection of the cell seems to be context dependent. Through studies employing phosphomimetic forms of αB-crystallin, it has been shown that phosphorylation at all three residues decreases oligomer size, with the dominant species being 12-mers and 6-mers, resulting in a more flexible n-terminal domain and increased chaperone activity toward malate dehydrogenase and p53 (Peschek et al. 2013). Additional studies have shown both increases and decreases in chaperone activity of αB-crystallin with phosphorylation depending on the substrate and conditions (Ahmad et al. 2008; Ecroyd et al. 2007), and the ratio of phosphorylated to non-phosphorylated forms of αB-crystallin present in oligomers may be key to regulating its wide range of chaperone activity (Ahmad et al. 2008).

Phosphorylation at Ser-45 may disrupt dimer formation, resulting in an increase in oligomers with an odd number of subunits (Aquilina et al. 2004). One study showed that phosphorylation at Ser-59 is required for nuclear import, and localization to nuclear speckles required phosphorylation at Ser-45 in HeLa cells (den Engelsman et al. 2005). Though a different study employing transient transfection

of a phospho-defective form of αB-crystallin, demonstrated that phosphorylation was not required for nuclear localization (Vandenijssel et al. 2003). Phosphorylation at Ser-59 occurs in response to I/R stress in cardiomyocytes (Ito et al. 1997). A phosphomimetic at Ser-59 was shown to be necessary and sufficient for attenuating hyperosmotic or hypoxic stress-induced apoptosis in rat neonatal cardiomyocytes through inhibition of caspase 3 activation (Morrison et al. 2003). In differentiating C2C12 myoblasts, overexpression of wildtype αB-crystallin inhibits caspase 3 activation thereby blocking differentiation-induced apoptosis, and pseudophosphorylation of αB-crystallin at all three serine residues prevents αB-crystallin from performing this function (Kamradt et al. 2002). In light of these data showing varying effects of phosphorylation of αB-crystallin on its structure, localization, and function, it is likely that phosphorylation may be a mechanism for fine-tuning the activity of αB-crystallin, which is context dependent. In addition to phosphorylation, αB-crystallin undergoes O-GlcNAcylation at threonine 170, which has been linked to effects on αB-crystallin subcellular localization, protein-protein interactions, chaperone function, and degradation (Krishnamoorthy et al. 2013).

11.2.4 Roles

11.2.4.1 Chaperone

The major role of αB-crystallin is as a molecular chaperone. Chaperones bind hydrophobic regions of unfolded proteins, stabilizing the protein and preventing it from precipitating out of solution (Ellis and van der Vies 1991). αB-Crystallin, functions in an ATP-independent manner to bind severely compromised, aggregation-prone, late unfolding protein intermediates that are about to precipitate out of solution, and forms a stable, soluble complex that is resistant to aggregation (Carver et al. 1995; Rajaraman et al. 2001). Additionally, αB-crystallin transiently interacts with early unfolding intermediates and promotes their refolding (Rajaraman et al. 2001). Substrate recognition by αB-crystallin is not fully defined, but occurs through interaction of its hydrophobic regions, possibly various regions throughout the protein with exposed hydrophobic regions of unfolded proteins. This provides αB-crystallin with the ability to recognize a wide range of substrates (Basha et al. 2012).

The importance of αB-crystallin in maintaining cytoskeletal integrity is exemplified by its ability to bind and stabilize actin microfilaments, intermediate filaments, including desmin, vimentin, and GFAP, as well as microtubules reviewed in (Liang and MacRae 1997). In addition to binding cytoskeletal elements, αB-crystallin also has the ability to bind and prevent the aggregation of some growth factors, including FGF-2 and VEGF (Ghosh et al. 2007a, b). An in vitro study demonstrated the transient appearance of dimeric αB-crystallin interacting with the model destabilized substrate, α-lactalbumin, indicating that dimer release from the larger oligomers may be important for the chaperone function of αB-crystallin (Smirnova et al. 2013).

Desmin, a major intermediate filament protein in striated muscle, is responsible for connecting myofibrils together through Z-discs (Lockard and Bloom 1993). αB-Crystallin interacts with and functions as a chaperone for desmin (Perng et al. 1999a), and a mutant form of αB-crystallin, R120G, can increase its affinity for desmin resulting in aberrant desmin aggregation (Perng et al. 2004; Vicart et al. 1998). A study identifying that the interaction between αB-crystallin with desmin involved the β3 and β8 strands as well as c-terminal residues 155–165, also suggests that binding or cosedimentation of αB-crystallin with desmin does not necessarily increase αB-crystallin chaperone function towards desmin (Houck et al. 2011).

The muscle contractile protein titin, responsible for the elastic properties of muscle, contains spring-like immunoglobulin (Ig) domains that can unfold and allow contracted muscles to stretch (Minajeva et al. 2001), which can result in aggregation of the unfolded titin domains (Minajeva et al. 2001; Rief 1997). Titin and αB-crystallin were co-immunoprecipitated in pig hearts following ischemia and αB-crystallin was shown to bind to the I-band region of titin, with extraction of actin, in ischemic rat cardiomyocytes (Golenhofen et al. 2002). A following study more specifically identified that αB-crystallin binds to the N2B region of the cardiac titin isoform in physiologically stretched cardiomyocytes, and that higher stretching forces are required to unfold the titin domains in the presence of αB-crystallin (Bullard et al. 2004). Whereas binding of αB-crystallin appears to be specific to the N2B element of titin in cardiac muscle, in skeletal muscle, αB-crystallin shows scattered binding along the length of the I-band in rats, indicating it may bind to other Ig domains (Golenhofen et al. 2004). In vitro work shows that unfolded Ig domains, including cardiac N2B and skeletal N2A, of titin aggregate with increased aggregation under acidic conditions, and the presence of αB-crystallin prevents this aggregation (Kotter et al. 2014). αB-Crystallin was also localized to the Ig domain regions of titin in diseased, human cardiomyocytes and skeletal muscle, suggesting that this localization is necessary to prevent aggregation of unfolded Ig domains in overstretched muscle cells, and this interaction may also be relevant in skeletal muscle during exercise (Kotter et al. 2014). Additionally, in I/R experiments using isolated papillary muscles from *CRYAB*/*HSPB2* double knockout (DKO) mouse hearts, it was speculated that more pronounced contracture in mutant muscles may be due to loss of αB-crystallin chaperone function of titin, thereby causing increased stiffness in response to ischemia (Golenhofen et al. 2006).

αB-Crystallin interacts with an f-box protein, FBX4, an important component of the SCF complex, which carries out ubiquitination of proteins, marking them for degradation (den Engelsman et al. 2003). This interaction is increased with phosphomimetics at Ser-19 and Ser-45 and also by the R120G mutation. These data suggest a potential role for αB-crystallin in directing substrate ubiquitination in the ubiquitin proteasome pathway, which may assist in maintaining cellular homeostasis by degrading proteins that will not refold properly. Activation of autophagy or the inflammatory response may also be a role for αB-crystallin in protein quality control as has been suggested for other sHSPs (Carra et al. 2008, 2009; Bruinsma et al. 2011).

11.2.4.2 Anti-apoptotic

Exogenous αB-crystallin expression in human lens epithelial cells prevented UVA-induced apoptosis through inhibition of the RAF/MEK/ERK pathway (Liu et al. 2004) via inhibition of RAS activation (Li et al. 2005). αB-Crystallin binds and modulates caspase 3 and Bax in the lens, regulating differentiation (Hu et al. 2012). It was also shown in retinal pigment epithelial cells that αB-crystallin is able to inhibit the translocation of Bax and Bcl-2 to the mitochondria (Mao et al. 2004). In cancer cell lines, αB-crystallin was identified as a target gene directly trans-activated by p53. αB-Crystallin binds to the DNA binding domain of p53 and reduced p53-induced apoptosis (Watanabe et al. 2009). In response to hydrogen peroxide treatment of C2C12 myogenic cells, αB-crystallin interacts with p53 in the cytoplasm, possibly preventing its translocation to the mitochondria and abrogating oxidative stress-induced apoptosis (Liu et al. 2007).

When myoblasts are stimulated to differentiate by growth factor deprivation, they will undergo apoptosis if they do not develop resistance to apoptosis, allowing differentiation to ensue. In differentiating C2C12 myoblasts, αB-crystallin is induced in those myoblasts that develop resistance to apoptosis and overexpression of αB-crystallin prevents differentiation-induced apoptosis through inhibition of caspase 3 activation (Kamradt et al. 2001, 2002). An independent experiment confirmed that overexpression of αB-crystallin decreased the levels of cleaved, activated caspase 3 in differentiating C2C12 myoblasts (Singh et al. 2010). These results suggest a critical role for αB-crystallin in the prevention of apoptosis during normal differentiation of myoblasts to myotubes. Additionally, DKO mice exhibit increases in both apoptosis and necrosis in response to I/R injury suggesting a protective role for one or both of these chaperones towards cardiomyocytes (Morrison et al. 2004). In αB-crystallin transgenic mice, Das and Dillmann have demonstrated ischemic cardioprotection (Ray et al. 2001).

11.2.4.3 Redox Modulation

Muscle contains high levels of mitochondria to comply with high energy requirements. The heart is made up of 55 % cardiomyocytes, with up to 35 % of the cardiomyocyte volume occupied by mitochondria and since mitochondria are the main source of reactive oxygen species (ROS), cells must adapt to deal with these harmful byproducts (Christians et al. 2012). Implications of αB-crystallin on redox state have mainly been explored through studies of the R120G mutant form. Transgenic mice overexpressing R120G αB-crystallin specifically in cardiomyocytes were shown to have a redox balance skewed towards reductive stress (Rajasekaran et al. 2007). In this model, R120G αB-crystallin-induced cardiomyopathy and aggregate formation were rescued by the intercross with mice having decreased levels of an antioxidative enzyme glucose-6-phosphate dehydrogenase, implicating an effect of the mutant form of αB-crystallin on redox state. αB-Crystallin cannot be thiolated due to its lack of cysteine residues, indicating that αB-crystallin does not undergo modification in response to extreme shifts of redox conditions.

11.3 Protective Effects of αB-Crystallin in Stressed or Pathological States

Many instances of protective roles for αB-crystallin have been described in the literature and correspond with its role as a stress response protein. Roles for αB-crystallin in I/R injury of the heart and exercise-induced injury in skeletal muscle will be discussed here.

11.3.1 Cardiac Muscle: Ischemia/Reperfusion

Neonatal and adult rat cardiomyocytes are protected from I/R injury by overexpression of αB-crystallin (Martin et al. 1997). Transgenic overexpression of αB-crystallin also protects the mouse heart in ex vivo I/R, decreasing the extent of infarction, lowering levels of oxidative stress, and decreasing apoptosis and necrosis (Ray et al. 2001). Conversely, DKO mouse hearts were more prone to I/R damage, and showed reduced contractile recovery, increased apoptosis and necrosis, and lower levels of the reduced form of glutathione, a protective molecule for oxidative damage (Morrison et al. 2004). To better understand the individual roles of αB-crystallin and HspB2 during I/R, Pinz and colleagues crossed DKO mice with mice transgenically overexpressing *CRYAB* and through I/R experiments, determined that αB-crystallin seems to be important for maintaining structure and diastolic function (Pinz et al. 2008). Through its mitochondrial interactions, as discussed previously, αB-crystallin may aid in maintaining mitochondrial integrity in response to I/R stress (Boelens 2014). In response to I/R, αB-crystallin also translocates to the mitochondria (Whittaker et al. 2009) and interacts with VDAC; this interaction may be critical for preventing apoptosis induced through the mitochondrial pathway (Mitra et al. 2013; Chis et al. 2012).

Sixty-minute cardiac ischemia in pigs resulted in overstretching of cardiomyocytes as observed by increased Z-disc spacing and increased distance between α-actinin and titin antibody staining (Golenhofen et al. 1999). In this study, αB-crystallin translocated from the cytoplasm to the I-band portion of titin in response to ischemia and following reperfusion, it remained bound to titin in cardiomyocytes that were no longer capable of contraction (Golenhofen et al. 1999). This result suggests that αB-crystallin is essential for mitigating the refolding of elastic titin domains in response to cardiomyocyte stretch as a result of ischemia, and αB-crystallin remains bound to the unfolded domains of titin in cardiomyocytes that are too damaged to recover contractile function.

11.3.2 Skeletal Muscle: Exercise

Eccentric contraction is the repeated stretching of actively contracting muscles and this can damage muscle fibers especially in untrained muscles, whereby damage occurs with concomitant inflammation (Koh 2002). Using ex vivo rabbit skeletal

muscles, it was shown that desmin is lost in damaged fibers immediately after eccentric contraction and continues up to 3 days following injury (Friden and Lieber 2001). Dystrophin seems to be affected in a similar manner as a result of eccentric contraction in rat tibialis anterior muscles (Komulainen et al. 1998). An increase in free radical production in rabbit muscle occurred 24 h post-eccentric contraction, attributable to infiltrating inflammatory cells (Best et al. 1999).

Increases in the level of *CRYAB* were seen at 6 and 24 h after eccentric contraction (Kostek et al. 2007), which may be induced by mechanical and/or oxidative stress (Koh 2002). In a study involving human subjects using biopsies of the quadriceps muscle, αB-crystallin was upregulated 30 min following eccentric exercise and gradually decreased for 1 week after (Paulsen et al. 2007). Additionally, αB-crystallin responded immediately to eccentric exercise by binding to and fractioning with the cytoskeletal/myofibrillar proteins. Mice exposed to eccentric contractions showed immediate translocation of αB-crystallin from the soluble to insoluble fraction by western blot and cytosol to the Z-disc by immunostaining (Koh and Escobedo 2004). Phosphorylation of αB-crystallin was also observed during this time and may be important for its protective activity.

The temperature of muscles rises during exercise and may result in thermal injury. Chicken skeletal muscle myosin was unfolded by heat shock in vitro and in the presence of αB-crystallin, myosin retained enzymatic activity and aggregation was prevented (Melkani et al. 2006). αB-Crystallin was shown in vitro to prevent the acidic-induced aggregation of the N2A region of skeletal muscle titin, which contains Ig domains that are prone to unfolding during exercise (Kotter et al. 2014). It also is bound to the Ig domain regions of titin in skeletal muscle biopsies from patients with limb girdle muscular dystrophy type 2a; while in healthy human biopsies, αB-crystallin had cytosolic localization with faint Z-disc staining (Kotter et al. 2014). Ischemic rat skeletal muscle showed αB-crystallin bound along the length of the I-band, likely to the Ig domains of titin (Golenhofen et al. 2004). It is likely that this ability of αB-crystallin to protect titin Ig domains from aggregation upon unfolding due to stretch is also active during exercise (Kotter et al. 2014), especially eccentric contraction, where muscle is damaged from overstretching (Koh 2002).

11.4 αB-Crystallin-Opathies: Mutations and Human Pathologies

To date, 14 naturally occurring mutations in human *CRYAB* have been identified and published in the literature (Christians et al. 2012). Of these, ten are dominant mutations and four exhibit recessive inheritance patterns with disease pathologies ranging from skeletal myopathy, cardiomyopathy, cataracts, or some combination of the three. Eight of these mutations result in skeletal and/or cardiac myopathy (see Table 11.1) and can be classified as αB-crystallin-opathies (Selcen 2011; Sanbe et al. 2011; Christians et al. 2012). Variable penetrance and expressivity of the myopathy-causing

Table 11.1 Myopathy causing mutations in *CRYAB*

Genetic mutation	Resulting protein change	Type of myopathy	Dominant or recessive	Onset	Reference
c.60delC	S21Afs24X	Skeletal	Recessive	Infantile	Del Bigio et al. (2011)
350 G>C	D109H	Both	Dominant	Adult	Sacconi et al. (2012)
c.343delT	S115Pfs129X	Skeletal	Recessive	Infantile	Forrest et al. (2011)
358 A>G	R120G	Both	Dominant	Adult	Vicart et al. (1998)
451 C>T	Q151X	Skeletal	Dominant	Adult	Selcen and Engel 2003)
460 G>A	G154S	Skeletal or Cardiac	Dominant	Adult	Pilotto et al. (2006), Reilich et al. (2010)
c.464delCT	L155fs163X	Skeletal	Dominant	Adult	Selcen and Engel (2003)
495 G>A	R157H	Cardiac	Dominant	Adult	Inagaki et al. (2006)

mutations in *CRYAB* suggest genetic modifier and/or environmental factor contribution to the disease state (Christians et al. 2014). Additionally, for the dominant mutations, relative levels of the wildtype compared with the mutant form of αB-crystallin may also contribute to disease and could be modified by degradation, which may change with environmental stressors (Christians et al. 2014).

11.4.1 Point Mutations

First described in 1978 (Fardeau et al. 1978), the prototype and most well studied of the human mutations in αB-crystallin, arginine 120 mutated to a glycine (R120G) (Vicart et al. 1998), resulting in multisystem disorders and pathologies, was not identified until 1998 (Vicart et al. 1998). This disease affects a large, French pedigree and muscle biopsies characterized by electron microscopy revealed the buildup of dense, granulo-filamentous material within the sarcoplasm (Fardeau et al. 1978), which contained the intermediate filament protein desmin (Rappaport et al. 1988; Fardeau et al. 1978) as well as αB-crystallin, and therefore is classified as a desmin-related myopathy (DRM) (Vicart et al. 1998). Patient biopsies revealed a "rubbed-out" appearance when stained for myosin adenosine triphosphatase (ATPase) activity, potentially indicating a loss of myosin (Brady et al. 2001; Vicart et al. 1998; Fardeau et al. 1978). The R120G mutation (358 A>G) occurs in the α-crystallin domain and disrupts the structure as well as reduces the chaperone activity of αB-crystallin (Bova et al. 1999; Perng et al. 1999b). The binding affinity of αB-crystallin for desmin in vitro is increased by R120G, and results in the aberrant aggregation of desmin, preferentially during de novo desmin network synthesis rather than the aggregation of previously formed networks (Perng et al. 2004). This mutation shows closure of the hydrophobic groove present in αB-crystallin dimers, which may alter substrate binding as well as oligomerization (Clark et al. 2011).

In vitro work shows that the R120G mutant form of αB-crystallin has complete loss of chaperone activity towards the N2B region of cardiac titin (Zhu et al. 2009).

Transgenic overexpression of R120G in the mouse heart portrays pathology similar to patients, showing dense desmin and αB-crystallin positive aggregates, and disruption of the cytoskeletal structure and mitochondrial architecture, resulting in cardiomyopathy and death in early adulthood (Wang et al. 2001). Overexpression of wildtype *CRYAB*, on the other hand, was relatively unremarkable (Wang et al. 2001). A knockin mouse model of R120G exhibits early onset cataracts and skeletal myopathy, with increased severity depending on dose (heterozygous versus homozygous knockin), though mortality was not increased (Andley et al. 2011), as is the case in the cardiac-specific overexpression of R120G (Wang et al. 2001). Cardiac function was not reported on in the publication of the R120G knockin animals (Andley et al. 2011).

Aggregates formed as a result of the R120G mutation contain amyloid oligomers and are classified as aggresomes (Sanbe et al. 2004), characteristic of neurodegenerative diseases, which result from transport of the aggregates along microtubules to the perinuclear region (Garcia-Mata et al. 2002). The dysfunction of mitochondria is one of the first defects observed in R120G overexpressing mouse hearts (Maloyan et al. 2005). Cardiomyocytes exhibit reduced mitochondrial oxygen consumption, changes in the permeability transition pore, and poor inner membrane potential, thereby activating apoptotic pathways and adversely affecting the hearts of transgenic animals. Transgenic overexpression of R120G in the heart also yields reductive stress, due to altered activity of enzymes that generate redox intermediates, including glucose-6-phosphate dehydrogenase, glutathione reductase, and glutathione peroxidase (Rajasekaran et al. 2007). These animals have elevated levels of autophagic activity by the age of 2 months, and this response is thought to be cytoprotective, possibly minimizing aggregate presence (Tannous et al. 2008). A study involving treatment of R120G transgenic mouse hearts with oxypurinol to rescue mitochondrial defects, determined that contractility was not rescued indicating further mechanical defects due to disarray of sarcomeres and accumulation of aggregates (Maloyan et al. 2009). Additionally, it has been suggested that aggregate formation and disease onset may be repressed at a young age due to competition with wildtype αB-crystallin (Andley et al. 2011; Vicart et al. 1998; Perng et al. 2004), which may also be the case for other dominant mutations described below.

The less studied ability of αB-crystallin to localize to nuclear speckles is eliminated by the R120G mutation, indicating a possible impact of the mutation on transcript processing (Vandenijssel et al. 2003). Overexpression of certain interacting partners has been found to attenuate the detrimental effects of R120G.

Interaction of R120G with BAG3, a co-chaperone involved in chaperone-assisted selective autophagy, increased R120G solubility, prevented its aggregation, and inhibited cell death induced by R120G overexpression in cell culture (Hishiya et al. 2011). Overexpression of HspB8 can inhibit R120G-induced aggresome formation and block the progression of cardiomyopathy (Sanbe et al. 2007, 2009). Voluntary exercise (Maloyan et al. 2007) and BCL-2 overexpression (Maloyan et al. 2009) also delay the onset and reduce the unfavorable effects of the R120G mutation.

The R120G disease state is likely due to a combination of loss and gain of function effects of the mutation (Sanbe et al. 2011). The broad range of roles played by αB-crystallin invites the potential for many factors to contribute to the R120G disease state, including: aggregation with desmin, loss of/altered chaperone function, altered mitochondrial architecture and function, and reductive stress. Since the initial discovery of R120G, other mutations have been identified in patient populations and can also be described as αB-crystallin-opathies.

A family with members harboring the dominant point mutation, D109H, in αB-crystallin exhibits similar multisystem pathology to patients with the R120G mutation (Sacconi et al. 2012). Residues D109 and R120 interact with each other during dimerization of αB-crystallin, and therefore disruption of this interaction may be responsible for the similar disease characteristics among patients with these two mutations (Sacconi et al. 2012) including effects on the hydrophobic groove, oligomerization (Clark et al. 2011), and desmin interaction (Perng et al. 2004). Overexpression of YFP-tagged constructs in HeLa cells showed similar aggregation of D109H and R120G as well as a similar decrease in aggregation and levels of apoptosis with Hsp27 co-overexpression (Raju and Abraham 2013), supporting a similar mechanism of action of the two mutations; however, further analysis is necessary.

A dominant glycine 154 to serine (G154S) mutation in a conserved residue was identified in a 48 year old patient diagnosed with mild dilated cardiomyopathy and slightly elevated skeletal creatine phosphokinase levels, indicating potential involvement of the skeletal muscle as well (Pilotto et al. 2006). The turnover rate of the protein is predicted to increase with this mutation (Pilotto et al. 2006). A second patient with this same mutation, G154S, presented in his sixties with progressive distal leg weakness and atrophy affecting mostly limb muscles, as well as mild difficulty swallowing (Reilich et al. 2010). The patient's biopsy showed disrupted myofibrillar structure, vacuolization, and desmin/αB-crystallin positive aggregates. No cataracts, cardiac or respiratory involvement were noted in this patient. The G154S mutation appears to have affects in both cardiac and skeletal muscle, and the specific presentation of the patient's symptoms may rely upon other confounding genetic or environmental factors causing stress in the muscle that result in the apparent tissue-specific disease manifestation. A potential increased turnover rate of this mutant form of the protein (Pilotto et al. 2006) may help to suppress symptoms exhibited by patients into later adulthood.

A patient with familial dilated cardiomyopathy, presenting after age 40, was identified to have a dominant, mutation of arginine 157 to a histidine residue (R157H), which was shown to decrease binding to the cardiac-specific N2B region of titin (Inagaki et al. 2006). This mutation, unlike the others, did not result in aberrant localization of αB-crystallin or in aggregation, and therefore, there may be an alternate disease mechanism causing dilated cardiomyopathy in this patient compared with the desmin-related cardiomyopathy in other patients with αB-crystallin-opathies. Reduced ability of αB-crystallin to bind to titin leaves titin vulnerable to stress and may predispose patients to heart failure (Inagaki et al. 2006). An in vitro chaperone assay showed that R157H maintained some chaperone activity towards the N2B region of titin, albeit reduced compared to wildtype

αB-crystallin (Zhu et al. 2009). Interestingly, this patient and family members did not exhibit skeletal muscle weakness or disease, though αB-crystallin does bind and chaperone the Ig domains in the N2A region of titin in skeletal muscle (Kotter et al. 2014; et al. 2004), in addition to the cardiac N2B region (Kotter et al. 2014), which may indicate that αB-crystallin binds the alternate regions of titin in a different way and the R157H mutation specifically disrupts the association of αB-crystallin with the N2B region. In vitro binding assays using the skeletal N2A region of titin with R157H αB-crystallin could verify this. Alternatively, absence of specific environmental stress to the skeletal muscle may be responsible for apparent lack of skeletal muscle involvement. The R157H mutation may also have other yet-unstudied implications that leave cardiac muscle more vulnerable than skeletal muscle.

11.4.2 Dominant C-Terminal Truncation Mutations

Other than the aforementioned missense mutations, the remaining mutations in αB-crystallin causing myopathy are due to frameshift or nonsense mutations resulting in varying degrees of c-terminal truncation, some with additional, novel peptide sequences present. In vitro work using site-directed mutagenesis to mutate the two terminal lysine residues in αB-crystallin to leucine or glycine greatly reduced its chaperone activity, suggesting that the lysines in the c-terminus may be critical for interacting with unfolded proteins through charge-charge interactions (Plater et al. 1996). Loss of this ability by c-terminal truncation of αB-crystallin may prevent stable substrate binding and therefore reduce chaperone activity. It has also been suggested that the flexible c-terminal region folds over, and through the I/V/L-X-I/V/L motif, binds to the β4/8 groove of the adjacent monomer, contributing to dimer formation, and potentially blocking the substrate binding face of αB-crystallin, thereby modulating substrate binding and chaperone activity (Ghosh et al. 2006; Delbecq et al. 2012). Expression of only the α-crystallin domain of αB-crystallin results in dimer formation with retained chaperone activity, but the lost ability to oligomerize (Feil et al. 2001). The high potential of c-terminal truncated mutants to aggregate, suggests a critical role for the c-terminus in preventing self-aggregation of αB-crystallin possibly through promotion of oligomerization, and expression of the mutant forms may induce co-aggregation with wildtype αB-crystallin inducing a dominant negative effect, thereby inhibiting the chaperone function of wildtype αB-crystallin (Hayes et al. 2008). The myopathy-causing, dominant, c-terminal truncation mutations will now be described.

A patient harboring the dominant 464delCT mutation in *CRYAB* presented at age 52 with respiratory trouble due to reduced diaphragmatic movement, as well as leg weakness and difficulty swallowing, and died at age 58 due to respiratory failure (Selcen and Engel 2003). This mutation generates a frameshift resulting in eight missense codons before a premature stop codon. A 53 year old patient with a dominant 451C→T transition generating a nonsense mutation (Q151X) suffered for 10 years with slowly progressive leg weakness and atrophy and exhibited elevated

creatine kinase levels (Selcen and Engel 2003). Neither patient had cataracts or cardiomyopathy. Abnormal fiber regions in both patients show intense desmin and αB-crystallin staining, and in both patients, the wildtype allele was preferentially expressed compared with the mutant forms.

Q151X results in extreme loss of protein stability and prevents oligomerization, while increasing in vitro chaperone activity towards citrate synthase and desmin (Hayes et al. 2008). The increase in chaperone activity may be due to potential loss of capping of the chaperone site by interaction with the c-terminal region (Delbecq et al. 2012; Ghosh et al. 2006), suggesting the c-terminus may be responsible for reducing αB-crystallin substrate binding for some substrates under normal conditions (Hayes et al. 2008). The 464delCT mutation results in the introduction of a novel peptide into the c-terminus resulting in decreased in vitro chaperone function towards desmin, as well as aggregation and loss of solubility that can be partially recovered through mixture with wildtype αB-crystallin (Hayes et al. 2008). Overexpression of Hsp27 also rescues the solubility and prevents aggregation of 464delCT, mediated by the ubiquitin proteasome system in H9C2 cells (a rat embryonic cardiomyocyte cell line) (Zhang et al. 2010).

11.4.3 Recessive Mutations

With mutations in *CRYAB*, especially the recessive mutations, a major question is to what extent the pathology observed is due to loss of function effects of αB-crystallin. DKO mice show progressive skeletal muscle deterioration with age following a normal development, with no apparent impact on the heart (Brady et al. 2001), except under stressful conditions such as I/R or transverse aortic constriction (TAC) (Morrison et al. 2004; Kumarapeli et al. 2008). These mice grow normally until 40 weeks, after which they lose weight, due to the inability to eat properly and exhibit severe kyphosis, hunched posture, both due to loss of corresponding musculature, with the tongue, head, and axial muscles being most greatly affected. Fatty replacement, macrophage infiltration, fibrosis, and vacuolization were observed in deteriorating muscles. Amorphous, flocculent, electron-opaque material was also noted corresponding with loss of myofibrils. Increased staining for desmin was also observed in affected fibers. Attempted determination of fiber type based on fiber type-specific myosin failed due to lack of myosin detection in deteriorating fibers (Brady et al. 2001), as confirmed in additional studies showing reduced levels of myosin heavy chain in skeletal muscle of DKO mice by western blot (Neppl et al. 2014). This may be similar to muscles of patients with the R120G mutation who have loss of myosin in their muscle cells (Vicart et al. 1998; Fardeau et al. 1978). Potentially, oxidative, slow-twitch fibers, which have the highest levels of αB-crystallin and are enriched in large truncal muscles, are preferentially degraded in the DKO mice (Brady et al. 2001) and in patients with recessive *CRYAB* mutations (Forrest et al. 2011; Del Bigio et al. 2011). Neppl and colleagues showed that 1 year old DKO mice have a significantly reduced number of satellite cells in their skeletal

muscle and a reduced ability to regenerate muscle following cardiotoxin-induced injury, shown by decreased cross-sectional myofiber area and increased fibrosis 2 weeks post-injury, indicating a potential role for αB-crystallin in skeletal muscle regeneration (Neppl et al. 2014).

This DKO mouse model is confounded due to the double knockout nature. HspB2, or myotonic dystrophy protein kinase binding protein (MKBP), activates and protects myotonic dystrophy protein kinase (DMPK) (Suzuki et al. 1998). *DMPK* -/- mice show minor decreases in size of head and neck muscles with age (Jansen et al. 1996) and late onset myopathy (Reddy et al. 1996). It is, therefore, possible that through its activation and protection of DMPK and other potential functions of HspB2, the loss of HspB2 also contributes to the pathogenesis seen in DKO animals. Subsequent studies have attempted to define the specific roles for loss of αB-crystallin and HspB2. A genetic study comparing the effects of I/R or inotropic stimulation in the hearts of wildtype, DKO, *CRYAB* transgenic, and DKO crossed with *CRYAB* transgenic (effectively expressing αB-crystallin without HspB2) concluded that αB-crystallin is responsible for structural remodeling and mechanical maintenance, while HspB2 is tasked with energetic balance maintenance in the stressed heart (Pinz et al. 2008).

CRYAB transgenic mouse hearts subjected to TAC showed reduced NFAT transactivation and attenuated hypertrophic response, while DKO hearts exhibit increased NFAT transactivation at baseline and develop cardiac insufficiencies in response to TAC, leading the authors to conclude that αB-crystallin prevents cardiac hypertrophic responses, possibly through inhibition of NFAT signaling (Kumarapeli et al. 2008). A single, cardiac specific knockout of *HSPB2* was also generated and shows under basal conditions that cardiac function, hypertrophic responses, and mitochondrial metabolism were unchanged; however, when animals were subjected to TAC, mitochondrial energetics were reduced (Ishiwata et al. 2012), in agreement with the previously suggested role for HspB2 in maintaining energetic balance (Pinz et al. 2008). To our knowledge, a whole body knockout of either *CRYAB* or *HSPB2* has yet to be published and would further distinguish the distinct roles for each in both skeletal and cardiac muscle. Additionally, identification of recessive mutants in *CRYAB* affecting muscle, discussed below, may assist in identifying loss of αB-crystallin function phenotypes, though these mutants may also have gain of function effects since the mutant proteins are expressed to some extent.

Fatal, infantile onset muscular dystrophy was identified in a cohort of Canadian aboriginals all harboring a homozygous c.60C deletion in the n-terminus of *CRYAB*, predicting a serine to alanine mutation at residue 21 and a premature stop codon after 23 missense residues, with unaffected parents both being heterozygous for this mutation (Del Bigio et al. 2011). Patients developed rigid muscles with elevated serum creatine kinase levels and died of respiratory insufficiency shortly after birth, except one child surviving to 4 years of age on mechanical ventilation. Axial muscles were more severely affected than appendicular muscles, Z-disc disarray, dense inclusions, vacuole presence, immune cell infiltration, and necrotic and regenerating fibers were noted. Deteriorating fibers stained strongly for myotilin, desmin, which concentrated at the periphery of inclusions, and αB-crystallin (using an N-terminal

specific antibody), which was highly expressed in inclusions and dimly throughout other regions of the fibers. Hearts examined in these patients were normal. This mutant mRNA is likely a target for nonsense-mediated mRNA decay due to the premature stop codon occurring upstream of the final splice junction (Amrani et al. 2006), which may attenuate its expression, though mutant protein is still expressed (Del Bigio et al. 2011). The authors hypothesize that the lack of association of αB-crystallin with titin in this case may be responsible for the severe muscle stiffness observed in patients.

A second recessive mutation in *CRYAB*, c.343delT, results in a frameshift mutation generating a predicted 127 amino acid protein, instead of the wildtype 175 amino acids (Forrest et al. 2011). The patient identified with this mutation, born from unrelated, heterozygous parents, presented starting at age 4 months with progressive feeding difficulties and respiratory distress, requiring ventilation, severe muscle stiffness affecting mostly axial muscles with some limb involvement, and elevated creatine kinase levels. No cardiomyopathy or cataracts were noted. Muscle biopsy showed increased vacuolization, increased lipid content, globular inclusions, fibrosis, and disrupted myofibrillar structure. Abnormal fibers were intensely positive for myotilin, desmin, and αB-crystallin, which was also detected in a 15 kDa truncated form by western blot. Appearance of symptoms following normal development suggests a role for αB-crystallin in remodeling of myofibrillar structure following contraction, rather than a developmental role.

Similarities between patients with these two recessive mutations in *CRYAB* and DKO mice, including skeletal muscle deterioration with fatty deposits, fibrosis, inflammation, and vacuolization, indicate potentially that the effects of these recessive mutants result from loss of αB-crystallin function. Patients develop more severe symptoms as infants, whereas the DKO mice develop progressive symptoms into adulthood. Additionally, patients exhibit severe muscle stiffness, which is not reported in the DKO mice. The phenotypic differences could be due to multiple factors including: the confounding effects of loss of HspB2 in the DKO mice, species variability of requirement for αB-crystallin in skeletal muscle, or potential additional gain of toxic function effects of the mutant protein expression in patients with these recessive mutations. Further examination is necessary to resolve these issues.

11.5 Differential Functions of αB-Crystallin in Skeletal and Cardiac Muscle

Tissue specificity of pathology correlating with the various mutations brings about interesting questions with regards to the roles and requirements for αB-crystallin in cardiac and skeletal muscle. Though the muscles are both striated, the structure and function is very different. Potentially, various mutations in αB-crystallin could affect tissues differently. The late-onset of disease with the majority of these mutations also suggests age-related stress and/or the presence of genetic modifiers may be key factors in disease manifestation. With variable patient lifestyles and

different stress encounters, it is difficult to determine in the relatively small number of patients whether, given time and/or the correct stress, patients may also develop clinical symptoms in the yet-unaffected tissue. Nevertheless, we discuss in this section some potential reasons for tissue-specific impacts of αB-crystallin.

Detailed analysis of the cellular localization of αB-crystallin using immunohistochemistry of rat organs indicates potential expression of αB-crystallin in highly oxidative cells, as suggested by a correlation between αB-crystallin expression and markers of oxidative activity (Iwaki et al. 1990). All type 1 aerobic fibers (slow-twitch) and about half of type 2 anaerobic fibers (fast-twitch), corresponding to mostly type 2A fibers, were positive for αB-crystallin, with more intense staining in type 1 fibers. Additional studies confirmed higher expression of αB-crystallin in slow- compared to fast-twitch fibers (Golenhofen et al. 2004; Atomi et al. 2000). Variable expression in different types of skeletal muscle fibers may account for specific fiber-type degradation, but this would not account for the lack of cardiac involvement, since αB-crystallin levels are comparably high in the heart (Golenhofen et al. 2004). Higher αB-crystallin expression in oxidative muscle (cardiac and type 1 skeletal fibers) may also be due to requirements of αB-crystallin for maintaining redox balance (Rajasekaran et al. 2007).

αB-Crystallin plays a role in maintaining the desmin network in muscle, which is crucial for proper sarcomere alignment as well as mitochondrial architecture (Perng et al. 1999a; Lockard and Bloom 1993; Wang et al. 2001; Maloyan et al. 2005). Differences between muscle types in mitochondrial architecture and requirements for appropriate coupling (Milner et al. 2000; Reipert et al. 1999; Rambourg and Segretain 1980; Rappaport et al. 1998) could underlie tissue specificity of disease as well as exemplify normal roles for αB-crystallin.

Sarcomeric localization of αB-crystallin in ischemic skeletal muscle is similar to cardiac muscle, with I-band and intermediate filament localization, though at the I-band, αB-crystallin binds to titin along the length of the I-band region in skeletal muscle, where in cardiac muscle it binds to a narrow region (Golenhofen et al. 2004), identified as the N2B element of titin (Bullard et al. 2004; Golenhofen et al. 2002). Skeletal muscle is susceptible to stretch injury on a day-to-day basis as a result of exercise, which can unfold titin Ig domains (Friden and Lieber 2001; Koh 2002), whereas in cardiac muscle, titin plays a role in the maintenance of passive stiffness during diastole, and, in patients with heart failure, isoforms of titin switch to more compliant forms, with stretching of titin isoforms occurring in cardiomyocytes due to I/R injury and hypertrophic response in heart failure (Linke 2008; Golenhofen et al. 1999). Stretching induces unfolding of the elastic domains of titin (Rief 1997; Minajeva et al. 2001), which may require αB-crystallin to prevent aggregation (Bullard et al. 2004; Golenhofen et al. 2002, 2004; Kotter et al. 2014). Potentially the different isoforms of titin expressed in cardiac and skeletal muscle (Labeit and Kolmerer 1995), as well the apparent variable binding of αB-crystallin to the titin domains may be a reason for tissue specificity of disease. Or more simply, tissue susceptibility to stretch may also explain this phenomenon.

Development of cardiac and skeletal muscle appear not to require αB-crystallin, since DKO mice (Brady et al. 2001), as well as all patients with mutations in *CRYAB*,

develop symptoms following normal development (see Table 11.1). The major role of αB-crystallin seems to be in the maintenance of muscle tissue as well as protection during stress, as described above. Figure 11.1 discusses the potential impacts of alterations in levels of αB-crystallin or mutations in *CRYAB* on various stages of skeletal muscle myogenesis. Maintenance of skeletal muscle requires the activation of resident, quiescent progenitor cells, known as satellite cells, identified by expression of the transcription factor Pax7, to sequentially express the myogenic regulatory factors (MRFs), including MyoD and myogenin, which regulate muscle differentiation (Weintraub 1993; Le Grand and Rudnicki 2007). Proliferating myoblasts expressing MyoD must turn off MyoD expression, exit the cell cycle, turn on myogenin, and fuse to form multinucleated myotubes (Weintraub 1993;

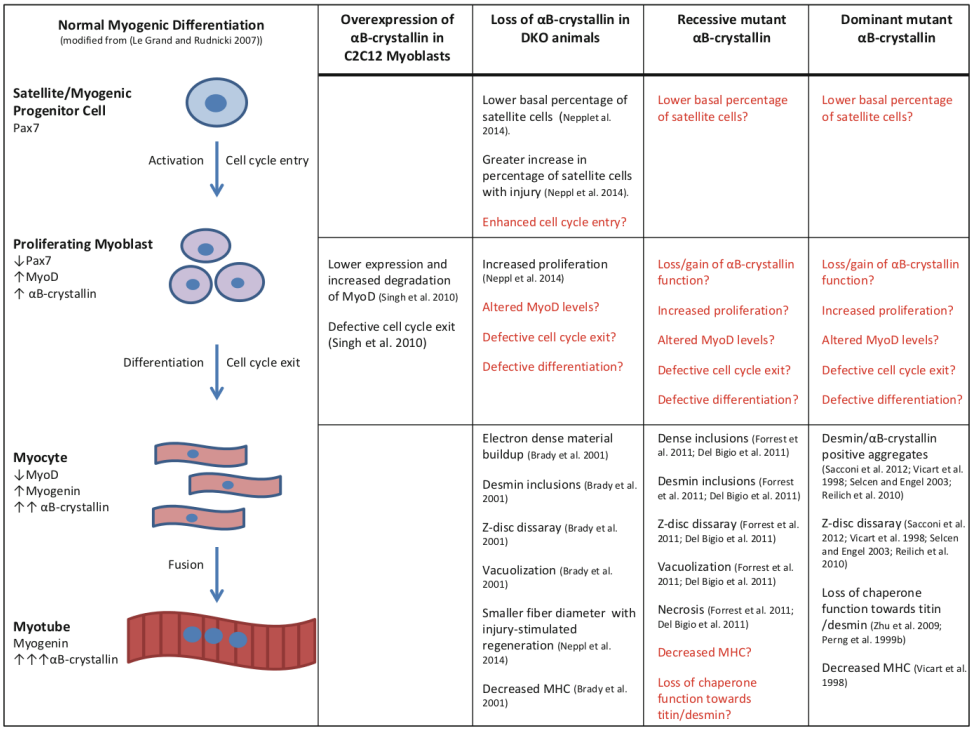

Overexpression of αB-crystallin in C2C12 Myoblasts	Loss of αB-crystallin in DKO animals	Recessive mutant αB-crystallin	Dominant mutant αB-crystallin
	Lower basal percentage of satellite cells (Nepplet al. 2014). Greater increase in percentage of satellite cells with injury (Neppl et al. 2014). Enhanced cell cycle entry?	Lower basal percentage of satellite cells?	Lower basal percentage of satellite cells?
Lower expression and increased degradation of MyoD (Singh et al. 2010) Defective cell cycle exit (Singh et al. 2010)	Increased proliferation (Neppl et al. 2014) Altered MyoD levels? Defective cell cycle exit? Defective differentiation?	Loss/gain of αB-crystallin function? Increased proliferation? Altered MyoD levels? Defective cell cycle exit? Defective differentiation?	Loss/gain of αB-crystallin function? Increased proliferation? Altered MyoD levels? Defective cell cycle exit? Defective differentiation?
	Electron dense material buildup (Brady et al. 2001) Desmin inclusions (Brady et al. 2001) Z-disc dissaray (Brady et al. 2001) Vacuolization (Brady et al. 2001) Smaller fiber diameter with injury-stimulated regeneration (Neppl et al. 2014) Decreased MHC (Brady et al. 2001)	Dense inclusions (Forrest et al. 2011; Del Bigio et al. 2011) Desmin inclusions (Forrest et al. 2011; Del Bigio et al. 2011) Z-disc dissaray (Forrest et al. 2011; Del Bigio et al. 2011) Vacuolization (Forrest et al. 2011; Del Bigio et al. 2011) Necrosis (Forrest et al. 2011; Del Bigio et al. 2011) Decreased MHC? Loss of chaperone function towards titin/desmin?	Desmin/αB-crystallin positive aggregates (Sacconi et al. 2012; Vicart et al. 1998; Selcen and Engel 2003; Reilich et al. 2010) Z-disc dissaray (Sacconi et al. 2012; Vicart et al. 1998; Selcen and Engel 2003; Reilich et al. 2010) Loss of chaperone function towards titin /desmin (Zhu et al. 2009; Perng et al. 1999b) Decreased MHC (Vicart et al. 1998)

Fig. 11.1 The schematic represents normal myogenic differentiation of satellite cells to myotubes, indicating relative expression levels of defining transcription factors throughout the process (Modified from Le Grand and Rudnicki 2007). Satellite cells/myogenic progenitor cells, expressing Pax7, are activated and enter the cell cycle to become proliferating myoblasts, with an increase in MyoD expression and concomitant decrease in Pax7 expression. Proliferating myoblasts must exit the cell cycle to fulfill differentiation to myocytes, which downregulate MyoD expression and upregulate myogenin. Myocytes then fuse into multi-nucleated myotubes, which maintain expression of myogenin. During myogenesis, αB-crystallin is expressed at low levels in proliferating myoblasts and is greatly upregulated upon differentiation to myotubes (Adhikari et al. 2004; Singh et al. 2010). The table to the right of the schematic indicates variations in myogenesis that occur as a result of overexpression of αB-crystallin, loss of αB-crystallin, recessive mutations in αB-crystallin, and dominant mutations in αB-crystallin. *Red text* indicates a testable hypothesis for that condition

Le Grand and Rudnicki 2007). Overexpression of αB-crystallin significantly delays this process in C2C12 myoblasts, with cells showing a defect in cell cycle exit and lower levels of MyoD (Singh et al. 2010). DKO mice exhibit reduced levels of satellite cells under basal conditions at 1 year of age, and unexpectedly, a cardiotoxin injury model of DKO mouse tibialis anterior muscles revealed a threefold increase in the percentage of satellite cells in response to injury; though the mice also showed decreased cross-sectional myofiber area and increased fibrosis (Neppl et al. 2014). This study suggests that loss of αB-crystallin results in an increase in proliferation, with lower levels of p21 and notch signaling molecules, possibly through modulation of Argonaute 2 activity, as shown by enrichment of miRNAs on Argonaute 2 in injured DKO skeletal muscles and co-immunoprecipitation of Argonaute 2 with αB-crystallin (Neppl et al. 2014). Argonaute 2 is an essential component of the RISC complex for miRNA-mediated silencing; the possibility of αB-crystallin as an allosteric regulator of the RISC complex may be a reason for its broad cellular impact (Neppl et al. 2014). The study by Neppl and colleagues suggests that with the loss of αB-crystallin, the regenerative response of satellite cells is skewed towards proliferation with inefficient differentiation to myotubes (Neppl et al. 2014). This is contradictory to data suggesting that overexpression of αB-crystallin in C2C12 myoblasts leads to increased proliferation through delayed exit from the cell cycle with a decrease in p21 expression (Singh et al. 2010). Both studies indicate a role for αB-crystallin in cell cycle regulation during skeletal muscle regeneration (Neppl et al. 2014; Singh et al. 2010). Additional experiments addressing the model system used (i.e. in vivo or cell culture, loss of αB-crystallin or overexpression) are necessary to reconcile the exact role for αB-crystallin in cell cycle regulation under basal and stressed conditions.

Due to withdrawal of growth factors, myoblasts must also resist apoptosis when differentiating to myotubes. αB-crystallin is induced in and contributes to apoptosis-resistance in C2C12 myoblasts through inhibition of caspase 3 activation, and overexpression of αB-crystallin prevents apoptosis occurring as a result of differentiation (Kamradt et al. 2001, 2002). These studies suggest that αB-crystallin may be important for modulating myoblast differentiation during tissue regeneration by multifaceted means including impact on proliferation and cell cycle exit, levels of regulatory MyoD, and inhibition of apoptosis. Cardiac muscle does not have the luxury to regenerate as skeletal muscle does (Mercola et al. 2011), implicating that loss of αB-crystallin function may manifest in skeletal muscle instead of cardiac muscle under healthy conditions due to requirements in regenerative myogenesis.

11.6 Stem Cells as a Model Systems for Studying αB-Crystallin in Cardiac and Skeletal Muscle

Many model systems have been employed in the study of αB-crystallin as discussed above, including rodents and larger mammalian models, some with whole body or tissue-specific overexpression/knockout, human tissue biopsies from healthy and

diseased patients, cell culture with primary cells or cell lines, as well as in vitro biochemical analysis. To more fully understand the differential implications of αB-crystallin in cardiac and skeletal muscle, it is crucial to use models in which both cell types can be analyzed in parallel. Animal models with whole body genetic modifications, cell culture using both cardiac and skeletal muscle cell lines, and in vitro experiments analyzing interactions with cardiac- and skeletal-specific isoforms will be useful in accomplishing this feat. Stem cells offer additional potential for analyzing the impact of αB-crystallin on cardiac and skeletal muscle. Induced pluripotent stem cells (iPSCs), a technology first developed in the lab of 2012 Nobel Prize winner, Shinya Yamanaka (Takahashi and Yamanaka 2006), are an invaluable tool offering the ability to model cell-autonomous disease using a patient's own cells and the potential to screen drug compounds or provide cell therapy (Robinton and Daley 2012). Somatic cells are isolated from patients, which can be done now through minimally invasive procedures including blood draws and urine sample collection, and reprogrammed into induced pluripotent stem cells through a variety of techniques involving the overexpression of key transcription factors (Chou et al. 2011; Zhou et al. 2012). Once reprogrammed, these cells are pluripotent and can be directed to differentiate to either cardiac or skeletal muscle cells, which can be studied in culture (Hosoyama et al. 2014; Zhang et al. 2012; Lian et al. 2013; Darabi et al. 2012).

Our lab has previously generated and characterized mouse iPSC-derived cardiomyocytes from transgenic R120G *CRYAB* mice, and shown that cardiomyocytes derived from these cells exhibit αB-crystallin positive aggregates as well as activation of the hypertrophic response (Limphong et al. 2013), indicating that iPSCs have the potential to recapitulate at least some phenotypes observed in αB-crystallinopathies. Many published examples of the use of iPSCs for modeling cardiac diseases exist in the literature, including long QT (Itzhaki et al. 2011) and LEOPARD syndromes (Carvajal-Vergara et al. 2010), with the list rapidly growing. Genetic manipulation is also feasible in iPSCs (Yusa et al. 2011; An et al. 2012; Fong et al. 2013), which allows for the generation of gene-corrected control cells from patient cells harboring mutations, or for insertion of mutations of interest into wildtype iPSC lines for analysis. Caveats of the use of iPSCs as a model include purity of differentiated cultures, which has improved drastically over time and is likely to continue improving with advancement of differentiation methods, lack of support cell presence in the culture (i.e. fibroblasts, endothelial cells, etc.) that may play a role in disease pathogenesis, and variability between iPSC lines with differentiation, which can be minimized through the use of genetic manipulation for the generation of appropriate controls. The iPSC system could be very effective for looking at cell-type specific impacts of αB-crystallin in mutant and wildtype form, which is a focus of pursuit in our laboratory.

11.7 Conclusions and Future Directions

Overall, much work has been done to describe the function of αB-crystallin in cardiac and skeletal muscle both in healthy and diseased states. The use of model systems that allow for direct comparison of the two cell/tissue types will better

define differential roles of αB-crystallin in each tissue and help to determine stressors or genetic modifiers that may contribute to disease susceptibility. The study of mutant forms of αB-crystallin existing in diseased patients will provide insights into not only how the mutation affects the structure and function of αB-crystallin, but also into the function and requirements of wildtype αB-crystallin during tissue maintenance and in disease compromised tissues.

The use of iPSCs to model protein misfolding disorders such as αB-crystallin-opathies, provides not only an in vitro disease model with the ability to analyze various impacted cell types and determine mechanistic details of the disease, but also the potential for small molecule screening and possibly regenerative cell therapies to treat patients. Small molecules that reduce the presence of toxic protein aggregates may be beneficial in protein misfolding diseases and can be screened for using the clinically relevant cell type generated from iPSCs (Ebert et al. 2012). The probable impact of loss of αB-crystallin on satellite cells suggests the potential for cell therapy in transplant of gene-corrected autologous or unaffected, nonautologous muscle progenitor cells to prevent skeletal myopathy in patients with recessive, early onset αB-crystallin-opathies. Engraftment of human iPSC-derived skeletal muscle progenitor cells has been shown to seed the satellite compartment in dystrophic mice suggesting the potential for long term benefits from this type of cell therapy (Darabi et al. 2012). The rapidly advancing field of iPSCs will likely lend itself to mechanistic disease modeling, small molecule screening, and regenerative therapies in protein misfolding disorders in the years to come.

Acknowledgments Lindsey Barber provided excellent editorial assistance during preparation of this manuscript.

References

Adhikari AS, Sridhar Rao K, Rangaraj N, Parnaik VK, Mohan Rao C (2004) Heat stress-induced localization of small heat shock proteins in mouse myoblasts: intranuclear lamin A/C speckles as target for alphaB-crystallin and Hsp25. Exp Cell Res 299(2):393–403. doi:10.1016/j.yexcr.2004.05.032

Ahmad MF, Raman B, Ramakrishna T, Rao Ch M (2008) Effect of phosphorylation on alpha B-crystallin: differences in stability, subunit exchange and chaperone activity of homo and mixed oligomers of alpha B-crystallin and its phosphorylation-mimicking mutant. J Mol Biol 375(4):1040–1051. doi:10.1016/j.jmb.2007.11.019

Amrani N, Sachs MS, Jacobson A (2006) Early nonsense: mRNA decay solves a translational problem. Nat Rev Mol Cell Biol 7(6):415–425. doi:10.1038/nrm1942

An MC, Zhang N, Scott G, Montoro D, Wittkop T, Mooney S, Melov S, Ellerby LM (2012) Genetic correction of Huntington's disease phenotypes in induced pluripotent stem cells. Cell Stem Cell 11(2):253–263. doi:10.1016/j.stem.2012.04.026

Andley UP, Hamilton PD, Ravi N, Weihl CC (2011) A knock-in mouse model for the R120G mutation of alphaB-crystallin recapitulates human hereditary myopathy and cataracts. PLoS one 6(3):e17671. doi:10.1371/journal.pone.0017671

Aquilina JA, Benesch JL, Ding LL, Yaron O, Horwitz J, Robinson CV (2004) Phosphorylation of alphaB-crystallin alters chaperone function through loss of dimeric substructure. J Biol Chem 279(27):28675–28680. doi:10.1074/jbc.M403348200

Atomi Y, Yamada S, Nishida T (1991) Early changes of αB-crystallin mRNA in rat skeletal muscle to mechanical tension and denervation. Biochem Biophys Res Commun 181(3):1323–1330

Atomi Y, Toro K, Masuda T, Hatta H (2000) Fiber-type-specific aB-crystallin distribution and its shifts with T3 and PTU treatments in rat hindlimb muscles. J Appl Physiol 88:1355–1364

Bagneris C, Bateman OA, Naylor CE, Cronin N, Boelens WC, Keep NH, Slingsby C (2009) Crystal structures of alpha-crystallin domain dimers of alphaB-crystallin and Hsp20. J Mol Biol 392(5):1242–1252. doi:10.1016/j.jmb.2009.07.069

Basha E, O'Neill H, Vierling E (2012) Small heat shock proteins and alpha-crystallins: dynamic proteins with flexible functions. Trends Biochem Sci 37(3):106–117. doi:10.1016/j.tibs.2011.11.005

Bennardini F, Wrzosek A, Chiesi M (1992) Alpha B-crystallin in cardiac tissue. Association with actin and desmin filaments. Circ Res 71(2):288–294. doi:10.1161/01.res.71.2.288

Best TM, Fiebig R, Corr DT, Brickson S, Ji L (1999) Free radical activity antioxidant enzyme and glutathione changes with muscle stretch injury in rabbits. J Appl Physiol 87:74–82

Bloemendal H (1981) The lens proteins. Molecular and cellular biology of the eye lens. Wiley, New York, pp 1–47

Boelens WC (2014) Cell biological roles of alphaB-crystallin. Prog Biophys Mol Biol. doi:10.1016/j.pbiomolbio.2014.02.005

Bova MP, Ding LL, Horwitz J, Fung BKK (1997) Subunit exchange of aA-crystallin. J Biol Chem 272(47):29511–29517

Bova MP, Yaron O, Huang Q, Ding L, Haley DA, Stewart PL, Horwitz J (1999) Mutation R120G in aB-crystallin, which is linked to a desmin-related myopathy, results in an irregular structure and defective chaperone-like function. Proc Natl Acad Sci U S A 96:6137–6142

Brady JP, Garland DL, Green DE, Tamm ET, Giblin FJ, Wawrousek EF (2001) aB-crystallin in lens development and muscle integrity: a gene knockout approach. IOVS 42(12):2924–2934

Bruinsma IB, de Jager M, Carrano A, Versleijen AA, Veerhuis R, Boelens W, Rozemuller AJ, de Waal RM, Verbeek MM (2011) Small heat shock proteins induce a cerebral inflammatory reaction. J Neurosci 31(33):11992–12000. doi:10.1523/JNEUROSCI. 0945-11.2011

Bullard B, Ferguson C, Minajeva A, Leake MC, Gautel M, Labeit D, Ding L, Labeit S, Horwitz J, Leonard KR, Linke WA (2004) Association of the chaperone alphaB-crystallin with titin in heart muscle. J Biol Chem 279(9):7917–7924. doi:10.1074/jbc.M307473200

Carra S, Seguin SJ, Lambert H, Landry J (2008) HspB8 chaperone activity toward poly(Q)-containing proteins depends on its association with Bag3, a stimulator of macroautophagy. J Biol Chem 283(3):1437–1444. doi:10.1074/jbc.M706304200

Carra S, Brunsting JF, Lambert H, Landry J, Kampinga HH (2009) HspB8 participates in protein quality control by a non-chaperone-like mechanism that requires eIF2{alpha} phosphorylation. J Biol Chem 284(9):5523–5532. doi:10.1074/jbc.M807440200

Carvajal-Vergara X, Sevilla A, D'Souza SL, Ang YS, Schaniel C, Lee DF, Yang L, Kaplan AD, Adler ED, Rozov R, Ge Y, Cohen N, Edelmann LJ, Chang B, Waghray A, Su J, Pardo S, Lichtenbelt KD, Tartaglia M, Gelb BD, Lemischka IR (2010) Patient-specific induced pluripotent stem-cell-derived models of LEOPARD syndrome. Nature 465(7299):808–812. doi:10.1038/nature09005

Carver JA, Guerreiro N, Nicholls KA, Truscott RJW (1995) On the interaction of a-crystallin with unfolded proteins. Biochem Biophys Acta 1252:251–260

Chis R, Sharma P, Bousette N, Miyake T, Wilson A, Backx PH, Gramolini AO (2012) Alpha-crystallin B prevents apoptosis after H2O2 exposure in mouse neonatal cardiomyocytes. Am J Physiol Heart Circ Physiol 303:H967–H978. doi:10.1152/ajpheart.00040.2012.-/-Crystallin

Chou BK, Mali P, Huang X, Ye Z, Dowey SN, Resar LM, Zou C, Zhang YA, Tong J, Cheng L (2011) Efficient human iPS cell derivation by a non-integrating plasmid from blood cells with unique epigenetic and gene expression signatures. Cell Res 21(3):518–529. doi:10.1038/cr.2011.12

Christians ES, Yan LJ, Benjamin IJ (2002) Heat shock factor 1 and heat shock proteins: critical partners in protection against acute cell injury. Crit Care Med 30(1):S43–S50

Christians ES, Ishiwata T, Benjamin IJ (2012) Small heat shock proteins in redox metabolism: implications for cardiovascular diseases. Int J Biochem Cell Biol 44(10):1632–1645. doi:10.1016/j.biocel.2012.06.006

Christians ES, Banerjee Mustafi S, Benjamin IJ (2014) Chaperones and cardiac misfolding protein diseases. Curr Protein Pept Sci 15(3):189–204

Clark AR, Naylor CE, Bagneris C, Keep NH, Slingsby C (2011) Crystal structure of R120G disease mutant of human alphaB-crystallin domain dimer shows closure of a groove. J Mol Biol 408(1):118–134. doi:10.1016/j.jmb.2011.02.020

Darabi R, Arpke RW, Irion S, Dimos JT, Grskovic M, Kyba M, Perlingeiro RC (2012) Human ES- and iPS-derived myogenic progenitors restore DYSTROPHIN and improve contractility upon transplantation in dystrophic mice. Cell Stem Cell 10(5):610–619. doi:10.1016/j.stem.2012.02.015

de Jong WW, Caspers GJ, Leunissen JAM (1998) Genealogy of the alpha-crystallin—small heatshock protein superfamily. Int J Biol Macromol 22:151–162

Del Bigio MR, Chudley AE, Sarnat HB, Campbell C, Goobie S, Chodirker BN, Selcen D (2011) Infantile muscular dystrophy in Canadian aboriginals is an alphaB-crystallinopathy. Ann Neurol 69(5):866–871. doi:10.1002/ana.22331

Delbecq SP, Jehle S, Klevit R (2012) Binding determinants of the small heat shock protein, alphaB-crystallin: recognition of the 'IxI' motif. EMBO J 31(24):4587–4594. doi:10.1038/emboj.2012.318

den Engelsman J, Keijsers V, de Jong WW, Boelens WC (2003) The small heat-shock protein alpha B-crystallin promotes FBX4-dependent ubiquitination. J Biol Chem 278(7):4699–4704. doi:10.1074/jbc.M211403200

den Engelsman J, Gerrits D, de Jong WW, Robbins J, Kato K, Boelens WC (2005) Nuclear import of {alpha}B-crystallin is phosphorylation-dependent and hampered by hyperphosphorylation of the myopathy-related mutant R120G. J Biol Chem 280(44):37139–37148. doi:10.1074/jbc.M504106200

Dubin RA, Wawrousek EF, Piatigorsky J (1989) Expression of the murine alpha B-crystallin gene is not restricted to the lens. Mol Cell Biol 9(3):1083–1091. doi:10.1128/mcb.9.3.1083

Ebert AD, Liang P, Wu JC (2012) Induced pluripotent stem cells as a disease modeling and drug screening platform. J Cardiovasc Pharmacol 60(4):408–416. doi:10.1097/FJC.0b013e318247f642

Ecroyd H, Meehan S, Horwitz J, Aquilina JA, Benesch JL, Robinson CV, Macphee CE, Carver JA (2007) Mimicking phosphorylation of alphaB-crystallin affects its chaperone activity. Biochem J 401(1):129–141. doi:10.1042/BJ20060981

Ellis RJ, van der Vies SM (1991) Molecular chaperones. Annu Rev Biochem 60(1):321–347. doi:10.1146/annurev.bi.60.070191.001541

Fardeau M, Godet-Guillain J, Tome FM, Collin H, Gaudeau S, Boffety C, Vernant P (1978) Une nouvelle affection musculaire familiale définie par l'accumulation intra-sarcoplasmique d'un matériel granulofilamentaire dense en microscopie electronique. [A new familial muscular disorder demonstrated by the intra-sarcoplasmic accumulation of a granulo-filamentous material which is dense on electron microscopy (author's transl)]. Rev Neurol (Paris) 134:411–425

Feil IK, Malfois M, Hendle J, van Der Zandt H, Svergun DI (2001) A novel quaternary structure of the dimeric alpha-crystallin domain with chaperone-like activity. J Biol Chem 276(15):12024–12029. doi:10.1074/jbc.M010856200

Fong H, Wang C, Knoferle J, Walker D, Balestra ME, Tong LM, Leung L, Ring KL, Seeley WW, Karydas A, Kshirsagar MA, Boxer AL, Kosik KS, Miller BL, Huang Y (2013) Genetic correction of tauopathy phenotypes in neurons derived from human induced pluripotent stem cells. Stem Cell Rep 1(3):226–234. doi:10.1016/j.stemcr.2013.08.001

Forrest KM, Al-Sarraj S, Sewry C, Buk S, Tan SV, Pitt M, Durward A, McDougall M, Irving M, Hanna MG, Matthews E, Sarkozy A, Hudson J, Barresi R, Bushby K, Jungbluth H, Wraige E (2011) Infantile onset myofibrillar myopathy due to recessive CRYAB mutations. Neuromuscul Disord 21(1):37–40. doi:10.1016/j.nmd.2010.11.003

Friden J, Lieber RL (2001) Eccentric exercise-induced injuries to contractile and cytoskeletal muscle fibre components. Acta Physiol Scand 171:321–326

Garcia-Mata R, Gao Y, Sztul E (2002) Hassles with taking out the garbage: aggravating aggresomes. Traffic 3:388–396

Ghosh JG, Estrada MR, Clark JI (2006) Structure-based analysis of the beta8 interactive sequence of human alphaB crystallin. Biochemistry 45:9878–9886

Ghosh JG, Houck SA, Clark JI (2007a) Interactive sequences in the stress protein and molecular chaperone human alphaB crystallin recognize and modulate the assembly of filaments. Int J Biochem Cell Biol 39(10):1804–1815. doi:10.1016/j.biocel.2007.04.027

Ghosh JG, Shenoy AK, Clark JI (2007b) Interactions between important regulatory proteins and human alphaB crystallin. Biochemistry 46:6308–6317

Golenhofen N, Htun P, Ness W, Koob R, Schaper W, Drenckhahn D (1999) Binding of stress protein cryab to cardiac myofibrils correlates with the degree of myocardial damage during I/R in vivo. J Mol Cell Cardiol 31:569–580

Golenhofen N, Arbeiter A, Koob R, Drenckhahn D (2002) Ischemia-induced association of the stress protein alpha B-crystallin with I-band portion of cardiac titin. J Mol Cell Cardiol 34(3):309–319. doi:10.1006/jmcc.2001.1513

Golenhofen N, Perng MD, Quinlan RA, Drenckhahn D (2004) Comparison of the small heat shock proteins alphaB-crystallin, MKBP, HSP25, HSP20, and cvHSP in heart and skeletal muscle. Histochem Cell Biol 122(5):415–425. doi:10.1007/s00418-004-0711-z

Golenhofen N, Redel A, Wawrousek EF, Drenckhahn D (2006) Ischemia-induced increase of stiffness of alphaB-crystallin/HSPB2-deficient myocardium. Pflugers Arch 451(4):518–525. doi:10.1007/s00424-005-1488-1

Gopal-Srivastava R, Piatigorsky J (1993) The murine alpha B-crystallin/small heat shock protein enhancer: identification of alpha BE-1, alpha BE-2, alpha BE-3 and MRF control elements. Mol Cell Biol 13(11):7144–7152

Gopal-Srivastava R, Haynes JI II, Piatigorsky J (1995) Regulation of the murine aB-crystallin/small heath shock protein gene in cardiac muscle. Mol Cell Biol 15(12):7081–7090

Hayes VH, Devlin G, Quinlan RA (2008) Truncation of alphaB-crystallin by the myopathy-causing Q151X mutation significantly destabilizes the protein leading to aggregate formation in transfected cells. J Biol Chem 283(16):10500–10512. doi:10.1074/jbc.M706453200

Hishiya A, Salman MN, Carra S, Kampinga HH, Takayama S (2011) BAG3 directly interacts with mutated alphaB-crystallin to suppress its aggregation and toxicity. PLoS ONE 6(3):e16828. doi:10.1371/journal.pone.0016828

Horwitz J (1992) a-Crystallin can function as a molecular chaperone. Proc Natl Acad Sci U S A 89:10449–10453

Hosoyama T, McGivern JV, Van Dyke JM, Ebert AD, Suzuki M (2014) Derivation of myogenic progenitors directly from human pluripotent stem cells using a sphere-based culture. Stem Cells Transl Med. doi:10.5966/sctm.2013-0143

Houck SA, Landsbury A, Clark JI, Quinlan RA (2011) Multiple sites in alphaB-crystallin modulate its interaction with desmin filaments assembled in vitro. PLoS ONE 6(11):e25859. doi:10.1371/journal.pone.0025859.g001

Hu WF, Gong L, Cao Z, Ma H, Ji W, Deng M, Liu M, Hu XH, Chen P, Yan Q, Chen HG, Liu J, Sun S, Zhang L, Liu JP, Wawrousek E, Li DW (2012) αA- and αB-crystallins interact with caspase-3 and Bax to guard mouse lens development. Curr Mol Med 12(2):177–187

Ignolia TD, Craig EA (1982) Four small Drosophila heat shock proteins are related to each other and to mammalian alpha crystallin. Proc Natl Acad Sci U S A 79:2360–2364

Inagaki N, Hayashi T, Arimura T, Koga Y, Takahashi M, Shibata H, Teraoka K, Chikamori T, Yamashina A, Kimura A (2006) Alpha B-crystallin mutation in dilated cardiomyopathy. Biochem Biophys Res Commun 342(2):379–386. doi:10.1016/j.bbrc.2006.01.154

Ishiwata T, Orosz A, Wang X, Mustafi SB, Pratt GW, Christians ES, Boudina S, Abel ED, Benjamin IJ (2012) HSPB2 is dispensable for the cardiac hypertrophic response but reduces mitochondrial energetics following pressure overload in mice. PLoS one 7(8):e42118. doi:10.1371/journal.pone.0042118

Ito H, Okamoto K, Nakayama H, Isobe T, Kato K (1997) Phosphorylation of alphaB-crystallin in response to various types of stress. J Biol Chem 272:29934–29941

Itzhaki I, Maizels L, Huber I, Zwi-Dantsis L, Caspi O, Winterstern A, Feldman O, Gepstein A, Arbel G, Hammerman H, Boulos M, Gepstein L (2011) Modelling the long QT syndrome with induced pluripotent stem cells. Nature 471(7337):225–229. doi:10.1038/nature09747

Iwaki T, Kume-Iwaki A, Goldman JE (1990) Cellular distribution of alpha B-crystallin in non-lenticular tissues. J Histochem Cytochem 38(1):31–39. doi:10.1177/38.1.2294148

Jansen G, Groenen PJTA, Bachner D, Jap PHK, Coerwinkel M, Oerlemans F, van den Broek W, Gohlsch B, Pette D, Plomp JJ, Molenaar PC, Nederhoff MGJ, van Echteld CJA, Dekker M, Berns A, Hameister H, Wieringa B (1996) Abnormal myotonic dystrophy protein kinase levels produce only mild myopathy in mice. Nat Genet 13:316–324

Jehle S, Rajagopal P, Bardiaux B, Markovic S, Kuhne R, Stout JR, Higman VA, Klevit RE, van Rossum BJ, Oschkinat H (2010) Solid-state NMR and SAXS studies provide a structural basis for the activation of alphaB-crystallin oligomers. Nat Struct Mol Biol 17(9):1037–1042. doi:10.1038/nsmb.1891

Kamradt MC, Chen F, Cryns VL (2001) The small heat shock protein alpha B-crystallin negatively regulates cytochrome c- and caspase-8-dependent activation of caspase-3 by inhibiting its autoproteolytic maturation. J Biol Chem 276(19):16059–16063. doi:10.1074/jbc.C100107200

Kamradt MC, Chen F, Sam S, Cryns VL (2002) The small heat shock protein alpha B-crystallin negatively regulates apoptosis during myogenic differentiation by inhibiting caspase-3 activation. J Biol Chem 277(41):38731–38736. doi:10.1074/jbc.M201770200

Kappé G, Leunissen JM, Jong W (2002) Evolution and diversity of prokaryotic small heat shock proteins. In: Arrigo A-P, Müller WEG (eds) Small stress proteins, vol 28, Progress in molecular and subcellular biology. Springer, Berlin/Heidelberg, pp 1–17. doi:10.1007/978-3-642-56348-5_1

Kato K, Ito H, Kamei K, Inaguma Y, Iwamoto I, Saga S (1998) Phosphorylation of αB-crystallin in mitotic cells and identification of enzymatic activities responsible for phosphorylation. J Biol Chem 273:28346–28354

Koh TJ (2002) Do small heat shock proteins protect skeletal muscle from injury. Exerc Sports Sci Rev 30(3):117–121

Koh TJ, Escobedo J (2004) Cytoskeletal disruption and small heat shock protein translocation immediately after lengthening contractions. Am J Physiol Cell Physiol 286(3):C713–C722. doi:10.1152/ajpcell.00341.2003

Komulainen J, Takala TES, Kuipers H, Hesselink MKC (1998) The disruption of myofibre structures in rat skeletal muscle after forced lengthening contractions. Eur J Physiol 436:735–741

Kostek MC, Chen YW, Cuthbertson DJ, Shi R, Fedele MJ, Esser KA, Rennie MJ (2007) Gene expression responses over 24 h to lengthening and shortening contractions in human muscle: major changes in CSRP3, MUSTN1, SIX1, and FBXO32. Physiol Genomics 31:42–52. doi:10.1152/physiolgenomics.00151.2006.-Resistance

Kotter S, Unger A, Hamdani N, Lang P, Vorgerd M, Nagel-Steger L, Linke WA (2014) Human myocytes are protected from titin aggregation-induced stiffening by small heat shock proteins. J Cell Biol 204(2):187–202. doi:10.1083/jcb.201306077

Krishnamoorthy V, Donofrio AJ, Martin JL (2013) O-GlcNAcylation of alphaB-crystallin regulates its stress-induced translocation and cytoprotection. Mol Cell Biochem 379(1–2):59–68. doi:10.1007/s11010-013-1627-5

Kumarapeli AR, Su H, Huang W, Tang M, Zheng H, Horak KM, Li M, Wang X (2008) Alpha B-crystallin suppresses pressure overload cardiac hypertrophy. Circ Res 103(12):1473–1482. doi:10.1161/CIRCRESAHA.108.180117

Labeit S, Kolmerer B (1995) Titins: giant proteins in charge of muscle ultrastructure and elasticity. Science 270:293–296

Laganowsky A, Benesch JL, Landau M, Ding L, Sawaya MR, Cascio D, Huang Q, Robinson CV, Horwitz J, Eisenberg D (2010) Crystal structures of truncated alphaA and alphaB crystallins reveal structural mechanisms of polydispersity important for eye lens function. Protein Sci 19(5):1031–1043. doi:10.1002/pro.380

Le Grand F, Rudnicki MA (2007) Skeletal muscle satellite cells and adult myogenesis. Curr Opin Cell Biol 19(6):628–633. doi:10.1016/j.ceb.2007.09.012

Li DW, Liu JP, Mao YW, Xiang H, Wang J, Ma WY, Dong Z, Pike HM, Brown RE, Reed JC (2005) Calcium-activated RAF/MEK/ERK signaling pathway mediates p53-dependent apoptosis and is abrogated by alpha B-crystallin through inhibition of RAS activation. Mol Biol Cell 16(9):4437–4453. doi:10.1091/mbc.E05-01-0010

Lian X, Zhang J, Azarin SM, Zhu K, Hazeltine LB, Bao X, Hsiao C, Kamp TJ, Palecek SP (2013) Directed cardiomyocyte differentiation from human pluripotent stem cells by modulating Wnt/beta-catenin signaling under fully defined conditions. Nat Protoc 8(1):162–175. doi:10.1038/nprot.2012.150

Liang P, MacRae TH (1997) Molecular chaperones and the cytoskeleton. J Cell Sci 110:1431–1440

Limphong P, Zhang H, Christians E, Liu Q, Riedel M, Ivey K, Cheng P, Mitzelfelt K, Taylor G, Winge D, Srivastava D, Benjamin I (2013) Modeling human protein aggregation cardiomyopathy using murine induced pluripotent stem cells. Stem Cells Transl Med 2(3):161–166. doi:10.5966/sctm. 2012-0073

Linke WA (2008) Sense and stretchability: the role of titin and titin-associated proteins in myocardial stress-sensing and mechanical dysfunction. Cardiovasc Res 77(4):637–648. doi:10.1016/j.cardiores.2007.03.029

Liu JP, Schlosser R, Ma WY, Dong Z, Feng H, Liu L, Huang XQ, Liu Y, Li DW (2004) Human alphaA- and alphaB-crystallins prevent UVA-induced apoptosis through regulation of PKCalpha, RAF/MEK/ERK and AKT signaling pathways. Exp Eye Res 79(3):393–403. doi:10.1016/j.exer.2004.06.015

Liu S, Li J, Tao Y, Xiao X (2007) Small heat shock protein alphaB-crystallin binds to p53 to sequester its translocation to mitochondria during hydrogen peroxide-induced apoptosis. Biochem Biophys Res Commun 354(1):109–114. doi:10.1016/j.bbrc.2006.12.152

Lockard VG, Bloom S (1993) Trans-cellular desmin-lamin B intermediate filament network in cardiac myocytes. J Mol Cell Cardiol 25:303–309

Lutsch G, Vetter R, Offhauss U, Wieske M, Gröne H-J, Klemenz R, Schimke I, Stahl J, Benndorf R (1997) Abundance and location of the small heat shock proteins HSP25 and αB-crystallin in rat and human heart. Circulation 96:3466–3476

Maloyan A, Sanbe A, Osinska H, Westfall M, Robinson D, Imahashi K, Murphy E, Robbins J (2005) Mitochondrial dysfunction and apoptosis underlie the pathogenic process in alpha-B-crystallin desmin-related cardiomyopathy. Circulation 112(22):3451–3461. doi:10.1161/CIRCULATIONAHA.105.572552

Maloyan A, Gulick J, Glabe CG, Kayed R, Robbins J (2007) Exercise reverses preamyloid oligomer and prolongs survival in alphaB-crystallin-based desmin-related cardiomyopathy. Proc Natl Acad Sci U S A 104(14):5995–6000. doi:10.1073/pnas.0609202104

Maloyan A, Osinska H, Lammerding J, Lee RT, Cingolani OH, Kass DA, Lorenz JN, Robbins J (2009) Biochemical and mechanical dysfunction in a mouse model of desmin-related myopathy. Circ Res 104(8):1021–1028. doi:10.1161/CIRCRESAHA.108.193516

Mao YW, Liu JP, Xiang H, Li DW (2004) Human alphaA- and alphaB-crystallins bind to Bax and Bcl-X(S) to sequester their translocation during staurosporine-induced apoptosis. Cell Death Differ 11(5):512–526. doi:10.1038/sj.cdd.4401384

Martin JL, Mestril R, Hilal-Dandan R, Brunton LL, Dillmann WH (1997) Small heat shock proteins and protection against ischemic injury in cardiac myocytes. Circulation 96:4343–4348

Melkani GC, Cammarato A, Bernstein SI (2006) AlphaB-crystallin maintains skeletal muscle myosin enzymatic activity and prevents its aggregation under heat-shock stress. J Mol Biol 358(3):635–645. doi:10.1016/j.jmb.2006.02.043

Mercola M, Ruiz-Lozano P, Schneider MD (2011) Cardiac muscle regeneration: lessons from development. Genes Dev 25(4):299–309. doi:10.1101/gad.2018411

Milner D, Mavroidis M, Weisleder N, Capetanaki Y (2000) Desmin cytoskeleton linked to muscle mitochondrial distribution and respiratory function. J Cell Biol 150(6):1283–1297

Minajeva A, Kulke M, Fernandez JM, Linke WA (2001) Unfolding of titin domains explains the viscoelastic behavior of skeletal myofibrils. Biophys J 80:1442–1451

Mitra A, Basak T, Datta K, Naskar S, Sengupta S, Sarkar S (2013) Role of alpha-crystallin B as a regulatory switch in modulating cardiomyocyte apoptosis by mitochondria or endoplasmic reticulum during cardiac hypertrophy and myocardial infarction. Cell Death Dis 4:e582. doi:10.1038/cddis.2013.114

Morimoto RI (1998) Regulation of the heat shock transcriptional response: cross talk between a family of heat shock factors, molecular chaperones, and negative regulators. Genes Dev 12(24):3788–3796. doi:10.1101/gad.12.24.3788

Morner CT (1894) Untersuchung der Proteinsubstanzen in den lichtbrechenden Medien des Auges (Examination of the protein-substances in the refractory media of the eye). Hoppe Seyler's Z Physiol Chem 18(61):106

Morrison LE, Hoover HE, Thuerauf DJ, Glembotski CC (2003) Mimicking phosphorylation of alphaB-crystallin on serine-59 is necessary and sufficient to provide maximal protection of cardiac myocytes from apoptosis. Circ Res 92(2):203–211. doi:10.1161/01.res.0000052989.83995.a5

Morrison LE, Whittaker RJ, Klepper RE, Wawrousek EF, Glembotski CC (2004) Roles for αB-crystallin and HSPB2 in protecting the myocardium from ischemia-reperfusion-induced damage in a KO mouse model. Am J Physiol Heart Circ Physiol 286:H847–H855

Mymrikov EV, Seit-Nebi AS, Gusev NB (2011) Large potentials of small heat shock proteins. Physiol Rev 91:1123–1159. doi:10.1152/physrev.00023.2010.-Modern

Neppl RL, Kataoka M, Wang DZ (2014) Crystallin-alphaB regulates skeletal muscle homeostasis via modulation of argonaute2 activity. J Biol Chem 289(24):17240–17248. doi:10.1074/jbc.M114.549584

Neufer PD, Benjamin IJ (1996) Differential expression of alpha B-crystallin and Hsp27 in skeletal muscle during continuous contractile activity. Relationship to myogenic regulatory factors. J Biol Chem 271(39):24089–24095. doi:10.1074/jbc.271.39.24089

Ogata T, Yamaksak Y (1997) Ultra-high-resolution scanning electron microscopy of mitochondria and sarcoplasmic reticulum arrangement in human red, white, and intermediate muscle fibers. Anat Rec 248:214–223

Paulsen G, Vissing K, Kalhovde JM, Ugelstad I, Bayer ML, Kadi F, Schjerling P, Hallen J, Raastad T (2007) Maximal eccentric exercise induces a rapid accumulation of small heat shock proteins on myofibrils and a delayed HSP70 response in humans. Am J Physiol Regul Integr Comp Physiol 293:R844–R853. doi:10.1152/ajpregu.00677.2006.-In

Perng MD, Cairns L, Vandenijssel P, Prescott A, Hutcheson AM, Quinlan RA (1999a) Intermediate filament interactions can be altered by HSP27 and alphaB-crystallin. J Cell Sci 112:2099–2112

Perng MD, Muchowski PJ, Vandenijssel P, Wu JS, Hutcheson AM, Clark JI, Quinlan RA (1999b) The cardiomyopathy and lens cataract mutation in alphaB-crystalln alters its protein structure, chaperone activity, and interaction with intermediate filaments in vitro. J Biol Chem 274:33235–33243

Perng MD, Wen SF, van den IP, Prescott AR, Quinlan RA (2004) Desmin aggregate formation by R120G alphaB-crystallin is caused by altered filament interactions and is dependent upon network status in cells. Mol Biol Cell 15(5):2335–2346. doi:10.1091/mbc.E03-12-0893

Peschek J, Braun N, Rohrberg J, Back KC, Kriehuber T, Kastenmüller A, Weinkauf S, Buchner J (2013) Regulated structural transitions unleash the chaperone activity of alphaB-crystallin. Proc Natl Acad Sci U S A 110(40):E3780–E3789

Pilotto A, Marziliano N, Pasotti M, Grasso M, Costante AM, Arbustini E (2006) AlphaB-crystallin mutation in dilated cardiomyopathies: low prevalence in a consecutive series of 200 unrelated probands. Biochem Biophys Res Commun 346(4):1115–1117. doi:10.1016/j.bbrc.2006.05.203

Pinz I, Robbins J, Rajasekaran NS, Benjamin IJ, Ingwall JS (2008) Unmasking different mechanical and energetic roles for the small heat shock proteins CryAB and HSPB2 using genetically modified mouse hearts. FASEB J 22(1):84–92. doi:10.1096/fj.07-8130com

Plater ML, Goode D, Crabbe MJC (1996) Effects of site-directed mutations on the chaperone-like activity of alphaB-crystallin. J Biol Chem 271(45):28558–28566

Rajaraman K, Raman B, Ramakrishna T, Rao Ch M (2001) Interaction of human recombinant alphaA- and alphaB-crystallins with early and late unfolding intermediates of citrate synthase on its thermal denaturation. FEBS Lett 497:118–123

Rajasekaran NS, Connell P, Christians ES, Yan LJ, Taylor RP, Orosz A, Zhang XQ, Stevenson TJ, Peshock RM, Leopold JA, Barry WH, Loscalzo J, Odelberg SJ, Benjamin IJ (2007) Human alpha B-crystallin mutation causes oxido-reductive stress and protein aggregation cardiomyopathy in mice. Cell 130(3):427–439. doi:10.1016/j.cell.2007.06.044

Raju I, Abraham EC (2013) Mutants of human alphaB-crystallin cause enhanced protein aggregation and apoptosis in mammalian cells: influence of co-expression of HspB1. Biochem Biophys Res Commun 430(1):107–112. doi:10.1016/j.bbrc.2012.11.051

Rambourg A, Segretain D (1980) Three-dimensional electron microscopy of mitochondria and endoplasmic reticulum in the red muscle fiber of the rat diaphragm. Anat Rec 197(1):33–48

Rappaport L, Contard F, Samuel JL, Delcayre C, Marotte F, Tome F, Fardeau M (1988) Storage of phosphorylated desmin in a familial myopathy. FEBS Lett 231(2):421–425

Rappaport L, Oliviero P, Samuel JL (1998) Cytoskeleton and mitochondrial morphology and function. Mol Cell Biochem 184:101–105

Ray PS, Martin JL, Swanson EA, Otani H, Dillmann WH, Das DK (2001) Transgene overexpression of aB crystallin confers simultaneous protection against cardiomyocyte apoptosis and necrosis during myocardial ischemia and reperfusion. FASEB J 15:393–402

Reddy S, Smith DBJ, Rich MM, Leferovich JM, Reilly P, Davis BM, Tran K, Rayburn H, Bronson R, Cros D, Balice-Gordon RJ, Housman D (1996) Mice lacking the myotonic dystrophy protein kinase develop a late onset progressive myopathy. Nat Genet 13:325–335

Reilich P, Schoser B, Schramm N, Krause S, Schessl J, Kress W, Muller-Hocker J, Walter MC, Lochmuller H (2010) The p.G154S mutation of the alpha-B crystallin gene (CRYAB) causes late-onset distal myopathy. Neuromuscul Disord 20(4):255–259. doi:10.1016/j.nmd.2010.01.012

Reipert S, Steinbock F, Fischer I, Bittner RE, Zeold A, Wiche G (1999) Association of mitochondria with plectin and desmin intermediate filaments in striated muscle. Exp Cell Res 252:479–491

Rief M (1997) Reversible unfolding of individual titin immunoglobulin domains by AFM. Science 276(5315):1109–1112. doi:10.1126/science.276.5315.1109

Robinton DA, Daley GQ (2012) The promise of induced pluripotent stem cells in research and therapy. Nature 481(7381):295–305. doi:10.1038/nature10761

Sacconi S, Feasson L, Antoine JC, Pecheux C, Bernard R, Cobo AM, Casarin A, Salviati L, Desnuelle C, Urtizberea A (2012) A novel CRYAB mutation resulting in multisystemic disease. Neuromuscul Dis 22(1):66–72. doi:10.1016/j.nmd.2011.07.004

Sanbe A, Osinska H, Saffitz JE, Glabe CG, Kayed R, Maloyan A, Robbins J (2004) Desmin-related cardiomyopathy in transgenic mice: a cardiac amyloidosis. Proc Natl Acad Sci U S A 101(27):10132–10136. doi:10.1073/pnas.0401900101

Sanbe A, Yamauchi J, Miyamoto Y, Fujiwara Y, Murabe M, Tanoue A (2007) Interruption of CryAB-amyloid oligomer formation by HSP22. J Biol Chem 282(1):555–563. doi:10.1074/jbc.M605481200

Sanbe A, Daicho T, Mizutani R, Endo T, Miyauchi N, Yamauchi J, Tanonaka K, Glabe C, Tanoue A (2009) Protective effect of geranylgeranylacetone via enhancement of HSPB8 induction in desmin-related cardiomyopathy. PLoS one 4(4):e5351. doi:10.1371/journal.pone.0005351

Sanbe A, Marunouchi T, Yamauchi J, Tanonaka K, Nishigori H, Tanoue A (2011) Cardioprotective effect of nicorandil, a mitochondrial ATP-sensitive potassium channel opener, prolongs survival in HSPB5 R120G transgenic mice. PLoS one 6(4):e18922. doi:10.1371/journal.pone.0018922

Selcen D (2011) Myofibrillar myopathies. Neuromuscular Dis NMD 21(3):161–171. doi:10.1016/j.nmd.2010.12.007

Selcen D, Engel AG (2003) Myofibrillar myopathy caused by novel dominant negative cryAB mutations. Ann Neurol 54(6):804–810

Singh BN, Rao KS, Rao Ch M (2010) Ubiquitin-proteasome-mediated degradation and synthesis of MyoD is modulated by alphaB-crystallin, a small heat shock protein, during muscle differentiation. Biochim Biophys Acta 1803(2):288–299. doi:10.1016/j.bbamcr.2009.11.009

Smirnova E, Chebotareva N, Gurvits B (2013) Transient transformation of oligomeric structure of alpha-crystallin during its chaperone action. Int J Biol Macromol 55:62–68. doi:10.1016/j.ijbiomac.2012.12.013

Spector DL, Lamond AI (2011) Nuclear speckles. Cold Spring Harb Perspect Biol 3(2):1–12. a000646. doi:10.1101/cshperspect.a000646

Suzuki A, Sugiyama Y, Hayashi Y, Nyu-i N, Yoshida M, Nonaka I, Ishiura S, Arahata K, Ohno S (1998) MKBP, a novel member of the small heat shock protein family, binds and activates the myotonic dystrophy protein kinase. J Cell Biol 140:1113–1124

Takahashi, Yamanaka (2006) Induction of pluripotent stem cells from mouse embryonic and adult fibroblast cultures by defined factors. Cell 126(4):663–676

Tannous P, Zhu H, Johnstone JL, Shelton JM, Rajasekaran NS, Benjamin IJ, Nguyen L, Gerard RD, Levine B, Rothermel BA, Hill JA (2008) Autophagy is an adaptive response in desmin-related cardiomyopathy. Proc Natl Acad Sci U S A 105(28):9745–9750. doi:10.1073/pnas.0706802105

Taylor RP, Benjamin IJ (2005) Small heat shock proteins: a new classification scheme in mammals. J Mol Cell Cardiol 38(3):433–444. doi:10.1016/j.yjmcc.2004.12.014

Thompson HS, Scordilis SP, Clarkson PM, Lohrer WA (2001) A single bout of eccentric exercise increases Hsp27 and HSC/HSP70 in human skeletal muscle. Acta Physiol Scand 171:187–193

Vandenijssel P, Wheelock R, Prescott A, Russell P, Quinlan R (2003) Nuclear speckle localisation of the small heat shock protein alphaB-crystallin and its inhibition by the R120G cardiomyopathy-linked mutation. Exp Cell Res 287(2):249–261. doi:10.1016/s0014-4827(03)00092-2

Vicart CA, Guicheney P, Li Z, Prévost MC, Faure A, Chateau D, Chapon F, Tomé F, Dupret JM, Paulin D, Fardeau M (1998) A missense mutation in the alphaB-crystallin chaperone gene causes a desmin-related myopathy. Nat Genet 20(1):92–95

Wang X, Osinska H, Klevitsky R, Gerdes AM, Nieman M, Lorenz J, Hewett T, Robbins J (2001) Expression of R120G- B-crystallin causes aberrant desmin and B-crystallin aggregation and cardiomyopathy in mice. Circ Res 89(1):84–91. doi:10.1161/hh1301.092688

Watanabe G, Kato S, Nakata H, Ishida T, Ohuchi N, Ishioka C (2009) alphaB-crystallin: a novel p53-target gene required for p53-dependent apoptosis. Cancer Sci 100(12):2368–2375. doi:10.1111/j.1349-7006.2009.01316.x

Weintraub H (1993) The MyoD family and myogenesis- redundancy, networks, and thresholds. Cell 75:1241–1244

Whittaker R, Gude GN, Sussman MA, Gottlieb RA, Glembotski CC (2009) Kinetics of the translocation and phosphorylation of alphaB-crystallin in mouse heart mitochondria during ex vivo ischemia. Am J Physiol Heart Circ Physiol 296:H1633–H1642. doi:10.1152/ajpheart.01227.2008.-/Bcrystallin

Yan LJ, Christians EC, Liu L, Xiao X, Sohal RS, Benjamin IJ (2002) Mouse heat shock transcription factor 1 deficiency alters cardiac redox homeostasis and increases mitochondrial oxidative damage. EMBO J 21(19):5164–5172

Yusa K, Rashid ST, Strick-Marchand H, Varela I, Liu PQ, Paschon DE, Miranda E, Ordonez A, Hannan NR, Rouhani FJ, Darche S, Alexander G, Marciniak SJ, Fusaki N, Hasegawa M, Holmes MC, Di Santo JP, Lomas DA, Bradley A, Vallier L (2011) Targeted gene correction of alpha1-antitrypsin deficiency in induced pluripotent stem cells. Nature 478(7369):391–394. doi:10.1038/nature10424

Zhang H, Rajasekaran NS, Orosz A, Xiao X, Rechsteiner M, Benjamin IJ (2010) Selective degradation of aggregate-prone CryAB mutants by HSPB1 is mediated by ubiquitin-proteasome pathways. J Mol Cell Cardiol 49(6):918–930. doi:10.1016/j.yjmcc.2010.09.004

Zhang J, Klos M, Wilson GF, Herman AM, Lian X, Raval KK, Barron MR, Hou L, Soerens AG, Yu J, Palecek SP, Lyons GE, Thomson JA, Herron TJ, Jalife J, Kamp TJ (2012)

Extracellular matrix promotes highly efficient cardiac differentiation of human pluripotent stem cells: the matrix sandwich method. Circ Res 111(9):1125–1136. doi:10.1161/CIRCRESAHA.112.273144

Zhou T, Benda C, Dunzinger S, Huang Y, Ho JC, Yang J, Wang Y, Zhang Y, Zhuang Q, Li Y, Bao X, Tse HF, Grillari J, Grillari-Voglauer R, Pei D, Esteban MA (2012) Generation of human induced pluripotent stem cells from urine samples. Nat Protoc 7(12):2080–2089. doi:10.1038/nprot.2012.115

Zhu Y, Bogomolovas J, Labeit S, Granzier H (2009) Single molecule force spectroscopy of the cardiac titin N2B element: effects of the molecular chaperone alphaB-crystallin with disease-causing mutations. J Biol Chem 284(20):13914–13923. doi:10.1074/jbc.M809743200

CHAPTER 2

INTRODUCTION ADDENDUM: INDUCED PLURIPOTENT STEM CELLS AND GENOME EDITING

Two major technological advances in the last ten years have revolutionized the ability for researchers to study disease *in vitro* using human cells while simultaneously accelerating and expanding the prospects of transplantation therapy (Figure 2.1). The first advance being the advent of induced pluripotent stem cells (iPSCs) by the lab of 2012 Nobel Prize winner, Shinya Yamanaka (Takahashi and Yamanaka, 2006), providing the ability to generate patient-specific pluripotent stem cells from somatic cells. The second, concurrent advance is the vast improvements in the efficiency of genome editing allowing specific, user-defined modification of the genome. Both advances have surpassed critical hurdles quickly bringing the use of this system into everyday practice for a multitude of laboratories. As alluded to in the Introduction (Chapter 1), iPSCs offer utility in the study of mutations in αB-crystallin (or HSPB5). Indeed, among the many diseases studied exploiting iPSCs to date (Tiscornia et al., 2011), the Benjamin Laboratory has generated both murine and human iPSC model systems for the study of mutant forms of HSPB5 (Limphong et al., 2013; Mitzelfelt et al., 2016) (Chapter 3). This chapter acts as an addendum to the introduction (Chapter 1) providing background information with regards to iPSCs and genome editing.

Embryonic Stem Cells: A Brief History

Mouse embryonic stem cells (mESCs), derived from the inner cell mass of the blastocyst, were first isolated 35 years ago (Evans and Kaufman, 1981; Martin, 1981). A similar feat for

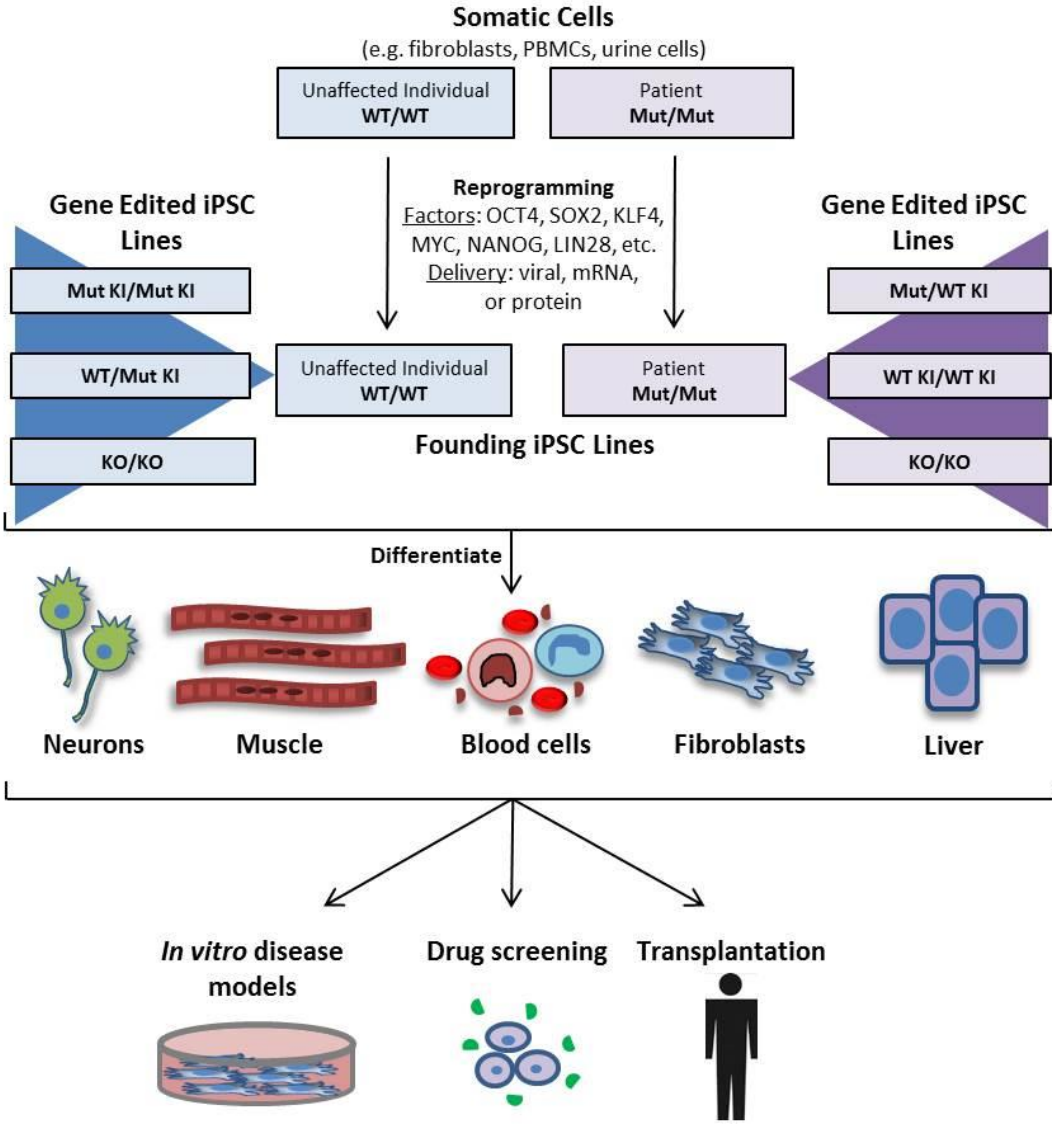

Figure 2.1 Schematic representation of combined iPSC and genome editing applications. Somatic cells (e.g., fibroblasts, peripheral blood mononuclear cells (PBMCs), cells isolated from urine, etc.) from patients with a mutation (Mut) or unaffected individuals with a wildtype locus (WT) can be reprogrammed into iPSCs using reprogramming factors (e.g., OCT4, SOX2, KLF4, MYC, NANOG, LIN28) through delivery methods such as virus, mRNA, or protein for generating founding iPSC lines. Genome editing can be performed on founding iPSC lines to generate knock-in (KI) cell lines in either direction (from WT to Mut or from Mut to WT) by inserting or correcting the mutation of interest to generate isogenic cell lines differing only at a specified location. Additionally, knockout (KO) of a gene of interest can also be performed. Differentiation of founding and gene edited iPSC lines into cell types of interest (e.g., neurons, muscle, blood cells, fibroblasts, liver cells, etc.) provides a platform for *in vitro* disease modeling, drug screening, and therapeutic transplantation studies.

human ESCs (hESCs) was not accomplished until 17 years later (Thomson et al., 1998). The defining characteristics of mammalian ESCs, unlimited self-renewal and pluripotency, made them uniquely attractive as a model for early development. Technology to modify the genome of mESCs (discussed in Section: Homologous Recombination) was later devised and utilized for generating genetically altered mice by research from Mario Capecchi, Martin Evans, and Oliver Smithies (Doetschman et al., 1987; Kuehn et al., 1987; Thomas and Capecchi, 1987), revolutionizing scientific approaches for understanding biological function.

Most existing hESCs for experimentation, including the widely used H1 and H9 lines (Thomson et al., 1998), were derived from donated *in vitro* fertilized (IVF) embryos. The idea of "therapeutic cloning" as a strategy for cell therapy involved the generation of "designer" ESCs through somatic cell nuclear transfer (SCNT). SCNT, initially described by John Gurdon in tadpoles in 1962, involves the removal of the nucleus from an oocyte and its replacement with a donor nucleus derived from a somatic cell; therefore the genetic material (except the mitochondrial DNA) of the resulting oocyte comes entirely from the donor nucleus (Gurdon, 1962). Gurdon later shared the Nobel Prize in Physiology or Medicine with Yamanaka in 2012, for the discovery that mature cells can be reprogrammed into pluripotent cells. Unlike reproductive cloning, in which the nuclear transfer oocyte develops into a new organism (e.g., Gurdon's original experiments (Gurdon, 1962) and the infamous "Dolly" the sheep (Campbell et al., 1996)), the goal of therapeutic cloning is to derive ESCs from the nuclear transfer embryo, which may be used as therapeutic cell replacement to treat disease. Indeed, a hallmark paper in 2002 demonstrated the utility of combining therapeutic cloning and gene editing for the treatment of genetic disorders in mice (Rideout III et al., 2002). Several years later, therapeutic cloning was also accomplished with human cells (Tachibana et al., 2013; Yamada et al., 2014). Patient-specific ESCs derived from SCNT contain the patient's nuclear DNA and would, therefore, reduce the risk of rejection upon transplantation.

The advances with hESCs have not been accompanied without debates about the ethical,

regulatory, and societal issues involving human cloning (Wert and Mummery, 2003). Whereas there are guidelines and restrictions for the uses of existing hESCs allowed in federally funded biomedical research, what purposes they may be used has come into question with varying degrees of acceptance world-wide and continuing changes in national policies. The advent of iPSCs, as discussed below, has largely ameliorated but not totally resolved these issues.

Induced Pluripotent Stem Cells (iPSCs)

Discovery

As discussed above, the ethical and regulatory issues accompanying hESC research have curtailed progress especially for investigations into cell replacement therapy for degenerative diseases and spinal cord injury in humans. The exciting discovery in 2006 of the relatively simple method to reprogram somatic cells into pluripotent cells has circumvented the need for human embryos. In their pioneering work, Takahashi and Yamanaka selected 24 candidate genes for their high expression in pluripotent cells (Takahashi and Yamanaka, 2006). They used retrovirus to ectopically express these factors in mouse embryonic fibroblasts (MEFs) beginning with each factor individually and all 24 factors combined. Individual expression did not result in colonies with an ESC-like morphology. Conversely, expression of all 24 factors did result in ESC-like morphology. Factors were subsequently removed to narrow the pool with the final determination being octamer-binding protein 4 (OCT4), kruppel-like factor 4 (KLF4), SRY (sex-determining region Y)-box 2 (SOX2), and V-Myc Avian Myelocytomatosis Viral Oncogene Homolog (c-MYC) (also called OKSM or the "Yamanaka factors") as sufficient to induce pluripotent cells from MEFs and adult mouse tail-tip fibroblasts. A myriad of assays were used to determine the similarity of these newly termed iPSCs with ESCs including examination of gene expression with RT-PCR and microarrray, alkaline phosphatase staining, immunostaining with SSEA-1, *in vivo* teratoma formation, and *in vitro* embryoid body differentiation. One year following their initial publication, the Yamanaka group published the ability of the same four factors, OKSM, to

reprogram human dermal fibroblasts into iPSCs (Takahashi et al., 2007). Because this technology has been reproducible and widely adopted by laboratories worldwide, the Nobel Prize for Physiology and Medicine was awarded within 6 years in 2012 to Shinya Yamanaka and shared with John Gurdon for their groundbreaking discoveries.

Improving the protocol

In the original work the "Yamanaka factors" resulted in 0.02% efficiency for reprogramming MEFs (Takahashi and Yamanaka, 2006); though excitingly successful, there was room for improvement in efficiency. Additionally, retrovirus used in the pioneering work only infects dividing cells and results with the integration of the factors into the genome, a less than desirable outcome especially for clinical use. Subsequent work aimed to improve efficiency and employ footprint-free methods for iPSC generation (Malik and Rao, 2013). In the same year Yamanaka's group showed OKSM were sufficient for reprogramming human somatic cells (Takahashi et al., 2007), a second group used lentivirus to deliver OCT4, SOX2, NANOG, and LIN28 for successful reprogramming of human fibroblasts (Yu et al., 2007). Equal stoichiometry of the reprogramming factors was shown to be crucial for successful reprogramming (Papapetrou et al., 2009) and to this end, polycistronic delivery systems were designed with self-cleaving sequences between the factors (Carey et al., 2009; Chang et al., 2009; Sommer et al., 2009), some of which were Cre-excisable (Chang et al., 2009; Soldner et al., 2009; Somers et al., 2010; Sommer et al., 2009). Nonintegrating Sendai virus has also been used for reprogramming (Ban et al., 2011; Fusaki et al., 2009; Seki et al., 2010) with ready-made viruses now commercially available. Additional methods employed include protein (Kim et al., 2009; Zhou et al., 2009), mRNA (Warren et al., 2010), and microRNA (Miyoshi et al., 2011; Subramanyam et al., 2011) transfection as well as integration followed by excision of the reprogramming factors through incorporation into transposable elements (*PiggyBac*) (Kaji et al., 2009; Woltjen et al., 2009) and long-term transient expression of the factors from episomal plasmids (Chou et al., 2011; Hu et al.,

2011; Yu et al., 2009).

A myriad of donor cell types have been used for reprogramming since the initial experiments were performed in fibroblasts, including more recently cells derived from noninvasive urine collection (Zhou et al., 2012). Streamlined protocols now exist for the derivation, maintenance, and differentiation of iPSCs allowing the technology to be used by labs with no prior experience in stem cell research, thus expanding the impact and broad application of the technology. A wide variety of cell types can be generated from iPSCs including cardiomyocytes (Burridge et al., 2015; Lian et al., 2013; Zhang et al., 2012), skeletal myotubes (Darabi et al., 2012; Hosoyama et al., 2014), neural cells (Chambers et al., 2009), kidney podocytes (Song et al., 2012), pancreatic cells (Zhang et al., 2009), hepatocytes (Mallanna and Duncan, 2013), and hematopoietic and endothelial cells (Choi et al., 2009).

Applications

Isolation of patient-specific iPSCs made permissible the "disease in a dish" modeling of genetic diseases. It has nearly replaced the systems of overexpression in cancer cells and complements studies using animal models, which do not always faithfully recapitulate human disease (Avior et al., 2016). With disease in a dish modeling comes mechanistic insights into disease pathogenesis as well as the ability to test drugs to treat the disease in a patient's own cells. Potentially the most appealing yet far reaching goal of iPSCs is either cell therapy or regenerative medicine. Though many obstacles exist that must be overcome before this platform develops into a standard practice (see Section: Limitation and caveats), some promising success has been demonstrated with transplantation of human iPSC-derived cells into animal models (Lamba et al., 2010; Lian et al., 2010; Morizane et al., 2013; Rufaihah et al., 2011; Tedesco et al., 2012).

Limitations and caveats

As with all model systems, it is critical to understand the limitations and caveats of utilizing iPSCs as model systems (Hockemeyer and Jaenisch, 2016). An apparent limitation of

iPSC technology is the relative immaturity of differentiated cells, more closely resembling embryonic as opposed to adult cell types (Bedada et al., 2016; Hrvatin et al., 2014; Spence et al., 2011). Organoids containing multiple different cell types are becoming increasingly popular in studies to enhance maturation, examine paracrine factors functioning in tissues, and as developmental models (Lancaster and Knoblich, 2014). Another important caveat with iPSCs is the variability between iPSC lines with regards to differentiation efficiency resulting from both genetic background and the reprogramming process. Thus modest phenotypic variability is more difficult to discern than a robust phenotype with this model system (Soldner and Jaenisch, 2012). Generation of isogenic cell lines through genome editing (see Section: Genome Editing) that differ only at a mutation of interest aids in circumventing this limitation (Hockemeyer and Jaenisch, 2016).

The use of pluripotent stem cells (PSCs, either ESCs or iPSCs) for cell replacement therapies faces its own set of hurdles that must be overcome before this becomes a common reality (Wu and Hochedlinger, 2011). The propensity of PSCs to form tumors containing cells of all three germ layers (i.e., teratoma) precludes the direct injection of undifferentiated cells into patients. Therefore, appropriately differentiated cells to the cell type of interest must be purified prior to replacement in patients to ensure removal of all PSCs. Cell delivery method and engraftment also remains a major hurdle and will no doubt vary depending on the tissue being targeted. Tissue rejection, depending on whether the source is allogenic or autologous, must also be taken into consideration. Because some research suggests that even autologous transplant of certain cell types may be immunogenic (Zhao et al., 2011), this active area warrants further investigation.

Altogether, the unique qualities of iPSCs as discussed here make them increasingly promising for studying disease models and potential treatment of multiple diseases. Coupling iPSCs with recent advances in genome editing as discussed below (see Section Genome Editing) promises many exciting prospects for the future.

Genome Editing

As discussed in Section: Induced Pluripotent Stem Cells (iPSCs), line to line variability in iPSCs makes it difficult to compare among lines that have different genetic background and reprogramming history. The generation of isogenic iPSC lines aids in addressing these issues while providing investigators with the appropriate control cell lines for phenotypic analysis. Additionally, a requirement exists for genome editing in order to correct a disease allele *ex vivo* within a patient's own cells for cell replacement therapy. Alternatively, genome editing may be performed *in vivo* for genetic correction of disease alleles. Though useful in mESCs (Doetschman et al., 1987; Thomas and Capecchi, 1987), homologous recombination alone as a method for genome editing is highly inefficient and impractical in hiPSCs (see Section: Homologous recombination). The advent of site-specific nucleases (SSNs) in recent years has greatly enhanced the efficiency of genome editing in PSCs and will be discussed in this section.

Homologous recombination

Homologous recombination refers to the genetic base pairing that occurs when nucleotide sequences are exchanged between two homologous (similar or identical) regions of DNA. Conventional genome modification through homologous recombination, discovered by work from 2007 Nobel Prize winners Mario Capecchi, Oliver Smithies, and Martin Evans (Doetschman et al., 1987; Kuehn et al., 1987; Thomas and Capecchi, 1987) provided a means to generate specific gene modifications in mESCs. However, hPSCs are more refractory to this type of modification, likely due to lower rates of endogenous homologous recombination. Though some success of modifying the genome in this way has been presented in hPSCs (An et al., 2012; Costa et al., 2007; Davis et al., 2008; Howden et al., 2011; Irion et al., 2007; Ruby and Zheng, 2009; Urbach et al., 2004; Zwaka and Thomson, 2003), it remains a highly inefficient and time consuming process. SSNs (described in Sections: ZFNs and TALENS and CRISPR/Cas9), namely zinc finger nucleases (ZFNs), transcription activator-like effector nucleases (TALENs),

and more recently, the clustered regularly interspaced short palindromic repeats (CRISPR)/CRISPR-associated 9 (Cas9) (CRISPR/Cas9) system have enhanced the efficiency of homologous recombination making specified genetic modification in human cells more feasible.

ZFNs and TALENs

SSNs are designed to generate targeted double strand breaks (DSBs) in the genome, which require repair for cell survival and proliferation (Figure 2.2). The repair pathways for DSBs include homology-directed repair (HDR), repair that occurs through homologous recombination (Jasin and Rothstein, 2013), and nonhomologous end joining (NHEJ), a DSB repair that results in direct ligation of the cut ends of DNA and can generate insertion or deletion mutations in the process (Lees-Miller and Meek, 2003) (Figure 2.2). The observation that a DSB in the genome enhances the efficiency of HDR was first made in mammalian cells during experiments utilizing the restriction enzyme I-Sce I to examine the modes of repair (Rouet et al., 1994a, b). This initial observation formed the basis for which SSNs where investigated as a tool for genome editing.

Zinc finger nucleases (ZFNs), which are a coupling of zinc finger proteins with a restriction enzyme, such as *FokI*, specifically cut DNA at the zinc finger protein recognizing sequence (Kim et al., 1996; Smith et al., 1999). For *FokI* cleavage of DNA, it must form a dimer; therefore, two adjacent ZFNs are designed in specific orientations, each coupled with a single *FokI*, to accomplish this feat, providing increased specificity (Smith et al., 1999). Zinc finger domains recognize nucleotides in triplets and have been designed to recognize nearly all possible nucleotide triplet combinations (Gaj et al., 2013). ZFNs were first shown to enhance gene targeting in 2003 (Bibikova et al., 2003) and utilized in 2005 to modify the endogenous human genome and the term “genome editing” was coined (Urnov et al., 2005).

TALENs are transcription activator-like effector (TALE) proteins fused to a nuclease, such as *FokI*, and recognize their targets based on a protein/DNA interaction, similar to ZFNs.

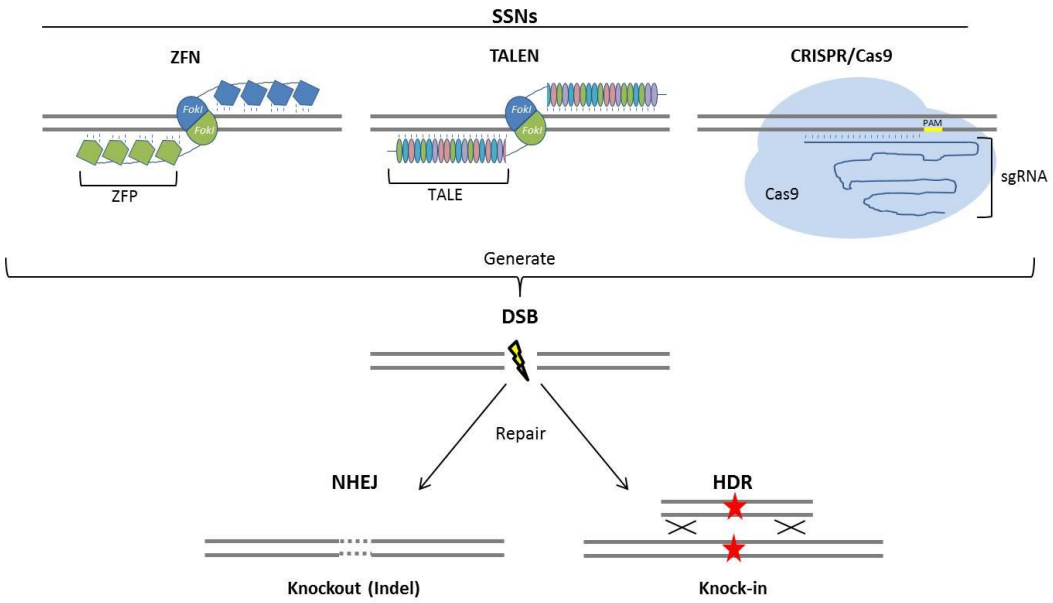

Figure 2.2 Schematic representation of genome editing. Site specific nucleases (SSNs) are designed to generate targeted double strand breaks (DSBs) within the genome and include zinc finger nucleases (ZFNs), transcription activator-like effector nucleases (TALENs), and the clustered regularly interspaced short palindromic repeats (CRISPR)/CRISPR-associated 9 (Cas9) (CRISPR/Cas9) system. DSBs are repaired either through nonhomologous end joining (NHEJ) or homology-directed repair (HDR). The former generates insertion/deletion mutations (indels)- potentially gene knockouts- and the latter allows targeted knock-in of specific sequences (denoted by the red star) into the specified locations.

TALEs were discovered as naturally occurring proteins in plant pathogenic bacteria (Gu et al., 2005; Kay et al., 2007; Sugio et al., 2007; Yang et al., 2006) and shown to have a simple recognition pattern of a pair of amino acid residues recognizing one nucleotide (Boch et al., 2009; Moscou and Bogdanove, 2009), making them simpler to design compared with ZFNs, though initially more difficult to generate due to the presence of repeat sequences (Gaj et al., 2013).

Despite the time intensive and costly nature of generating and/or purchasing custom ZFNs and TALENs, many studies have utilized them for genome editing in hPSCs generating gene knockouts, insertion or repair of point mutations, insertion of transgenes, and generation of reporters (DeKelver et al., 2010; Hockemeyer et al., 2009; Lombardo et al., 2007; Mitzelfelt et al., 2016; Soldner et al., 2011; Yusa et al., 2011). The simpler, cheaper, next generation version of SSNs came in the form of CRISPR/Cas9 (see Section: CRISPR/Cas9).

CRISPR/Cas9

As described in Section: ZFN and TALEN, both ZFNs and TALENs interact with DNA through a protein/DNA interaction, making them more difficult to design and construct. The recently adapted use of the CRISPR/Cas9 system as an engineered SSN provided an answer to these issues as it works through an RNA/DNA interaction- Watson and Crick base pairing- making design and construction simple.

The CRISPR/Cas system is a naturally occurring adaptive immunity response in bacteria and archaea where viral infection results in the insertion of a small sequence of the viral genome into the CRISPR locus of the bacterium (or archaeum) that is then transcribed into RNA to bind and direct the cleavage of the viral genome by Cas proteins (Marraffini, 2015). Much research has gone in to understanding the bacterial system (Hsu et al., 2014) stemming from the initial finding of a set of a novel type of repeat interspaced by nonrepetitive sequences in the *Escherichia coli* genome in 1987 (Ishino et al., 1987). Similar sequences were later shown to be present in 90% of archaea and >40% of bacteria (Mojica et al., 2000), with the term CRISPR being coined in 2002 along with the identification of associated *Cas* genes (Jansen et al., 2002). Three types of CRISPR systems exist (Type I-III) based on the associated *Cas* genes (Haft et al., 2005; Makarova et al., 2011) with Type II being the system adopted for genome editing utilizing Cas9.

Though CRISPRs were known to be transcribed in bacteria/archaea (Tang et al., 2002), their exogenous, viral origin was not appreciated until 2005 (Bolotin et al., 2005; Mojica et al., 2005; Pourcel et al., 2005). The role of CRISPRs as an adaptive immune response was predicted from this finding, and the first experimental evidence showing that CRISPRs direct Cas9 cleavage of viral DNA came in 2007 (Barrangou et al., 2007).

In the native Type II CRISPR/Cas9 system, the genomic CRISPR array is transcribed as a single RNA and then cleaved to form short CRISPR RNAs (crRNAs), providing specificity for Cas9 targeting. A noncoding *trans*-activating crRNA (tracrRNA) hybridizes with a crRNA and is

required for cleavage of the CRISPR array. These two components (crRNA and tracrRNA) together with the target DNA provide a scaffold for Cas9 to fold and bind for DNA cleavage (Hsu et al., 2014). A crRNA and a tracrRNA can be fused into a single guide RNA (sgRNA) for efficient engineered cleavage suggesting its use as a SSN similar to ZFNs and TALENs in genome editing (Jinek et al., 2012). The protospacer-adjacent motif (PAM) within the target DNA is essential for Cas9 nuclease activity. The specific sequence and location vary between species and Cas proteins (Hsu et al., 2014). Overall the components for DSB generation by the CRISPR/Cas9 system include: crRNA/tracrRNA complex (or sgRNA), Cas9 protein, and target DNA containing a PAM site.

Adapting the CRISPR/Cas9 bacterial system to applications in genome editing is relatively simple. One must design a guide sequence (originally 20 nucleotides, with many online tools available for assistance http://zifit.partners.org/ZiFiT/ and http://www.rgenome.net/) and incorporate this into a sgRNA coexpressed with Cas9. Design limitation stems from the requirement for a PAM site in the appropriate orientation to the target site (Hsu et al., 2014). Design and construction are much simpler compared with their predecessors ZFNs and TALENs. The first demonstration of genome editing utilizing CRISPR/Cas9 in eukaryotic cells occurred in 2013 (Cong et al., 2013; Mali et al., 2013b), with exponential expansion of the use of the technology since then, including in hPSCs (Hinson et al., 2015; Smith et al., 2014; Wang et al., 2014; Xie et al., 2014). Multiple published protocols exist for genome editing in hPSCs (Blair et al., 2016; Byrne and Church, 2015; Chiba and Hockemeyer, 2015; Yusa, 2013).

Improving genome editing

As with any new application, modifications to genome editing protocols optimize the impact. The CRISPR/Cas9 system continues to be widely studied with the hopes of further improving efficiency, enhancing specificity, and broadening flexibility.

Though the efficiency of genome editing with SSNs is many fold greater than through

homologous recombination alone, there still exists room for improvement. An elegant strategy aimed to alleviate this issue incorporates positive selection for the editing event. Kosuke Yusa, developed and utilized this strategy for the correction of a mutation causing α-1 antitrypsin deficiency (Yusa et al., 2011). Targeting was performed at the region of interest to knock-in a selection cassette flanked by *PiggyBac* repeats followed by subsequent excision of the selection cassette through transfection with *PiggyBac* transposase resulting in seamless or 'scar-free' editing of the locus of interest (Yusa, 2013; Yusa et al., 2011). A similar approach utilizing the Cre-LoxP system was utilized to correct point mutations in the beta-globin gene leaving a single LoxP site within an intronic region (Zou et al., 2011). A downfall to these approaches is the requirement for two separate targeting steps, the first to incorporate the selection cassette and the second to remove it. A separate strategy develop by Bruce Conklin's group involves serial enrichment of positive subfractions (sib-selection) that allows for more efficient isolation of rare editing events (Miyaoka et al., 2014).

Cell cycle synchronization and transfection of preassembled Cas9-guide RNA ribonucleoprotein (RNP) has been shown to enhance HDR efficiency preferentially over NHEJ depending on cell cycle timing of RNP application (Lin et al., 2014). This is important as NHEJ remains the dominant repair pathway for DSBs (Chapman et al., 2012). Additional work has utilized chemical inhibitors, such as Scr7, to block NHEJ resulting in higher rates of HDR (Maruyama et al., 2015). hPSC lines with knock-in of doxycycline-inducible Cas9 into the *AAVS1* safe-harbor locus have been generated thereby requiring only transfection of an sgRNA for targeting simplifying the process (González et al., 2014). Genome editing has also been combined with iPSC reprogramming in a simultaneous process beginning with patient fibroblasts thereby creating a streamlined approach for regenerative therapy (Howden et al., 2015).

Despite these improvements in this exciting, rapidly progressing field, it has not yet reached an optimal point in which efficient editing can be performed at virtually any locus leaving room for improvement. A strategy designed and tested by our laboratory in which

isolation of cells bearing a selectable, HDR-mediated editing event at one locus enriches many-fold for the introduction of additional HDR-mediated edits at secondary, investigator-specified loci (see Chapter 4) is aimed towards this goal.

Specificity and off-target cleavage are concerns for all SSNs, especially CRISPR/Cas9, which is thought to be more promiscuous compared with ZFNs and TALENS due to their cooperative nature. Enhancing the specificity of Cas9 and identifying unbiased methods to screen for off-target effects are high priorities. Mismatches occurring throughout the guide sequence impact Cas9's ability to cleave DNA and interestingly, though guides with lower levels of homology result in binding, cleavage efficacy is negatively impacted through mismatches (Wu et al., 2014). Higher concentrations of Cas9 correlate with elevated off-target effects (Hsu et al., 2013; Pattanayak et al., 2013) suggesting that using lower levels of Cas9 should enhance specificity, though the efficiency of on-target cleavage is also reduced (Hsu et al., 2013).

Modification of Cas9 to generate single strand breaks or nicks in the DNA opposed to DSBs has allowed a dimeric approach similar to ZFNs and TALENs, which requires pairs of guide RNAs specifically placed to generate DSBs and therefore increases the number of matching bases required for cleavage (Mali et al., 2013a; Ran et al., 2013). Single DNA nicks cannot be repaired by NHEJ, but can be repaired by HDR, though the efficiency is lower compared with DSBs (Hsu et al., 2013). Shorter guide RNAs (17-19 bp as opposed to 20 bp) have been shown to decrease off-target effects without the loss of on-target efficiency (Fu et al., 2014). A high fidelity version of endogenous Cas9 has been generated that contains sequence alterations designed to reduce nonspecific DNA contacts while retaining on-target activity (Kleinstiver et al., 2016). Though significant off-target effects have been observed in cancer cells, it is generally thought that primary cells, such as hPSCs with intact cell cycle checkpoints, undergo lower levels of off-target nuclease cutting though this has not been fully addressed (Hockemeyer and Jaenisch, 2016).

Efficient methods to screen for off-target effects of SSNs have also been a priority, which

becomes increasingly important as we envisage their clinical use. Initially, off-target sites were computationally identified looking for similarity in genomic sequences using available online tools (e.g., http://zifit.partners.org/ZiFiT/ or http://www.rgenome.net/) followed by subsequent screening for off-target cutting with direct sequencing. Recent studies have shown that computationally identified off-target sites do not always account for actual off-target sites (Tsai et al., 2015). Keith Joung's group has developed a rigorous strategy for unbiased off-target site identification, termed GUIDE-Seq, which involves the incorporation of a double-stranded piece of exogenous DNA into a DSB (Tsai et al., 2015). Though strategies such as GUIDE-Seq should be used as a preclinical screening mechanism, for most basic research purposes appropriate experimental controls should account for differences generated due to off-target effects.

Improving the flexibility of the CRISPR/Cas system is another pursued endeavor. Much of the initial work was performed with the CRISRP/Cas9 system adopted from *Streptococcus pyogenes* (Cong et al., 2013; Jinek et al., 2012; Mali et al., 2013b), with limited work also performed using the *Streptococcus thermophilus* LMD-9 CRISPR1 system (Cong et al., 2013), termed SpCas9 and StCas9, respectively. SpCas9 utilizes a 5'-NGG-3' PAM sequence, while StCas9 recognizes a 5'-NNAGAAW-3' (W= A or T) PAM sequence, limiting target design to locations in the genome adjacent to those sequences. Additional work with other species of Cas9 including *Neisseria meningitidis* (NmCas9) provides further options for PAM sequences (Hou et al., 2013). Additionally, the use of Cpf1 in place of Cas9 offers variability as well since it recognizes a T-rich PAM upstream of the target site, does not require a tracrRNA, and introduces a staggered DSBs as opposed to the blunt DSBs introduced by Cas9 (Zetsche et al., 2015). Additional work has been performed by Keith Joung's group to modify SpCas9 and Cas9 derived from *Staphylococcus aureus* (SaCas9) altering their PAM recognition sequences generating 'designer' Cas9 (Kleinstiver et al., 2015a; Kleinstiver et al., 2015b).

Summary and perspectives

The rapid-paced genome engineering field continues to grow and expand with more labs feasibly utilizing the now simplified techniques. The first clinical trials involving transplantation studies using ZFNs to disrupt the CCR5 locus in autologous patient CD4 T cells were performed with relative success in a small cohort (Tebas et al., 2014). Many companies are currently investigating therapeutic treatments utilizing genome editing with SSNs with many likely therapeutic prospects such as transplantation of autologous T cells genetically modified at the CCR5 locus for treatment of human immunodeficiency virus (HIV) and treatment of Duchenne's muscular dystrophy through either *in vivo* or *ex vivo* restoration of the dystrophin reading frame by exon deletion (Maeder and Gersbach, 2016; Sheridan, 2015).

Though most agree therapeutic modifications of the genome warrant investigation, engineering the human germline is not met with such enthusiasm and much skepticism exists in terms of societal benefits. The ease of CRISPR/Cas9 genome editing sparked this ethical debate, as now any molecular biology-equipped laboratory can perform editing experiments, and will require policy regulation (Hockemeyer and Jaenisch, 2016). Policy will likely vary worldwide, as already two separate groups in China have performed editing in nonviable human embryos (Kang et al., 2016; Liang et al., 2015). A distinction must be made between modification for therapeutic purposes and germline modification, which results in permanent, transmissible modification of the human genome (Hockemeyer and Jaenisch, 2016).

The Combined Power of iPSCs and Genome Editing

Ten years of exciting recent work with the advent of iPSCs and the CRISPR/Cas9 system for genome engineering have opened the door for regenerative therapies involving cell and gene replacement. This work is based on the foundational discoveries of ESCs and homologous recombination/ZFNs, studied since the 1980s. Though many challenges to bring these grand ideas into reality lie ahead, the prospect is certainly exhilarating. Continued small steps of progress will

lead towards standard clinical treatments. Chapter 3 of this work provides an example incorporating the use of iPSC and genome editing technologies in the study of 343delT HSPB5 associated with early-onset skeletal myopathy, introduced in Chapter 1. Chapter 4 presents a strategy for efficient genome editing in hiPSCs.

References

An, M.C., Zhang, N., Scott, G., Montoro, D., Wittkop, T., Mooney, S., Melov, S., and Ellerby, L.M. (2012). Genetic correction of Huntington's disease phenotypes in induced pluripotent stem cells. Cell Stem Cell 11, 253-263.

Avior, Y., Sagi, I., and Benvenisty, N. (2016). Pluripotent stem cells in disease modelling and drug discovery. Nat. Rev. Mol. Cell Biol. 17, 170-182.

Ban, H., Nishishita, N., Fusaki, N., Tabata, T., Saeki, K., Shikamura, M., Takada, N., Inoue, M., Hasegawa, M., Kawamata, S., et al. (2011). Efficient generation of transgene-free human induced pluripotent stem cells (iPSCs) by temperature-sensitive Sendai virus vectors. Proc. Natl. Acad. Sci. 108, 14234-14239.

Barrangou, R., Fremaux, C., Deveau, H., Richards, M., Boyaval, P., Moineau, S., Romero, D.A., and Horvath, P. (2007). CRISPR provides acquired resistance against viruses in prokaryotes. Science 315, 1709-1712.

Bedada, F.B., Wheelwright, M., and Metzger, J.M. (2016). Maturation status of sarcomere structure and function in human iPSC-derived cardiac myocytes. BBA Mol. Cell Res. 1863, 1829-1838.

Bibikova, M., Beumer, K., Trautman, J.K., and Carroll, D. (2003). Enhancing gene targeting with designed zinc finger nucleases. Science 300, 764-764.

Blair, J.D., Bateup, H.S., and Hockemeyer, D.F. (2016). Establishment of genome-edited human pluripotent stem cell lines: From targeting to isolation. JoVE, 53583.

Boch, J., Scholze, H., Schornack, S., Landgraf, A., Hahn, S., Kay, S., Lahaye, T., Nickstadt, A., and Bonas, U. (2009). Breaking the code of DNA binding specificity of TAL-type III effectors. Science 326, 1509-1512.

Bolotin, A., Quinquis, B., Sorokin, A., and Ehrlich, S.D. (2005). Clustered regularly interspaced short palindrome repeats (CRISPRs) have spacers of extrachromosomal origin. Microbiology 151, 2551-2561.

Burridge, P.W., Holmström, A., and Wu, J.C. (2015). Chemically defined culture and cardiomyocyte differentiation of human pluripotent stem cells. In Current Protocols in Human Genetics (John Wiley & Sons, Inc.).

Byrne, S.M., and Church, G.M. (2015). CRISPR-mediated gene targeting of human induced pluripotent stem cells. In Current Protocols in Stem Cell Biology (John Wiley & Sons, Inc.).

Campbell, K.H.S., McWhir, J., Ritchie, W.A., and Wilmut, I. (1996). Sheep cloned by nuclear transfer from a cultured cell line. Nature 380, 64-66.

Carey, B.W., Markoulaki, S., Hanna, J., Saha, K., Gao, Q., Mitalipova, M., and Jaenisch, R. (2009). Reprogramming of murine and human somatic cells using a single polycistronic vector. PNAS 106, 157-162.

Chambers, S.M., Fasano, C.A., Papapetrou, E.P., Tomishima, M., Sadelain, M., and Studer, L. (2009). Highly efficient neural conversion of human ES and iPS cells by dual inhibition of SMAD signaling. Nat. Biotech. 27, 275-280.

Chang, C.-W., Lai, Y.-S., Pawlik, K.M., Liu, K., Sun, C.-W., Li, C., Schoeb, T.R., and Townes, T.M. (2009). Polycistronic lentiviral vector for "hit and run" reprogramming of adult skin fibroblasts to induced pluripotent stem cells. Stem Cells 27, 1042-1049.

Chapman, J.R., Taylor, Martin R.G., and Boulton, Simon J. (2012). Playing the end game: DNA double-strand break repair pathway choice. Molec. Cell 47, 497-510.

Chiba, K., and Hockemeyer, D. (2015). Genome editing in human pluripotent stem cells using site-specific nucleases. In Chromosomal Mutagenesis, M.S. Pruett-Miller, ed. (New York, NY: Springer New York), pp. 267-280.

Choi, K.-D., Yu, J., Smuga-Otto, K., Salvagiotto, G., Rehrauer, W., Vodyanik, M., Thomson, J., and Slukvin, I. (2009). Hematopoietic and endothelial differentiation of human induced pluripotent stem cells. Stem Cells 27, 559-567.

Chou, B.K., Mali, P., Huang, X., Ye, Z., Dowey, S.N., Resar, L.M., Zou, C., Zhang, Y.A., Tong, J., and Cheng, L. (2011). Efficient human iPS cell derivation by a non-integrating plasmid from blood cells with unique epigenetic and gene expression signatures. Cell Res. 21, 518-529.

Cong, L., Ran, F.A., Cox, D., Lin, S., Barretto, R., Habib, N., Hsu, P.D., Wu, X., Jiang, W., Marraffini, L.A., et al. (2013). Multiplex genome engineering using CRISPR/Cas systems. Science 339, 819-823.

Costa, M., Dottori, M., Sourris, K., Jamshidi, P., Hatzistavrou, T., Davis, R., Azzola, L., Jackson, S., Lim, S.M., Pera, M., et al. (2007). A method for genetic modification of human embryonic stem cells using electroporation. Nat. Protocols 2, 792-796.

Darabi, R., Arpke, R.W., Irion, S., Dimos, J.T., Grskovic, M., Kyba, M., and Perlingeiro, R.C. (2012). Human ES- and iPS-derived myogenic progenitors restore DYSTROPHIN and improve contractility upon transplantation in dystrophic mice. Cell Stem Cell 10, 610-619.

Davis, R.P., Ng, E.S., Costa, M., Mossman, A.K., Sourris, K., Elefanty, A.G., and Stanley, E.G. (2008). Targeting a GFP reporter gene to the MIXL1 locus of human embryonic stem cells identifies human primitive streak–like cells and enables isolation of primitive hematopoietic precursors. Blood 111, 1876-1884.

DeKelver, R.C., Choi, V.M., Moehle, E.A., Paschon, D.E., Hockemeyer, D., Meijsing, S.H., Sancak, Y., Cui, X., Steine, E.J., Miller, J.C., et al. (2010). Functional genomics, proteomics, and regulatory DNA analysis in isogenic settings using zinc finger nuclease-driven transgenesis into a safe harbor locus in the human genome. Genome Res. 20, 1133-1142.

Doetschman, T., Gregg, R.G., Maeda, N., Hooper, M.L., Melton, D.W., Thompson, S., and Smithies, O. (1987). Targeted correction of a mutant HPRT gene in mouse embryonic stem cells. Nature 330, 576-578.

Evans, M.J., and Kaufman, M.H. (1981). Establishment in culture of pluripotential cells from mouse embryos. Nature 292, 154-156.

Fu, Y., Sander, J.D., Reyon, D., Cascio, V.M., and Joung, J.K. (2014). Improving CRISPR-Cas nuclease specificity using truncated guide RNAs. Nat. Biotech. 32, 279-284.

Fusaki, N., Ban, H., Nishiyama, A., Saeki, K., and Hasegawa, M. (2009). Efficient induction of transgene-free human pluripotent stem cells using a vector based on Sendai virus, an RNA virus that does not integrate into the host genome. Proc. of the Japan Academy, Series B 85, 348-362.

Gaj, T., Gersbach, C.A., and Barbas, C.F., III (2013). ZFN, TALEN, and CRISPR/Cas-based methods for genome engineering. Trends Biotech. 31, 397-405.

González, F., Zhu, Z., Shi, Z.-D., Lelli, K., Verma, N., Li, Qing V., and Huangfu, D. (2014). An iCRISPR platform for rapid, multiplexable, and inducible genome editing in human pluripotent stem cells. Cell Stem Cell 15, 215-226.

Gu, K., Yang, B., Tian, D., Wu, L., Wang, D., Sreekala, C., Yang, F., Chu, Z., Wang, G.-L., White, F.F., et al. (2005). R gene expression induced by a type-III effector triggers disease resistance in rice. Nature 435, 1122-1125.

Gurdon, J.B. (1962). The developmental capacity of nuclei taken from intestinal epithelium cells of feeding tadpoles. Development 10, 622-640.

Haft, D.H., Selengut, J., Mongodin, E.F., and Nelson, K.E. (2005). A guild of 45 CRISPR-associated (Cas) protein families and multiple CRISPR/Cas subtypes exist in prokaryotic genomes. PLoS Comput. Biol. 1, e60.

Hinson, J.T., Chopra, A., Nafissi, N., Polacheck, W.J., Benson, C.C., Swist, S., Gorham, J., Yang, L., Schafer, S., Sheng, C.C., et al. (2015). Titin mutations in iPS cells define sarcomere insufficiency as a cause of dilated cardiomyopathy. Science 349, 982-986.

Hockemeyer, D., and Jaenisch, R. (2016). Induced pluripotent stem cells meet genome editing. Cell Stem Cell 18, 573-586.

Hockemeyer, D., Soldner, F., Beard, C., Gao, Q., Mitalipova, M., DeKelver, R.C., Katibah, G.E., Amora, R., Boydston, E.A., Zeitler, B., et al. (2009). Efficient targeting of expressed and silent genes in human ESCs and iPSCs using zinc-finger nucleases. Nat. Biotech. 27, 851-857.

Hosoyama, T., McGivern, J.V., Van Dyke, J.M., Ebert, A.D., and Suzuki, M. (2014). Derivation of myogenic progenitors directly from human pluripotent stem cells using a sphere-based culture. Stem Cells Trans. Med.

Hou, Z., Zhang, Y., Propson, N.E., Howden, S.E., Chu, L.-F., Sontheimer, E.J., and Thomson, J.A. (2013). Efficient genome engineering in human pluripotent stem cells using Cas9 from Neisseria meningitidis. Proc. Natl. Acad. Sci. 110, 15644-15649.

Howden, S.E., Gore, A., Li, Z., Fung, H.-L., Nisler, B.S., Nie, J., Chen, G., McIntosh, B.E., Gulbranson, D.R., Diol, N.R., et al. (2011). Genetic correction and analysis of induced pluripotent stem cells from a patient with gyrate atrophy. Proc. Natl. Acad. Sci. 108, 6537-6542.

Howden, Sara E., Maufort, John P., Duffin, Bret M., Elefanty, Andrew G., Stanley, Edouard G., and Thomson, James A. (2015). Simultaneous reprogramming and gene correction of patient fibroblasts. Stem Cell Rep. 5, 1109-1118.

Hrvatin, S., O'Donnell, C.W., Deng, F., Millman, J.R., Pagliuca, F.W., DiIorio, P., Rezania, A., Gifford, D.K., and Melton, D.A. (2014). Differentiated human stem cells resemble fetal, not adult, β cells. Proc. Natl. Acad. Sci. 111, 3038-3043.

Hsu, Patrick D., Lander, Eric S., and Zhang, F. (2014). Development and applications of CRISPR-Cas9 for genome engineering. Cell 157, 1262-1278.

Hsu, P.D., Scott, D.A., Weinstein, J.A., Ran, F.A., Konermann, S., Agarwala, V., Li, Y., Fine, E.J., Wu, X., Shalem, O., et al. (2013). DNA targeting specificity of RNA-guided Cas9 nucleases. Nat. Biotech. 31, 827-832.

Hu, K., Yu, J., Suknuntha, K., Tian, S., Montgomery, K., Choi, K.D., Stewart, R., Thomson, J.A., and Slukvin, II (2011). Efficient generation of transgene-free induced pluripotent stem cells from normal and neoplastic bone marrow and cord blood mononuclear cells. Blood 117, e109-119.

Irion, S., Luche, H., Gadue, P., Fehling, H.J., Kennedy, M., and Keller, G. (2007). Identification and targeting of the ROSA26 locus in human embryonic stem cells. Nat. Biotech. 25, 1477-1482.

Ishino, Y., Shinagawa, H., Makino, K., Amemura, M., and Nakata, A. (1987). Nucleotide sequence of the iap gene, responsible for alkaline phosphatase isozyme conversion in Escherichia coli, and identification of the gene product. J. of Bacteriology 169, 5429-5433.

Jansen, R., Embden, J.D.A.v., Gaastra, W., and Schouls, L.M. (2002). Identification of genes that are associated with DNA repeats in prokaryotes. Molec. Microbiol. 43, 1565-1575.

Jasin, M., and Rothstein, R. (2013). Repair of strand breaks by homologous recombination. Cold Spring Harbor Persp.Biol. 5, a012740.

Jinek, M., Chylinski, K., Fonfara, I., Hauer, M., Doudna, J.A., and Charpentier, E. (2012). A programmable dual-RNA–guided DNA endonuclease in adaptive bacterial immunity. Science 337, 816-821.

Kaji, K., Norrby, K., Paca, A., Mileikovsky, M., Mohseni, P., and Woltjen, K. (2009). Virus-free induction of pluripotency and subsequent excision of reprogramming factors. Nature 458, 771-775.

Kang, X., He, W., Huang, Y., Yu, Q., Chen, Y., Gao, X., Sun, X., and Fan, Y. (2016). Introducing precise genetic modifications into human 3PN embryos by CRISPR/Cas-mediated genome editing. J. Assist. Reprod. Gen. 33, 581-588.

Kay, S., Hahn, S., Marois, E., Hause, G., and Bonas, U. (2007). A bacterial effector acts as a plant transcription factor and induces a cell size regulator. Science 318, 648-651.

Kim, D., Kim, C.-H., Moon, J.-I., Chung, Y.-G., Chang, M.-Y., Han, B.-S., Ko, S., Yang, E., Cha, K.Y., Lanza, R., et al. (2009). Generation of human induced pluripotent stem cells by direct delivery of reprogramming proteins. Cell Stem Cell 4, 472-476.

Kim, Y.G., Cha, J., and Chandrasegaran, S. (1996). Hybrid restriction enzymes: zinc finger fusions to Fok I cleavage domain. Proc. Natl. Acad. Sci. USA 93, 1156-1160.

Kleinstiver, B.P., Pattanayak, V., Prew, M.S., Tsai, S.Q., Nguyen, N.T., Zheng, Z., and Joung, J.K. (2016). High-fidelity CRISPR–Cas9 nucleases with no detectable genome-wide off-target effects. Nature 529, 490-495.

Kleinstiver, B.P., Prew, M.S., Tsai, S.Q., Nguyen, N.T., Topkar, V.V., Zheng, Z., and Joung, J.K. (2015a). Broadening the targeting range of Staphylococcus aureus CRISPR-Cas9 by modifying PAM recognition. Nat. Biotech. 33, 1293-1298.

Kleinstiver, B.P., Prew, M.S., Tsai, S.Q., Topkar, V.V., Nguyen, N.T., Zheng, Z., Gonzales, A.P.W., Li, Z., Peterson, R.T., Yeh, J.-R.J., et al. (2015b). Engineered CRISPR-Cas9 nucleases with altered PAM specificities. Nature 523, 481-485.

Kuehn, M.R., Bradley, A., Robertson, E.J., and Evans, M.J. (1987). A potential animal model for Lesch-Nyhan syndrome through introduction of HPRT mutations into mice. Nature 326, 295-298.

Lamba, D.A., McUsic, A., Hirata, R.K., Wang, P.-R., Russell, D., and Reh, T.A. (2010). Generation, purification and transplantation of photoreceptors derived from human induced pluripotent stem cells. PloS One 5, e8763.

Lancaster, M.A., and Knoblich, J.A. (2014). Organogenesis in a dish: Modeling development and disease using organoid technologies. Science 345.

Lees-Miller, S.P., and Meek, K. (2003). Repair of DNA double strand breaks by non-homologous end joining. Biochimie 85, 1161-1173.

Lian, Q., Zhang, Y., Zhang, J., Zhang, H.K., Wu, X., Zhang, Y., Lam, F.F.-Y., Kang, S., Xia, J.C., Lai, W.-H., et al. (2010). Functional mesenchymal stem cells derived from human induced pluripotent stem cells attenuate limb ischemia in mice. Circulation 121, 1113-1123.

Lian, X., Zhang, J., Azarin, S.M., Zhu, K., Hazeltine, L.B., Bao, X., Hsiao, C., Kamp, T.J., and Palecek, S.P. (2013). Directed cardiomyocyte differentiation from human pluripotent stem cells by modulating Wnt/beta-catenin signaling under fully defined conditions. Nat. Prot. 8, 162-175.

Liang, P., Xu, Y., Zhang, X., Ding, C., Huang, R., Zhang, Z., Lv, J., Xie, X., Chen, Y., Li, Y., et al. (2015). CRISPR/Cas9-mediated gene editing in human tripronuclear zygotes. Protein & Cell 6, 363-372.

Limphong, P., Zhang, H., Christians, E., Liu, Q., Riedel, M., Ivey, K., Cheng, P., Mitzelfelt, K., Taylor, G., Winge, D., et al. (2013). Modeling human protein aggregation cardiomyopathy using murine induced pluripotent stem cells. Stem Cells Trans. Med. 2, 161-166.

Lin, S., Staahl, B.T., Alla, R.K., and Doudna, J.A. (2014). Enhanced homology-directed human genome engineering by controlled timing of CRISPR/Cas9 delivery. eLife 3, e04766.

Lombardo, A., Genovese, P., Beausejour, C.M., Colleoni, S., Lee, Y.-L., Kim, K.A., Ando, D., Urnov, F.D., Galli, C., Gregory, P.D., et al. (2007). Gene editing in human stem cells using zinc finger nucleases and integrase-defective lentiviral vector delivery. Nat. Biotech. 25, 1298-1306.

Maeder, M.L., and Gersbach, C.A. (2016). Genome-editing technologies for gene and cell therapy. Mol. Ther. 24, 430-446.

Makarova, K.S., Haft, D.H., Barrangou, R., Brouns, S.J.J., Charpentier, E., Horvath, P., Moineau, S., Mojica, F.J.M., Wolf, Y.I., Yakunin, A.F., et al. (2011). Evolution and classification of the CRISPR–Cas systems. Nat. Rev. Micro. 9, 467-477.

Mali, P., Aach, J., Stranges, P.B., Esvelt, K.M., Moosburner, M., Kosuri, S., Yang, L., and Church, G.M. (2013a). CAS9 transcriptional activators for target specificity screening and paired nickases for cooperative genome engineering. Nat Biotech 31, 833-838.

Mali, P., Yang, L., Esvelt, K.M., Aach, J., Guell, M., DiCarlo, J.E., Norville, J.E., and Church, G.M. (2013b). RNA-guided human genome engineering via Cas9. Science 339, 823-826.

Malik, N., and Rao, M.S. (2013). A review of the methods for human iPSC derivation. In Pluripotent Stem Cells: Methods and Protocols, U. Lakshmipathy, and C.M. Vemuri, eds. (Totowa, NJ: Humana Press), pp. 23-33.

Mallanna, S.K., and Duncan, S.A. (2013). Differentiation of hepatocytes from pluripotent stem cells. In Current Protocols in Stem Cell Biology (John Wiley & Sons, Inc.).

Marraffini, L.A. (2015). CRISPR-Cas immunity in prokaryotes. Nature 526, 55-61.

Martin, G.R. (1981). Isolation of a pluripotent cell line from early mouse embryos cultured in medium conditioned by teratocarcinoma stem cells. Proc. of the Natl. Acad. of Sci. USA 78, 7634-7638.

Maruyama, T., Dougan, S.K., Truttmann, M.C., Bilate, A.M., Ingram, J.R., and Ploegh, H.L. (2015). Increasing the efficiency of precise genome editing with CRISPR-Cas9 by inhibition of nonhomologous end joining. Nat. Biotech. 33, 538-542.

Mitzelfelt, K.A., Limphong, P., Choi, M.J., Kondrat, F.D.L., Lai, S., Kolander, K.D., Kwok, W.-M., Dai, Q., Grzybowski, M.N., Zhang, H., et al. (2016). Human 343delT HSPB5 chaperone associated with early-onset skeletal myopathy causes defects in protein solubility. J. Biol. Chem. 291, 14939-14953.

Miyaoka, Y., Chan, A.H., Judge, L.M., Yoo, J., Huang, M., Nguyen, T.D., Lizarraga, P.P., So, P.-L., and Conklin, B.R. (2014). Isolation of single-base genome-edited human iPS cells without antibiotic selection. Nat. Meth. 11, 291-293.

Miyoshi, N., Ishii, H., Nagano, H., Haraguchi, N., Dewi, Dyah L., Kano, Y., Nishikawa, S., Tanemura, M., Mimori, K., Tanaka, F., et al. (2011). Reprogramming of mouse and human cells to pluripotency using mature microRNAs. Cell Stem Cell 8, 633-638.

Mojica, F.J.M., Díez-Villaseñor, C., Soria, E., and Juez, G. (2000). Biological significance of a family of regularly spaced repeats in the genomes of Archaea, Bacteria and mitochondria. Molec. Micro. 36, 244-246.

Mojica, F.J.M., Díez-Villaseñor, C.s., García-Martínez, J., and Soria, E. (2005). Intervening sequences of regularly spaced prokaryotic repeats derive from foreign genetic elements. J. Mol. Evo. 60, 174-182.

Morizane, A., Doi, D., Kikuchi, T., Okita, K., Hotta, A., Kawasaki, T., Hayashi, T., Onoe, H., Shiina, T., Yamanaka, S., et al. (2013). Direct comparison of autologous and allogeneic transplantation of iPSC-derived neural cells in the brain of a nonhuman primate. Stem Cell Rep. 1, 283-292.

Moscou, M.J., and Bogdanove, A.J. (2009). A simple cipher governs DNA recognition by TAL effectors. Science 326, 1501-1501.

Papapetrou, E.P., Tomishima, M.J., Chambers, S.M., Mica, Y., Reed, E., Menon, J., Tabar, V., Mo, Q., Studer, L., and Sadelain, M. (2009). Stoichiometric and temporal requirements of Oct4, Sox2, Klf4, and c-Myc expression for efficient human iPSC induction and differentiation. Proc. Natl. Acad. Sci. 106, 12759-12764.

Pattanayak, V., Lin, S., Guilinger, J.P., Ma, E., Doudna, J.A., and Liu, D.R. (2013). High-throughput profiling of off-target DNA cleavage reveals RNA-programmed Cas9 nuclease specificity. Nat. Biotech. 31, 839-843.

Pourcel, C., Salvignol, G., and Vergnaud, G. (2005). CRISPR elements in Yersinia pestis acquire new repeats by preferential uptake of bacteriophage DNA, and provide additional tools for evolutionary studies. Microbiology 151, 653-663.

Ran, F.A., Hsu, Patrick D., Lin, C.-Y., Gootenberg, Jonathan S., Konermann, S., Trevino, A.E., Scott, David A., Inoue, A., Matoba, S., Zhang, Y., et al. (2013). Double nicking by RNA-guided CRISPR Cas9 for enhanced genome editing specificity. Cell 154, 1380-1389.

Rideout III, W.M., Hochedlinger, K., Kyba, M., Daley, G.Q., and Jaenisch, R. (2002). Correction of a genetic defect by nuclear transplantation and combined cell and gene therapy. Cell 109, 17-27.

Rouet, P., Smih, F., and Jasin, M. (1994a). Expression of a site-specific endonuclease stimulates homologous recombination in mammalian cells. Proc. Natl. Acad. Sci. USA 91, 6064-6068.

Rouet, P., Smih, F., and Jasin, M. (1994b). Introduction of double-strand breaks into the genome of mouse cells by expression of a rare-cutting endonuclease. Mol. Cell. Biol. 14, 8096-8106.

Ruby, K.M., and Zheng, B. (2009). Gene targeting in a HUES line of human embryonic stem cells via electroporation. Stem Cells 27, 1496-1506.

Rufaihah, A.J., Huang, N.F., Jamé, S., Lee, J.C., Nguyen, H.N., Byers, B., De, A., Okogbaa, J., Rollins, M., Reijo-Pera, R., et al. (2011). Endothelial cells derived from human iPSCS increase capillary density and improve perfusion in a mouse model of peripheral arterial disease. Arteriosclerosis Thrombosis Vasc. Boil. 31, e72-e79.

Seki, T., Yuasa, S., Oda, M., Egashira, T., Yae, K., Kusumoto, D., Nakata, H., Tohyama, S., Hashimoto, H., Kodaira, M., et al. (2010). Generation of induced pluripotent stem cells from human terminally differentiated circulating T cells. Cell Stem Cell 7, 11-14.

Sheridan, C. (2015). CRISPR germline editing reverberates through biotech industry. Nat. Biotech. 33, 431-432.

Smith, C., Gore, A., Yan, W., Abalde-Atristain, L., Li, Z., He, C., Wang, Y., Brodsky, R.A., Zhang, K., Cheng, L., et al. (2014). Whole-genome sequencing analysis reveals high specificity of CRISPR/Cas9 and TALEN-based genome editing in human iPSCs. Cell Stem Cell 15, 12-13.

Smith, J., Berg, J.M., and Chandrasegaran, S. (1999). A detailed study of the substrate specificity of a chimeric restriction enzyme. Nucl. Acids Res. 27, 674-681.

Soldner, F., Hockemeyer, D., Beard, C., Gao, Q., Bell, G.W., Cook, E.G., Hargus, G., Blak, A., Cooper, O., Mitalipova, M., et al. (2009). Parkinson's disease patient-derived induced pluripotent stem cells free of viral reprogramming factors. Cell 136, 964-977.

Soldner, F., and Jaenisch, R. (2012). iPSC disease modeling. Science 338, 1155-1156.

Soldner, F., Laganiere, J., Cheng, A.W., Hockemeyer, D., Gao, Q., Alagappan, R., Khurana, V., Golbe, L.I., Myers, R.H., Lindquist, S., et al. (2011). Generation of isogenic pluripotent stem cells differing exclusively at two early onset Parkinson point mutations. Cell 146, 318-331.

Somers, A., Jean, J.-C., Sommer, C.A., Omari, A., Ford, C.C., Mills, J.A., Ying, L., Sommer, A.G., Jean, J.M., Smith, B.W., et al. (2010). Generation of transgene-free lung disease-specific human induced pluripotent stem cells using a single excisable lentiviral stem cell cassette. Stem Cells 28, 1728-1740.

Sommer, C.A., Stadtfeld, M., Murphy, G.J., Hochedlinger, K., Kotton, D.N., and Mostoslavsky, G. (2009). Induced pluripotent stem cell generation using a single lentiviral stem cell ccassette. Stem Cells 27, 543-549.

Song, B., Smink, A.M., Jones, C.V., Callaghan, J.M., Firth, S.D., Bernard, C.A., Laslett, A.L., Kerr, P.G., and Ricardo, S.D. (2012). The directed differentiation of human iPS cells into kidney podocytes. PloS One 7, e46453.

Spence, J.R., Mayhew, C.N., Rankin, S.A., Kuhar, M.F., Vallance, J.E., Tolle, K., Hoskins, E.E., Kalinichenko, V.V., Wells, S.I., Zorn, A.M., et al. (2011). Directed differentiation of human pluripotent stem cells into intestinal tissue in vitro. Nature 470, 105-109.

Subramanyam, D., Lamouille, S., Judson, R.L., Liu, J.Y., Bucay, N., Derynck, R., and Blelloch, R. (2011). Multiple targets of miR-302 and miR-372 promote reprogramming of human fibroblasts to induced pluripotent stem cells. Nat. Biotech. 29, 443-448.

Sugio, A., Yang, B., Zhu, T., and White, F.F. (2007). Two type III effector genes of Xanthomonas oryzae pv. oryzae control the induction of the host genes OsTFIIAγ1 and OsTFX1 during bacterial blight of rice. Proc. Natl. Acad. Sci. 104, 10720-10725.

Tachibana, M., Amato, P., Sparman, M., Gutierrez, Nuria M., Tippner-Hedges, R., Ma, H., Kang, E., Fulati, A., Lee, H.-S., Sritanaudomchai, H., et al. (2013). Human embryonic stem cells derived by somatic cell nuclear transfer. Cell 153, 1228-1238.

Takahashi, K., Tanabe, K., Ohnuki, M., Narita, M., Ichisaka, T., Tomoda, K., and Yamanaka, S. (2007). Induction of pluripotent stem cells from adult human fibroblasts by defined factors. Cell

131, 861-872.

Takahashi, K., and Yamanaka, S. (2006). Induction of pluripotent stem cells from mouse embryonic and adult fibroblast cultures by defined factors. Cell 126, 663-676.

Tang, T.-H., Bachellerie, J.-P., Rozhdestvensky, T., Bortolin, M.-L., Huber, H., Drungowski, M., Elge, T., Brosius, J., and Hüttenhofer, A. (2002). Identification of 86 candidates for small non-messenger RNAs from the archaeon Archaeoglobus fulgidus. Proc. Natl. Acad. Sci. 99, 7536-7541.

Tebas , P., Stein , D., Tang , W.W., Frank , I., Wang , S.Q., Lee , G., Spratt , S.K., Surosky , R.T., Giedlin , M.A., Nichol , G., et al. (2014). Gene editing of CCR5 in autologous CD4 T cells of persons infected with HIV. New Eng. J. Med. 370, 901-910.

Tedesco, F.S., Gerli, M.F.M., Perani, L., Benedetti, S., Ungaro, F., Cassano, M., Antonini, S., Tagliafico, E., Artusi, V., Longa, E., et al. (2012). Transplantation of genetically corrected human iPSC-derived progenitors in mice with limb-girdle muscular dystrophy. Sci. Trans. Med. 4, 140ra189-140ra189.

Thomas, K.R., and Capecchi, M.R. (1987). Site-directed mutagenesis by gene targeting in mouse embryo-derived stem cells. Cell 51, 503-512.

Thomson, J.A., Itskovitz-Eldor, J., Shapiro, S.S., Waknitz, M.A., Swiergiel, J.J., Marshall, V.S., and Jones, J.M. (1998). Embryonic Stem Cell Lines Derived from Human Blastocysts. Science 282, 1145-1147.

Tiscornia, G., Vivas, E.L., and Belmonte, J.C.I. (2011). Diseases in a dish: modeling human genetic disorders using induced pluripotent cells. Nat. Med. 1570-1576.

Tsai, S.Q., Zheng, Z., Nguyen, N.T., Liebers, M., Topkar, V.V., Thapar, V., Wyvekens, N., Khayter, C., Iafrate, A.J., Le, L.P., et al. (2015). GUIDE-seq enables genome-wide profiling of off-target cleavage by CRISPR-Cas nucleases. Nat. Biotech. 33, 187-197.

Urbach, A., Schuldiner, M., and Benvenisty, N. (2004). Modeling for Lesch-Nyhan disease by gene targeting in human embryonic stem cells. Stem Cells 22, 635-641.

Urnov, F.D., Miller, J.C., Lee, Y.-L., Beausejour, C.M., Rock, J.M., Augustus, S., Jamieson, A.C., Porteus, M.H., Gregory, P.D., and Holmes, M.C. (2005). Highly efficient endogenous human gene correction using designed zinc-finger nucleases. Nature 435, 646-651.

Wang, G., McCain, M.L., Yang, L., He, A., Pasqualini, F.S., Agarwal, A., Yuan, H., Jiang, D., Zhang, D., Zangi, L., et al. (2014). Modeling the mitochondrial cardiomyopathy of Barth syndrome with induced pluripotent stem cell and heart-on-chip technologies. Nat. Med. 20, 616-623.

Warren, L., Manos, P.D., Ahfeldt, T., Loh, Y.-H., Li, H., Lau, F., Ebina, W., Mandal, P.K., Smith, Z.D., Meissner, A., et al. (2010). Highly efficient reprogramming to pluripotency and directed differentiation of human cells with synthetic modified mRNA. Cell Stem Cell 7, 618-630.

Wert, G.d., and Mummery, C. (2003). Human embryonic stem cells: research, ethics and policy.

Human Reprod. 18, 672-682.

Woltjen, K., Michael, I.P., Mohseni, P., Desai, R., Mileikovsky, M., Hamalainen, R., Cowling, R., Wang, W., Liu, P., Gertsenstein, M., et al. (2009). piggyBac transposition reprograms fibroblasts to induced pluripotent stem cells. Nature 458, 766-770.

Wu, S.M., and Hochedlinger, K. (2011). Harnessing the potential of induced pluripotent stem cells for regenerative medicine. Nat. Cell Biol. 13, 497-505.

Wu, X., Scott, D.A., Kriz, A.J., Chiu, A.C., Hsu, P.D., Dadon, D.B., Cheng, A.W., Trevino, A.E., Konermann, S., Chen, S., et al. (2014). Genome-wide binding of the CRISPR endonuclease Cas9 in mammalian cells. Nat. Biotech. 32, 670-676.

Xie, F., Ye, L., Chang, J.C., Beyer, A.I., Wang, J., Muench, M.O., and Kan, Y.W. (2014). Seamless gene correction of β-thalassemia mutations in patient-specific iPSCs using CRISPR/Cas9 and piggyBac. Gen. Res. 24, 1526-1533.

Yamada, M., Johannesson, B., Sagi, I., Burnett, L.C., Kort, D.H., Prosser, R.W., Paull, D., Nestor, M.W., Freeby, M., Greenberg, E., et al. (2014). Human oocytes reprogram adult somatic nuclei of a type 1 diabetic to diploid pluripotent stem cells. Nature 510, 533-536.

Yang, B., Sugio, A., and White, F.F. (2006). Os8N3 is a host disease-susceptibility gene for bacterial blight of rice. Proc. Natl. Acad. Sci. 103, 10503-10508.

Yu, J., Hu, K., Smuga-Otto, K., Tian, S., Stewart, R., Slukvin, I.I., and Thomson, J.A. (2009). Human induced pluripotent stem cells free of vector and transgene sequences. Science 324, 797-801.

Yu, J., Vodyanik, M.A., Smuga-Otto, K., Antosiewicz-Bourget, J., Frane, J.L., Tian, S., Nie, J., Jonsdottir, G.A., Ruotti, V., Stewart, R., et al. (2007). Induced pluripotent stem cell lines derived from human somatic cells. Science 318, 1917-1920.

Yusa, K. (2013). Seamless genome editing in human pluripotent stem cells using custom endonuclease–based gene targeting and the piggyBac transposon. Nat. Prot. 8, 2061-2078.

Yusa, K., Rashid, S.T., Strick-Marchand, H., Varela, I., Liu, P.Q., Paschon, D.E., Miranda, E., Ordonez, A., Hannan, N.R., Rouhani, F.J., et al. (2011). Targeted gene correction of alpha1-antitrypsin deficiency in induced pluripotent stem cells. Nature 478, 391-394.

Zetsche, B., Gootenberg, Jonathan S., Abudayyeh, Omar O., Slaymaker, Ian M., Makarova, Kira S., Essletzbichler, P., Volz, Sara E., Joung, J., van der Oost, J., Regev, A., et al. (2015). Cpf1 is a single RNA-guided endonuclease of a class 2 CRISPR-Cas system. Cell 163, 759-771.

Zhang, D., Jiang, W., Liu, M., Sui, X., Yin, X., Chen, S., Shi, Y., and Deng, H. (2009). Highly efficient differentiation of human ES cells and iPS cells into mature pancreatic insulin-producing cells. Cell Res. 19, 429-438.

Zhang, J., Klos, M., Wilson, G.F., Herman, A.M., Lian, X., Raval, K.K., Barron, M.R., Hou, L., Soerens, A.G., Yu, J., et al. (2012). Extracellular matrix promotes highly efficient cardiac differentiation of human pluripotent stem cells: the matrix sandwich method. Circ. Res. 111, 1125-1136.

Zhao, T., Zhang, Z.N., Rong, Z., and Xu, Y. (2011). Immunogenicity of induced pluripotent stem cells. Nature 474, 212-215.

Zhou, H., Wu, S., Joo, J.Y., Zhu, S., Han, D.W., Lin, T., Trauger, S., Bien, G., Yao, S., Zhu, Y., et al. (2009). Generation of induced pluripotent stem cells using recombinant proteins. Cell Stem Cell 4, 381-384.

Zhou, T., Benda, C., Dunzinger, S., Huang, Y., Ho, J.C., Yang, J., Wang, Y., Zhang, Y., Zhuang, Q., Li, Y., et al. (2012). Generation of human induced pluripotent stem cells from urine samples. Nat. Prot. 7, 2080-2089.

Zou, J., Mali, P., Huang, X., Dowey, S.N., and Cheng, L. (2011). Site-specific gene correction of a point mutation in human iPS cells derived from an adult patient with sickle cell disease. Blood 118, 4599-4608.

Zwaka, T.P., and Thomson, J.A. (2003). Homologous recombination in human embryonic stem cells. Nat. Biotech. 21, 319-321.

CHAPTER 3

THE HUMAN 343DELT HSPB5 CHAPERONE ASSOCIATED WITH EARLY-ONSET SKELETAL MYOPTAHTY CAUSES DEFECTS IN PROTEIN SOLUBILITY

This research was originally published in the *Journal of Biological Chemistry*. Katie A. Mitzelfelt, Pattraranee Limphong, Melinda J. Choi, Frances D. L. Kondrat, Shuping Lai, Kurt D. Kolander, Wai-Meng Kwok, Qiang Dai, Michael N. Grzybowski, Huali Zhang, Graydon M. Taylor, Qiang Lui, Mai T. Thao, Judith A. Hudson, Rita Barresi, Kate Bushby, Heinz Jungbluth, Elizabeth Wraige, Aron M. Geurts, Justin L. P. Benesch, Michael Riedel, Elisabeth S. Christians, Alex C. Minella, and Ivor J. Benjamin. The Human 343delT HSPB5 Chaperone Associated with Early-onset Skeletal Myopathy Causes Defects in Protein Solubility. *Journal of Biological Chemistry*. 2016; Vol: 291, NO. 29: pp. 14939-14953.

THE JOURNAL OF BIOLOGICAL CHEMISTRY VOL. 291, NO. 29, pp. 14939–14953, July 15, 2016

The Human 343delT HSPB5 Chaperone Associated with Early-onset Skeletal Myopathy Causes Defects in Protein Solubility*[S]

Received for publication, April 1, 2016, and in revised form, May 14, 2016 Published, JBC Papers in Press, May 19, 2016, DOI 10.1074/jbc.M116.730481

Katie A. Mitzelfelt,[a1] Pattraranee Limphong,[b] Melinda J. Choi,[c] Frances D. L. Kondrat,[d2] Shuping Lai,[c] Kurt D. Kolander,[c] Wai-Meng Kwok,[e] Qiang Dai,[c] Michael N. Grzybowski,[c] Huali Zhang,[f] Graydon M. Taylor,[g] Qiang Lui,[g] Mai T. Thao,[c] Judith A. Hudson,[h] Rita Barresi,[i] Kate Bushby,[j] Heinz Jungbluth,[k,l,m] Elizabeth Wraige,[k] Aron M. Geurts,[c] Justin L. P. Benesch,[d] Michael Riedel,[n] Elisabeth S. Christians,[o] Alex C. Minella,[p] and Ivor J. Benjamin[a,c,3]

From the [a]Department of Biochemistry, University of Utah, Salt Lake City, Utah 84112-5650, [b]Arcturus Therapeutics, San Diego, California 92121, the [c]Cardiovascular Center, Departments of [e]Anesthesiology and Pharmacology and Toxicology, Medical College of Wisconsin, Milwaukee, Wisconsin 53226, the [d]Department of Chemistry, University of Oxford, Oxford OX1 3TA, United Kingdom, the [f]Department of Pathophysiology, Xiangya School of Medicine, Central South University, Changsha City, Hunan 410078, China, the [g]Division of Cardiology, Department of Medicine, University of Utah, Salt Lake City, Utah 84132, the [h]Northern Genetics Service, Newcastle upon Tyne Hospitals NHS Foundation Trust, Newcastle upon Tyne NE1 3BZ, United Kingdom, the [i]National Health Service England Health Science Services for Rare Neuromuscular Diseases, Muscle Immunoanalysis Unit, Dental Hospital, Richardson Road, Newcastle upon Tyne NE2 4AZ, United Kingdom, [j]Neuromuscular Genetics, Newcastle University John Walton Centre for Muscular Dystrophy Research, Medical Research Council Centre for Neuromuscular Diseases, Institute of Genetic Medicine, International Centre for Life, Newcastle upon Tyne NE1 3BZ, United Kingdom, the [k]Department of Paediatric Neurology, Neuromuscular Service Evelina Children's Hospital, Guy's and St. Thomas' National Health Service Foundation Trust, London SE1 7EH, United Kingdom, the [l]Randall Division of Cell and Molecular Biophysics, Muscle Signalling Section, King's College London, London SE1 1UL, United Kingdom, the [m]Department of Basic and Clinical Neuroscience Institute of Psychiatry, Psychology and Neuroscience, King's College London SE5 9RX, United Kingdom, [n]PharmaCell, Maastricht, Netherlands, 6229 EV Maastricht, the [o]Sorbonne Universités, University Pierre and Marie Curie, Univ Paris 06, CNRS, Laboratoire de Biologie du Dévelopment de Villefranche sur mer (LBDV), UMR 7009, 181 Chemin du Lazaret, 06230 Villefranche sur mer, France, and the [p]Blood Research Institute, BloodCenter of Wisconsin, Milwaukee, Wisconsin 53226

Mutations of HSPB5 (also known as CRYAB or αB-crystallin), a *bona fide* heat shock protein and molecular chaperone encoded by the *HSPB5* (crystallin, alpha B) gene, are linked to multisystem disorders featuring variable combinations of cataracts, cardiomyopathy, and skeletal myopathy. This study aimed to investigate the pathological mechanisms involved in an early-onset myofibrillar myopathy manifesting in a child harboring a homozygous recessive mutation in *HSPB5*, 343delT. To study HSPB5 343delT protein dynamics, we utilize model cell culture systems including induced pluripotent stem cells derived from the 343delT patient (343delT/343delT) along with isogenic, heterozygous, gene-corrected control cells (WT KI/343delT) and BHK21 cells, a cell line lacking endogenous HSPB5 expression. 343delT/343delT and WT KI/343delT-induced pluripotent stem cell-derived skeletal myotubes and cardiomyocytes did not express detectable levels of 343delT protein, contributable to the extreme insolubility of the mutant protein. Overexpression of HSPB5 343delT resulted in insoluble mutant protein aggregates and induction of a cellular stress response. Co-expression of 343delT with WT prevented visible aggregation of 343delT and improved its solubility. Additionally, *in vitro* refolding of 343delT in the presence of WT rescued its solubility. We demonstrate an interaction between WT and 343delT both *in vitro* and within cells. These data support a loss-of-function model for the myopathy observed in the patient because the insoluble mutant would be unavailable to perform normal functions of HSPB5, although additional gain-of-function effects of the mutant protein cannot be excluded. Additionally, our data highlight the solubilization of 343delT by WT, concordant with the recessive inheritance of the disease and absence of symptoms in carrier individuals.

HSPB5 (also known as CRYAB or αB-crystallin) is a small molecular weight heat shock protein encoded by the *HSPB5* (crystallin, alpha B) gene and functions as a molecular chaperone. Its promoter contains a heat shock element, a stress-responsive binding site of heat shock transcription factor 1 (HSF1), that functionally up-regulates the expression of *HSPB5*. Increased levels of HSPB5 can then go on to provide

* This work was supported by National Institute of Health Director's Pioneer Award Grant 8DP1HL17650-04 (to I. J. B.) and a Royal Society University Research Fellowship (to J. L. P. B.). The authors declare that they have no conflicts of interest with the contents of this article. The content is solely the responsibility of the authors and does not necessarily represent the official views of the National Institutes of Health.
We dedicate this work to the patient and her family.
[S] This article contains supplemental Figures S1–S5.
[1] Supported by Ruth L. Kirschstein National Research Service Award F31 Individual Fellowship 1F31AR067618-01A1.
[2] Supported by the Biotechnology and Biological Sciences Research Council (BB/J018082/1).
[3] To whom correspondence should be addressed: Cardiovascular Center, Medical College of Wisconsin, 8701 Watertown Plank Rd., Milwaukee, WI 53226. Tel.: 414-955-6780; Fax: 414-456-6515; E-mail: ibenjamin@mcw.edu.

distinct cytoprotective effects engaged in restoring cellular homeostasis (reviewed in Refs. 1, 2). Additionally, *HSPB5* contains tissue-specific enhancer elements in its promoter that allow constitutive high expression in the lens, heart, and skeletal muscle (3, 4).

As a member of the small molecular weight heat shock protein family, HSPB5 contains a well conserved central "α-crystallin" domain (ACD),[4] flanked by N- and C-terminal regions (5). The ACDs dimerize and assemble to form a polydisperse ensemble of oligomers, largely through dynamic interactions mediated by the terminal regions (6). The isolated ACD has been shown to have potent chaperone activity *in vitro* (7), and it is hypothesized that it might become exposed within the context of the wild-type protein in a manner regulated by phosphorylation (8) or cellular stress directly (9). The HSPB5 ACD contains two hydrophobic grooves, one between the β4 and β8 strands and the other at the dimer interface, both of which serve as putative binding sites for chaperone action (10). In addition, evidence also points at the involvement of the N terminus in target binding (11). Current data suggest that HSPB5 is a dynamic protein that is flexible in how it interacts with its diverse range of clients.

In striated muscle, HSPB5 acts as a chaperone for important structural client proteins, including desmin (12–14), titin (15–18), and actin (14, 19), a property that becomes particularly important under conditions of pathology or stress. *HSPB5/HSPB2* double knockout (DKO) mice exhibit progressive skeletal myopathy throughout life (20), with an impact on cardiac muscle only observed under conditions of exogenous stress (21, 22). More recently, a requirement for HSPB5 in muscle homeostasis has been demonstrated via modulation of argonaute 2 activity (23). DKO mice show reduced basal levels of skeletal muscle progenitor cells or satellite cells and defective muscle regeneration with cellular injury (23).

Multiple mutations in *HSPB5* are linked to human pathologies affecting the lens, heart, skeletal muscle, or some combination thereof, with the underlying disease mechanism(s) only partially understood (reviewed in Refs. 24, 25). These mutations are either dominant or recessive and have variable penetrance and expressivity. Of the known mutations in *HSPB5* linked with (cardio)myopathy, all but one result in aberrant protein aggregation of the mutant protein (reviewed in Ref. 25). For the well studied R120G mutation in HSPB5, the aggregates are thought to sequester other metastable proteins, such as desmin (26–28). The relative contribution of loss- *versus* gain-of-toxic function effects remain unclear for specific mutations.

An enhanced understanding of HSPB5 as a chaperone is needed to inform therapy development. Here we have investigated a recessive mutation in *HSPB5*, 343delT, found in a patient who presented at age 4 months with profound muscle stiffness, persistent creatine kinase elevation, and histopathological features of a myofibrillar myopathy (29). This homozygous recessive, single base deletion results in a frameshift and formation of a premature stop codon following addition of 14 missense residues (S115fs129X). The truncated protein is predicted to contain residues 1–115, having lost the C-terminal extension, as well as a significant portion of the ACD. The skeletal muscle biopsy of the patient shows dense, irregular staining of HSPB5, detectable only by an antibody recognizing the N terminus of HSPB5 (NT-HSPB5). This band runs at the predicted molecular weight of 15 kDa on a Western blot, smaller than the 22-kDa WT HSPB5 protein (29). Additionally, the biopsy shows intense, irregular staining of desmin and myotilin. At presentation, the patient exhibited neither signs of an associated cardiomyopathy nor cataracts, although with age, these symptoms may develop. Of note, the non-consanguineous parents, each heterozygous for 343delT, have no known symptoms attributed to this mutation; however, potential development of late-onset symptoms cannot be excluded.

To understand 343delT protein dynamics and their contribution to disease, we have incorporated the use of induced pluripotent stem cells (iPSCs) (30) derived from the patient as a unique system to permit the study of endogenous 343delT protein within cell types of interest. Additionally, we used systems of overexpression in a cell line that lacks endogenous HSPB5 expression (reviewed in Ref. 31) because of the recessive nature of the mutation as well as *in vitro* analysis of 343delT. Here we describe our findings, which provide insights into the molecular defects of 343delT in disease pathogenesis.

Results

Generation of iPSCs for the Investigation of 343delT—Fig. 1*A* shows the family pedigree of the patient harboring the homozygous, recessive 343delT mutation. The non-consanguineous parents are each heterozygous for the mutation and are asymptomatic, whereas the homozygous 343delT patient exhibits a severe, infantile-onset myopathy (29). To examine the effects of 343delT (strategy outlined in Fig. 1*B*), we generated iPSCs from dermal fibroblasts of the patient through four-factor reprogramming. Isogenic, heterozygous, gene-corrected control cells were then engineered from the patient iPSCs with a strategy adapted from Yusa *et al.* (32) through zinc finger nuclease-stimulated homologous recombination (see "Experimental Procedures"). The genotypes of both the patient (343delT/343delT) and heterozygous wild-type knockin control (WT KI/343delT) iPSCs are outlined in Fig. 1*B* and were confirmed through direct Sanger sequencing (Fig. 1*C*). Both iPSC lines expressed relevant pluripotency markers, including NANOG, stage-specific embryonic antigen 4 (SSEA-4), octamer-binding protein 4 (OCT-4), and TRA-1–81 at the protein level (Fig. 1, *D* and *E*) and *NANOG*, *OCT-4* (*POU5F1*), *SOX2*, and *TRA-1-60* at the RNA level (Fig. 1*F*). *In vitro* EZ sphere differentiations of both cell lines resulted in up-regulation of markers from all three germ layers (Fig. 1*G*). Karyotypes were normal (Fig. 1*H*). These data validate the use of generated iPSC lines for further investigations.

343delT Protein Is Not Detectable in iSKMs or iCMs although RNA Is Present—Validated iPSC lines were differentiated into skeletal myotubes (iSKMs) and cardiomyocytes (iCMs) using established protocols (see "Experimental Procedures"). iCMs

[4] The abbreviations used are: ACD, α-crystallin domain; DKO, double knockout; NT, N-terminal; iPSC, induced pluripotent stem cell; iSKM, iPSC-derived skeletal myotube; iCM, iPSC-derived cardiomyocyte; qRT-PCR, quantitative real-time PCR; TnT, Troponin T; IP, immunoprecipitation; RIPA, radioimmune precipitation assay; SUMO, small ubiquitin-related modifier; WCL, whole cell lysate.

contracted rhythmically in the dish, stained positive for cardiomyocyte markers, including Troponin T (TnT) (Fig. 2*A*), and exhibited cardiomyocyte-like action potential profiles (Fig. 2*C*). iSKMs elongate as they mature in culture, many appear multinucleated, some cells can be observed to twitch spontaneously, and they stain positively for muscle markers, including TnT (Figs. 2*B* and 4*A*) and desmin (Fig. 4*B*). No obvious phenotypic differences were observed between WT KI/343delT and 343delT/343delT iCMs or iSKMs when characterizing cell differentiation in this way.

The major difference observed between the muscle-differentiated cell lines was a complete lack of detectable 343delT pro-

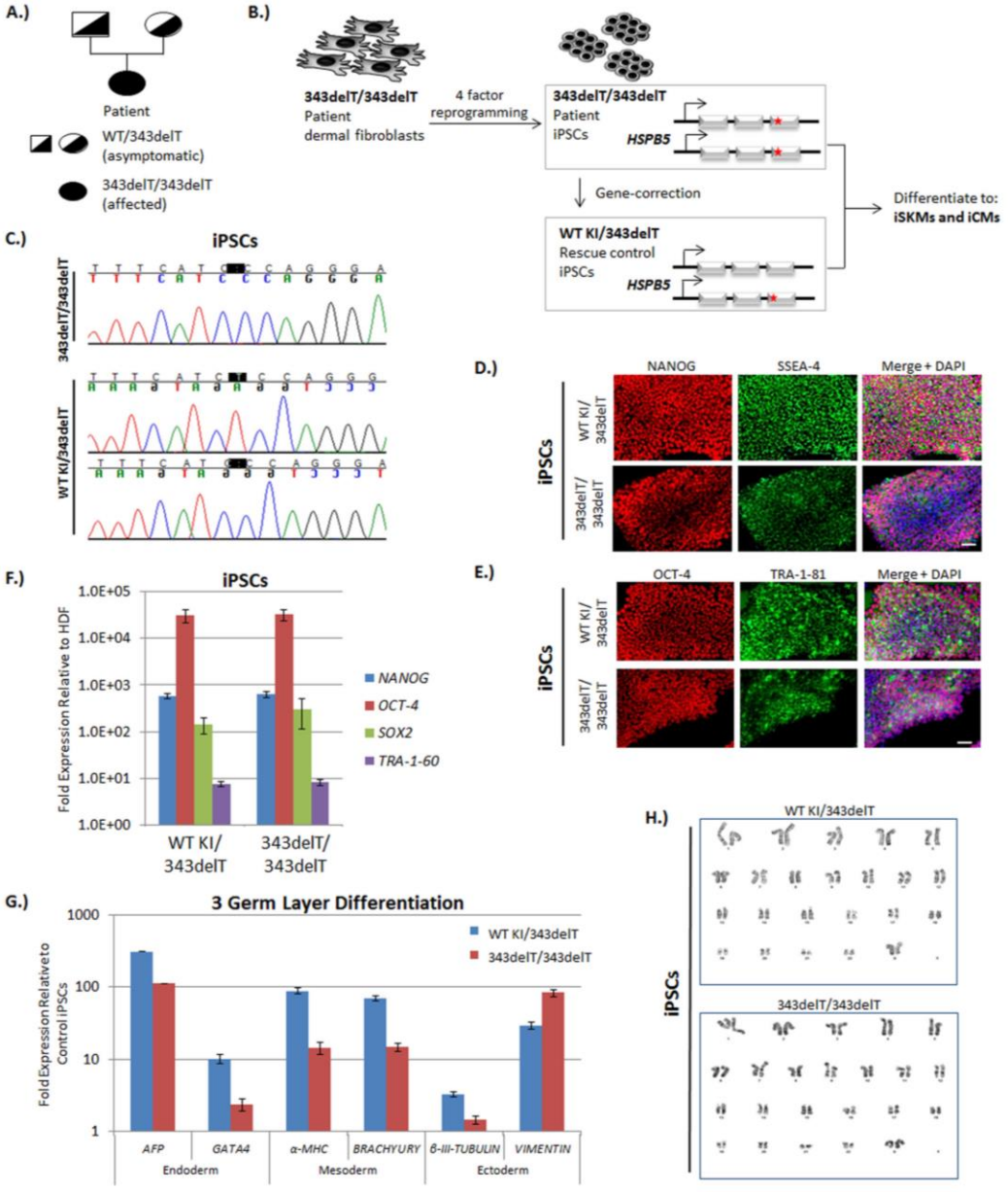

tein both through immunocytochemistry (Fig. 2, *A* and *B*) and Western blotting (Fig. 2, *D* and *E*) in the 343delT/343delT line when probed with an NT HSPB5 antibody. In the WT KI/343delT control, predicted to express both a 22-kDa-sized WT protein and a 15-kDa-sized 343delT protein, only the WT form of the protein is detectable (Fig. 2, *D* and *E*), indicating that lack of detectable 343delT is not due to immaturity of the cells. This result was surprising to us because the muscle biopsy from the patient showed dense, irregular staining of HSPB5 through immunohistochemistry and a 15-kDa-sized protein detectable by Western blotting with the NT HSPB5 antibody (29). Lack of 343delT protein was confirmed in a second iPSC line derived from the patient as well as the isogenic, heterozygous, gene-corrected control line derived from that iPSC line (supplemental Fig. S1). Additionally, homozygous knockin of the 343delT mutation into the endogenous *HSPB5* locus of an iPSC line derived from an unrelated, healthy individual also exhibited a complete lack of detectable 343delT protein (data not shown).

Because 343delT protein was not detectable, we next investigated whether this was due to defects in RNA levels. The 343delT transcript is not predicted to be a target for nonsense-mediated mRNA decay because the premature stop codon is downstream of the final exon-exon junction complex (33). Therefore, we hypothesized that 343delT transcript levels would be comparable with the WT. Quantitative real-time PCR (qRT-PCR) of iCMs and iSKMs revealed expression of *HSPB5* mRNA in both WT KI/343delT and 343delT/343delT (Fig. 2, *F* and *G*). *HSPB5* mRNA levels may differ depending on the efficiency of differentiation, which varies between iPSC lines and differentiation attempts, as noted by differences in expression of the muscle-specific gene *Troponin T* (*TNNT2*) (Fig. 2, *F* and *G*). Therefore, although the level of *HSPB5* mRNA cannot be directly compared between samples, we confirm that 343delT mRNA is present. Additionally, in contrast to an unstable mRNA control, *MYC*, levels of *HSPB5* mRNA did not decline in WT KI/343delT or 343delT/343delT iCMs with treatment of actinomycin D to inhibit transcription over 24 h (supplemental Fig. S2), indicating similar transcript stability in WT and 343delT. These results show that the defect in 343delT protein expression is not due to deficient transcript levels.

Lack of 343delT Protein Is Not Due to Degradation, MicroRNA Targeting, or Defective Translation—To further investigate the reason for lack of 343delT protein detection, we next examined protein degradation as a possible mechanism. iCMs were treated with the proteasomal inhibitor MG132 (34) (Fig. 3*A*). In contrast to the increase in the short-lived cell cycle inhibitor p21 with MG132 treatment (35), 343delT protein (15 kDa) remained undetectable in both WT KI/343delT and 343delT/343delT with inhibition of proteasomal degradation. Inhibition of autophagosome maturation with bafilomycin A1 for 12 h (36) was also insufficient to evoke 343delT protein detection in iCMs, although LC3-II (lower band) increased as expected with treatment (supplemental Fig. S3*A*). Additionally, treatment of 343delT/343delT iSKMs with the proteasomal inhibitor bortezomib for up to 48 h (37) (supplemental Fig. S3*B*) or MG132 for 12 h (supplemental Fig. S3*C*) and inhibition of autophagosome maturation with bafilomycin A1 for 12 h (supplemental Fig. S3*C*) were also insufficient to evoke 343delT detection. These data suggest that the lack of detectable 343delT protein is not due to degradation by the proteasome or autophagy. Complementary experiments of overexpression of 343delT in a human breast cancer cell line (MCF7 cells) showed that both inhibition of the proteasome (MG132) and autophagy (bafilomycin A1) resulted in slight increases in 343delT protein (supplemental Fig. S3, *D* and *E*). This result suggests that 343delT protein is likely degraded to some extent by the proteasome and autophagy, but this is not the major cause for our inability to detect 343delT protein in our iPSC model.

Another possibility we considered is that 343delT mRNA is differentially targeted compared with WT by a microRNA that inhibits translation. To examine this possibility, we transfected iCMs with siRNA to knock down dicer, the protein responsible for processing pre-microRNAs into mature microRNAs (38). Although knockdown of dicer was confirmed through decreased levels of dicer protein and elevated levels of c-MYC, a known target of dicer-dependent microRNAs (39), we were unable to detect 343delT protein in either WT KI/343delT or 343delT/343delT (Fig. 3*B*). This result suggests that 343delT is not differentially targeted by a dicer-dependent microRNA.

To confirm that there is no inherent defect in the translation efficiency of 343delT compared with WT, we performed an *in vitro* transcription/translation assay using rabbit reticulocyte lysate labeling-translated proteins with [^{35}S]L-methionine and [^{35}S]L-cysteine. We utilized a plasmid containing N-terminally MYC-tagged versions of WT (pCS2-MYC-WT) and 343delT (pCS2-MYC-343delT) and an SP6 promoter as the template for this reaction. Both WT and 343delT are visible after 30 min of incubation and increase after 90 min (Fig. 3*C*). No significant

FIGURE 1. **343delT iPSC generation and pluripotency characterization.** *A*, representative pedigree for the family of the homozygous recessive 343delT patient. Females are represented by *circles*, males by *squares*. *Filled shapes* represent homozygous 343delT. *Half-filled shapes* represent heterozygous 343delT. *B*, schematic of the experimental strategy. Dermal fibroblasts derived from the homozygous 343delT patient were reprogrammed into iPSCs (*343delT/343delT*), with the 343delT mutation indicated by *red stars*. Heterozygous gene-corrected control iPSCs were generated from the 343delT/343delT iPSCs through gene editing and have one copy of WT knocked into the *HSPB5* locus (*WT KI/343delT*). WT KI/343delT and 343delT/343delT iPSCs were differentiated to iCMs and iSKMs, respectively. *C*, direct Sanger sequencing of a PCR product covering the region of interest reveals deletion of the T at position 343 (highlighted in *black*) in the 343delT/343delT iPSCs. The PCR product from the WT KI/343delT iPSC line was TOPO-cloned into a vector, and multiple clones were sequenced. Reads showing WT (*top panel*) and 343delT (*bottom panel*) were observed, indicating that the WT KI/343delT iPSC line is heterozygous for this mutation. *D* and *E*, WT KI/343delT and 343delT/343delT iPSCs were stained with immunocytochemistry for the pluripotency markers nanog (*red*) and SSEA-4 (*green*) (*D*) and OCT-4 (*red*) and TRA-1–81 (*green*) (*E*). Nuclei were counterstained and merged with DAPI (*blue*). *Scale bars* = 50 μm. *F*, qRT-PCR was performed on WT KI/343delT and 343delT/343delT iPSCs, with the graph depicting mean ± S.E. relative expression levels of the pluripotency markers *NANOG*, *OCT-4*, *SOX2*, and *TRA-1–60* normalized to 18S rRNA and compared with human dermal fibroblasts (*HDF*) derived from the patient. *G*, WT KI/343delT and 343delT/343delT iPSCs differentiated to EZ spheres were taken at week 5 of differentiation for qRT-PCR analysis with markers of the three germ layers: endoderm (*AFP* and *GATA4*), mesoderm (*α-MHC* and *BRACHYURY*), and ectoderm (*β-III-TUBULIN* and *VIMENTIN*). The graph shows mean ± S.E. expression values normalized to 18s rRNA and compared with WT KI/343delT iPSCs. *H*, 20 proliferating cells were counted and fully analyzed using G-banding for each cell line, with representative karyotype images showing no consistent abnormalities.

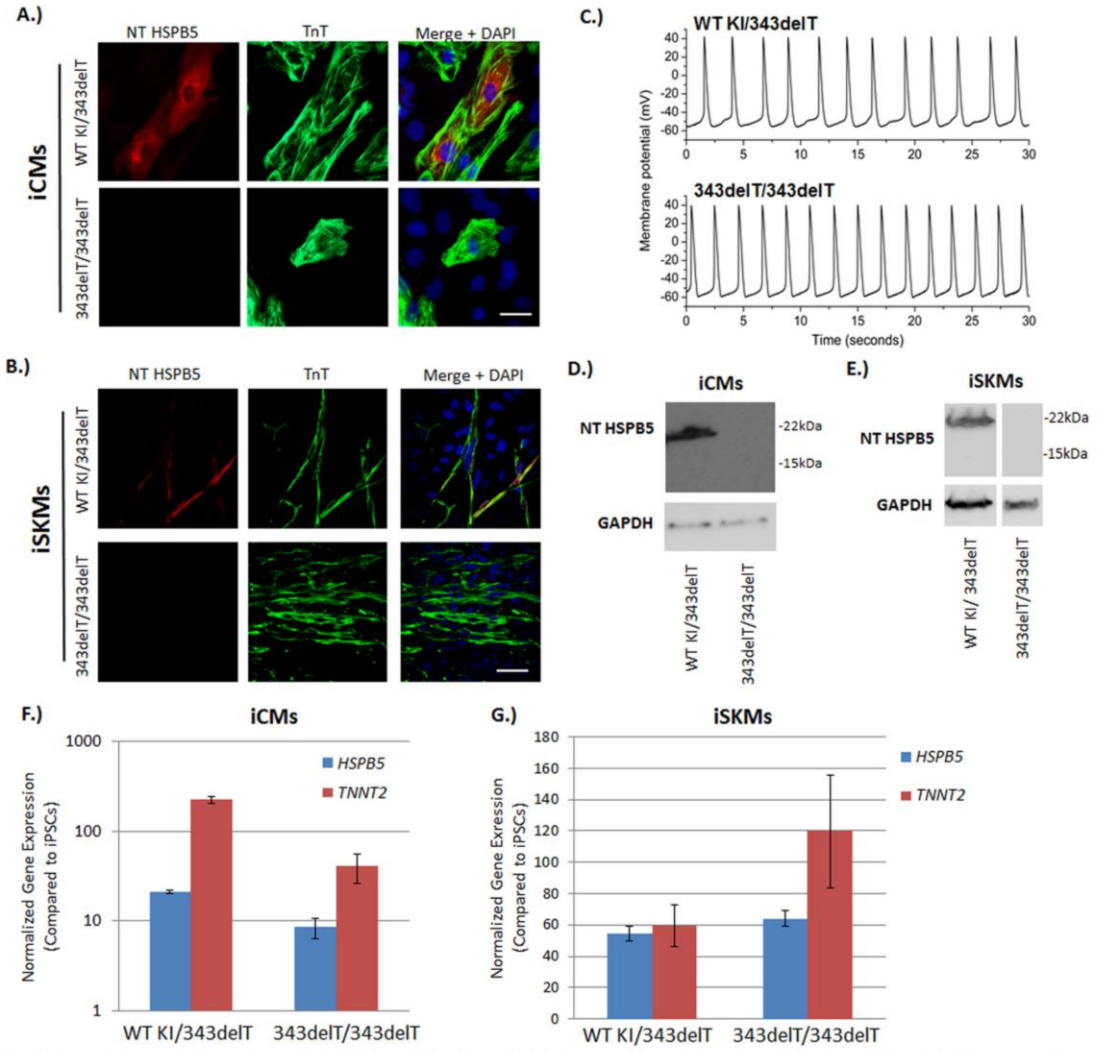

FIGURE 2. **343delT protein is not detectable in iSKMs or iCMs although RNA is present.** *A* and *B*, WT KI/343delT and 343delT/343delT iPSCs were differentiated to iCMs (*A*) or iSKMs (*B*)and stained with antibodies that recognized NT HSPB5 (*red*) and TnT (*green*) and merged with DAPI (*blue*). *Scale bars* = 50 μm. *C*, representative action potentials recorded from spontaneously beating WT KI/343delT (*top panel*) and 343delT/343delT iPSCs (*bottom panel*) cardiomyocytes ($n = 6$). Western blotting and qRT-PCR were performed on paired samples derived from WT KI/343delT and 343delT/343delT cells. *D* and *E*, Western blotting of WCL from iCMs (*D*) and iSKMs (*E*) probed with antibodies that recognize NT HSPB5 and GAPDH as a loading control. *F* and *G*, qRT-PCR of iCMs (*F*) and iSKMs (*G*) showing mean ± S.E. gene expression for *HSPB5* and *TROPONIN T* (*TNNT2*) normalized to 18s rRNA. Expression is shown as -fold change compared with undifferentiated iPSCs.

difference is observed between WT and 343delT in the rate of synthesis over time (21.8 ± 3.4 and 19.1 ± 6.9, respectively) of the recombinant protein. This result shows that 343delT is translated efficiently, at least in this reticulocyte lysate. *In toto*, these results demonstrate that lack of detectable 343delT protein in iCMs and iSKMs generated from 343delT/343delT and WT KI/343delT is not attributable to proteasomal degradation, autophagic degradation, microRNA targeting, or defective translation.

343delT Forms Insoluble Protein Aggregates and Induces a Cellular Stress Response When Overexpressed—The results presented above utilizing iCMs and iSKMs show an absence of detectable 343delT protein. The presence of mutant protein in the biopsy specimen of the protein suggests that accumulation of 343delT in the affected tissue may contribute to disease. For this reason, we attempted to simulate these conditions with our model to determine whether high levels of 343delT expression would result in aggregation in muscle cells.

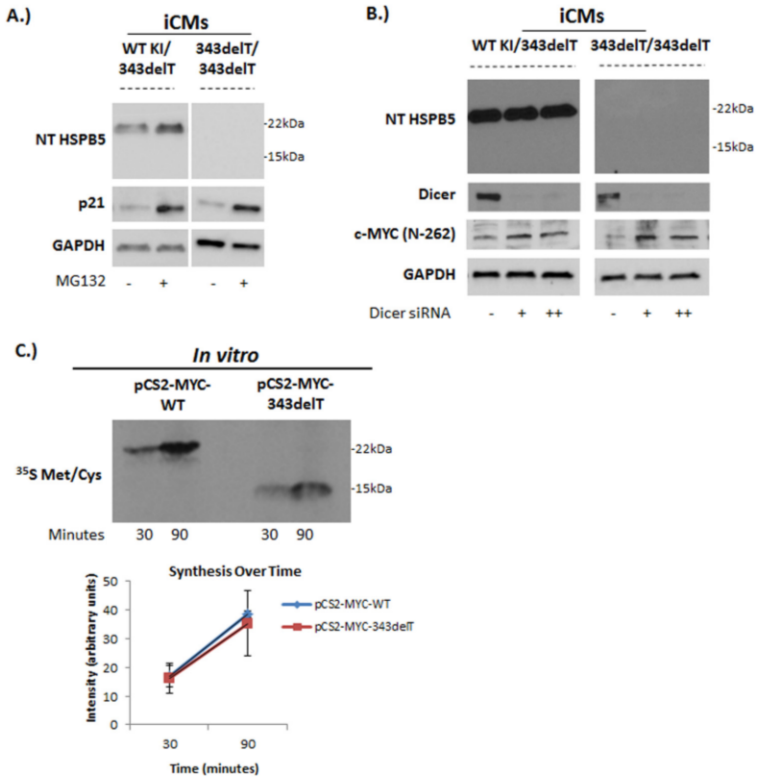

FIGURE 3. **Lack of 343delT protein is not due to degradation, microRNA targeting, or disrupted translation.** *A*, WT KI/343delT and 343delT/343delT iCMs were treated with DMSO or 10 μM MG132 to inhibit the proteasome for 12 h. Western blots of WCL were probed with antibodies recognizing NT HSPB5, p21, and GAPDH. Results are representative of two independent experiments. *B*, WT KI/343delT and 343delT/343delT iCMs were transfected with scrambled siRNA control (−) or either 40 pmol (+) or 80 pmol (++) of siRNA targeting dicer. Samples were harvested 72 h post-transfection, and WCL was run on a Western blot and probed with antibodies against NT HSPB5, dicer, c-MYC (N-262), and GAPDH. *C*, equal amounts of pCSC-MYC-WT and pCS2-MYC-343delT plasmids were entered into an *in vitro* transcription/translation (TnT) assay along with ^{35}S-labeled methionine/cysteine. Aliquots were taken from reactions at 30 and 90 min as indicated and separated by SDS-PAGE, transferred to nitrocellulose membranes, and exposed to film (*top panel*). The image is representative of three independent experiments, with the quantification (*bottom panel*) expressing synthesis over time as arbitrary units, indicating band intensity, showing mean ± S.D. There is no significant difference in the rate of synthesis over time for WT (21.8 ± 3.4) and 343delT (19.1 ± 6.9) as calculated by Student's *t* test ($p > 0.5$).

We transiently transfected N-terminally MYC-tagged WT or 343delT constructs (pCMV-MYC-WT and pCMV-MYC-343delT) into 343delT/343delT iSKMs. Overexpression of 343delT resulted in aggregation in iSKMs marked by TnT (Fig. 4*A*) or desmin (Fig. 4*B*), whereas overexpression of WT resulted in diffuse cytoplasmic staining (Fig. 4, *A* and *B*). 343delT aggregates exclude TnT and desmin. Similar aggregates of 343delT were observed with overexpression in 343delT/343delT iCMs (data not shown). These results indicate that, at high levels, 343delT forms aggregates in muscle cells.

Because overexpression of 343delT in iSKMs recapitulates aggregation observed in the biopsy of the patient, we examined whether overexpression in non-muscle cell lines also results in 343delT aggregation. Transfection is difficult in iCMs and iSKMs, and variances in differentiation efficiency may impact results, making overexpression studies in commercially available cells lines that lack endogenous HSPB5 expression, such as BHK21 cells (baby hamster kidney fibroblasts), more appealing. Overexpression of pCMV-MYC-343delT forms cytoplasmic aggregates in BHK21 cells (Fig. 4*C*), which are detectable with both NT HSPB5 and MYC tag antibodies. The absence of additional cell staining with NT HSPB5 relative to the MYC tag exemplifies the lack of endogenous HSPB5 expression. Aggregates in BHK21 cells typically appear in the perinuclear region and look similar to aggregates observed with overexpression in iSKMs (Fig. 4, *A* and *B*). Overexpression of pCMV-MYC-WT in BHK21 cells results in diffuse cytoplasmic staining (Fig. 4*C*). These experiments provide a proof of concept for the use of overexpression of 343delT in BHK21 cells as a platform to investigate 343delT aggregation and protein dynamics.

We noted that levels of 343delT protein expression were consistently lower than WT levels by immunocytochemistry and Western blotting when overexpressed in all cell lines tested. We confirmed equal transfection efficiency through co-transfection with a pCMV-dsRed plasmid (data not shown). Additionally, the levels of WT and 343delT mRNA were assessed

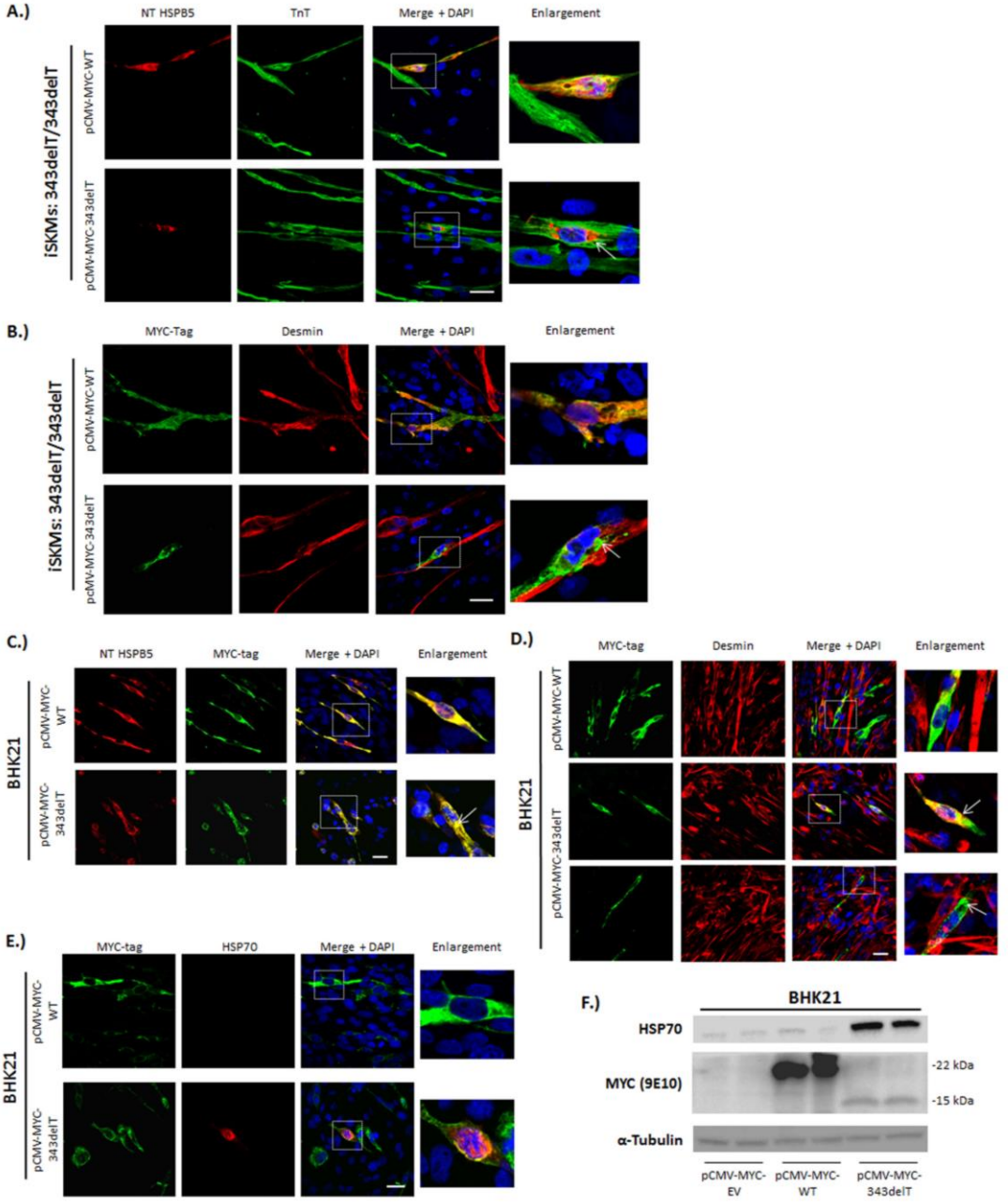

FIGURE 4. **343delT forms visible aggregates when overexpressed and induces a cellular stress response.** *A* and *B*, 343delT/343delT iSKMs were transfected with pCMV-MYC-WT or pCMV-MYC-343delT constructs. Cells were stained 48 h post-transfection with antibodies recognizing NT HSPB5 (*red*) and TnT (*green*) (*A*) and MYC tag (*green*) and desmin (*red*) (*B*). *Scale bars* = 25 μm. *C–E*, BHK21 cells were transfected with pCMV-MYC-WT or pCMV-MYC-343delT constructs for 24 h and co-stained with antibodies against NT HSPB5 (*red*) and MYC tag (*green*) (*C*) MYC tag (*green*) and desmin (*red*) (*D*), and MYC-tag (*green*) and HSP70 (*red*) (*E*). *Scale bars* = 50 μm. In all merged immunocytochemistry images, nuclei were counterstained and merged with DAPI (*blue*). Enlargements of the area within the *white dotted box* are shown at the *right*. *Arrows* indicate 343delT aggregates. F, WCL from BHK21 cells transfected as above or similarly with pCMV-MYC-empty vector (*EV*) were analyzed by Western blotting with antibodies recognizing HSP70, MYC (9E10), and α-tubulin as a loading control. Samples were run in duplicate.

between 2 and 24 h after transfection and determined to be similar (supplemental Fig. S4*A*). RNA levels correlated with transfection efficiency for the WT construct (supplemental Fig. S4*B*). Transfection with either WT or 343delT impacted neither cell proliferation nor viability (supplemental Fig. S5, *A* and *B*) when compared with empty vector transfection over a similar period. These results indicate that transfection efficiencies and RNA levels were equal and that cell proliferation and viability were unaffected by transfection.

The metastable desmin protein is a known client for HSPB5 (12–14) and is present in aggregates in patients with desmin-related (cardio)myopathy (25, 26, 40). Although 343delT aggregates did not colocalize with desmin in iSKMs, we wanted to examine this in BHK21 cells, which express endogenous desmin as well (26, 31). 343delT aggregates in BHK21 cells colocalize with desmin in some (Fig. 4*D*, *center panels*) but not all cells (Fig. 4*D*, *bottom panels*), potentially indicating stochastic incorporation of desmin into aggregates.

Misfolded proteins and protein aggregates are triggers for the induction of a cellular stress response driven by the master regulatory transcription factor HSF1 (41). This response results in the up-regulation of genes whose promoters contain heat shock response elements, including HSP70 (as reviewed in Ref. 2). Indeed, overexpression of 343delT in BHK21 cells resulted in induction of HSP70 in some but not all transfected cells (Fig. 4*E*), whereas, in WT, it does not result in HSP70 induction (Fig. 4*E*). We further confirmed this induction by Western blotting (Fig. 4*F*). These results indicate that 343delT can induce a cellular stress response when overexpressed. Consistent up-regulation of HSP70 in 343delT/343delT iCMs under basal conditions was not observed (data not shown), indicating that perhaps the detectable, aggregated form of 343delT and/or the presence of other proteins in the aggregates is required for up-regulation of HSP70.

Together, these results show the ability of 343delT to form visible, cytoplasmic aggregates when overexpressed in muscle and non-muscle cells, with potentially stochastic incorporation of desmin into these aggregates, at least in non-muscle cells. Additionally, HSP70 induction demonstrates disruption in overall protein homeostasis with overexpression of 343delT.

Co-Expression with WT Solubilizes 343delT—Because 343delT is a recessively inherited mutation, to mimic the unaffected heterozygous parents, we co-transfected HA-tagged WT and MYC-tagged 343delT constructs (pCMV-HA-WT HSPB5 and pCMV-MYC-343delT HSPB5) into cell lines in equimolar ratios. In the presence of WT, 343delT no longer formed aggregates in BHK21 cells (Fig. 5*A*, *bottom panels*). Additionally, when expressed alone, 343delT was present almost entirely in the insoluble fraction (99 ± 1%, mean ± S.D., $n = 3$), whereas, when co-expressed with WT, the percentage of insoluble 343delT was reduced 6.6-fold (15% ± 6%, mean ± S.D., $n = 3$, $p < 0.01$ as calculated by Student's t test) (Fig. 5, *B* and *C*). The percentage of insoluble 343delT was quantified using the 15-kDa-sized band ($[\text{insoluble}]_{\text{density}} \times 100/([\text{insoluble}]_{\text{density}} + [\text{soluble}]_{\text{density}})$). Larger molecular weight bands may be post-translationally modified forms of the protein. Inclusion of these bands in the analysis does not impact the relative percentage of insoluble 343delT. These results indicate that the presence of WT shifts 343delT from the insoluble to the soluble fraction.

To determine whether 343delT and WT are interacting, we co-transfected HA-tagged WT and MYC-tagged 343delT and performed co-immunoprecipitation (Co-IP). IP of HA resulted in the pulldown of MYC-tagged 343delT only in the co-transfected sample (Fig. 5*D*). Reciprocally, IP of MYC resulted in the pulldown of HA-tagged WT only in the co-transfected sample (Fig. 5*D*). The insoluble pellet fraction demonstrated that much of the 343delT protein, when transfected alone, was insoluble (Fig. 5*D*), consistent with the idea that WT solubilizes 343delT. These results demonstrate an interaction between WT and 343delT proteins within the cell.

343delT Solubility: in Vitro and in Vivo—In line with overexpression in mammalian cell lines, the overexpression of recombinant 343delT in *Escherichia coli* resulted in an insoluble product exclusively found in inclusion bodies (Fig. 6*A*). Refolding of 343delT in the absence of WT predominantly led to the formation of insoluble aggregates (Fig. 6*B*). Conversely, the presence of an excess of WT during the entire refolding process resulted in the formation of a soluble product (Fig. 6*B*). This mixture eluted from gel filtration in a single peak with a slight shoulder at an elution volume of ~10 ml, slightly earlier than refolded WT, which eluted at 10.5 ml (Fig. 6*C*). SDS-PAGE of the resulting fractions showed the co-elution of 343delT (14.7 kDa) with WT (20.2 kDa) across the entire peak, whereas only a single band at the WT mass was visible in the control (Fig. 6*C*, *inset*). To obtain a higher-resolution view of the oligomers formed, we performed native mass spectrometry (42). A spectrum of WT reveals a broad region of signal centered around 10,000 *m/z*, resulting from the overlap of a large number of charge states (Fig. 6*D*), and consistent with a polydisperse ensemble of oligomers (43). A spectrum obtained for the 343delT:WT mixture at identical mass spectrometry conditions reveals an additional charge series at ~2000 *m/z*, corresponding to a mass of 14,695 Da, which can be assigned to the monomeric form of 343delT (Fig. 6*D*). Interestingly, the charge states populated are relatively low, indicative of a largely folded conformation of the 343delT monomers free in solution. Examination of the high *m/z* region of the spectrum for WT allows the assignment of overlapping charge state envelopes to the oligomers comprising the ensemble. Strikingly, many additional features are observed in the spectra for the 343delT:WT mixture (Fig. 6*D*, *inset*). The complexity of the spectrum is such that individual oligomers cannot be directly identified; however, by comparison with the WT data it is clear that they cannot be explained by integer stoichiometries of WT HSPB5 but, rather, that an ensemble of hetero-oligomers is present, resulting from a direct interaction between the two proteins. These *in vitro* data further support the notion that WT solubilizes 343delT through a direct interaction.

We hypothesized that extreme insolubility of 343delT was responsible for our inability to detect the mutant protein in iSKMs and iCMs and for lower levels of 343delT compared with WT upon overexpression. We have excluded many reasons for the absence of detectable 343delT protein noted above, including mRNA instability, degradation by the proteasome or autophagy, targeting by a dicer-dependent microRNA, and defective translation. Decreased detectable 343delT protein compared with WT was consistently observed both through analyses by Western blotting and immunocytochemistry. We

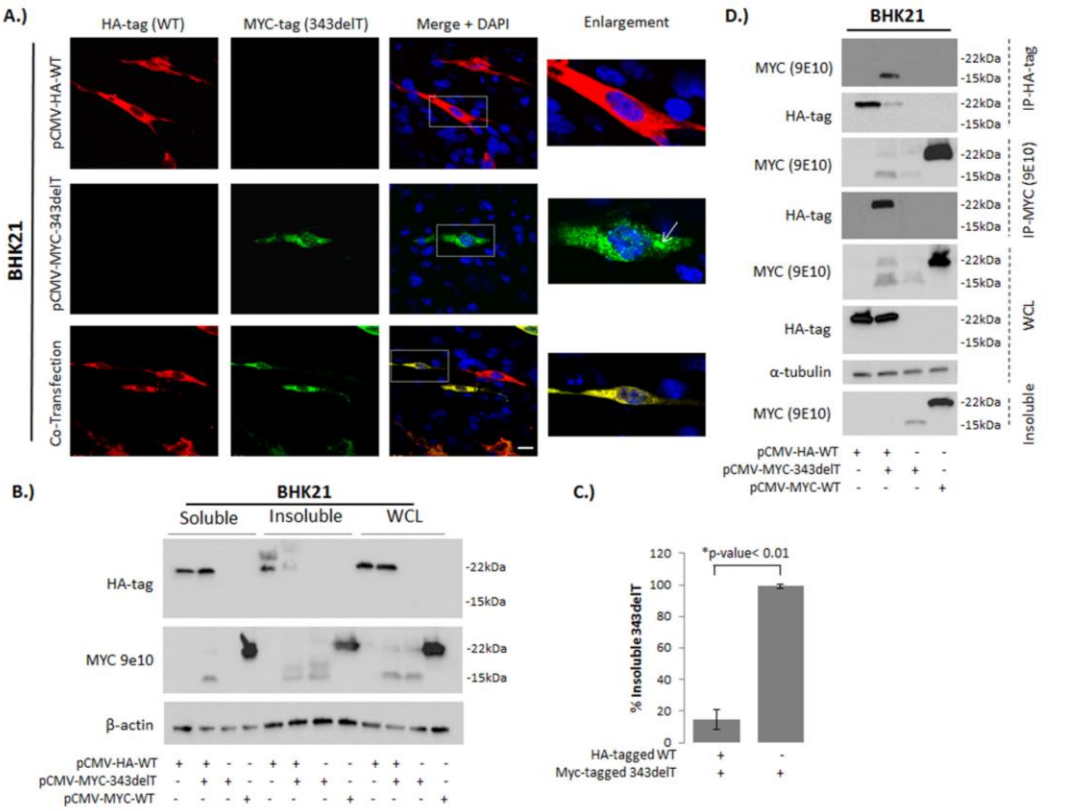

FIGURE 5. **WT co-expression reduces 343delT aggregates and increases solubility of the mutant protein.** *A*, BHK21 cells were transfected with pCMV-HA-WT, pCMV-MYC-343delT, or both (co-transfection) and stained with antibodies against HA tag and MYC tag after 24 h. Nuclei were counterstained and merged with DAPI (*blue*). Enlargements of the area within the *white dotted box* are shown at the *right*. *Arrows* indicate 343delT aggregates. *Scale bar* = 50 μm. *B*, BHK21 cells were transfected with pCMV-HA-WT, pCMV-HA-WT, and pCMV-MYC-343delT (co-transfection), pCMV-MYC-343delT, or pCMV-MYC-WT, harvested 24 h post-transfection, and fractionated into soluble and insoluble fractions or WCL. Equal amounts of protein were loaded for Western blotting using an anti-MYC (9E10) antibody and an HA tag antibody with β-actin as a loading control. The image depicts representative blots from three independent experiments. *C*, the percentage of insoluble 343delT, quantified using the 15-kDa-sized band ([insoluble] $_{density}$ × 100/([insoluble] $_{density}$ + [soluble] $_{density}$). Insoluble 343delT is reduced 6.6-fold by co-expression with WT (343delT alone = 99% ± 1% insoluble 343delT, 343delT + WT = 15% ± 6% insoluble 343delT, mean ± S.D., $n = 3$, $p < 0.01$ as calculated by Student's *t* test). *D*, BHK21 cells transfected as in *B* were harvested after 24 h for co-IP using RIPA buffer and immunoblotted with anti-HA tag or anti-MYC (9E10) antibodies. Western blotting was performed, showing IP fractions as well as WCL and the insoluble fraction (the remaining pellet from the sample solubilized in RIPA buffer) and stained with antibodies against MYC (9E10), HA tag, and α-tubulin as a loading control.

tested additional lysis buffers to determine whether we could detect 343delT by Western blotting, including RIPA buffer, 100% formic acid, and 8 M urea plus 2% SDS. We observed a consistent lack of 343delT protein in iCMs with all tested buffers (data not shown).

Addition of a small ubiquitin-related modifier (SUMO) to proteins has been shown to enhance their solubility (44, 45). To directly test our hypothesis that the insolubility of 343delT is the reason for low levels of detection with overexpression, we generated SUMO-HSPB5 fusion constructs. These plasmids contain a version of WT and 343delT HSPB5 that are N-terminally MYC-tagged followed by SUMO, preceding the HSPB5 variant. We used a non-cleavable version of SUMO3 Q89P (46) in this construct to prevent removal of SUMO by endogenous deSUMOylases. MYC tag-only versions of the constructs were used as controls. Expression of SUMOylated constructs in BHK21 cells results in a 130 ± 60 and 5 ± 1 (mean ± S.D.) -fold increase in 343delT and WT, respectively (Fig. 6*E*). The larger increase of 343delT compared with WT through the addition of SUMO ($p < 0.05$, calculated by Student's *t* test) suggests that the increase in mutant protein is likely not due to inherent stabilization and/or enhanced transcription/translation of proteins by SUMO addition. If this were the case, similar increases in WT and 343delT would be expected. Elevated detection of 343delT was also observed with overexpression of 343delT and SUMOylated 343delT in 343delT/343delT iCMs, resulting in 811 ± 218-fold (mean ± S.D.) enhanced detection of the SUMOylated protein by Western blotting (Fig. 6*F*). These results suggest that our suboptimal ability to detect 343delT is due to extreme insolubility of the mutant protein in both non-muscle and muscle cells.

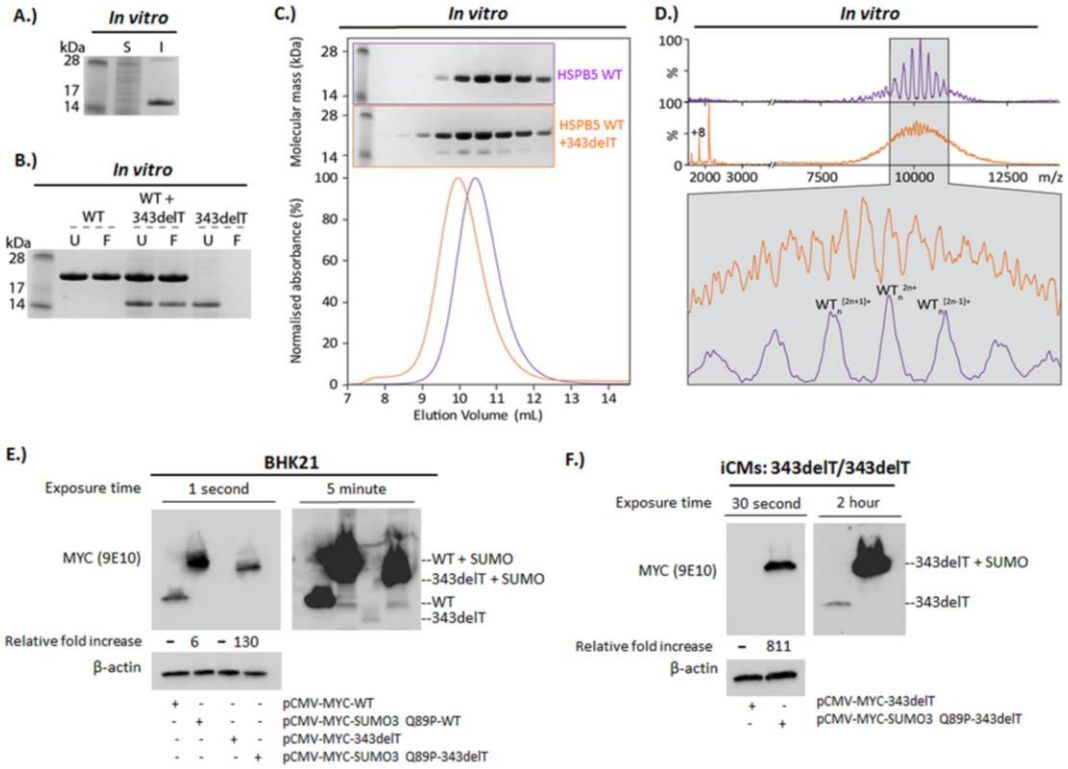

FIGURE 6. **In vitro refolding of 343delT in the presence of WT and SUMOylation in cells rescue 343delT insolubility.** *A*, recombinant 343delT expressed in *E. coli* was found to accumulate within insoluble inclusion bodies (*I*) and not within the soluble lysate (*S*). *B*, refolding WT or a 343delT:WT mixture resulted in a soluble product that was not removed upon passing through a 0.22-μm filtration device. Refolding of 343delT in the absence of WT resulted in aggregates that were removed from solution upon filtration. *U*, unfiltered; *F*, filtered. *C*, 300 μl of refolded WT and refolded 343delT:WT mixture from *B* was loaded in subsequent runs onto a Superdex 200 10/300 column (pre-equilibrated into 200 mM ammonium acetate (pH 6.9). Separation was carried out at a flow rate of 0.4 ml/min, and absorbance was monitored at 280 nm. The chromatogram for the 343delT:WT mixture (*orange*) had a slight shoulder and was shifted to earlier elution volumes compared with WT alone (*purple*). 9 μl of fractions 9–17 were analyzed by SDS-PAGE for each run, alongside molecular weight markers. These revealed the co-elution of 343delT with WT. *D*, corresponding fractions from each run in *C* were analyzed by means of native mass spectrometry. The control containing WT displayed a complicated overlapping signal centered near 10,000 *m/z*, relating to multiple charge state series of WT oligomers. For the mixture, two areas of interest were identified, a region around 10,000 *m/z* akin to the WT spectra and a charge state series at 2000 *m/z*. This was identified to correspond to monomeric 343delT (molecular mass = 14,695 Da). Close inspection of the region at high *m/z* (*inset*) reveals peaks in the 343delT:WT mixture that cannot arise from WT homo-oligomers but, rather, correspond to an ensemble of hetero-oligomers comprising both HSPB5 components. *E*, BHK21 cells were transfected with pCMV-MYC-WT, pCMV-MYC-SUMO3 Q89P-WT, pCMV-MYC-343delT, or pCMV-MYC-SUMO3 Q89P-343delT and harvested 24 h post-transfection, and WCL was isolated. Equal amounts of protein were loaded for Western blotting using an anti-MYC (9E10) antibody with β-actin as a loading control. The image depicts a representative blot from three independent experiments, with longer exposure shown at the *right*. The relative increase in WT and 343delT proteins with the addition of SUMO is indicated below the respective lanes. WT increased 6 $\pm$ 1-fold, whereas 343delT increased 130 $\pm$ 60-fold (mean $\pm$ S.D. of three independent experiments) with $p < 0.05\%$ as calculated by Student's *t* test. *F*, 343delT/343delT iCMs were transfected with pCMV-MYC-343delT or pCMV-MYC-SUMO3 Q89P-343delT and harvested 24 h post-transfection. Analysis of WCL by Western blotting was performed using an anti-MYC (9E10) antibody with β-actin as a loading control, with longer exposure shown at the *right*. The relative increase in 343delT protein with the addition of SUMO is indicated (811 $\pm$ 218-fold) as mean $\pm$ S.D. of three independent experiments.

Discussion

Together, the data presented here describe molecular defects observed with disease-causing 343delT. Although mRNA is unaffected, basal levels of 343delT protein in iCMs or iSKMs were undetectable in both WT KI/343delT and 343delT/343delT cell lines. Detection of the WT-sized protein, but not the truncated 343delT-sized protein in the heterozygous WT KI/343delT iPSC-derived cells, indicates that the absence of 343delT is not due to lack of maturation. Several possibilities, such as proteasomal degradation, autophagic degradation, Dicer-dependent microRNA targeting, and inherent translational defects, were examined and proved to be unlikely mechanisms responsible for the lack of detectable 343delT protein. Overexpression of 343delT consistently resulted in much lower levels of protein compared with WT as well. Greatly enhanced detection of 343delT when fused to SUMO3 Q89P, a non-cleavable form of SUMO known to enhance protein solubility, is consistent with extreme insolubility of 343delT as the reason for lack of protein detection.

It is conceivable that insoluble 343delT would be unavailable to perform essential, normal functions of HSPB5 in muscle cells, suggesting that loss of HSPB5 function contributes to myopathy in the patient harboring homozygous 343delT. HSPB5 specifically plays key chaperone roles for proteostasis and

protein quality control, differentiation, and maintenance in muscle cells (12–23). Loss of these or other functions of HSPB5 may leave myotubes vulnerable to stress, prone to muscle breakdown with increased usage, and/or have an impact on regeneration of skeletal muscle from satellite cells. Although absent at presentation, the early onset of the skeletal myopathy in the patient does not preclude later development of cardiac manifestations.

Although 343delT protein is observed in the patient skeletal muscle biopsy, it does appear at lower levels when compared with a control individual (29). Nonetheless, endogenous detection of the mutant protein was not observed in our iPSC-derived cells. Potentially, our model does not recapitulate 343delT expression observed in the patient for reasons related to the culture environment (pH differences, two-dimensional cell culture *versus* three-dimensional tissue structure, oxygen levels, etc.), stress (contraction, muscle turnover), variability in experimental techniques, age- and tissue-dependent, and other factors. This may illustrate the inherent limitations of iPSCs in modeling diseases because of an accumulation of stressors over time, also corresponding to the observation that the patient was entirely normal until disease onset at 4 months of age. Therefore, we hypothesize that the iPSCs recapitulate what may have occurred early in the patient, *i.e.* prior to disease manifestation. 343delT may be packaged into a completely insoluble state when expressed at basal levels, and its accumulation over time could result in 343delT surpassing a threshold, thereby allowing detection. The potential change in protein status may or may not contribute to disease. It is of interest that the severity and early-onset nature of the autosomal recessive disease in the 343delT patient is not consistent with the DKO mouse (20), which develops progressive myopathy into adulthood. We recognize that these differences could be due to species variation and/or the DKO mouse also lacking HSPB2. Alternatively, the presence of 343delT protein could exacerbate the phenotypes observed in the complete loss of function scenario (DKO mouse).

Co-aggregation of 343delT with desmin was observed upon overexpression of 343delT in some but not all BHK21 cells but was not observed with overexpression in iSKMs. Other mutations in *HSPB5*, such as R120G (26, 40), result in co-aggregation of the mutant protein with desmin, and patients are termed to have desmin-related (cardio)myopathy. The stochastic accumulation of desmin in 343delT aggregates is likely due to loss of 343delT chaperone function toward aggregation-prone desmin, resulting in the two proteins clustered together, among other proteins, in aggregates. The extent of desmin accumulation in aggregates likely depends on overall protein homeostasis within the cell. The finding that overexpression of 343delT induced elevated levels of HSP70 in BHK21 cells is consistent with cells suffering from an imbalance in protein homeostasis. We did not observe consistently elevated HSP70 levels in 343delT/343delT iCMs under basal conditions, which indicates that the presence of detectable 343delT (*i.e.* the visible aggregated form) and potentially other proteins present in the aggregates are required for disruption of protein homeostasis.

The recessive nature of 343delT led us to investigate the interaction between 343delT and WT HSPB5. It is unknown whether the heterozygous parents, who are non-consanguineous and healthy, express detectable levels of the 343delT protein. Potentially, expression of 343delT in the heterozygous state may not be detrimental, as we have shown increased solubility of 343delT and loss of aggregate formation upon co-expression with equimolar WT. Our co-IP experiments demonstrate an interaction between 343delT and WT within the cell. Together, these data suggest that WT solubilizes 343delT. Additionally, the presence of WT during refolding of 343delT rescues the protein from forming insoluble aggregates *in vitro*. The shift in elution volume during size exclusion and co-elution of the proteins, as observed by SDS-PAGE, suggest the formation of a complex between WT and 343delT, which is confirmed directly by native mass spectrometry experiments. The observation of a large proportion of what appears, from the absence of highly charged 343delT species, to be solution-phase monomeric 343delT in the mass spectrum suggests a labile interaction, especially under the conditions used, consistent with a chaperone-like interaction. The ability of WT to solubilize 343delT and the presence of unaffected WT protein to perform normal cellular functions likely result in the parents being asymptomatic.

Overall, our data support loss of HSPB5 function as a likely mechanism contributing to the myopathy. Given the substantial number of protein aggregation diseases, the findings reported here have direct implications for understanding the mechanisms of variable expressivity of both disease susceptibility and resistance. Although we cannot exclude the presence of the mutant protein directly contributing to disease, any detrimental effects of the 343delT protein would likely be ameliorated by the presence of WT through solubilization. Exogenous expression of WT HSPB5 by a gene therapy approach may therefore improve symptoms in mutant HSPB5-induced myopathy. Design of effective delivery methods for exogenous chaperones to the tissue or gene/cell therapy would be necessary for this treatment.

Experimental Procedures

Reprogramming Patient Dermal Fibroblasts to iPSCs—Dermal fibroblasts were isolated from the patient containing the 343delT mutation (29) with written consent of the mother of the patient and with research ethics committee approval at Guy's and St. Thomas' NHS Foundation Trust (London, UK) for biobank storage and transfer of samples for use in an ethically approved research project. Fibroblast culture and further research in the laboratory were performed with appropriate institutional review board approval at the University of Utah (Salt Lake City, UT) and the Medical College of Wisconsin (Milwaukee, WI) for use of human cells. Dermal fibroblasts expanded in DMEM supplemented with 10% FBS and 100 units of penicillin/100 μg of streptomycin/ml of medium (P/S) (all from Life Technologies) were reprogrammed into iPSCs through transduction with four retroviruses carrying the genes *OCT-4*, *SOX2*, *c-MYC*, and *KLF4* as described previously (30). Following transduction, transduced fibroblasts were seeded onto SNL feeder cells (Cell Biolabs) that were mitotically inactivated through treatment with Mitomycin C (ATCC) in ESC medium composed of knockout DMEM supplemented with 20% knockout serum replacement, minimum essential medi-

um-non-essential amino acids, 2 mM L-glutamine (all from Life Technologies), P/S, 0.1 mM β-mercaptoethanol (Sigma), 10 ng/ml human basic FGF (Cell Signaling Technology), and 50 ng/ml L-ascorbic acid (Sigma). The resulting iPSC clones were manually picked and maintained on feeder cells in ESC medium for four passages before transitioning to feeder-free culture as described below.

iPSC Culture—iPSCs were routinely cultured under feeder-free conditions on Matrigel (Corning)-coated dishes with mTeSR1 (Stem Cell Technologies) or StemMACS iPS-Brew XF (Miltenyi Biotec). Cells were passaged every 3–4 days using Accutase (Life Technologies) and seeded in medium containing 10 μM Rho-associated kinase inhibitor (Y-27632, Selleck) for 24 h following passaging.

Gene Editing in iPSCs, Genotyping, and Sequencing—iPSCs derived from the homozygous recessive 343delT patient (343delT/343delT) were gene-corrected to generate heterozygous 343delT iPSCs (WT KI/343delT) using a protocol modified from a previously defined strategy that involves knockin/excision of a selection cassette (32). Briefly, zinc finger nucleases were designed and generated by Sigma (CompoZr custom zinc finger nucleases). The targeting vector was designed and synthesized using Gene Art (Life Technologies) containing a portion of the WT *HSPB5* sequence with a silent mutation (435 G>T) to generate a TTAA site for *piggyBac* excision. The puromycin/thymidine kinase selection cassette driven by the phosphoglycerate kinase promoter (PGK-*puroΔtk*) and flanked by *piggyBac* repeats was cloned from the pPB-CAG-OSKM-puDtk vector (Sanger Institute) into the targeting vector through In-Fusion Cloning (CloneTech). Components were transfected into iPSCs using a 4D-Nucleofector and P4 nucleofector solution with program CB-150 (Lonza), followed by seeding onto SNL feeder cells and selection with 0.5–1 μg/ml puromycin (InvivoGen) from days 5–12 post-transfection. The resulting puromycin-resistant clones were manually picked and genotyped. Heterozygous knockin clones were selected for excision of the selection cassette and transfected with an excision-only *piggyBac* transposase (PBx, Transposagen), followed by negative selection with 0.5 μM ganciclovir (Cayman Chemicals). The resulting colonies were picked and genotyped. PCR products from WT KI/343delT iPSCs were cloned into a TOPO vector (Life Technologies), and plasmids were isolated from bacterial colonies and Sanger-sequenced by Retrogen (San Diego, CA) to confirm heterozygosity for the 343delT mutation and incorporation of the engineered silent mutation. WT KI/343delT iPSCs were expanded and transitioned to feeder-free culture as described above.

Immunocytochemistry—Cells on 4% paraformaldehyde (Sigma)-fixed glass coverslips were permeabilized with 0.1% Triton X-100 (Sigma), blocked with 3% bovine serum albumin (Ultrapure BSA, Cell Signaling Technology), and stained appropriately before finally mounting with Ultracruz Hard Set mounting medium plus DAPI (Santa Cruz Biotechnology). Primary antibodies were as follows: NANOG (Cell Signaling Technology, 4903p, 1:200), SSEA-4 (Stem Cell Technologies, 60062AD, 1:40), OCT-4 (Cell Signaling Technology, 2840, 1:400), TRA-1–81 (Abcam, ab16289, 1:100), NT HSPB5 (NovaCastra ABCrys513, Leica, 1:100), TnT (Abcam, 45932, 1:500), MYC tag (Cell Signaling Technology, 2278, 1:100), desmin (Dako, M0760, 1:100), HSP70 (Stress Marq, SMC-100A/B, 1:100), and HA tag (Invivogen, ab-hatag, 1:500). Secondary antibodies were as follows: Alexa Fluor 488 donkey anti-rabbit IgG and Alexa Fluor 555 donkey anti-mouse IgG (Life Technologies, 1:500). Images were taken on a Nikon A1 confocal microscope.

qRT-PCR—RNA was isolated using the PureLink RNA Mini-Prep kit (Life Technologies), followed by treatment with the DNA-free DNA removal kit (Life Technologies). cDNA was generated using the high-capacity cDNA reverse transcription kit (Life Technologies). qRT-PCR was performed using a Bio-Rad CFX 96 thermocycler with Qiagen QuantiTect SYBR Green PCR mixture and QuantiTect primer assays (Qiagen). Bio-Rad CFX Manager software was used for data analysis.

Karyotyping—Karyotyping was performed by Wisconsin Diagnostic Laboratories (formerly Dynacare Laboratories, Milwaukee, WI).

iCM and iSKM Differentiation—iCM differentiation was performed using chemical modulation of the Wnt pathway modified from a previously described protocol (47). Briefly, iPSCs at 100% confluency were overlaid with Matrigel in mTeSR1 or StemMACS iPS-Brew XF medium on day 1. On day 0, cells were treated with 12 μmol/liter Chir-99021 (Selleck) and 10 ng/ml human Activin-A (R&D Systems) in RPMI minus insulin medium (RPMI supplemented with 1× B27 supplement minus insulin (both from Life Technologies). On day 2, the medium was changed to RPMI minus insulin. On day 3, cells were treated with 5 μmol/liter IWP-2 (Stem Cell Technologies) in RPMI minus insulin, with medium subsequently changed on day 5 to RPMI minus insulin. The medium was changed to Complete medium, RPMI supplemented with 1× B27 supplement (Life Technologies) and P/S, on day 7 and changed every 2–3 days thereafter until cells were utilized for experiments around day 30 of differentiation. iCMs were passaged prior to experiments using TrypLE Express (Life Technologies) and seeded in Complete medium containing 10% FBS and 10 μM Rho-associated kinase inhibitor on 0.1% gelatin-coated surfaces.

iSKMs were differentiated using the EZ sphere protocol as described previously (48). Week 5 EZ spheres where treated with Accutase and pelleted for qRT-PCR of markers for all three germ layers. Week 6 EZ spheres were terminally differentiated as described previously (48) for 3 weeks prior to the experiments. Immunocytochemistry was performed directly on cells differentiated on coverslips.

Electrophysiology of iCMs—Action potentials were recorded using intracellular sharp electrodes. Coverslips containing beating clusters of iCMs were placed in Tyrode solution and held at physiological temperature with a heated recording chamber (TC-344B, Warner Instruments). Sharp electrodes were pulled from borosilicate glass (FHC, Inc.) using a Sutter model P-97 to resistances of 50–70 MΩ when backfilled with 3 M KCl. Recordings were acquired using a Multiclamp 700B amplifier (Molecular Devices) interfaced with a Digidata 1449A (Molecular Devices). The pClamp software suite (version 10, Molecular Devices) was used for data acquisition and analysis.

Graphing of representative action potentials was performed using Origin software (OriginLab).

Cell Fractionation Assay and Western Blotting—Detergent-soluble, detergent-insoluble, and whole cell lysate (WCL) fractions were isolated, and Western blotting was performed as described previously (49), except equal amounts of protein were separated on Mini-Protean TGX gels, 4–20% (Bio-Rad). Primary antibodies were as follows: NT HSPB5 (NovaCastra ABCrys513, Leica, 1:100), GAPDH (Cell Signaling Technology, 2118, 1:10,000), p21 (Santa Cruz Biotechnology, sc-sc397, 1:250), LC3 (Novus, NB100–2220, 1:10,000), dicer (Santa Cruz Biotechnology, sc-393328, 1:100), c-MYC N-262 (Santa Cruz Biotechnology, sc-764, 1:500), MYC 9E10 (Santa Cruz Biotechnology, sc-40, 1:200), HSP70 (Stress Marq, SMC-100A/B, 1:1,000), α-tubulin (Santa Cruz Biotechnology, sc-5546, 1:500), β-actin (Abcam, ab6276, 1:5000), and HA tag (Invivogen, ab-hatag, 1:1000). Quantification of band intensity was performed using ImageJ or Image Lab 5.2.1 (Bio-Rad) software.

Inhibition of the Proteasome and Autophagosome Maturation—iCMs and iSKMs were treated with DMSO, 10 μM MG132, or 10 or 100 nM bortezomib to inhibit the proteasome or 80 nM bafilomycin A1 to inhibit autophagosome maturation for 12 h.

Dicer Knockdown—iCMs were transfected with scrambled siRNA control (−) or either 40 pmol (+) or 80 pmol (++) of siRNA targeting dicer (Santa Cruz Biotechnology) using Lipofectamine RNAi Max (Life Technologies). Samples were harvested 72 h post-transfection.

HSPB5 Vector Constructs—pCMV N-terminal MYC-tagged WT and HA-tagged WT (pCMV-MYC-WT and pCMV-HA-WT, respectively) were generated previously (49). The pCMV-MYC-343delT construct was produced by *in vitro* site-directed mutagenesis as described previously (49). MYC-WT and MYC-343delT were PCR-amplified from pCMV-MYC vectors and cloned into a pCS2 vector that contained an SP6 promoter required for the TnT assay (see below). For SUMOylated constructs, a gBlock gene fragment (Integrated DNA Technologies) was purchased, containing the non-cleavable SUMO3 Q89P sequence obtained from the pcDNA3 MYC-SUMO3Q89P vector (Addgene plasmid 48963) (46), and cloned into the pCMV-MYC-WT and 343delT constructs. The resulting constructs, pCMV-MYC-SUMO3 Q89P-WT and pCMV-MYC-SUMO3 Q89P-343delT, were a fusion in the N to C-terminal direction of MYC-SUMO3Q89P-WT and 343delT HSPB5, respectively.

In Vitro Transcription/Translation Assay—The TnT SP6 quick-coupled transcription/translation system (Promega) was used with EXPRE^{35}S^{35}S protein labeling mix (PerkinElmer Life Sciences) containing both [^{35}S]L-methionine and [^{35}S]L-cysteine. The pCS2-MYC-WT and 343delT plasmids were used as template DNA in the reaction according to the instructions of the manufacturer. Samples were subsequently run on a 12% SDS-PAGE gel, transferred to nitrocellulose membranes, and exposed to film at −80 °C. Quantification of band intensity was performed using ImageJ software.

Transfection—iSKMs were transfected using Lipofectamine 3000 (Life Technologies) according to the instructions of the manufacturer.

BHK21 cells (ATCC) were cultured in Glasgow medium supplemented with 5% tryptose phosphate broth (both from Life Technologies), 15% FBS, and P/S. BHK21 cells were transfected with Lipofectamine 3000 according to the instructions of the manufacturer. For co-transfection of two plasmids, equal amounts of each plasmid were used, with empty vector plasmid added to single-plasmid transfections to control for the total DNA amount.

iCMs were passaged and resuspended in P3 nucleofection solution (Lonza) and transected using the CA-137 program on the 4D nucleofector system (Lonza). Following transfection, cells were seeded onto fibronectin-coated surfaces (Corning) in Complete medium supplemented with 10% FBS and Rho-associated kinase inhibitor.

Co-immunoprecipitation—Cell pellets were resuspended in RIPA buffer (Thermo Scientific) supplemented with Halt protease and phosphatase inhibitor (Thermo Scientific), sonicated on ice, and centrifuged at 4 °C for 10 min at 12,000 × *g*. A portion was removed here for WCL, diluted with 4× XT sample buffer (Bio-Rad), and boiled for 5 min. The remaining WCL was used for IP performed with protein G-Sepharose 4 Fast Flow beads (Genesee). Samples were precleared through incubation with beads for 45 min on a rotisserie shaker at 4 °C, followed by preincubation with 200 μg/ml antibody, either MYC 9E10 (Santa Cruz Biotechnology, sc-40) or HA (Invivogen, ab-hatag) for 30 min at 4 °C with intermittent vortexing. Beads were added to the sample/antibody mixture and incubated on a rotisserie shaker for 1 h at 4 °C. Bead-bound samples were washed six times with RIPA buffer and finally resuspended in RIPA buffer with 4× XT sample buffer, boiled for 5 min, and centrifuged for 30 s at 12,000 × *g*. The insoluble pellet, prior to IP, was washed twice with RIPA buffer, resuspended in 4× XT sample buffer, boiled for 5 min, and centrifuged for 30 s at 12,000 × *g*. All fractions were loaded onto Mini-Protean TGX gels, 4–20% (Bio-Rad). Western blotting was performed as described above.

In vitro 343delT Protein Expression, Refolding, and Purification—The 343delT plasmid, purchased from GenScript, was transformed into BL21 (DE3) Stratagene Gold-competent cells (Agilent Technologies) and plated on kanamycin-selective plates. A single colony was picked and used to inoculate 5 ml of Luria-Bertani broth (Fisher). This culture was incubated at 37 °C, 220 rpm overnight until a high optical density was achieved. 1 liter of Luria-Bertani broth was then inoculated with 10 ml of the overnight culture and grown at 37 °C, 200 rpm, until an optical density of between 0.6–0.8 was obtained. To induce 343delT expression, a final concentration of 0.5 mM isopropyl 1-thio-β-D-galactopyranoside (Merck) was added, and cultures were grown for a further 3 h before harvesting by centrifugation. Cell pellets were then stored at −80 °C for future use. Cells were thawed, resuspended, and lysed in 50 mM Tris (Sigma), 0.1 mM EDTA (Sigma), 0.1 mM DTT (Sigma), 0.1 M NaCl (Sigma), 5% glycerol (Fisher) (pH 7.9) (lysis buffer) containing a cOmplete EDTA-free protease inhibitor tablet (Roche). Post-clarification, overexpressed 343delT was shown to reside within insoluble inclusion bodies and not within the soluble lysate. The insoluble pellet was resuspended in lysis buffer, and any remaining cells were lysed by an additional son-

ication step. Membrane elements were solubilized by the addition of a final concentration of 1% Triton X-100 (Promega). This preparation was left to incubate for 15 min on ice before centrifugal clarification. Two further washes of the inclusion body pellet were carried out in lysis buffer to remove the remaining Triton X-100. Clean inclusion body pellets were then solubilized in 6 M GuHCl (Sigma), 50 mM Tris, 0.1 mM EDTA, 0.1 mM DTT, 5% glycerol (pH 7.9) and agitated at room temperature for 1 h, with any remaining insoluble material being removed by centrifugation. The protein concentration of the sample was estimated from UV absorbance measurements, and 2 molar equivalents of WT HSPB5 were added. Protein refolding was achieved by gradually reducing the concentration of GuHCl by stepwise dialysis, initially to 2 M, 1 M, and then 0 M to ensure that refolding was complete. Samples were passed through a 0.22 μM Spin X centrifuge tube (Fisher Scientific) and loaded onto a Superdex 200 10/300 column (GE Healthcare) to further purify and exchange buffer into 200 mM ammonium acetate (Sigma, pH 6.9). Fractions could then be analyzed by SDS-PAGE before being selected for mass spectrometry analysis.

Mass Spectrometry—Complex-containing samples were analyzed by nanoelectrospray mass spectrometry without the need for further sample preparation or concentration. Transmission pressures and energies on a Synapt G1 HDMS (Waters Corp.) were optimized to preserve non-covalent interactions but to maintain the transmission of large assemblies. Spectra were obtained using a previously defined protocol (42) under the following conditions: capillary, 1.5 kV; cone, 50 V; extractor, 3.0 V; trap, 8.0 V; transfer, 8.0 V; analyzer pressure, 1.58 e^{-3} millibar; backing pressure, 5.8 e^{0} millibar. All spectra were processed and analyzed in MassLynx V4.1.

Author Contributions—K. A. M., P. L., F. D. L. K., H. J., E. W., A. M. G., J. L. P. B., M. R., E. S. C., A. C. M., and I. J. B. conceived and designed the experiments. K. A. M., P. L., M. J. C., F. D. L. K, S. L., K. D. K., Q. D., M. N. G., H. Z., G. M. T., Q. L., J. A. H., R. B., and J. L. P. B. performed the experiments. K. A. M., P. L., F. D. L. K., W. M. K., M. T. T., K. B., A. M. G., J. L. P. B., M. R., E. S. C., A. C. M., and I. J. B interpreted the data. K. A. M. wrote the manuscript. F. D. L. K., K. D. K., H. J., J. L. P. B., E. S. C., A. C. M., and I. J. B. edited the article.

Acknowledgments—We are grateful to the clinicians involved in the care of our patient, including Dr. Andrew Durward and Dr. Jane Heraghty at the Evelina Children's Hospital, Guy's and St. Thomas NHS Foundation Trust (London, UK). We also thank Stefan Buk and Dr. Safa Al-Saraj (both King's College, London, UK) and Dr. Caroline Sewry (Dubowitz Neuromuscular Centre, Great Ormond Street Children's Hospital) for expert neuropathological input. We are grateful to Dr. Allison Ebert and Dr. Jered McGivern (both Medical College of Wisconsin, Milwaukee, WI) for instruction in the EZ sphere protocol for skeletal muscle differentiation.

References

1. Morimoto, R. I. (1998) Regulation of the heat shock transcriptional response: cross talk between a family of heat shock factors, molecular chaperones, and negative regulators. *Genes Dev.* **12,** 3788–3796
2. Christians, E. S., Yan, L. J., and Benjamin, I. J. (2002) Heat shock factor 1 and heat shock proteins: critical partners in protection against acute cell injury. *Crit. Care Med.* **30,** S43–S50
3. Gopal-Srivastava, R., and Piatigorsky, J. (1993) The murine α B-crystallin/small heat shock protein enhancer: identification of α BE-1, α BE-2, α BE-3 and MRF control elements. *Mol. Cell. Biol.* **13,** 7144–7152
4. Gopal-Srivastava, R., Haynes, J. I., 2nd, and Piatigorsky, J. (1995) Regulation of the murine aB-crystallin/small heath shock protein gene in cardiac muscle. *Mol. Cell. Biol.* **15,** 7081–7090
5. Poulain, P., Gelly, J. C., and Flatters, D. (2010) Detection and architecture of small heat shock protein monomers. *PLoS ONE* **5,** e9990
6. Hochberg, G. K., and Benesch, J. L. (2014) Dynamical structure of αB-crystallin. *Prog. Biophys. Mol. Biol.* **115,** 11–20
7. Hochberg, G. K., Ecroyd, H., Liu, C., Cox, D., Cascio, D., Sawaya, M. R., Collier, M. P., Stroud, J., Carver, J. A., Baldwin, A. J., Robinson, C. V., Eisenberg, D. S., Benesch, J. L., and Laganowsky, A. (2014) The structured core domain of αB-crystallin can prevent amyloid fibrillation and associated toxicity. *Proc. Natl. Acad. Sci. U.S.A.* **111,** E1562–1570
8. Peschek, J., Braun, N., Rohrberg, J., Back, K. C., Kriehuber, T., Kastenmüller, A., Weinkauf, S., and Buchner, J. (2013) Regulated structural transitions unleash the chaperone activity of αB-crystallin. *Proc. Natl. Acad. Sci. U.S.A.* **110,** E3780–E3789
9. Rajagopal, P., Tse, E., Borst, A. J., Delbecq, S. P., Shi, L., Southworth, D. R., and Klevit, R. E. (2015) A conserved histidine modulates HSPB5 structure to trigger chaperone activity in response to stress-related acidosis. *eLife* **4,** 1–21
10. Clark, A. R., Naylor, C. E., Bagnéris, C., Keep, N. H., and Slingsby, C. (2011) Crystal structure of R120G disease mutant of human αB-crystallin domain dimer shows closure of a groove. *J. Mol. Biol.* **408,** 118–134
11. Mainz, A., Peschek, J., Stavropoulou, M., Back, K. C., Bardiaux, B., Asami, S., Prade, E., Peters, C., Weinkauf, S., Buchner, J., and Reif, B. (2015) The chaperone αB-crystallin uses different interfaces to capture an amorphous and an amyloid client. *Nat. Struct. Mol. Biol.* **22,** 898–905
12. Houck, S. A., Landsbury, A., Clark, J. I., and Quinlan, R. A. (2011) Multiple sites in αB-crystallin modulate its interaction with desmin filaments assembled *in vitro*. *PLoS ONE* **6,** e25859
13. Perng, M. D., Cairns, L., van den Ijssel, P., Prescott, A., Hutcheson, A. M., and Quinlan, R. A. (1999) Intermediate filament interactions can be altered by HSP27 and αB-crystallin. *J. Cell Sci.* **112,** 2099–2112
14. Bennardini, F., Wrzosek, A., and Chiesi, M. (1992) α B-crystallin in cardiac tissue: association with actin and desmin filaments. *Circ. Res.* **71,** 288–294
15. Bullard, B., Ferguson, C., Minajeva, A., Leake, M. C., Gautel, M., Labeit, D., Ding, L., Labeit, S., Horwitz, J., Leonard, K. R., and Linke, W. A. (2004) Association of the chaperone αB-crystallin with titin in heart muscle. *J. Biol. Chem.* **279,** 7917–7924
16. Golenhofen, N., Arbeiter, A., Koob, R., and Drenckhahn, D. (2002) Ischemia-induced association of the stress protein α B-crystallin with I-band portion of cardiac titin. *J. Mol. Cell. Cardiol.* **34,** 309–319
17. Golenhofen, N., Perng, M. D., Quinlan, R. A., and Drenckhahn, D. (2004) Comparison of the small heat shock proteins αB-crystallin, MKBP, HSP25, HSP20, and cvHSP in heart and skeletal muscle. *Histochem. Cell Biol.* **122,** 415–425
18. Kötter, S., Unger, A., Hamdani, N., Lang, P., Vorgerd, M., Nagel-Steger, L., and Linke, W. A. (2014) Human myocytes are protected from titin aggregation-induced stiffening by small heat shock proteins. *J. Cell Biol.* **204,** 187–202
19. Singh, B. N., Rao, K. S., Ramakrishna, T., Rangaraj, N., and Rao, C. M. (2007) Association of αB-crystallin, a small heat shock protein, with actin: role in modulating actin filament dynamics *in vivo*. *J. Mol. Biol.* **366,** 756–767
20. Brady, J. P., Garland, D. L., Green, D. E., Tamm, E. R., Giblin, F. J., and Wawrousek, E. F. (2001) aB-Crystallin in Lens development and muscle integrity: a gene knockout approach. *Invest. Ophthalmol. Vis. Sci.* **42,** 2924–2934
21. Morrison, L. E., Whittaker, R. J., Klepper, R. E., Wawrousek, E. F., and Glembotski, C. C. (2004) Roles for αB-crystallin and HSPB2 in protecting the myocardium from ischemia-reperfusion-induced damage in a KO mouse model. *Am. J. Physiol. Heart Circ. Physiol.* **286,** H847–H855
22. Kumarapeli, A. R., Su, H., Huang, W., Tang, M., Zheng, H., Horak, K. M.,

Li, M., and Wang, X. (2008) α B-crystallin suppresses pressure overload cardiac hypertrophy. *Circ. Res.* **103,** 1473–1482
23. Neppl, R. L., Kataoka, M., and Wang, D. Z. (2014) Crystallin-αB regulates skeletal muscle homeostasis via modulation of Argonaute2 activity. *J. Biol. Chem.* **289,** 17240–17248
24. Christians, E. S., Ishiwata, T., and Benjamin, I. J. (2012) Small heat shock proteins in redox metabolism: implications for cardiovascular diseases. *Int. J. Biochem. Cell Biol.* **44,** 1632–1645
25. Mitzelfelt, K. A., and Benjamin, I. J. (2015) in *The Big Book on Small Heat Shock Proteins* (Tanguay, R. M., and Hightower, L. E., eds.), 1st ed., pp. 269–299, Springer International Publishing, Switzerland
26. Vicart, P., Caron, A., Guicheney, P., Li, Z., Prévost, M. C., Faure, A., Chateau, D., Chapon, F., Tomé, F., Dupret, J. M., Paulin, D., and Fardeau, M. (1998) A missense mutation in the αB-crystallin chaperone gene causes a desmin-related myopathy. *Nat. Genet.* **20,** 92–95
27. Elliott, J. L., Der Perng, M., Prescott, A. R., Jansen, K. A., Koenderink, G. H., and Quinlan, R. A. (2013) The specificity of the interaction between αB-crystallin and desmin filaments and its impact on filament aggregation and cell viability. *Philos. Trans. R Soc. Lond. B Biol. Sci.* **368,** 20120375
28. Wang, X., Osinska, H., Klevitsky, R., Gerdes, A. M., Nieman, M., Lorenz, J., Hewett, T., and Robbins, J. (2001) Expression of R120G- B-crystallin causes aberrant Desmin and B-Crystallin aggregation and cardiomyopathy in mice. *Circ. Res.* **89,** 84–91
29. Forrest, K. M., Al-Sarraj, S., Sewry, C., Buk, S., Tan, S. V., Pitt, M., Durward, A., McDougall, M., Irving, M., Hanna, M. G., Matthews, E., Sarkozy, A., Hudson, J., Barresi, R., Bushby, K., *et al.* (2011) Infantile onset myofibrillar myopathy due to recessive CRYAB mutations. *Neuromuscul. Disord.* **21,** 37–40
30. Takahashi, K., Okita, K., Nakagawa, M., and Yamanaka, S. (2007) Induction of pluripotent stem cells from fibroblast cultures. *Nat. Protoc.* **2,** 3081–3089
31. Christians, E. S., Banerjee Mustafi, S., and Benjamin, I. J. (2014) Chaperones and cardiac misfolding protein diseases. *Curr. Protein Pept. Sci.* **15,** 189–204
32. Yusa, K., Rashid, S. T., Strick-Marchand, H., Varela, I., Liu, P. Q., Paschon, D. E., Miranda, E., Ordóñez, A., Hannan, N. R., Rouhani, F. J., Darche, S., Alexander, G., Marciniak, S. J., Fusaki, N., Hasegawa, M., *et al.* (2011) Targeted gene correction of α1-antitrypsin deficiency in induced pluripotent stem cells. *Nature* **478,** 391–394
33. Amrani, N., Sachs, M. S., and Jacobson, A. (2006) Early nonsense: mRNA decay solves a translational problem. *Nat. Rev. Mol. Cell Biol.* **7,** 415–425
34. Lee, D. H., and Goldberg, A. L. (1998) Proteasome inhibitors: valuable new tools for cell biologists. *Trends Cell Biol.* **8,** 397–403
35. Bloom, J., Amador, V., Bartolini, F., DeMartino, G., and Pagano, M. (2003) Proteasome-mediated degradation of p21 via N-terminal ubiquitinylation. *Cell* **115,** 71–82
36. Yamamoto, A., Tagawa, Y., Yoshimori, T., Moriyama, Y., Masaki, R., and Tashiro, Y. (1998) Bafilomycin A1 prevents maturation of autophagic vacuoles by inhibiting fusion between autophagosomes and lysosomes in rat hepatoma cell line, H-4-II-E cells. *Cell Struct. Funct.* **23,** 33–42
37. Nawrocki, S. T., Carew, J. S., Dunner, K., Jr., Boise, L. H., Chiao, P. J., Huang, P., Abbruzzese, J. L., and McConkey, D. J. (2005) Bortezomib inhibits PKR-like endoplasmic reticulum (ER) kinase and induces apoptosis via ER stress in human pancreatic cancer cells. *Cancer Res.* **65,** 11510–11519
38. Flores-Jasso, C. F., Arenas-Huertero, C., Reyes, J. L., Contreras-Cubas, C., Covarrubias, A., and Vaca, L. (2009) First step in pre-miRNAs processing by human Dicer. *Acta Pharmacol. Sin.* **30,** 1177–1185
39. Jackstadt, R., and Hermeking, H. (2015) MicroRNAs as regulators and mediators of c-MYC function. *Biochim. Biophys. Acta* **1849,** 544–553
40. Perng, M. D., Wen, S. F., van den Ijssel, P., Prescott, A. R., and Quinlan, R. A. (2004) Desmin aggregate formation by R120G αB-crystallin is caused by altered filament interactions and is dependent upon network status in cells. *Mol. Biol. Cell* **15,** 2335–2346
41. Vabulas, R. M., Raychaudhuri, S., Hayer-Hartl, M., and Hartl, F. U. (2010) Protein folding in the cytoplasm and the heat shock response. *Cold Spring Harb. Perspect. Biol.* **2,** 1–18
42. Kondrat, F. L., Struwe, W., and Benesch, J. P. (2015) in *Structural Proteomics* (Owens, R. J., ed.) pp. 349–371, Springer, New York
43. Aquilina, J. A., Benesch, J. L., Bateman, O. A., Slingsby, C., and Robinson, C. V. (2003) Polydispersity of a mammalian chaperone: mass spectrometry reveals the population of oligomers in αB-crystallin. *Proc. Natl. Acad. Sci. U.S.A.* **100,** 10611–10616
44. Peroutka, R. J., Elshourbagy, N., Piech, T., and Butt, T. R. (2008) Enhanced protein expression in mammalian cells using engineered SUMO fusions: secreted phospholipase A(2). *Protein Sci.* **17,** 1586–1595
45. Panavas, T., Sanders, C., and Butt, T. (2009) SUMO fusion technology for enhanced protein production in prokaryotic and eukaryotic expression systems. *Methods Mol. Biol.* **497,** 303–317
46. Békés, M., Prudden, J., Srikumar, T., Raught, B., Boddy, M. N., and Salvesen, G. S. (2011) The dynamics and mechanism of SUMO chain deconjugation by SUMO-specific proteases. *J. Biol. Chem.* **286,** 10238–10247
47. Lian, X., Zhang, J., Azarin, S. M., Zhu, K., Hazeltine, L. B., Bao, X., Hsiao, C., Kamp, T. J., and Palecek, S. P. (2013) Directed cardiomyocyte differentiation from human pluripotent stem cells by modulating Wnt/β-catenin signaling under fully defined conditions. *Nat. Protoc.* **8,** 162–175
48. Hosoyama, T., McGivern, J. V., Van Dyke, J. M., Ebert, A. D., and Suzuki, M. (2014) Derivation of myogenic progenitors directly from human pluripotent stem cells using a sphere-based culture. *Stem Cells Transl. Med.* **3,** 564–574
49. Zhang, H., Rajasekaran, N. S., Orosz, A., Xiao, X., Rechsteiner, M., and Benjamin, I. J. (2010) Selective degradation of aggregate-prone CryAB mutants by HSPB1 is mediated by ubiquitin-proteasome pathways. *J. Mol. Cell. Cardiol.* **49,** 918–930

Human 343delT HSPB5 Chaperone associated with Early-onset Skeletal Myopathy causes Defects in Protein Solubility

Katie A. Mitzelfelt, Pattraranee Limphong, Melinda J. Choi, Frances D.L. Konrat, Shuping Lai, Kurt D. Kolander, Wai-Meng Kwok, Qiang Dai, Michael N. Grzybowski, Huali Zhang, Graydon M. Taylor, Qiang Lui, Mai T. Thao, Judith A. Hudson, Rita Barresi, Kate Bushby, Heinz Jungbluth, Elizabeth Wraige, Aron M. Geurts, Justin L.P. Benesch, Michael Riedel, Elisabeth S. Christians, Alex C. Minella, Ivor J. Benjamin

SUPPLEMENTARY DATA

Supplementary Figure S1: Lack of 343delT Protein in an Alternate iPSC Line
An alternate iPSC line derived from 343delT/343delT patient dermal fibroblasts was gene-corrected using the same approach as described previously. Both lines were differentiated to iCMs and iSKMs and a western blot was performed and probed with antibodies that recognize NT HSPB5 and GAPDH as a loading control.

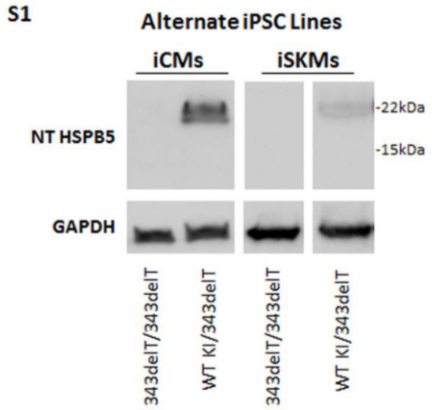

Supplementary Figure S2: 343delT Transcript Stability

To measure *HSPB5* transcript stability, iCMs were re-plated on day 27 as described in Experimental Procedures and seeded into a 12 well 0.1% gelatin coated plate at 80% confluency. The following day, cells were treated with 1μM actinomycin D (Sigma) to inhibit transcription and harvested at indicated time points for qRT-PCR. *HSPB5* mRNA and *MYC* (an unstable control mRNA) levels were normalized to *18s rRNA* and plotted as mean ± s.e.m. expression relative to 0 hour WT KI/343delT sample. Data is representative of two independent experiments performed. Decrease in *MYC* transcript levels from 0-4 hours indicates the actinomycin D treatment successfully inhibited transcription. *HSPB5* levels did not decline over 24 hours, indicating transcript stability. The unexpected increase in *HSPB5* mRNA levels may be explained by incomplete inhibition of transcription by actinomycin D, which acts as a cellular stress and upregulates stress response genes including *HSPB5.*

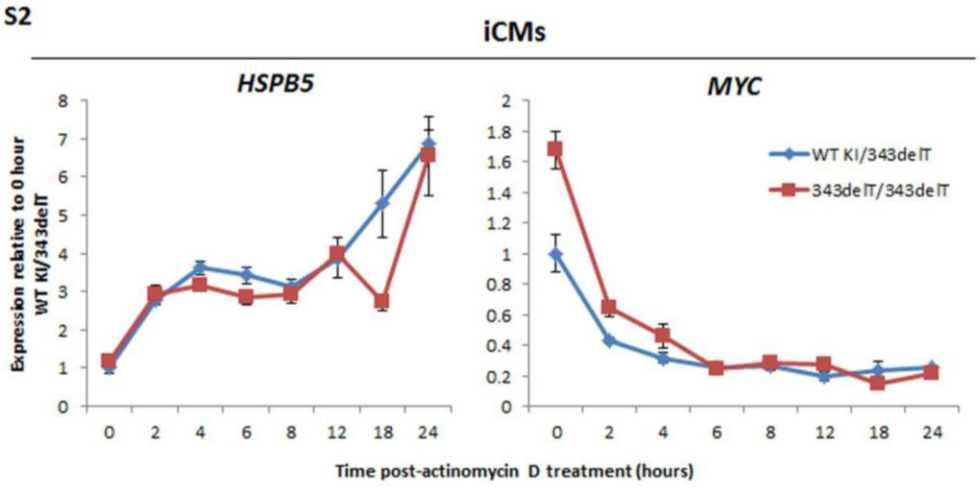

Supplementary Figure S3: Overexpressed 343delT Protein is Degraded by Both the Proteasome and Autophagy

A.) 343delT/343delT iCMs were treated with DMSO or 80 nM bafilomycin A1 to inhibit autophagy for 12 hours. Western blots of WCL were probed with antibodies recognizing NT HSPB5, LC3, and GAPDH. Results are representative of two independent experiments. B.) 343delT/343delT iSKMs were treated with DMSO (-) or 10 or 100nM bortezomib for 24 or 48 hours to inhibit the proteasome and WCLs were probed by western blot with antibodies recognizing NT HSPB5, p21, and GAPDH. C.) 343delT/343delT iSKMs were treated with DMSO (-), 80nM bafilomycin A1, or 10μM MG132 for 12 hours and WCL were run on western blots probed with antibodies recognizing NT HSPB5, LC3, p21, and GAPDH. MCF7 cells were transfected with pCMV-MYC-WT or 343delT constructs for 24 hours followed by treatment with DMSO, 5 μM MG132, or 80 nM bafilomycin (Baf) for 12 hours. D.) Western blots with 5 μg (WT) or 60 μg (343delT) of WCL were stained with antibodies against MYC (9E10) and GAPDH as a loading control. Samples are shown in duplicates. Results are representative of two independent experiments. E.) 5 μg of protein for each of the same samples in (D) was run on a gel and stained with antibodies against p21, LC3, and GAPDH. Both inhibition of the proteasome (MG132) and inhibition of autophagosome maturation (Baf) resulted in slightly elevated levels of 343delT.

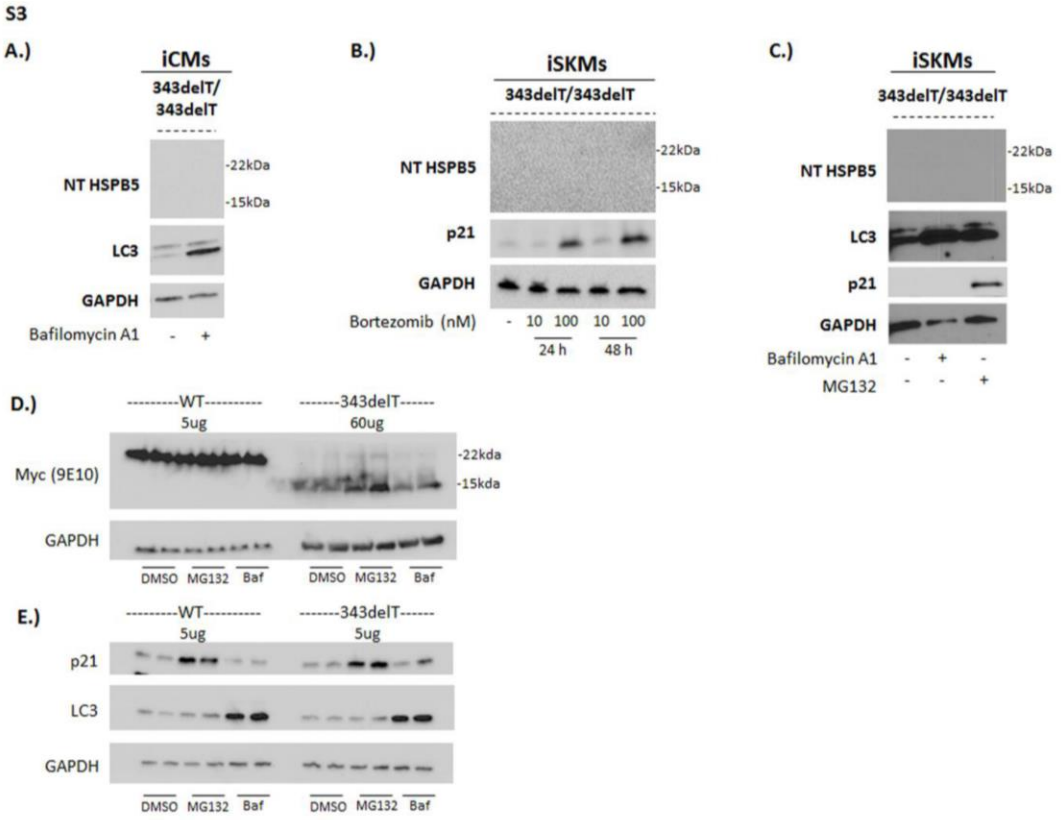

Supplementary Figure S4: Transfection and RNA levels are Equal between WT and 343delT
A.) MCF7 cells transfected with pCMV-MYC-WT or 343delT HSPB5 constructs were harvested 2, 4, 6, or 24 hour after transfection for qRT-PCR. Graph shows mean ± s.e.m. ΔCt values for *HSPB5* normalized to *18s rRNA* from n=3. B.) MCF7 cells were transfected with empty vector (EV) (1 μg) or pCMV-MYC-WT in increasing amounts (0.01 μg, 0.1 μg, 1 μg). Samples (n=4 for each group) were harvested 24 hours after transfection and divided using half for qRT-PCR analysis of gene expression (left graph) and the other half fixed and analyzed by flow cytometry (right graph). *HSPB5* gene expression is normalized to *18s rRNA*, with the graph expressing mean ± s.e.m. fold change relative to EV. Transfection efficiency was analyzed by flow cytometry using anti-MYC-tag (Cell Signaling 2278, 1:500) with the graph showing mean ± s.d. percentage of MYC-tag positive cells. Results indicate similar transfection efficiencies between WT and 343delT.

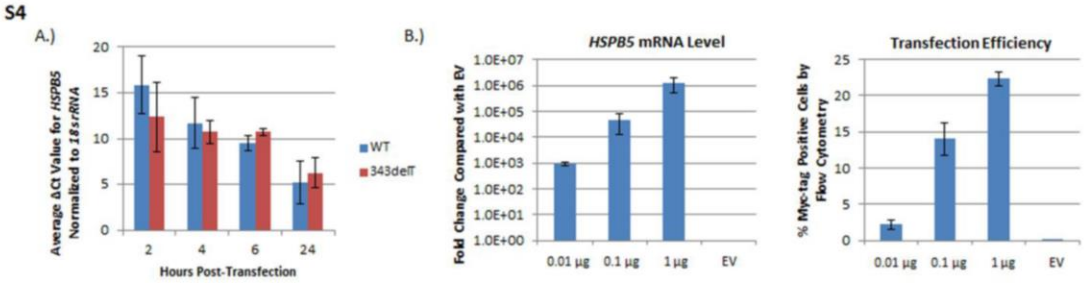

Supplementary Figure S5: Effects of 343delT Expression on Proliferation and Cell Toxicity
HEK 293FT cells transfected with EV, myc-tagged WT, or myc-tagged 343delT were harvested after 24 hours and A.) total cell number as well as B.) percent viable cells by trypan blue staining were counted using a Countess Automated Cell Counter (Life Technologies). Graphs depict mean ± s.d. from n=4 for each group. Results indicate no impact on cell proliferation or viability with transfection of WT or 343delT constructs.

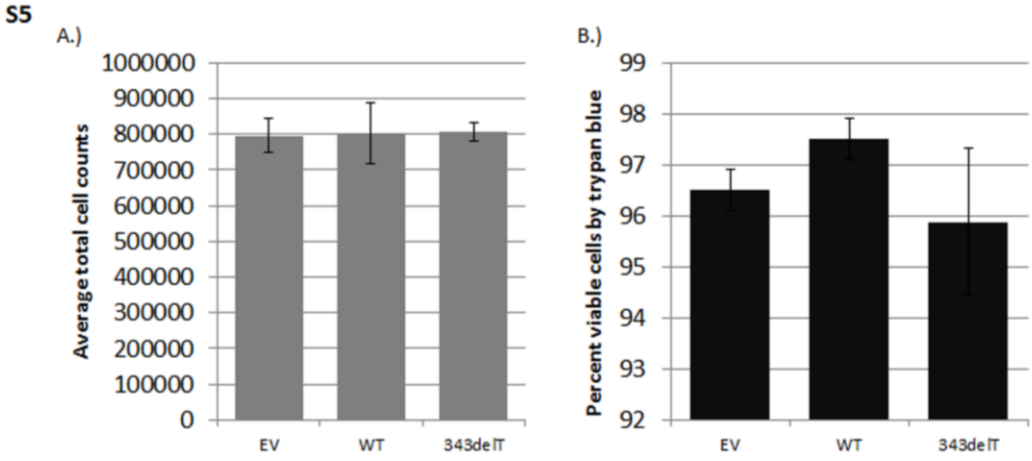

CHAPTER 4

EFFICIENT PRECISION GENOME EDITING IN IPSCS VIA GENETIC COTARGETING WITH SELECTION

Katie A. Mitzelfelt[1,9], Chris McDermott-Roe[2,3,9*], Michael N. Grzybowski[2,3], Maribel Marquez[2,3], Chieh-Ti Kuo[2], Michael Riedel[4], Shuping Lai[2], Melinda J. Choi[2], Kurt D. Kolander[2], Daniel Helbling[5], David P. Dimmock[5], Chuanchau J. Jou[6,7], Martin Tristani-Firouzi[6,7], James W. Verbsky[8], Ivor J. Benjamin[1,2,10], Aron M. Geurts[2,3,10*]

[1]Department of Biochemistry, University of Utah, Salt Lake City, UT 84112, USA

[2]Cardiovascular Center, Medical College of Wisconsin, Milwaukee, WI 53226, USA.

[3]Department of Physiology, Medical College of Wisconsin, Milwaukee, WI 53226, USA.

[4]PharmaCell, Maastricht, Netherlands

[5]Human Molecular Genetics Center and Division of Genetics, Department of Pediatrics, Medical College of Wisconsin, Milwaukee, WI 53226, USA

[6]Nora Eccles Harrison CVRTI, University of Utah School of Medicine, Salt Lake City, UT 84112, USA

[7]Division of Pediatric Cardiology, University of Utah School of Medicine, Salt Lake City, UT 83113, USA

[8]Department of Pediatrics, Medical College of Wisconsin, Milwaukee, WI 53226, USA

[9]Co-first authors

[10]Co-senior authors

*Corresponding authors

Summary

Genome editing in induced pluripotent stem cells is currently hampered by the laborious and expensive nature of identifying homology-directed repair- (HDR) modified cells. We present an approach where isolation of cells bearing a selectable, HDR-mediated editing event at one locus enriches for HDR-mediated edits at additional loci. This strategy, called cotargeting with selection, improves the probability of isolating cells bearing HDR-mediated variants and accelerates the production of disease models.

Introduction

Programmable nucleases are seeing widespread application in the genome engineering field on account of their ability to permit precise genetic modifications in cell cultures and whole organisms. The CRISPR (Clustered Regularly Interspaced Short Palindromic Repeats)/Cas9 (CRISPR-associated) system (Bhaya et al., 2011) has attracted particular attention on account of its flexibility, ease of use, and cost-effectiveness compared to alternative nucleases (e.g., Zinc finger nucleases (ZFNs) and Transcription activator-like effector nucleases (TALENs)). Approaches utilizing ZFNs, TALENs, and increasingly CRISPR/Cas9 for the creation of genetically-modified induced pluripotent stem cell (iPSC) lines which can be converted into pertinent somatic cell-types for exploration of contextually-relevant pathophysiological states have become a go-to strategy for delineating variant/disease association, reviewed in Hockemeyer and Jaenisch 2016 (Hockemeyer and Jaenisch, 2016). Precision genome editing typically involves incorporation of an exogenously-supplied DNA donor with the desired variant –often containing one or more additional sequence incorporations to prevent nuclease re-cutting (Long et al., 2014)- into the host cell's genome via the homology-directed repair (HDR) pathway following a nuclease-mediated double-strand break. Despite enhancements in the efficiency with which donor DNA can be incorporated into the genome, HDR-based editing in iPSCs using either vector- or single-stranded oligodeoxynucleotide (ssODN)-based donors occurs infrequently, often less than

1% (Soldner et al., 2011; Wang et al., 2014). Consequently, identifying a cell that bears a mutation of interest – which can entail extended maintenance, expansion, and analysis of hundreds of clonal populations - is laborious, expensive and not readily scalable.

Increasing evidence suggests HDR, which represents the lesser-used method of genome repair, is dependent on various cell-autonomous factors. Mitotic manipulation, temporal regulation of Cas9 expression, and suppression of the nonhomologous end joining (NHEJ) pathway have all been shown to enhance HDR editing *in vitro* to varying degrees (Gutschner et al., 2016; Lin et al., 2014; Maruyama et al., 2015; Yu et al., 2015). Elegant strategies have also been devised to enhance isolation of precision-modified clones, including precision knock-in of excisable selectable cassettes and serial enrichment of positive subfractions (Miyaoka et al., 2014; Yusa et al., 2011). Here we implemented a simple and adaptable method that obviates chemical perturbation, avoids stable Cas9 expression, maintains inherent DNA repair competence, does not require additional time or equipment, and is applicable to mismatch repair-proficient cell systems. We envisaged a potential HDR-competence spectrum across any population of transfected iPSCs, whereby a small subpopulation would naturally be more receptive to the incorporation of donor DNA via HDR while other cells remain refractory. In such a receptive cell, multiple independent HDR events could occur simultaneously meaning in theory an HDR-based primary editing event to incorporate a selectable marker at one locus could be accompanied by one or more independent, specified, HDR-mediated edits. Hence, isolation of cells based on the primary, selectable modification would enrich for the secondary, passenger modification(s).

To test our hypothesis, we devised and implemented a strategy that we refer to as cotargeting with selection (CTS). CTS involves simultaneous transfection of human iPSCs with (i) a nuclease and donor plasmid designed to incorporate, via HDR, an antibiotic-resistance cassette into the *AAVS1* safe-harbor site (Sadelain et al., 2012) on chromosome 19, and (ii) CRISPR/Cas9-based reagents and a cognate ssODN designed to introduce a variant of interest at a second locus, followed by maintenance in antibiotic-containing media for approximately ten

days to select for resistant (and theoretically HDR-competent) clones (Figure 4.1a-b). Antibiotic-resistant colonies are then isolated, clonally expanded and screened for knock-in of the variant of interest. CTS does not alter the duration from transfection to isolation and analysis, but based on our experience and data reported herein, markedly enhances the representation of cells bearing knock-in alleles in the final population.

Results and Discussion

We first applied the CTS method to a single gene (*CRYAB*) in hB53 hiPS6 iPSCs (Riedel et al., 2014). Following transfection of a prevalidated *CRYAB*-specific single guide RNA (sgRNA)-expressing pX330 vector and ssODN donor template as well as a commercially-available *AAVS1*-specific TALEN pair and puromycin N-acetyl-transferase (pac)-containing donor vector driven by a constitutive promoter, cells were treated with puromycin per our CTS protocol (to enrich for cells that underwent HDR, Figure 4.2), for 48 h (to eliminate untransfected cells) or not at all (to mimic a selection-free system) (Figure 4.3). Clones were then harvested and analyzed via Sanger sequencing. The total number of editing events (NHEJ and HDR) was >7-fold greater in CTS cells relative to unselected cells and, crucially, the HDR/NHEJ ratio was >4-fold greater (Figure 4.1c, left panel and Table 4.1). This corresponded to a ~40% likelihood of picking a precision-modified clone, both heterozygous and homozygous, from the final culture with CTS compared to 2% (no treatment) or 4% (transient puromycin treatment) (Figure 4.1c, middle and right panel and 4.1d). Contrary to previous findings in which merely selecting cells based on reagent delivery increased HDR (Ding et al., 2013), we did not observe enhancement in donor incorporation following isolation of transiently-transfected cells. In sum, this data suggested that selecting for HDR-receptive cells via a selectable modification significantly enriched for cells bearing precision edit events at the site of interest.

To benchmark the impact of CTS on HDR representation in a more quantitative manner and across multiple loci, we applied the workflow to a total of seven disease-associated variants

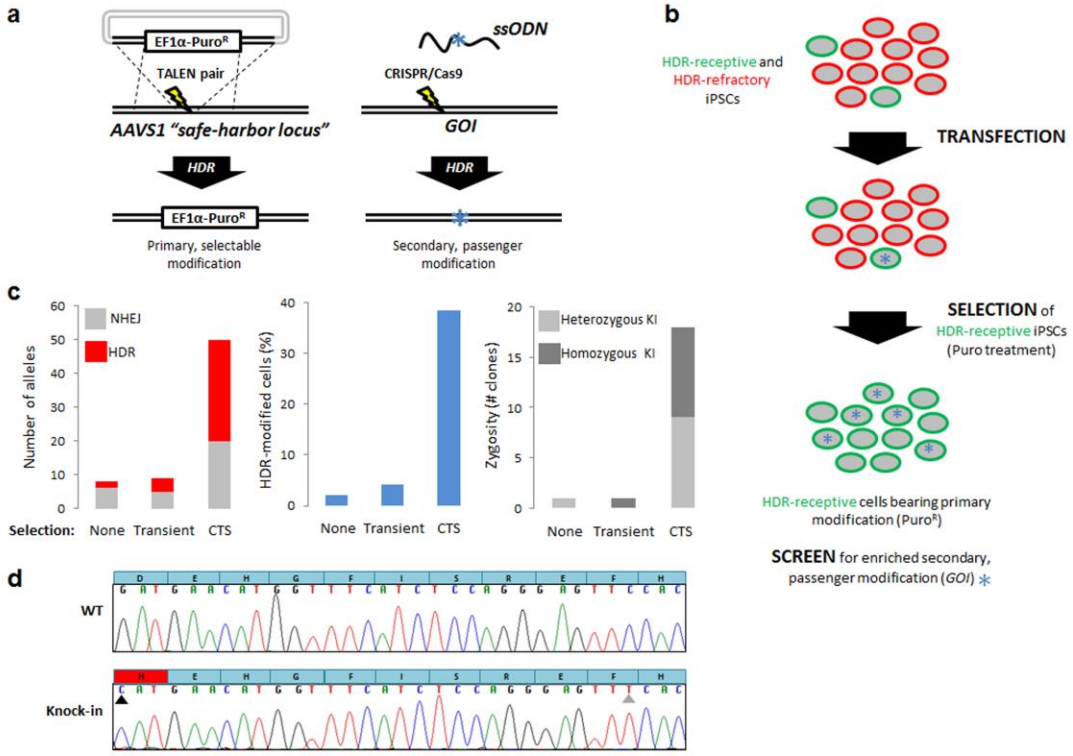

Figure 4.1: Rationale for cotargeting with selection (CTS) and proof of feasibility. (a) Cells are edited simultaneously with gene-specific CRISPR/Cas9 and ssODN containing a variant of interest (blue asterisk) as well as plasmids expressing *AAVS1*-specific TALENs and a puromycin resistant (Puro^R) donor cassette. (b) Components from (a) are transfected into iPSCs where HDR-receptive cells (green) are more likely to incorporate donor DNA than HDR-refractory cells (red). (c) Precision-edited versus indel-containing alleles, detected via Sanger-sequencing in hB53 hiPS6 iPSCs following CTS (n=39) compared to no selection (n=46) or transient exposure to puromycin (n=48) (left panel). Percent of clones bearing the *CRYAB*:c.325G>C variant (middle panel) and the number of heterozygous/homozygous clones (right panel). (d) Representative chromatograms showing local *CRYAB* sequence of a wild-type (WT) clone (top) and that of a clone bearing a *CRYAB*:c.325G>C (homozygous) knock-in allele (black arrow, c.325G>C variant; grey arrow, Cas9-blocking silent variant).

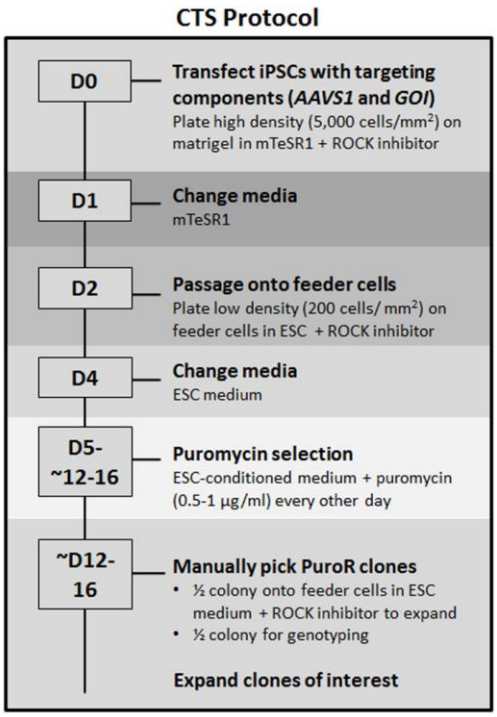

Figure 4.2: Timeline for CTS protocol. iPSCs are transfected with targeting components shown in Figure 4.1a on day 0 (D0) and plated at high density on matrigel to promote survival in mTeSR1 medium supplemented with ROCK inhibitor. On D1, media is changed to fresh mTeSR1 and dead cells are washed away. Cells are passaged on D2 to mitomycin-C-treated SNL feeders cells at low density. Puromycin selection (0.5 µg/ml) is performed D5-picking time (~D12-16) in order to limit selection based on transient expression of puromycin resistance and promote selection for incorporation of the puromycin cassette into the *AAVS1* locus. Selection is continued until picking to ensure all cells picked are puromycin resistant. Colonies are manually picked ~D12-16, with half of the colony utilized for genotyping while the other half is replated for expansion.

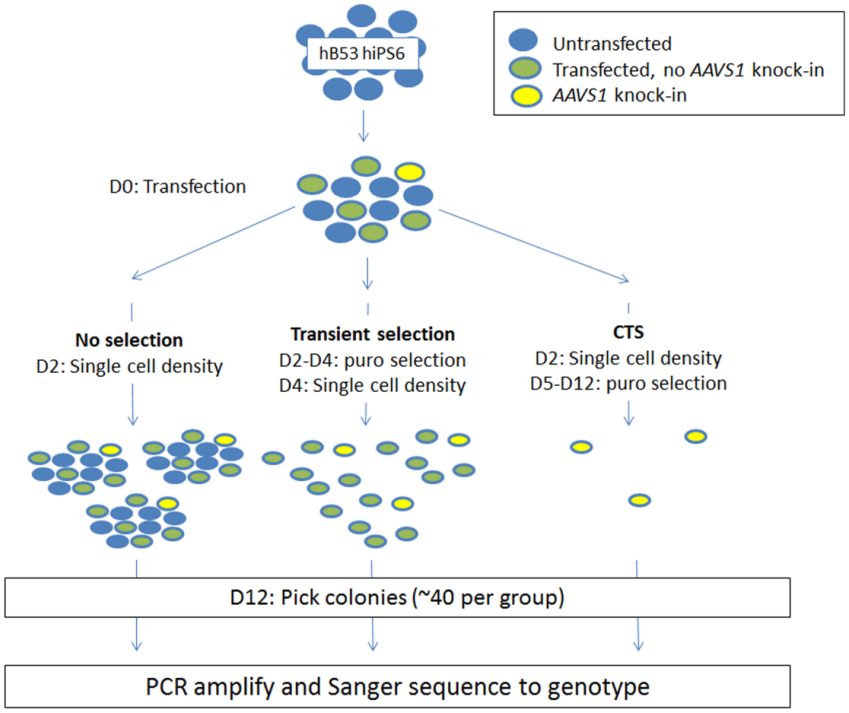

Figure 4.3: Experimental design comparing selection methods. Experimental design employed for comparing selection strategies (no selection, transient selection, and CTS) used for generating data shown in Table 4.1 and Figure 4.1c.

Table 4.1: Genotypes of clones analyzed comparing different selection strategies.

Selection	None	Transient	CTS
WT/WT	39	43	4
WT/Indel	3	1	4
Indel/Indel	1	1	6
Knock-in/Indel	1	2	3
Blocking/Indel	0	0	1
WT/Knock-in	0	0	2
Knock-in/Knock-in[#]	0	1	9
WT/Blocking	1	0	1
Blocking/Blocking[#]	0	0	2
Knock-in/Blocking	1	0	7
Total	46	48	39

Genotypes of clones analyzed and presented in Figure 4.1c. "Blocking" indicates knock-in of only the silent, Cas9-blocking mutation (i.e., without the variant of interest), whereas "Knock-in" indicates incorporation of both the silent mutation and variant of interest. 'WT' indicates unmodified alleles. CTS column from this table is the same data shown in Table 4.3.
[#]Though these clones appear to be homozygous through Sanger sequencing (i.e., "clean" sequence), a Southern blot would be required prior to phenotyping to ensure there is not a large deletion on one allele that prevents PCR amplification.

across four different genes (*CRYAB, BAG3*, *LMNA*, and *MTERF4*) in two separate iPSC lines (hB53 hiPS6 and hB119 hiPS9) and analyzed editing outcomes via deep-sequencing. Following CTS, cells were pooled and deep-sequenced using the Illumina MiSeq platform. Average sequencing coverage following read trimming and quality filtering across all experiments was >150,000x and error rate was estimated to be less than 0.1%. We observed an average 3.7-fold (hB53 hiPS6) and 3.3-fold (hB119 hiPS9) increase in the total number of edits (HDR and NHEJ) across all loci with CTS compared to without (Table 4.2). Focusing on precision editing events and considering all seven variants, we observed an average 50-fold increase in HDR with CTS compared to without in both cell lines (Figure 4.4a-c and Table 4.2). In support of our hypothesis that CTS enriches for HDR, we observed an overt shift in the balance between the two modes of repair such that the HDR/NHEJ ratio was enhanced on average 18-fold (hB53 hiPS6) and 27-fold (hB119 hiPS9) with CTS compared to without (Figure 4.4d-f and Table 4.2). Considering all loci and both cell lines, the HDR rate following CTS was ~14%, which corresponds to >1 in 10 clones bearing a precision edit.

While CTS led to a gross increase in precision editing, deep-sequencing data revealed significant variation in locus targetability. For example, representation of the *CRYAB*:c.343delT variant was 22% (hB53 hiPS6) and 25% (hB119 hiPS9) following CTS (1% (hB53 hiPS6) and 3% (hB119 hiPS9) without CTS), whereas representation of the *LMNA*:c.1346G>T variant was 1% (hB53 hiPS6) and 4% (hB119 hiPS9) HDR following CTS (<0.05% in both cell lines without CTS). Notwithstanding, the average >100-fold increase in HDR at *LMNA* with CTS means isolating a precision-edited clone is feasible (~1 cell in 40 with CTS compared to ~1 cell in ~3,800 without, assuming heterozygosity) and suggests that loci which are inherently refractory to precision editing may be amenable via CTS.

We next assessed how reflective the HDR editing rates calculated via deep-sequencing were of actual editing rates. Hence, the CTS protocol was repeated for all seven variants

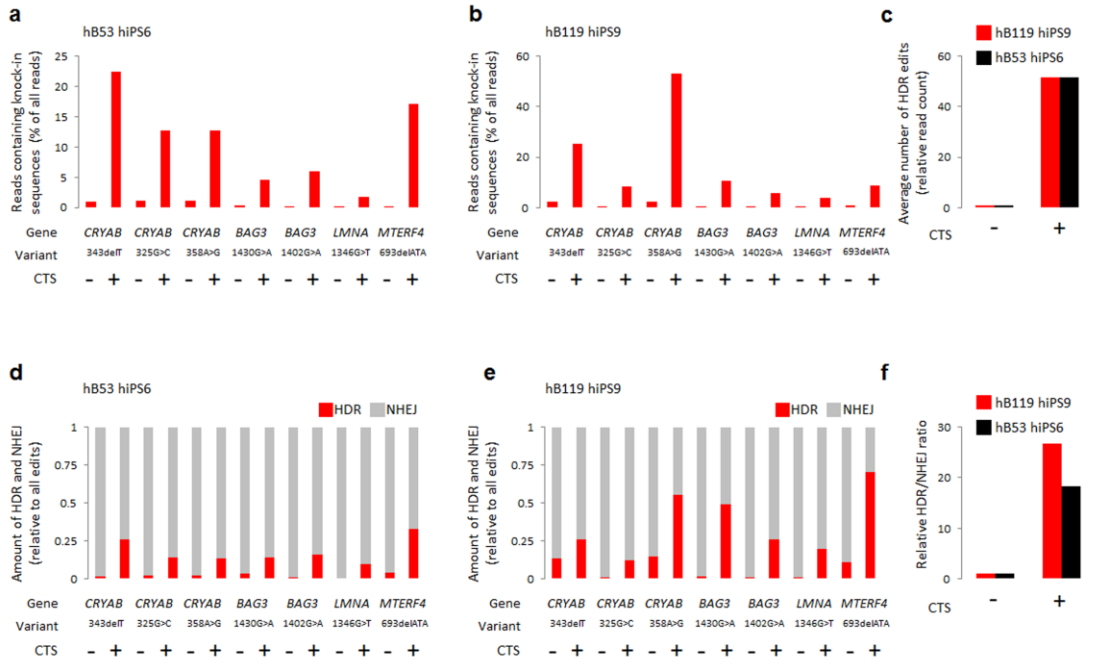

Figure 4.4: Quantitative analysis of CTS-enabled precision editing across multiple genes. Representation of precision (HDR only) editing events, based on read sequence and normalized to total read count, with (+) and without (-) CTS at multiple loci in hB53 hiPS6 (a) and hB119 hiPS9 (b) iPSC lines. (-) CTS indicates cells handled in the same way as (+) CTS except for the addition of puromycin. (c) Average fold-change in HDR-mediated knock-in with CTS relative to without, considering all loci in hB53 hiPS6 and hB119 hiPS9 iPSC lines. Relative proportions of reads bearing NHEJ- and HDR-based edits with (+) and without (-) CTS at multiple loci in hB53 hiPS6 (d) and hB119 hiPS9 (e) iPSC lines. (f) Average increase in the HDR/NHEJ ratio in hB53 hiPS6 and hB119 hiPS9 iPSC lines with CTS relative to without.

Table 4.2: Illumina MiSeq experimental results.

hB53 hiPS6	**Total # reads**	**Total # edits**	**HDR**		**NHEJ**		**WT**	
Sample			**# reads**	**% of total**	**# reads**	**% of total**	**# reads**	**% of total**
CRYAB:c.343delT_CTS-	262144	152720	**2458**	***1***	150262	*57*	109424	*42*
CRYAB:c.343delT_CTS+	134752	134752	**30210**	***22***	86683	*64*	17859	*13*
CRYAB:c.325G>C_CTS-	264167	168170	**2967**	***1***	165437	*63*	95997	*36*
CRYAB:c.325G>C_CTS+	135680	123981	**17227**	***13***	106754	*79*	11699	*9*
CRYAB:c.358A>G_CTS-	233189	129405	**2568**	***1***	126837	*54*	103784	*45*
CRYAB:c.358A>G_CTS+	299329	282460	**37946**	***13***	244515	*82*	16869	*6*
BAG3:c.1430G>A_CTS-	155400	13104	**439**	***0***	12665	*8*	142296	*92*
BAG3:c.1430G>A_CTS+	183997	61279	**8526**	***5***	52753	*29*	122718	*67*
BAG3:c.1402G>A_CTS-	180651	14651	**108**	***0***	14543	*8*	166000	*92*
BAG3:c.1402G>A_CTS+	160393	50311	**8042**	***5***	42269	*26*	110082	*69*
LMNA:c.1346G>T_CTS-	207467	9211	**20**	***0***	9191	*4*	198256	*96*
LMNA:c.1346G>T_CTS+	202658	25455	**2410**	***1***	23045	*11*	177203	*87*
MTERF4:c.693delATA_CTS-	188846	9255	**353**	***0***	8902	*5*	179591	*95*
MTERF4:c.693delATA_CTS+	174497	90735	**29916**	***17***	60819	*35*	83762	*48*
Average_CTS-	**213123**	**70931**	**1273**	**0.4**	**69691**	**28.4**	**142193**	**71.1**
Average_CTS+	**184472**	**109853**	**19182**	**10.9**	**88120**	**46.6**	**77170**	**42.7**

hB119 hiPS9	**Total # reads**	**Total # edits**	**HDR**		**NHEJ**		**WT**	
Sample			**# reads**	**% of total**	**# reads**	**% of total**	**# reads**	**% of total**
CRYAB:c.343delT_CTS-	121572	23748	**3108**	***3***	20640	*17*	97824	*80*
CRYAB:c.343delT_CTS+	110499	108887	**27905**	***25***	80982	*73*	1612	*1*
CRYAB:c.325G>C_CTS-	118811	69039	**774**	***1***	68265	*57*	49772	*42*
CRYAB:c.325G>C_CTS+	109238	75900	**9260**	***8***	66640	*61*	33338	*31*
CRYAB:c.358A>G_CTS-	100932	16806	**2447**	***2***	14359	*14*	84126	*83*
CRYAB:c.358A>G_CTS+	77869	75359	**41505**	***53***	33854	*43*	2510	*3*
BAG3:c.1430G>A_CTS-	91759	7878	**139**	***<1***	7739	*8*	83881	*91*
BAG3:c.1430G>A_CTS+	98513	21496	**10510**	***11***	10986	*11*	77017	*78*
BAG3:c.1402G>A_CTS-	95556	6920	**37**	***<1***	6883	*7*	88636	*93*
BAG3:c.1402G>A_CTS+	207563	45135	**11727**	***6***	33408	*16*	162428	*78*
LMNA:c.1346G>T_CTS-	112816	5463	**48**	***0***	5415	*5*	107623	*95*
LMNA:c.1346G>T_CTS+	220533	42597	8521	***4***	34436	*16*	177576	*81*
MTERF4:c.693delATA_CTS-	130614	9997	**1087**	***1***	8910	*7*	120617	*92*
MTERF4:c.693delATA_CTS+	93752	11555	**8111**	***9***	3444	*4*	82197	*88*
Average_CTS-	**110294**	**19979**	**1091**	**1.4**	**18887**	**16.4**	**90354**	**82.3**
Average_CTS+	**131138**	**54418**	**16791**	**16.6**	**37679**	**32.0**	**76668**	**51.4**

MiSeq experimental results for each cell line (hB53 hiPS6- top and hB119 hiPS9- bottom) including total number of reads, total number of edits, number of reads with HDR, percent of reads with HDR, number of reads with NHEJ, percent of reads with NHEJ, number of WT (unmodified) reads, and percent WT reads. Data for each variant with (CTS+) and without (CTS-) CTS are shown in individual rows with the final two rows showing average values including all variants.

independently and approximately 250 clonal populations were then picked and analyzed via Sanger sequencing. We successfully isolated cell lines for all seven mutations and observed a concordance between the quantities of HDR editing events determined via deep-sequencing and direct sequencing (Figure 4.5, Figure 4.6, and Table 4.2-4.3). We note that pooled deep-sequencing measures allelic representation at a specific time-point and does not reflect zygosity or account for differing cellular growth rates from which the pool was derived. Extent of heterozygosity seemed to correlate, at least for the *CRYAB* mutations, with increasing distance from the CRISPR/Cas9 cut-site (i.e., increased observation of heterozygous knock-in clones with *CRYAB*:c.325G>C), but not in the case of *BAG3*:c.1430G>A, where we failed to isolate any mutant homozygous lines even though the targeted nucleotide was immediately adjacent to the CRISPR/Cas9 cut-site. We speculate, as others have, that the nature and extent of zygosity is dictated by distance between the CRISPR/Cas9 cut-site and the targeted nucleotide as well as locus-dependent factors such as chromatin organization (Paquet et al., 2016; Ward, 2015; Yang et al., 2013). As expected representative cell lines harbored the pac cassette at *AAVS1* (Figure 4.5) and none displayed evidence of additional aspecific integration events (Experimental Procedures). Analyzing clones picked from two knock-in experiments revealed a 10% random integration rate of the *AAVS1* donor vector (Experimental Procedures). Additionally, all lines analyzed exhibited the typical pluripotent cell morphology and karyotypic stability as well as expression of pluripotency markers (Figure 4.5), and maintained a capacity to form high-representation cardiomyocyte cultures (data not shown).

Despite improvements in sgRNA design (Doench et al., 2016), we nevertheless analyzed the top potential off-target sites (Experimental Procedures) in multiple mutant cell lines via Sanger sequencing and detected no signs of aspecific cleavage (data not shown). Furthermore, deep-sequencing of 12 potential off-target sites (Experimental Procedures) associated with the most active sgRNA (*CRYAB*) in pooled populations of cells, with and without CTS, revealed no difference in off-target cutting (data not shown). The TALENs targeting *AAVS1* have been

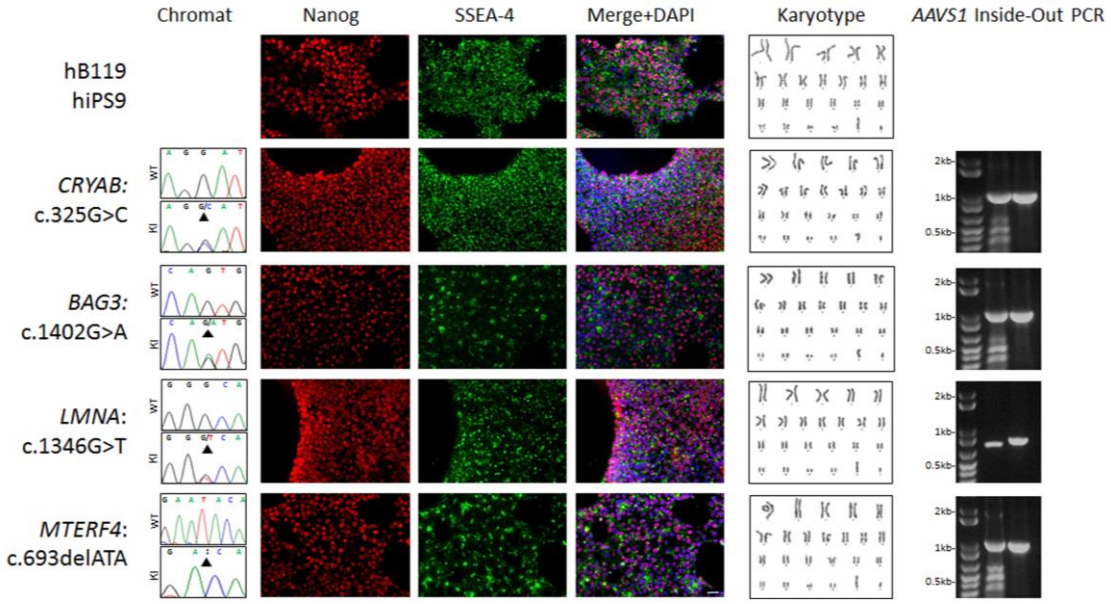

Figure 4.5: Validation of knock-in cell lines generated with CTS. Knock-in clones were generated for each disease-associated variant of interest shown in Table 4.3, with representative clones harboring variants in each gene shown here. Chromatograms (chromats) showing Sanger sequencing results of original cell line (WT) and knock-in line (KI) with variants indicated by black arrows. Immunocytochemistry showing pluripotency markers Nanog and SSEA-4 for each knock-in cell line harboring the respective variant of interest. Images were merged and counterstained with DAPI. Size bar indicates 100μm. Representative karyotypes for each cell line. Agarose gel showing *AAVS1* inside-out PCR for both the 5' (middle lane) and 3' (right lane) integration sites (Experimental Procedures), which demonstrates site-specific integration of the selection construct via HDR.

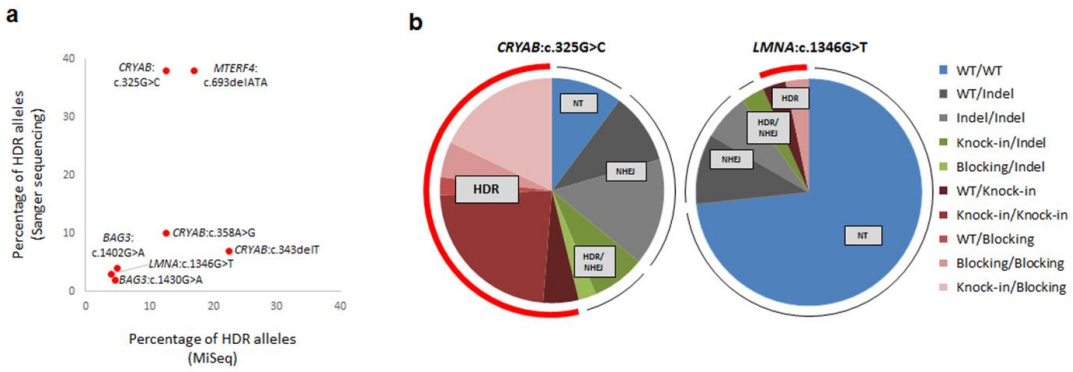

Figure 4.6: Concordance between deep-sequencing pooled samples and direct sequencing clonal samples. (a) Correlation of allelic HDR frequency between deep-sequencing (MiSeq) of pooled populations and Sanger sequencing of clonal populations. (b) Representative examples of high (CRYAB:c.325G>C) and low (LMNA:c.1346G>T) efficiency loci showing genotypes derived from clonally expanded populations. "Blocking" indicates knock-in of only the silent, Cas9-blocking mutation (i.e., without the variant of interest), whereas "Knock-in" indicates incorporation of both the silent mutation and variant of interest. "WT" indicates unmodified alleles. Genotypes are categorized as not-targeted (NT), NHEJ, HDR and NHEJ (HDR/NHEJ), or HDR.

Table 4.3: Information regarding generation of knock-in cell lines.

	Gene	*Crystallin, Alpha B or HSPB5 (CRYAB)*			*BCL2-Associated Athanogene 3 (BAG3)*		*Lamin A/C (LMNA)*	*Mitochondrial Transcription Termination Factor 4 (MTERF4)*
	Location	11q23.1			10q25.2-q26.2		1q22	2q37.3
Variant Information	Mutation	c.343delT	c.325G>C	c.358A>G	c.1430G>A	c.1402G>A	c.1346G>T	c.[693delATA]; [787C>T] *
	Protein change	p.S115Pfs*14	p.D109H	p.R120G	p.R477H	p.V468M	p.G449V	p.[E231D,Y232del]; [Q263*]
	Disease	skeletal myopathy	cardiomyopathy, skeletal myopathy, cataracts	cardiomyopathy, skeletal myopathy, cataracts	dilated cardiomyopathy	dilated cardiomyopathy	muscular atrophy	hypertrophic cardiomyopathy
	Reference	(Forrest et al., 2011)	(Sacconi et al., 2012)	(Vicart et al., 1998)	(Norton et al., 2011)	(Villard et al., 2011)	(Dialynas et al., 2012)	Unpublished data
Targeting Information	AAVS1 Targeting Vector	Transposagen	SBI	Transposagen	SBI	SBI	Transposagen	SBI
	sgRNA/ssODN Orientation	R+	R+	R+	R-	R-	R+	R-
	Cell Line	hB53 hiPS6	hB53 hiPS6	hB53 hiPS6	hB53 hiPS6	hB53 hiPS6	hB119 hiPS9	hB53 hiPS6
Genotype	Unmodified	9	4	13	61	75	22	13
	WT/Indel	0	4	0	2	7	3	0
	Indel/Indel	4	6	5	0	2	2	2
	Knock-in/indel	0	3	0	1	1	1	4
	Blocking/Indel	0	1	0	0	1	0	0
	WT/Knock-in	0	2	0	1	3	1	0
	Knock-in/Knock-in#	1	9	2	0	1	0	11
	WT/Blocking	0	1	0	0	0	0	0
	Blocking/Blocking#	0	2	0	0	0	1	0
	Knock-in/Blocking	0	7	0	0	1	0	0
	Total	14	39	20	65	91	30	30

Variants of interest knocked-in to iPSCs using CTS. Gene name, mutation, corresponding protein change, disease, and references are given for each variant. The *AAVS1* targeting vector utilized in each case is shown (see Experimental Procedures). The sgRNA/ssODN orientation is listed as either R+ or R-, indicating agreement or disagreement with the Richardson et al. model for ssODN strand design (Richardson et al., 2016). The cell line utilized to generate each variant is also listed (hB53 hiPS6 or hB119 hiPS9). The numbers of clones isolated with each genotype are indicated below each variant. *The patient variant *MTERF4*:c.[693delATA];[787C>T] was generated by an ssODN incorporating c.693delATA and screening for an indel on the second allele to mimic c.787C>T, which generates a stop codon. #Though these clones appear to be homozygous through Sanger sequencing (i.e., "clean" sequence), a Southern blot would be required prior to phenotyping to ensure there is not a large deletion on one allele that prevents PCR amplification.

previously demonstrated to have minimal off-target cleavage (Hockemeyer et al., 2011) and aspecific integration profiling revealed extremely low rates of random integration of the donor plasmid. Collectively, these data suggest negligible reagent promiscuity and that while CTS specifically enriches for cells bearing HDR-edited alleles, it does not enrich for off-target mutations. We note that GUIDE-Seq (Tsai et al., 2015) or similar would be required for whole genome examination of off-target cutting.

CTS is an inexpensive, rapid, straightforward, and readily scalable method, conceptually analogous to other marker-assisted enrichment strategies (Arribere et al., 2014), which increases the likelihood of isolating cells bearing knock-in alleles and hence significantly accelerates the production of *in vitro*-based disease models. We encountered significant variability with inter-locus targetability and suspect that local sequence composition and chromatin organization likely influences repair preference. Given the multifactorial nature of complex diseases and especially the role of modifier loci, we envisage CTS being of potential utility for simultaneous recapitulation of multiple candidate variants. Indeed, using CTS, we concurrently delivered editing reagents designed to incorporate mutations at two different loci and isolated multiple clones bearing both edits (Figure 4.7). It will be interesting to determine whether polycistronic sgRNA delivery systems (Cong et al., 2013) will permit highly parallelized HDR-based genome editing in conjunction with CTS.

Operationally, CTS provides a marked improvement in the efficiency of isolating precision-modified iPSC lines compared with no selection/direct cloning, without extended hands-on time or a requirement for additional instrumentation. Following methodological refinements and legislating for effect-range, we conservatively estimate that a single well-trained technician could generate ten precision-edited cell lines in one month. CTS is also generalizable in that while the system described uses antibiotic resistance as the selectable modification, alternative HDR-based modifications (e.g., insertion of a GFP cassette) could theoretically be employed. The site of the selectable modification could also be adapted depending on context and

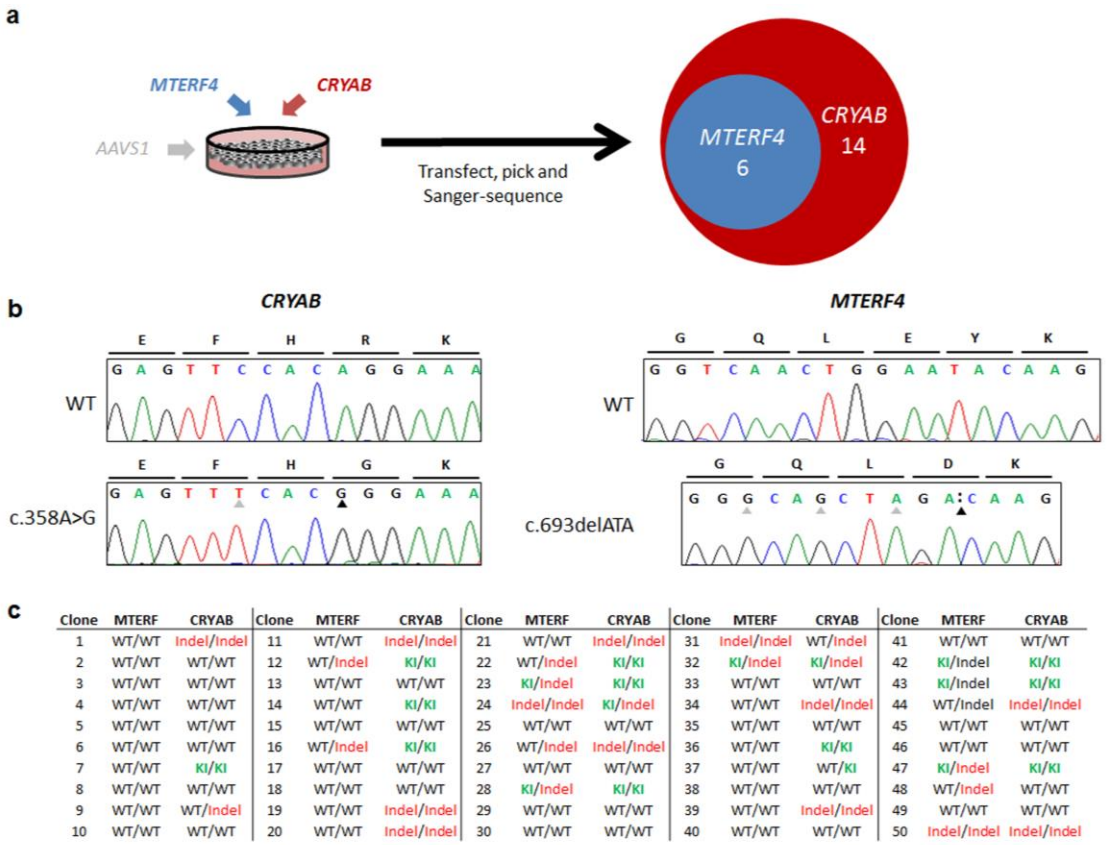

c

Clone	MTERF	CRYAB	Clone	MTERF	CRYAB	Clone	MTERF	CRYAB	Clone	MTERF	CRYAB	Clone	MTERF	CRYAB
1	WT/WT	Indel/Indel	11	WT/WT	Indel/Indel	21	WT/WT	Indel/Indel	31	Indel/Indel	WT/Indel	41	WT/WT	WT/WT
2	WT/WT	WT/WT	12	WT/Indel	KI/KI	22	WT/Indel	KI/KI	32	KI/Indel	KI/Indel	42	KI/Indel	KI/KI
3	WT/WT	WT/WT	13	WT/WT	WT/WT	23	KI/Indel	KI/KI	33	WT/WT	WT/WT	43	KI/Indel	KI/KI
4	WT/WT	WT/WT	14	WT/WT	KI/KI	24	Indel/Indel	KI/Indel	34	WT/WT	Indel/Indel	44	WT/Indel	Indel/Indel
5	WT/WT	WT/WT	15	WT/WT	WT/WT	25	WT/WT	WT/WT	35	WT/WT	WT/WT	45	WT/WT	WT/WT
6	WT/WT	WT/WT	16	WT/Indel	KI/KI	26	WT/Indel	Indel/Indel	36	WT/WT	KI/KI	46	WT/WT	WT/WT
7	WT/WT	KI/KI	17	WT/WT	WT/WT	27	WT/WT	WT/WT	37	WT/WT	WT/KI	47	KI/Indel	KI/KI
8	WT/WT	WT/WT	18	WT/WT	WT/WT	28	KI/Indel	KI/KI	38	WT/WT	WT/WT	48	WT/Indel	WT/WT
9	WT/WT	WT/Indel	19	WT/WT	Indel/Indel	29	WT/WT	WT/WT	39	WT/WT	Indel/Indel	49	WT/WT	WT/WT
10	WT/WT	WT/WT	20	WT/WT	Indel/Indel	30	WT/WT	WT/WT	40	WT/WT	WT/WT	50	Indel/Indel	Indel/Indel

Figure 4.7: Simultaneous, dual modification using CTS. (a) Dual modification was attempted on hB53 hiPS6 using components for targeting *MTERF4*:c.693delATA and *CRYAB*:c.358 A>G. Following CTS, 50 clones were sequenced, and of those, 15 had knock-in at *CRYAB* (depicted in the red circle) and 6 had knock-in at *MTERF4* (depicted in the blue circle). All 6 of the cells with *MTERF4* knock-in also had knock-in at *CRYAB*. Given individual editing rates, the likelihood of co-occurrence assuming random distribution of events is 5%. We observed a disproportionate co-occurrence of dual modification with a FET<0.001. (b) Representative chromatograms of dual-targeted clones at each loci and wild-type (WT) sequences. Black arrows indicate variant of interest position. Silent, engineered blocking mutations that prevent re-targeting by Cas9 are indicated by grey arrows. **(c)** Table including genotypes of individual clones at both (*MTERF4* and *CRYAB*) loci. WT indicates unmodified, KI indicates knock-in, Indel indicates insertion or deletion.

user requirements. For example, knock-in of a GFP tag into a cardiac transcription factor such as NKX2-5 (Elliott et al., 2011) would yield iPSCs that harbor a variant of interest in tandem with a reporter which assists with cardiomyocyte isolation. Furthermore, compared to alternative knock-in strategies facilitated by targeted insertion of a selectable marker, CTS does not require the production of gene-specific custom targeting vectors making it a readily scalable strategy. In addition, while we observed no adverse effects of *AAVS1* targeting or carriage of the *pac* cassette on cell behavior or differentiation potential, (although appropriate control cell lines harboring only the *pac* cassette should be utilized for phenotypic evaluation), removal of the *pac* cassette could be performed through transfection of cells with *piggyBac* transposase. Finally, although we show utility of CTS in iPSCs for enhancing the efficiency of isolating HDR-modified clones, we envisage CTS being widely applicable mismatch repair-competent cell types.

Experimental Procedures

CRISPR target site design and plasmid construction

CRISPR target sites proximal (within 35 bps) to the SNP of interest were identified using ZiFiT Targeter Version 4.2. Target sites as unique as possible – based on dissimilarity to other genomic loci - were selected (Table 4.4). Typically, sites were chosen that had zero or one "off by 0" or "off by 1" matches elsewhere in the genome. pX330-U6-Chimeric_BB-CBh-hSpCas9 was a gift from Feng Zhang (Addgene plasmid # 42230). Reverse complementary oligonucleotide pairs with BbsI overhangs were purchased from Sigma (or Life Technologies) and hybridized, and cloned into the pX330 vector as described previously (Cong et al., 2013).

Culture and transfection of HEK293T cells and Cel-1 surveyor assay

HEK293T cells, maintained in Dulbecco's modified Eagle medium (DMEM) with high glucose, sodium pyruvate and L-glutamine (Life Technologies) supplemented with 10% fetal bovine serum (FBS- Life Technologies) and 100 u penicillin/100ug streptomycin/ml media (P/S- Life Technologies), were passaged using 0.05% Trypsin (Life Technologies) for transfection. For

Table 4.4 CRISPR guide RNA sequences

Locus	Guide RNA complementarity regions (5'-3')
CRYAB	GGGATCCGGTATTTCCTG
BAG3	GGGACGAGCCGATGTGCGTC
LMNA	CATTGGACTTGTTGCGCAGC
MTERF4	ACTTGTATTCCAGTTGACCC

validating cleavage efficiencies of designed CRISPR guides, HEK 293T cells were mixed with SF nucleofection solution (Lonza) and various pX330 plasmids and transfected with the 4D Nucleofector™ (Lonza) using program CM-130. Cells were harvested 48 h later and CRISPR activity was validated using the Cel-1 Surveyor assay as previously described (Geurts et al., 2009; Miller et al., 2007).

ssODN design

We typically designed ssODNs to flank the variant and/or cut-site by approximately 60bp on either side. In keeping with previous reports (Chen et al., 2011; Long et al., 2014; Paquet et al., 2016; Ponce de León et al., 2014), silent mutations were incorporated into the ssODNs to prevent re-cutting by Cas9 following HDR. This was achieved either through disruption of the PAM sequence or multiple disruptions within the target sequence. ssODNs utilized in experiments are shown in Table 4.5.

AAVS1 targeting plasmids

The *AAVS1* Safe Harbor TALE-Nuclease kit was purchased from System Biosciences (SBI), including TALENs previously shown to have minimal off-target cleavage (Hockemeyer et al., 2011). Plasmids include the HDR donor vector, p*AAVS1* Dual Promoter Donor Vector (GE602A-1) containing GFP-Puromycin resistance cassette driven by an *EF1α* promoter, and the TALE-Nuclease Vectors, pZT-*AAVS1* L1 TALE-N Vector (GE601A-1) and pZT-*AAVS1* R1 TALE-N Vector (GE601A-1). These were used for all Illumina MiSeq experiments (except hB119 hiPS9 *LMNA*:c.1346 G>T), and for clonal knockin of *BAG3*:c.1430G>A,

Table 4.5 ssODN sequences

Variant	ssODN Sequence (5'-3')
CRYAB: c.343delT	TGTTCTTATCTCTCTGCCTCTTTCCTCATTCTTTTGGGTTAGGATGAACATGGTTTCATCCCAGGGAGTTCAACAGGAAATACCGGATCCCAGCTGATGTAGACCCTCTCACCATTACTTCATCCCTGTCATCTGA
CRYAB: c.325G>C	GCAGGTGATAATAGTTCCTGTTCTTATCTCTCTGCCTCTTTCCTCATTCTTTTGGGTTAGCATGAACATGGTTTCATCTCCAGGGAGTTTCACAGGAAATACCGGATCCCAGCTGATGTAGACCCTCTCACCATTACTTCATCCCTGTCATCTGA
CRYAB: c.358A>G	GCCTCTTTCCTCATTCTTTTGGGTTAGGATGAACATGGTTTCATCTCCAGGGAGTTTCACGGGAAATACCGGATCCCAGCTGATGTAGACCCTCTCACCATTACTTCATCCCTGTCATCTGA
BAG3: c.1430G>A	CCTGATGATCGAAGAGTATTTGACCAAAGAGCTGCTGGCCCTGGATTCAGTGGACCCCGAGGGGCGGGCAGACGTCCATCAGGCCAGGAGAGACGGTGTCAGGAAGGTTCAGACCATCTTGGAAAAACTTGAACAGAAAG
BAG3: c.1402G>A	CCTGATGATCGAAGAGTATTTGACCAAAGAGCTGCTGGCCCTGGATTCAATGGACCCCGAGGGGCGGGCAGACGTCCGGCAGGCCAGGAGAGACGGTGTCAGGAAGGTTCAGACCATCTTGGAAAAACTTGAACAGAAAG
LMNA: c.1346G>T	ACGCACTAGCGGGCGCGTGGCCGTGGAGGAGGTGGATGAGGAGGGCAAGTTTGTACGGCTGCGCAACAAGTCCAATGAGgtaggctcctgctcagggtctaaggggatacagctgcatca
MTERF4: c.693delATA	ccagtcattctcacctgaaactacgctaatcacgctatcagtcattctcacCTGAAACTTGTCTAGCTGCCCCAGGTCCTCTCGAAGAACAGAGGGGCAACTGTGCAAAATCTTGGTGACTTGCTGTACCGTGAAAAGGCA

*BAG3:*c.1402G>A, *MTERF4*:c.693delATA, and *CRYAB*:c.325G>C. A second *AAVS1* Safe-harbor kit was purchased from Transposagen (Puro-TK with XTN™ TALEN, Catalog # KSH-004) with the donor vector that includes a puromycin resistance gene and thymidine kinase selection cassette driven by a *PGK* promoter and flanked by *piggyBac* repeats, which can be sequentially, seamlessly removed with excision by *piggyBac* transposase if desired, as well as the accompanying *AAVS1*-specific XTN Forward and Reverse TALEN nucleases. The Transposagen system was used for generating *CRYAB*:c.358A>G and *CRYAB*:c.343delT clones. Additionally, we designed and validated a sgRNA targeting the *AAVS1* locus (guide RNA complementarity region (5'-3') GTCACCAATCCTGTCCCTAG) cloned into pX330 as described above. This pX330-*AAVS1* was used in concert with the *AAVS1* donor vector from Transposagen for generating *LMNA*:c.1346G>T clones and for Illumina MiSeq analysis of hB119 hiPS9

LMNA:c.1346G>T.

iPSC lines

All human subject research was approved by the Medical College of Wisconsin and University of Utah Institutional Review Boards. The human iPSC lines used in this study are hB53 hiPS6 (Riedel et al., 2014), derived from a 25-year-old Caucasian male and hB119 hiPS9, derived from peripheral blood mononuclear cells of a healthy 34-year-old Caucasian male using a polycistronic lentivirus containing *OCT4*, *KLF4*, *SOX2*, and *c-MYC* as previously described (Riedel et al., 2014). Informed consent was obtained for this procedure. hB53 hiPS6 was used for generating cell lines with the following knock-in mutations: *BAG3*:c.1402G>A, *BAG3*:c.1430G>A, *MTERF4*:c.693delATA, *CRYAB*:c.358A>G, *CRYAB*:c.325G>C and *CRYAB*:c.343delT, as well as the dual targeting experiment. hB119 hiPS9 was used for generating the cell line containing *LMNA*:c.1346G>T. We successfully applied our CTS method to two other iPSC lines (data not shown): knocking-in *CRYAB*:c.358A>G and *CRYAB:*c.325G>C mutations into hB119 hips10 (an alternate iPSC line derived from the same individual as hB119 hiPS9 using the same method, unpublished data) and reverting homozygous *CRYAB:*c.343delT to homozygous wildtype in a female iPSC line derived from the patient (Forrest et al., 2011), which was reprogrammed using retrovirus (Mitzelfelt et al., 2016).

iPSC culture

Prior to transfection, iPSCs were cultured as previously described (Mitzelfelt et al., 2016) in feeder-free conditions on Matrigel (Corning)-coated 6-well plates with mTeSR1 (Stem Cell Technologies) or StemMACS iPS-Brew XF (Miltenyi Biotec). Cells were passaged every 3-4 days using Accutase (Life Technologies) and seeded in media containing 10μM Rho-associated, coiled-coil containing protein kinase (ROCK) inhibitor (Y-27632, Selleck) for 24 h following passaging.

iPSC transfection

CTS for generation of knock-in iPSC lines. iPSCs were pretreated for 3-4 h with 10μM ROCK inhibitor, washed once with Dulbecco's phosphate buffered saline (DPBS- Life Technologies), and incubated with Accutase (Life Technologies) for 5-8 min. Wash medium (Knockout DMEM/F12 supplemented with 10% FBS- both from Life Technologies) was added and cells were pipette vigorously to generate a single cell solution and counted using a Countess Automated Cell Counter (Life Technologies). For each transfection (*day 0*), 1μg of the gene-specific pX330 CRISPR/Cas9 plasmid, 2μl of a 40μM stock solution or 1.5μl of a 20μM stock solution of the relevant ssODN, 1μg of each of the two *AAVS1*-specific TALEN plasmids (or 1μg of the *AAVS1*-specific pX330 CRISPR plasmid) and 1μg *AAVS1* donor plasmid (see Targeting Reagents above) were added to 100μl P4 solution (Lonza) and electroporated using program CB-150 on a 4D Nucleofector™ into iPSCs ($1x10^6$ cells/transfection). Cells from each transfection were then seeded into one well of Matrigel-coated 24-well plate (5,000 cells/mm^2) for recovery in mTeSR1 or StemMACS iPS-Brew XF supplemented with 10μM ROCK inhibitor. The following day (*day 1*), cells were washed once with DPBS to remove dead cells and media was changed to mTeSR1 or StemMACS iPSC-Brew XF. Two days post-transfection (*day 2*), iPSCs were dispersed using Accutase and distributed across a 6-well plate pre-seeded with Mitomycin C (SantaCruz) -treated SNL feeder cells (Cell Biolabs) in ESC medium, composed of Knockout DMEM (Life Technologies) supplemented with 20% Knockout Serum Replacement (Life Technologies), MEM-NEAA (Life Technologies), 2mM L-glutamine (Life Technologies), P/S, 0.1mM β-mercaptoethanol (Sigma), 10ng/ml human basic fibroblast growth factor (bFGF, Cell Signaling), and 50ng/ml L-ascorbic acid (Sigma), supplemented with 10μM ROCK inhibitor. Media was changed two days later (*day 4*) to ESC medium minus ROCK inhibitor. Three days post-seeding (*day 5*), puromycin (0.5-1μg/ml)-supplemented ESC-conditioned media (ESC media conditioned on SNL feeder cells with bFGF and vitamin C added post-conditioning) was added and replaced thereafter every 2 days until picking time (~7-10 days). Waiting until *day* 5 to begin

puromycin selection limits the extent of selection for transient expression of puromycin resistance and selecting until picking ensures that all colonies picked have integration of the *pac* cassette. Following ~7-10 days of maintenance in puromycin-containing media (*day 12-16*), distinct colonies (~1mm diameter) were apparent and manually/mechanically transferred each to a single well of a 24-well plate pre-seeded with feeder cells in ESC media plus ROCK inhibitor. Half of each isolate was retained for expansion and half for DNA isolation to genotype. Following genotyping (see below), desired clones were passaged to single wells of 12-well matrigel-coated dishes in mTeSR1 plus ROCK inhibitor and further expanded for pluripotency immunocytochemistry and karyotyping (see below) and frozen for future culture in freezing medium composed of FBS plus 10% dimethyl sulfoxide (DMSO- Sigma). Isolated knock-in iPSC lines were frequently subcloned to ensure homogeneity of the population.

Transfection and CTS for Illumina MiSeq experiments. With the aim to assess the effect of our CTS regimen on editing outcomes, we carried out next-generation sequencing using the Illumina MiSeq platform via a pooled amplicon strategy, including 7 different variants of interest (Table 4.3) across 4 different genes (*CRYAB, BAG3, LMNA* and *MTERF4*,) in two different cell lines (hB53 hiPS6 and hB119 hiPS9). Samples were prepared as described above except, two days post-transfection (*day 2*), iPSCs were dispersed such that 10,000 iPSCs were allocated across 3 wells ($Puro^-$) and the remainder across the other 3 wells ($Puro^+$) of a 6-well plate. Media was changed every other day for 1 week (*day 5-12*) with or without puromycin, accordingly. Following 1 week maintenance (*day 12*), all three $Puro^+$ wells and all three $Puro^-$ wells were collected and combined separately. In order to deplete the feeder cell sub-population, cells were reseeded in one Matrigel-coated 6-well plate wells in mTeSR1 plus ROCK inhibitor. At confluence, cells were again dispersed, combined and pelleted for isolation of genomic DNA and library preparation for Illumina MiSeq analysis (see below).

Genotyping PCR and Sanger sequencing for clones

To isolate genomic DNA from clones, 30µl Quick Extract Solution (Epicentre) was added to each cell pellet (half colony) and incubated for 15 min at 65°C, followed by 5 min at 95°C. PCR was carried out using gene-specific primers (Table 4.6) and the resulting amplicons were PCR-purified using a PureLink Quick PCR Purification Kit (Life Technologies) and Sanger sequencing was performed by Retrogen (San Diego, CA) with the same primers used for amplification. Sequences were analyzed using Sequencher software.

Illumina MiSeq library preparation

Genomic DNA was isolated from cell pellets using a PureLink Genomic DNA Mini Kit (Life Technologies). Samples were prepared for analysis with Illumina MiSeq as previously described (Kistler et al., 2015). PCR 1 primers are listed in Table 4.7 with adapter sequences in red and green text for the forward and reverse primers, respectively. PCR2 was performed using the Nextera XT Index Kit (#15055293) from Illumina according to manufacturer's instructions. Individual amplicons were quantified via qPCR (KAPA Biosystems) and pooled at 3nM concentrations. To ensure high sequencing quality, following pooling, final amplicon pools were quantitated by qPCR to determine the precise molarity of the pool as a whole. Samples were sequenced using Single read sequencing (250bp read) and dual indexing on an Illumina MiSeq following the manufacturer's instructions. The pool was run with a 30% spike-in of Phi-X to avoid issues with low-complexity Amplicon Libraries.

Illumina MiSeq analysis methods

In all cases, reads were inspected using the FASTX-Toolkit to assess general quality and then 3'-clipped where the Q score in a 4 nucleotide sliding window fell below 15 and filtered as to retain only those of 100 nucleotides or longer using Trimmomatic (Bolger et al., 2014). Pipeline error rate was estimated by deep-sequencing unedited amplicons derived from each target gene and aligning FATSTQ-derived sorted/indexed BAM file to reference sequences

Table 4.6 Genotyping primers

Primer Name	Primer Sequence (5'-3')
CRYAB_F	AGACAGTTATCTGTTGCTGAATGATATT
CRYAB_R	GGCAATTTCATCTTAGCTGCAA
BAG3_F	TGAAAGTGGAAGCCATCCTG
BAG3_R	GGCTGATCTGCTTCAAGGTT
LMNA_F	CCCCACTTGGTCTCCCTC
LMNA_R	GGCTCACCCTGGTCCACC
MTERF4_F	TTATATGCTTGCCTTTTTTGAA
MTERF4_R	GTCCGAGGCTTCTTATCCATAT

Table 4.7 Illumina MiSeq PCR 1 primers

Primer Name	Primer Sequence (5'-3')
CRYAB_MiSeq_F	TCGTCGGCAGCGTCAGATGTGTATAAGAGACAGCTGAGTTCTGGGCAGGTGAT
CRYAB_MiSeq_R	GTCTCGTGGGCTCGGAGATGTGTATAAGAGACAGTAATTTGGGCCTGCCCTTAG
BAG3_MiSeq_F	TCGTCGGCAGCGTCAGATGTGTATAAGAGACAGACCAAAGAGCTGCTGGCCCT
BAG3_MiSeq_R	GTCTCGTGGGCTCGGAGATGTGTATAAGAGACAGTCGCTGCTGCTGTGGCTTCT
LMNA_MiSeq_F	TCGTCGGCAGCGTCAGATGTGTATAAGAGACAGGCAGCAGCTTCTCACAGCAC
LMNA_MiSeq_R	GTCTCGTGGGCTCGGAGATGTGTATAAGAGACAGGGCACACGGATACCTTATCTTT
MTERF4_MiSeq_F	TCGTCGGCAGCGTCAGATGTGTATAAGAGACAGGGCAGAAAAGTTGAAGAATAGG TTT
MTERF4_MiSeq_R	GTCTCGTGGGCTCGGAGATGTGTATAAGAGACAGAGAAGTGCCTTTTCACGGTACA

(obtained from Ensembl release 84) with Bowtie2 and assessing sequence divergence in the informative segment (10 nucleotides up/downstream of the nucleotide to be mutated and the CRISPR PAM site) of each target read. Average coverage was ~240,000X and average sequence divergence from the reference at Q30 was 0.1%. For knock-in experiments, we quantified the extent of HDR-mediated donor integration by interrogating pre-processed FASTQ files (as described above) for informative segments of the donor sequence (typically ~50 nucleotides, spanning the targeted nucleotide and CRISPR cut site (not simply the targeted nucleotide, as this may occur in the presence of an indel and lead to overestimation of knock-in) using a Linux grep command (of format : grep -A 2 -B 1 'ssODN sequence' 'INPUT.FQ' | sed '/^--$/d' > 'OUTPUT.FQ') as well as via manual inspection of FASTQ files for confirmation. For comparative value, HDR was also quantified using the Church lab's CRISPR Genome Analyzer (Güell et al., 2014) and we observed good agreement with our estimates (data not shown).

PCR to confirm HDR at *AAVS1* locus

To confirm HDR at the *AAVS1* locus, inside-out PCR was performed on all knock-in variant cell lines. Primers were designed for the SBI and Transposagen *AAVS1* targeting vectors for both the 5' and 3' ends with one falling inside the homology arm (i.e., in the exogenous sequence) and one outside (i.e., in the endogenous locus) (Table 4.8) and PCR was performed with Accuprime Supermix II (Life Technologies).

PCR to screen for random integration of the *AAVS1* donor vector

To screen for random integration of the *AAVS1* donor construct, two sets of PCR primers were designed for each donor vector (SBI and Transposagen) that amplify the backbone region (i.e., the region of the vector outside of the homology arms) (Table 4.9). PCR was performed using Accuprime Supermix II (Life Technologies) with plasmid DNA as a positive control and DNA from hB53 hiPS6 and hB119 hiPS9 iPSCs as negative controls. Bands were undetectable in generated knock-in cell lines (data not shown). Additionally, of 44 clones screened from two

Table 4.8 Primers for confirming integration at *AAVS1*

Name	Primer Sequence (5'-3')	Expected PCR Product Size
SBI 5' Forward	AGTCCGGACCACTTTGAGCTCTACT	1061bp
SBI 5' Reverse	GAGGAGTAGAAGGTGGCGCGAA	
SBI 3' Forward	AGGTTTAGCCCCGGAATTGACTG	1036bp
SBI 3' Reverse	CCAAAAGGCAGCCTGGTAGACA	
Transposagen 5' Forward	CTCTTTCCGGAGCACTTCC	711bp
Transposagen 5' Reverse	CCGATAAAACACATGCGTCA	
Transposagen 3' Forward	ACTTACCGCATTGACAAGCA	805bp
Transposagen 3' Reverse	CCAGATAGCACTGGGGACTC	

Table 4.9 Primers for screening for random integration of the *AAVS1* vector

Name	Primer Sequence (5'-3')	Expected PCR Product Size
SBI Random Forward 1	GTGCCACCTAAATTGTAAGCGTT	495bp
SBI Random Reverse 1	AACAGTTGCGCAGCCTGAAT	
SBI Random Forward 2	TGCTGCTGCATTGACGTTGA	408bp
SBI Random Reverse 2	TGCTTCCGGCTCGTATGTTG	
Transposagen Random Forward 1	GCTTCCTCGCTCACTGACTC	409bp
Transposagen Random Reverse 1	CGACCTACACCGAACTGAGA	
Transposagen Random Forward 2	CGGTGAAAACCTCTGACACA	380bp
Transposagen Random Reverse 2	ATTCACTGGCCGTCGTTTTA	

knock-in experiments, 4 showed positive bands with the random integration primers indicating an approximate 10% rate of random integration of the *AAVS1* donor vector.

Immunocytochemistry

Immunocytochemistry was performed as previously described (Mitzelfelt et al., 2016). Briefly, iPSCs were seeded onto 12mm glass coverslips in 12 well plates coated with Matrigel in mTeSR1 or StemMACS iPS-Brew XF supplemented with 10μM ROCK inhibitor. The following day, media was changed minus ROCK inhibitor and incubated for 4 h. iPSCs on coverslips were washed with DPBS, fixed with 4% paraformaldehyde at room temperature for 15 min, washed two times with DPBS, and stored in DPBS at 4°C until staining. Cells were permeabolized with 0.1% triton-X 100 in DBPS for 10 min, washed once in DPBS, and blocked for 1 h at room temperature with 3% bovine serum albumin (BSA-Sigma) in DPBS. Primary antibody was added in 3% BSA/DPBS and incubated for 2 h at room temperature. Primary antibodies: Nanog (Cell Signaling 4903p, USA, 1:200) and stage-specific embryonic antigen-4 (SSEA-4) (Stem Cell Technologies 60062AD, USA, 1:40). Cells were washed three times with DPBS. Secondary antibody was added in DBPS and incubated for 1 h at room temperature. Secondary antibody: Alexa Fluor 555 donkey anti-rabbit IgG (A31572). Cells were washed three times and mounted with Ultracruz Hard Set Mounting Media plus DAPI (Santa Cruz). Representative images were taken using the inverted Nikon Eclipse TE 2000.

Karyotyping

Karyotyping, performed as previously described (Mitzelfelt et al., 2016), was carried out by Wisconsin Diagnostic Laboratories (formerly Dynacare Laboratories), Milwaukee WI. Chromosomes of 20 proliferating cells were counted and fully analyzed using G-banding with representative images shown (Figure 4.5).

Potential off-target analysis

Clone analysis. Potential off-target sites were predicted by CRISPR RGEN Tools Cas-OFFinder (Bae et al., 2014) and are shown in Table 4.10 (with lowercase text indicating mismatches from the guide sequence). We chose the top 3-5 off-target sites for each CRISPR guide and designed primers that amplify a 300-500bp region around the off-target site. Off-target genomic regions were amplified using Accuprime Supermix II in all isolated knock-in clones. Amplicons were PCR-purified using a PureLink Quick PCR Purification Kit and Sanger sequencing was performed by Retrogen in both the 5' and 3' directions with the amplification primers. Sequences were analyzed using Sequencher software. Sequencing results were compared with the originating cell line (either hB53 hiPS6 or hB119 hiPS9). No mutations were noted (data not shown).

Illumina MiSeq analysis. To ensure CTS does not enrich for off-target effects, we chose our most active CRISPR (targeting *CRYAB*), and analyzed the top 12 potential off-target sites by deep-sequencing using the Illumina MiSeq. CRISPR RGEN Tools Cas-OFFinder (Bae et al., 2014) was used to identify potential off-target sites with sequences identified in Table 4.11 (lowercase text indicates mismatches from the guide sequence). Primers were designed flanking these sites and samples were prepared and analyzed using the Illumina MiSeq (as described above). PCR 1 primers are listed in Table 4.11 (adapter sequences in red and green text for the forward and reverse primers, respectively). Reads were inspected and 3'-clipped as described above before being aligned to the appropriate off-target reference sequences using Bowtie2 (with the 'local' alignment setting to maximize the chance of finding indels). Resulting SAM files were converted to sorted/indexed BAM files and loaded into IGV for viewing. We found no measurable difference in indel presence between pooled populations following CTS compared to without CTS.

Table 4.10 Off –target sites screened by Sanger sequencing

CRISPR	Potential Off-Target Site	Chromosome	Position	Primer Name	Primer Sequence (5'-3')
CRYAB	GaGATCCGGTAaTTCCTGAGG	chrY	17785850	OT_1_F	AGCATGCAGTTTAATCATTG
				OT_1_R	CCTATAATGTGTTGGGGAAA
	GGGATCCaGTAaTTCCTGAGG	chrY	18489869	OT_2_F	CAGCATGCAGTTCAATCAT
				OT_2_R	TATAACGTGTTGGGCAAAGT
	GGGATCCaGTAaTTCCTGTGG	chrY	23737276	OT_3_F	AGCCTGCAGTTCAATCAT
				OT_3_R	CATAAGGTGTTGGGCATATT
	GGGAaCaGGTATTTCCTGCGG	chr6	40874614	OT_4_F	TTCCTTGCTTTCTTCCTATG
				OT_4_R	AGGCCAGGGAAGTTAAAGTA
	GGGAaCCGcTATTTCCTGAGG	chrX	153640375	OT_5_F	GGTCTGACAGGAAACAAGAT
				OT_5_R	GGAGAAACATTTGGATTGAA
BAG3	GGGAaGAGCCAGATGgGgGTCAGG	chr12	53068310	OT_1_F	CAGCTCCATGAGCAAAAA
				OT_1_R	AAGTGTGTGGGGGAAGAC
	GGGAaGAGCaGATTGTGCGTaGGG	chr3	62611736	OT_2_F	CACAGAGCTTGGCTTCTAGT
				OT_2_R	CTACAAGGCCTTTGATGAGT
	GGGACGAGCCaATGTGCtTtAGG	chr7	57160206	OT_3_F	TCTGCATGTTGAAATTGTTT
				OT_3_R	TGGGAAAATTTTGGAGATTA
	GGcACGAGCTACcATGTcCGTCTGG	chr4	147603021	OT_4_F	CAATCCTCCCACCTTAGC
				OT_4_R	TCCTTTTATGCACCAAGTTT
LMNA	tATTGGACTTcTTGgGCAGCCGG	chr12	26116974	OT_1_F	CTAATGGTTTTAGCCCACAA
				OT_1_R	TCACATACAGCAAGCAAAAC
	CATgGGACTTGTTGCGtAGaTGG	chr10	6557892	OT_2_F	ATGTTTCAAAGCAAGGAAGA
				OT_2_R	CCCCTGTATTCAACTCCATA
	CAcTGGAaTTtTTGCtCAGCAGG	chr8	4084793	OT_3_F	AACACATTCACTTCCTTTGG
				OT_3_R	TTGGGAGAGAGAAAATGAAA
	CATTGGgCTgGTTGgGCAcCAGG	chr8	41681653	OT_4_F	TCCTATGTGGGAGAAGCA
				OT_4_R	TGTCCAGAATCAGCTTCTTT
	CATTGGgCTTaggGCGCAGCTGG	chr8	69992997	OT_5_F	AAGTCCAAAACGAAGGTGTT
				OT_5_R	CTGAGGCAGGAGAATCACT
MTERF4	ACcTGTATTCCAGTCTGAtCCTGG	chr12	115848234	OT_1_F	TTTTGAAATTGGGAGATGAG
				OT_1_R	TGAAGCTTTGTTCTTCCTGT
	cCTTGTAcTCCATGTTGACCCAGG	chr3	105899012	OT_2_F	CGTGTACTTTATCATTTAACAGC
				OT_2_R	GATCTGTGGACAGAAAGTCC
	ACTTtTATTCCAGcTGACCACAGG	chr5	53828304	OT_3_F	TCTTGTTTTACTGTGGCTGA
				OT_3_R	ATGGCTGTACAAAATTGAGC

Table 4.11 *CRYAB* off-target sites analyzed by Illumina MiSeq

Potential Off-Target Site	Chr	Position	Primer Name	Primer Sequence (5'-3')
GaGATCCGGTA aTTCCTGAGG	chrY	17785850	COT_MS_F_1	TCGTCGGCAGCGTCAGATGTGTATAAGAGA CAGCAGGCATGTTGTTGTTAATC*
			COT_MS_R_1	GTCTCGTGGGCTCGGAGATGTGTATAAGAG ACAGTTAGCTGGAAATTGTGATCC*
GGGATCCaGTA aTTCCTGAGG	chrY	18489869	COT_MS_F_2	TCGTCGGCAGCGTCAGATGTGTATAAGAGA CAGATTCATCAACCAAGCAGGT*
			COT_MS_R_2	GTCTCGTGGGCTCGGAGATGTGTATAAGAG ACAGCTTCAGCATTAGCTGGAAAT*
GGGATCCaGTA aTTCCTGTGG	chrY	23737276	COT_MS_F_3	TCGTCGGCAGCGTCAGATGTGTATAAGAGA CAGCAAGCAGGTTGTTGTAGTCA*
			COT_MS_R_3	GTCTCGTGGGCTCGGAGATGTGTATAAGAG ACAGCTTCAGCATTAGCTGGAAAT*
GGGATCCaGTA aTTCCTGAGG	chrY	23941131	COT_MS_F_4	TCGTCGGCAGCGTCAGATGTGTATAAGAGA CAGTAAGCAGGTTGTTGTTGTCA*
			COT_MS_R_4	GTCTCGTGGGCTCGGAGATGTGTATAAGAG ACAGCTTCAGCATTAGCTGGAAAT*
GGGAaCaGGTA TTTCCTGCGG	chr6	40874614	COT_MS_F_5	TCGTCGGCAGCGTCAGATGTGTATAAGAGA CAGGACCCTGTGTGAGACAGAAA
			COT_MS_R_5	GTCTCGTGGGCTCGGAGATGTGTATAAGAG ACAGGTGCCTTCTCATAGGGAAT
GGGAaCCGcTA TTTCCTGAGG	chrX	153640375	COT_MS_F_6	TCGTCGGCAGCGTCAGATGTGTATAAGAGA CAGCCAAGCAAACTTGCACTC
			COT_MS_R_6	GTCTCGTGGGCTCGGAGATGTGTATAAGAG ACAGAAAGGCTTGGTGGGTGAG
GGtATCCtGTAT TTCCTcTGG	chr8	41832706	COT_MS_F_7	TCGTCGGCAGCGTCAGATGTGTATAAGAGA CAGTATTGCACAGGACAGACTTG
			COT_MS_R_7	GTCTCGTGGGCTCGGAGATGTGTATAAGAG ACAGCAGCAGATGTTAGGTCAGAA
GaGATCaGGTAc TTCCTGGGG	chr8	120828204	COT_MS_F_8	TCGTCGGCAGCGTCAGATGTGTATAAGAGA CAGGTGCTCTTTGTTCTGAAGGA
			COT_MS_R_8	GTCTCGTGGGCTCGGAGATGTGTATAAGAG ACAGCAGTGTTGACAAGCATCTGA
GGGATCaGGTg TTTCtTGTGG	chr12	128299314	COT_MS_F_9	TCGTCGGCAGCGTCAGATGTGTATAAGAGA CAGAGACCAGCTCATCTTTTCAA
			COT_MS_R_9	GTCTCGTGGGCTCGGAGATGTGTATAAGAG ACAGGGTATTTAACGCTGAGAGCA
aGaATCtGGTAT TTCCTGTGG	chr3	123694853	COT_MS_F_10	TCGTCGGCAGCGTCAGATGTGTATAAGAGA CAGAGGCAGCTTTTCCAACCT
			COT_MS_R_10	GTCTCGTGGGCTCGGAGATGTGTATAAGAG ACAGCCTATAGCAGAGCCTCCAG
GaGATtCGGTcT TTCCTGAGG	chr3	179083191	COT_MS_F_11	TCGTCGGCAGCGTCAGATGTGTATAAGAGA CAGGCATGGACATCTGACCTACT
			COT_MS_R_11	GTCTCGTGGGCTCGGAGATGTGTATAAGAG ACAGTGGGAGATTAGAATGTTGCT
GGGAaCaGGgA TTTCCTGCGG	chr7	45889831	COT_MS_F_12	TCGTCGGCAGCGTCAGATGTGTATAAGAGA CAGGGAGGAATTAGGACTTCCAT
			COT_MS_R_12	GTCTCGTGGGCTCGGAGATGTGTATAAGAG ACAGTCAGCTTCTCCATCCTTAAA

*Primers amplified >1 locus with same sequence

Acknowledgements

We thank Shirng-Wern Tsaih and Michael Tschannen (Human Molecular Genetics Center, Medical College of Wisconsin) for advice and technical support. This work was supported by NIH New Innovator Award OD008396 (A.M.G) and NIH Director's Pioneer Award Grant HL17650 (I.J.B.), the Steven Cullen Healthy Heart Award (A.M.G.), made possible by the Research and Education Program Fund, a component of the Advancing a Healthier Wisconsin endowment at the Medical College of Wisconsin, a W.M. Keck Foundation Medical Research Grant (J.W.V.), and Ruth L. Kirschstein National Research Service Award F31 Individual Fellowship AR067618 (K.A.M.).

Author Contributions

Conceptualization, A.M.G., K.A.M., and C.M.D.R.; Methodology, A.M.G., K.A.M., and C.M.D.R.; Software and Formal Analysis, C.M.D.R.; Investigation, K.A.M., C.M.D.R., M.N.G., M.M., C.T.K., M.J.C.; K.D.K., M.R., and S.L.; Resources, D.P.D., D.H., C.J.J., and M.T.F.; Writing – Original Draft, C.M.D.R.; Writing – Review & Editing, C.M.D.R., K.A.M., A.M.G., and I.J.B.; Visualization, C.M.D.R. and K.A.M.; Supervision - A.M.G., C.M.D.R., and K.A.M.; Funding Acquisition, A.M.G., I.J.B., K.A.M., C.M.D.R., and J.W.V.

References

Arribere, J.A., Bell, R.T., Fu, B.X.H., Artiles, K.L., Hartman, P.S., and Fire, A.Z. (2014). Efficient marker-free recovery of custom genetic modifications with CRISPR/Cas9 in *Caenorhabditis elegans*. Genetics 198, 837-846.

Bae, S., Park, J., and Kim, J.-S. (2014). Cas-OFFinder: A fast and versatile algorithm that searches for potential off-target sites of Cas9 RNA-guided endonucleases. Bioinformatics 30, 1473-1475.

Bhaya, D., Davison, M., and Barrangou, R. (2011). CRISPR-Cas systems in Bacteria and Archaea: Versatile small RNAs for adaptive defense and regulation. Ann. Rev. Gen. 45, 273-297.

Bolger, A.M., Lohse, M., and Usadel, B. (2014). Trimmomatic: A flexible trimmer for Illumina sequence data. Bioinformatics 30, 2114-2120.

Chen, F., Pruett-Miller, S.M., Huang, Y., Gjoka, M., Duda, K., Taunton, J., Collingwood, T.N.,

Frodin, M., and Davis, G.D. (2011). High-frequency genome editing using ssDNA oligonucleotides with zinc-finger nucleases. Nat. Meth. 8, 753-755.

Cong, L., Ran, F.A., Cox, D., Lin, S., Barretto, R., Habib, N., Hsu, P.D., Wu, X., Jiang, W., Marraffini, L.A., et al. (2013). Multiplex genome engineering using CRISPR/Cas systems. Science 339, 819-823.

Dialynas, G., Flannery, K.M., Zirbel, L.N., Nagy, P.L., Mathews, K.D., Moore, S.A., and Wallrath, L.L. (2012). LMNA variants cause cytoplasmic distribution of nuclear pore proteins in Drosophila and human muscle. Hum. Mol. Gen. 21, 1544-1556.

Ding, Q., Lee, Y.-K., Schaefer, Esperance A.K., Peters, Derek T., Veres, A., Kim, K., Kuperwasser, N., Motola, Daniel L., Meissner, Torsten B., Hendriks, William T., et al. (2013). A TALEN genome-editing system for generating human stem cell-based disease models. Cell Stem Cell 12, 238-251.

Doench, J.G., Fusi, N., Sullender, M., Hegde, M., Vaimberg, E.W., Donovan, K.F., Smith, I., Tothova, Z., Wilen, C., Orchard, R., et al. (2016). Optimized sgRNA design to maximize activity and minimize off-target effects of CRISPR-Cas9. Nat. Biotech. 34, 184-191.

Elliott, D.A., Braam, S.R., Koutsis, K., Ng, E.S., Jenny, R., Lagerqvist, E.L., Biben, C., Hatzistavrou, T., Hirst, C.E., Yu, Q.C., et al. (2011). NKX2-5eGFP/w hESCs for isolation of human cardiac progenitors and cardiomyocytes. Nat. Meth. 8, 1037-1040.

Forrest, K.M.L., Al-Sarraj, S., Sewry, C., Buk, S., Tan, S.V., Pitt, M., Durward, A., McDougall, M., Irving, M., Hanna, M.G., et al. (2011). Infantile onset myofibrillar myopathy due to recessive CRYAB mutations. Neuromuscular Disord. 21, 37-40.

Geurts, A.M., Cost, G.J., Freyvert, Y., Zeitler, B., Miller, J.C., Choi, V.M., Jenkins, S.S., Wood, A., Cui, X., Meng, X., et al. (2009). Knockout rats via embryo microinjection of zinc-finger nucleases. Science 325, 433-433.

Güell, M., Yang, L., and Church, G.M. (2014). Genome editing assessment using CRISPR Genome Analyzer (CRISPR-GA). Bioinformatics 30, 2968-2970.

Gutschner, T., Haemmerle, M., Genovese, G., Draetta, Giulio F., and Chin, L. (2016). Post-translational regulation of Cas9 during G1 enhances homology-directed repair. Cell Reports 14, 1555-1566.

Hockemeyer, D., and Jaenisch, R. (2016). Induced pluripotent stem cells meet genome editing. Cell Stem Cell 18, 573-586.

Hockemeyer, D., Wang, H., Kiani, S., Lai, C.S., Gao, Q., Cassady, J.P., Cost, G.J., Zhang, L., Santiago, Y., Miller, J.C., et al. (2011). Genetic engineering of human pluripotent cells using TALE nucleases. Nat. Biotech. 29, 731-734.

Kistler, Kathryn E., Vosshall, Leslie B., and Matthews, Benjamin J. (2015). Genome engineering with CRISPR-Cas9 in the mosquito *Aedes aegypti*. Cell Reports 11, 51-60.

Lin, S., Staahl, B.T., Alla, R.K., and Doudna, J.A. (2014). Enhanced homology-directed human genome engineering by controlled timing of CRISPR/Cas9 delivery. eLife 3, e04766.

Long, C., McAnally, J.R., Shelton, J.M., Mireault, A.A., Bassel-Duby, R., and Olson, E.N. (2014). Prevention of muscular dystrophy in mice by CRISPR/Cas9–mediated editing of germline DNA. Science 345, 1184-1188.

Maruyama, T., Dougan, S.K., Truttmann, M.C., Bilate, A.M., Ingram, J.R., and Ploegh, H.L. (2015). Increasing the efficiency of precise genome editing with CRISPR-Cas9 by inhibition of nonhomologous end joining. Nat. Biotech. 33, 538-542.

Miller, J.C., Holmes, M.C., Wang, J., Guschin, D.Y., Lee, Y.-L., Rupniewski, I., Beausejour, C.M., Waite, A.J., Wang, N.S., Kim, K.A., et al. (2007). An improved zinc-finger nuclease architecture for highly specific genome editing. Nat. Biotech. 25, 778-785.

Mitzelfelt, K.A., Limphong, P., Choi, M.J., Kondrat, F.D., Lai, S., Kolander, K.D., Kwok, W.M., Dai, Q., Grzybowski, M.N., Zhang, H., et al. (2016). Human 343delT HSPB5 Chaperone associated with Early-onset Skeletal Myopathy causes Defects in Protein Solubility. J Biol Chem.

Miyaoka, Y., Chan, A.H., Judge, L.M., Yoo, J., Huang, M., Nguyen, T.D., Lizarraga, P.P., So, P.-L., and Conklin, B.R. (2014). Isolation of single-base genome-edited human iPS cells without antibiotic selection. Nat. Meth. 11, 291-293.

Norton, N., Li, D., Rieder, Mark J., Siegfried, Jill D., Rampersaud, E., Züchner, S., Mangos, S., Gonzalez-Quintana, J., Wang, L., McGee, S., et al. (2011). Genome-wide studies of copy number variation and exome sequencing identify rare variants in BAG3 as a cause of dilated cardiomyopathy. Amer. J. Hum. Gen. 88, 273-282.

Paquet, D., Kwart, D., Chen, A., Sproul, A., Jacob, S., Teo, S., Olsen, K.M., Gregg, A., Noggle, S., and Tessier-Lavigne, M. (2016). Efficient introduction of specific homozygous and heterozygous mutations using CRISPR/Cas9. Nature advance online publication.

Ponce de León, V., Mérillat, A.-M., Tesson, L., Anegón, I., and Hummler, E. (2014). Generation of TALEN-Mediated GR^{dim} Knock-in rats by homologous recombination. PLoS One 9, e88146.

Richardson, C.D., Ray, G.J., DeWitt, M.A., Curie, G.L., and Corn, J.E. (2016). Enhancing homology-directed genome editing by catalytically active and inactive CRISPR-Cas9 using asymmetric donor DNA. Nat. Biotech. 34, 339-344.

Riedel, M., Jou, Chuanchau J., Lai, S., Lux, Robert L., Moreno, Alonso P., Spitzer, Kenneth W., Christians, E., Tristani-Firouzi, M., and Benjamin, Ivor J. (2014). Functional and pharmacological analysis of cardiomyocytes differentiated from human peripheral blood mononuclear-derived pluripotent stem cells. Stem Cell Rep. 3, 131-141.

Sacconi, S., Féasson, L., Antoine, J.C., Pécheux, C., Bernard, R., Cobo, A.M., Casarin, A., Salviati, L., Desnuelle, C., and Urtizberea, A. (2012). A novel CRYAB mutation resulting in multisystemic disease. Neuromuscular Disord. 22, 66-72.

Sadelain, M., Papapetrou, E.P., and Bushman, F.D. (2012). Safe harbours for the integration of new DNA in the human genome. Nat. Rev. Cancer 12, 51-58.

Soldner, F., Laganière, J., Cheng, Albert W., Hockemeyer, D., Gao, Q., Alagappan, R., Khurana, V., Golbe, Lawrence I., Myers, Richard H., Lindquist, S., et al. (2011). Generation of isogenic

pluripotent stem cells differing exclusively at two early onset Parkinson point mutations. Cell 146, 318-331.

Tsai, S.Q., Zheng, Z., Nguyen, N.T., Liebers, M., Topkar, V.V., Thapar, V., Wyvekens, N., Khayter, C., Iafrate, A.J., Le, L.P., et al. (2015). GUIDE-seq enables genome-wide profiling of off-target cleavage by CRISPR-Cas nucleases. Nat. Biotech. 33, 187-197.

Vicart, P., Caron, A., Guicheney, P., Li, Z., Prevost, M.-C., Faure, A., Chateau, D., Chapon, F., Tome, F., Dupret, J.-M., et al. (1998). A missense mutation in the αB-crystallin chaperone gene causes a desmin-related myopathy. Nat. Gen. 20, 92-95.

Villard, E., Perret, C., Gary, F., Proust, C., Dilanian, G., Hengstenberg, C., Ruppert, V., Arbustini, E., Wichter, T., Germain, M., et al. (2011). A genome-wide association study identifies two loci associated with heart failure due to dilated cardiomyopathy. Europ. Heart J. 32, 1065-1076.

Wang, G., McCain, M.L., Yang, L., He, A., Pasqualini, F.S., Agarwal, A., Yuan, H., Jiang, D., Zhang, D., Zangi, L., et al. (2014). Modeling the mitochondrial cardiomyopathy of Barth syndrome with induced pluripotent stem cell and heart-on-chip technologies. Nat. Med. 20, 616-623.

Ward, J.D. (2015). Rapid and precise engineering of the *Caenorhabditis elegans* genome with lethal mutation co-conversion and inactivation of NHEJ repair. Genetics 199, 363-377.

Yang, L., Guell, M., Byrne, S., Yang, J.L., De Los Angeles, A., Mali, P., Aach, J., Kim-Kiselak, C., Briggs, A.W., Rios, X., et al. (2013). Optimization of scarless human stem cell genome editing. Nuc. Acids Res. 41, 9049-9061.

Yu, C., Liu, Y., Ma, T., Liu, K., Xu, S., Zhang, Y., Liu, H., La Russa, M., Xie, M., Ding, S., et al. (2015). Small molecules enhance CRISPR genome editing in pluripotent stem cells. Cell Stem Cell 16, 142-147.

Yusa, K., Rashid, S.T., Strick-Marchand, H., Varela, I., Liu, P.-Q., Paschon, D.E., Miranda, E., Ordonez, A., Hannan, N.R.F., Rouhani, F.J., et al. (2011). Targeted gene correction of α1-antitrypsin deficiency in induced pluripotent stem cells. Nature 478, 391-394.

CHAPTER 5

DISCUSSION: HSPB5 IN MYOPATHY AND CTS CRITIQUE

Mechanisms of HSPB5 in (Cardio-) Myopathy

Chapter 3 presents molecular and biochemical data regarding 343delT HSPB5 protein dynamics (Mitzelfelt et al., 2016). Of interest, evidence for extreme insolubility of the mutant protein is evident and rescued by fusion with a SUMO moiety, a known solubilizing modification. Coexpression of 343delT with WT HSPB5 also solubilizes the mutant form of the protein. Insoluble 343delT is likely functionally unavailable, thereby supporting a loss of function disease mechanism. On a related theme, phenotypes of the *HSPB2/HPSB5* double knockout mouse (DKO) (Brady et al., 2001) are neither as severe nor early-onset as the signs observed in the patient (Forrest et al., 2011). In addition, the mutant protein accumulates as dense, irregular deposits in the patient's skeletal muscle biopsy (Forrest et al., 2011). This suggests a potential detrimental impact of the presence of the 343delT protein in disease progression. Indeed, overexpression of 343delT results in protein aggregates that can colocalize with the intermediate filament protein desmin and induce a cellular stress response indicating disruption of proteostasis (Mitzelfelt et al., 2016). These data suggest a model in which disease onset in the homozygous 343delT state is initiated by lack of HSPB5 (i.e., loss of function) leading to an "at risk" muscle. Activation of cellular stress response pathways leads to transcriptional upregulation of *HSPB5*, and this combined with a potential "second-hit stress" results in accumulated, aggregated mutant protein that then may impose detrimental effects on the cell (i.e., gain-of-toxic function) resulting in accelerated disease progression and increased severity. This working model is outlined in Figure 5.1.

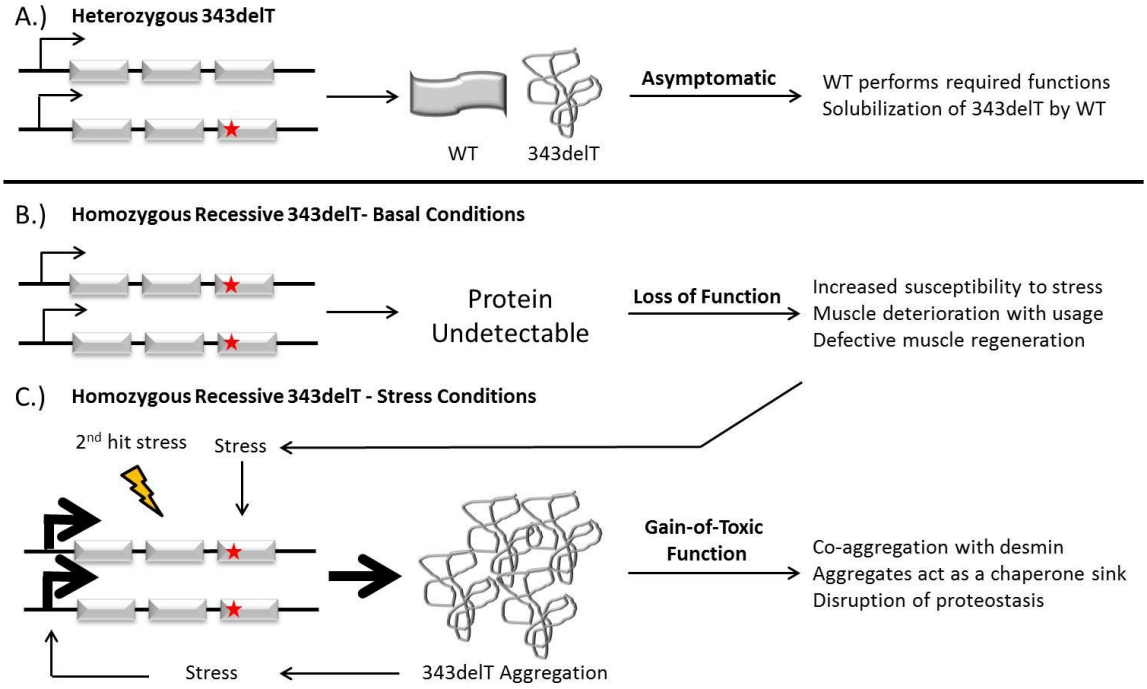

Figure 5.1: Working Model for Potential Gain and Loss of Function Effects of 343delT in Myopathy. A.) The heterozygous 343delT parents, with one WT and one 343delT (denoted by the red star) allele are asymptomatic, as WT is available to perform essential functions and 343delT is solubilized by WT. The homozygous recessive 343delT patient (B and C) can only produce 343delT protein. B.) Initially, 343delT protein is undetectable in the cells leading to loss of HSPB5 function that triggers increased susceptibility to stress, muscle deterioration with usage, and inability to properly regenerate muscle. In turn, cellular stress ensues. C.) As *HSPB5* is a stress response gene, we hypothesize that stress-inducible upregulation in conjunction with a potential "second hit stress" are both necessary and sufficient to produce detectable levels of 343delT protein, which is highly insoluble alone. Accumulation of 343delT protein aggregates in the cell resulting in gain-of-toxic function effects including perturbing the positive feedback stress loop and a deleterious cascade of events causing coaggregation with other metastable proteins including desmin, acting as a chaperone sink, and disrupting overall cellular proteostasis resulting in early onset disease.

These data provide an example of potential mechanisms for a recessive mutant contributing to myopathy. The general principles may be applicable to other mutant forms of HSPB5, including dominant and recessive variants. Indeed, it has been suggested that the well-studied variant, R120G, likely results in disease due to a combination of both loss and gain of function effects (Sanbe et al., 2011). Focusing only on variants that result in muscle (cardiac or skeletal) disease (reviewed in Chapter 1, Table 1.1) (Mitzelfelt and Benjamin, 2015), variability exists as to which tissue is affected, dominant or recessive presentation, and infantile or adult-onset. The recessive mutants, 343delT and 60delC, result in infantile-onset, severe skeletal myopathy; whereas dominant mutations affecting either or both tissue types result in adult-onset symptoms. With only the present data, it is unknown if the now unaffected, heterozygous parents of the patients with the recessive mutations will exhibit symptoms due to the presence of the heterozygous mutation later in life. If this proves to be the case, a dominant inheritance pattern could also be suggested for these mutants, with the homozygous state resulting in enhanced susceptibility and increased severity. However, the ability of at least 343delT to be solubilized by its WT counterpart (Chapter 3) (Mitzelfelt et al., 2016), suggests that potential detrimental effects of the mutant may be ameliorated by the presence of the WT protein.

All but one of the (cardio-) myopathy-associated mutations in HSPB5 result in aberrant accumulation or aggregation of the mutant protein. The nonaggregating mutation, R157H, results in reduced binding efficacy to titin and likely has alternative disease mechanisms compared with the other mutations (Inagaki et al., 2006). It is possible that the aggregating mutants may follow a similar disease progression as predicted for 343delT in Figure 5.1. Dominant variants may result in adult-onset due to competition of the mutant protein with the WT form early in life (Andley et al., 2011; Perng et al., 2004; Vicart et al., 1998), while in the recessive state, infantile-onset likely results due to lack of WT. Reaching a threshold of mutant protein may be a common required theme among variants. As insoluble mutant protein levels surpass a threshold, a tipping point is met that results in a downward spiral and disruption for maintaining proteostasis within the cell.

The relative insolubility of the specific variant, its ability to be solubilized by WT HSPB5, and the presence or absence of WT (i.e., heterozygous or homozygous) likely contribute to the tipping point at which this threshold is breached. Once surpassed, the so-called gain-of-toxic function effects of the mutants ensue. The fact that *HSPB5* is a stress response gene perpetuates the problem by creating a positive feedback loop where enhanced stress results in stress-inducible transcriptional upregulation of the mutant *HSPB5*, thereby producing more mutant protein in an already saturated system. Such protein aggregates are known contributors to disruption of proteostasis, functioning with a cascade effect, nucleating small aggregates that increase in size as additional meta-stable proteins and corresponding chaperones become sequestered within the aggregates, thereby enhancing the detrimental impact (McLendon and Robbins, 2011; Pattison et al., 2011; Wang et al., 2003; Wang and Robbins, 2006). Meta-stable components that are lost from the cytoplasm into the aggregates, and not resynthesized in a timely manner, likely contribute to myopathy through a loss of function mechanism (Yang and Hu, 2016; Yang et al., 2014).

HSPB5 is a key component for skeletal muscle maintenance over time as is shown by the DKO mouse model, which displays progressive myopathy throughout life (Brady et al., 2001). Whereas the DKO mouse only exhibits cardiac defects when subjected to stress conditions (Morrison et al., 2004; Pinz et al., 2008). Though each tissue has some variability in protein/isoform expression, both cardiac and skeletal muscle likely benefit in a similar fashion from the chaperone function of HSPB5. A major difference between the tissues is the unique ability of skeletal muscle to undergo regeneration from resident progenitor (or satellite) cells. HSPB5 has also been shown to play critical roles in the differentiation of satellite cells into myotubes (reviewed in Chapter 1) (Mitzelfelt and Benjamin, 2015). This unique role of HSPB5 in progenitor cell differentiation may be a reason for heightened sensitivity of skeletal muscle in a loss of function situation (e.g., DKO mouse or recessive mutation), resulting in early-onset defects.

The apparent tissue specificity of the various mutations poses interesting questions as well. It is difficult to discern true tissue specificity from the small number of patients harboring these disease-causing mutations with undoubtedly variable lifestyles and genetic/epigenetic backgrounds. Only a snapshot of current events is available, without taking into account what might occur in the future or under specific conditions. Stress undergone by the tissue is unmistakably a factor affecting tissue susceptibility. In addition, the expression of potential modifier genes most likely affects outcomes. Future experiments using model systems that allow controlled comparisons would be required to determine true tissue specificity.

Many questions remain as to the contribution of HSPB5 disruption in (cardio-) myopathy. Chapter 6 discusses future experiments designed for further investigation into mechanisms and treatments for 343delT in myopathy in the form of a proposal. Studies involving 343delT present a platform to provide a better understanding of how chaperones contribute to overall muscle homeostasis and how defects in chaperones contribute to disease. An understanding derived from these experiments will likely be adaptable to other systems.

Genome Editing with CTS: Advantages, Disadvantages, and Future Studies

Vast progress has been made with genome engineering, especially over the last ten years, necessitating its use in many aspects of research. Protocol publications and key advancements will make this technology more available and less intimidating to the common laboratory. CTS (described in Chapter 4), provides an efficient, innovative but simple strategy for enhancing the isolation of precision-modified clones that makes disease-in-a-dish model production readily available to the common user for the following reasons (see Table 5.1 for comparison with other published strategies):

- Simplicity- CTS requires only design of a gene-specific sgRNA and ssODN, not the design of an extensive targeting vector, which many laboratories that are less well versed in molecular biology may find to be a daunting task. Also, CTS does not require the use

Table 5.1: Comparison of CTS with previously published strategies

Task or Quality	NS	TS	Sib-selection	CTS
Hands on time for component design/generation (guide RNA and vector or ssODN)	1 h	4 h	1 h	1 h
Total time for preparing components (shipping, cloning, etc.)	1 week	1-4 weeks (depending on strategy)	1 week	1 week
Hands on time for transfection of iPSCs	2 h	4 h	2 h	2 h
Hands on time for sib-selection	None	None	8 h	None
Clone number to isolate	>2000	10	10	10-50
Hands on time for feeding cells	15-25 h	30 min	1 h	30 min
Hands-on time for isolating and genotyping clones	>100 h	4 h	1 h	4-6 h
Total time required (from design-genotype)	~3.5 weeks	~11-14 weeks	~3.5 weeks	~3.5 weeks
Total hands-on time required	~122-132 h	~13 h	~13 h	~9 h
Restrictiveness in targeting	None	Need a TTAA site	None	None
Factors for off-target damage	Nucleases	Nucleases and piggyBac transposon	Nucleases	Nucleases (GOI and AAVS1)
Scarless	Yes	Yes	Yes	Can be adapted
Technical difficulty	Low	Medium	Medium	Low
Required additional equipment	None	None	ddPCR	None

Adapted from Miyaoka and colleagues (Miyaoka et al., 2014). NS= no selection/direct cloning. TS= targeting with selection/ *piggyBac* system (Yusa et al., 2011). Sib-selection= digital droplet (dd) PCR method for prescreening pooled populations (Miyaoka et al., 2014).

of additional equipment over conventional targeting.

- Speed- CTS is a one-step editing process as opposed to other efficient two-step strategies that require subsequent removal of a selection cassette (Yusa, 2013; Yusa et al., 2011). CTS leave a selection cassette in a safe-harbor locus, which is an allowable and controllable presence for most research purposes, though not applicable for clinical use.
- Efficiency- CTS provides marked enhancement of efficiency for the incorporation of variants of interest over no selection and transient selection for transfection.
- Cost- CTS utilizes custom ssODNs, which are around 10-fold cheaper than custom targeting vectors and require less time for production. The upfront cost of purchasing the commercially available *AAVS1* targeting vector/TALEN kit utilized in CTS is generalizable to all future editing experiments performed by the laboratory.
- Scalability- Many genes can be targeted using the *AAVS1* components for CTS in concert with easily designed and generated gene-specific CRISPR/Cas9 guide RNAs and ssODNs.

As discussed in Chapter 2, the future holds further advances in efficiency and specificity of genome editing for both laboratory and clinical applications. Though CTS is not the "one size fits all" solution to genome editing, it provides a straightforward alternative to other available strategies allowing the common user a method for time-efficient, inexpensive, simple, and scalable genome editing, which is critical for the further dissemination and widespread use of the technology. Coupling CTS with other strategies such as inhibition of NHEJ (Maruyama et al., 2015), cell cycle synchronization (Lin et al., 2014), or delivery of targeting components as preassembled RNPs (Lin et al., 2014) will likely further enhance the efficiency of recovering HDR-modified clones. Additionally, alternative selection strategies to knock-in of the selection cassette at *AAVS1* could be employed. For example, selecting for HDR by fluorescence activated cell sorting (FACS) through incorporation of a fluorescent marker, knock-in of a cell type-specific reporter, or selection for alterations in a surface marker through FACS. These strategies

would utilize the hypothesis of CTS, while altering the selection method.

The CTS hypothesis, *selection for HDR at one locus enriches for HDR at a second locus*, suggests that certain "receptive" cells are more amenable to genome editing than other "refractory" cells. Though the efficiency data presented in Chapter 4 support this hypothesis, the mechanism remains elusive. Receptivity could be a transient state, brought on by stage of the cell cycle, expression of components necessary for editing, cell stress status, age, etc. Alternatively, receptivity could be a permanent state, retained by certain cells within a culture. The implications of the latter suggest heterogeneity within the culture that could be selected for with multiple rounds of targeting. Though at first glance this is appealing, it presents further questions as to the status of these "super-editable" cells that may confound future work performed for phenotypic analysis, etc. This idea could be tested through subsequent rounds of CTS to determine if efficiency of editing is enhanced in a population of cells that previously underwent CTS. Additional work to elucidate mechanisms behind CTS would likely require the ability to single-cell sort cells as they undergo the editing process to compare the cell cycle state, transcriptome, and proteome of receptive versus refractory cells in order to elucidate factors contributing to this HDR-receptive state. The ability to isolate and purify cells as they undergo editing is less well defined and warrants further investigation.

Extreme locus variability with respect to the efficiency of CTS was observed and is being actively investigated. Local sequence composition and chromatin organization likely affect both the ability of the SSN to bind and cleave DNA, as well as the repair pathway preference. It is difficult to generalize comparisons across loci due to the multitude of variables (e.g., sequence, chromatin state, etc.). Therefore, answers to these questions will require careful study design limiting variables in order to examine the impact of sequence, chromatin organization, and gene activity. Such studies must be performed over multiple loci.

An additional advantage of CTS is the ability to concurrently target multiple loci. Indeed, in Chapter 4, two variants of interest were knocked-in simultaneously along with the selection

cassette at *AAVS1*, for a total of three HDR events occurring concurrently in one cell. Experiments attempting to incorporate three variants of interest (four total editing events) were met with poor cell viability, due potentially to an overload of DNA upon transfection, too much Cas9 protein (since each gene of interest's sgRNA plasmid also contained Cas9 coding sequence), or overwhelming the cell with DSBs. Generation and use of plasmid arrays that include multiple sgRNAs and only one sequence for Cas9 may alleviate these issues making it efficient to target multiple loci simultaneously. This is important for the study of multifactorial diseases and modifier genes, where sequential editing of individual loci is time consuming and laborious.

Overall, CTS is an efficient, innovative but simple strategy for enhancing the isolation of precision-modified clones that is usable by a broad audience. Though it does not provide the magic bullet solution to genome editing efficiency, it does present a straightforward available solution making editing possible for a multitude of laboratories new to the field. Ease of use is key as genome editing quickly becomes a required technology for obtaining research funding for many applications. As progress in the field ensues, there will no doubt be further improvements and advances.

References

Andley, U.P., Hamilton, P.D., Ravi, N., and Weihl, C.C. (2011). A knock-in mouse model for the R120G mutation of alphaB-crystallin recapitulates human hereditary myopathy and cataracts. PloS One 6, e17671.

Brady, J.P., Garland, D.L., Green, D.E., Tamm, E.T., Giblin, F.J., and Wawrousek, E.F. (2001). aB-Crystallin in lens development and muscle integrity: A gene knockout approach. IOVS 42, 2924-2934.

Forrest, K.M., Al-Sarraj, S., Sewry, C., Buk, S., Tan, S.V., Pitt, M., Durward, A., McDougall, M., Irving, M., Hanna, M.G., et al. (2011). Infantile onset myofibrillar myopathy due to recessive CRYAB mutations. Neuromuscular Disord. NMD 21, 37-40.

Inagaki, N., Hayashi, T., Arimura, T., Koga, Y., Takahashi, M., Shibata, H., Teraoka, K., Chikamori, T., Yamashina, A., and Kimura, A. (2006). Alpha B-crystallin mutation in dilated cardiomyopathy. Biochem. Biophys. Res. Comm. 342, 379-386.

Lin, S., Staahl, B.T., Alla, R.K., and Doudna, J.A. (2014). Enhanced homology-directed human genome engineering by controlled timing of CRISPR/Cas9 delivery. eLife 3, e04766.

Maruyama, T., Dougan, S.K., Truttmann, M.C., Bilate, A.M., Ingram, J.R., and Ploegh, H.L. (2015). Increasing the efficiency of precise genome editing with CRISPR-Cas9 by inhibition of nonhomologous end joining. Nat. Biotech. 33, 538-542.

McLendon, P.M., and Robbins, J. (2011). Desmin-related cardiomyopathy: an unfolding story. Amer. J. Phys. Heart Circ. Phys. 301, H1220-H1228.

Mitzelfelt, K.A., and Benjamin, I.J. (2015). Multifunctional roles of αB-crystallin in skeletal and cardiac muscle homeostasis and disease. In The Big Book on Small Heat Shock Proteins, R.M. Tanguay, and L.E. Hightower, eds. (Springer International Publishing), pp. 269-299.

Mitzelfelt, K.A., Limphong, P., Choi, M.J., Kondrat, F.D.L., Lai, S., Kolander, K.D., Kwok, W.-M., Dai, Q., Grzybowski, M.N., Zhang, H., et al. (2016). Human 343delT HSPB5 chaperone associated with early-onset skeletal myopathy causes defects in protein solubility. J. Biol. Chem. 291, 14939-14953.

Miyaoka, Y., Chan, A.H., Judge, L.M., Yoo, J., Huang, M., Nguyen, T.D., Lizarraga, P.P., So, P.-L., and Conklin, B.R. (2014). Isolation of single-base genome-edited human iPS cells without antibiotic selection. Nat. Meth. 11, 291-293.

Morrison, L.E., Whittaker, R.J., Klepper, R.E., Wawrousek, E.F., and Glembotski, C.C. (2004). Roles for αB-crystallin and HSPB2 in protecting the myocardium from ischemia-reperfusion-induced damage in a KO mouse model. Amer. J. Phys. Heart Circ. Phys. 286, H847-H855.

Pattison, J.S., Osinska, H., and Robbins, J. (2011). Atg7 induces basal autophagy and rescues autophagic deficiency in CryABR120G cardiomyocytes. Circ. Res. 109, 151-160.

Perng, M.D., Wen, S.F., van den, I.P., Prescott, A.R., and Quinlan, R.A. (2004). Desmin aggregate formation by R120G alphaB-crystallin is caused by altered filament interactions and is dependent upon network status in cells. Mol. Biol. Cell 15, 2335-2346.

Pinz, I., Robbins, J., Rajasekaran, N.S., Benjamin, I.J., and Ingwall, J.S. (2008). Unmasking different mechanical and energetic roles for the small heat shock proteins CryAB and HSPB2 using genetically modified mouse hearts. FASEB J. 22, 84-92.

Sanbe, A., Marunouchi, T., Yamauchi, J., Tanonaka, K., Nishigori, H., and Tanoue, A. (2011). Cardioprotective effect of nicorandil, a mitochondrial ATP-sensitive potassium channel opener, prolongs survival in HSPB5 R120G transgenic mice. PloS One 6, e18922.

Vicart, C.A., Guicheney, P., Li, Z., Prévost, M.C., Faure, A., Chateau, D., Chapon, F., Tomé, F., Dupret, J.M., Paulin, D., et al. (1998). A missense mutation in the alphaB-crystallin chaperone gene causes a desmin-related myopathy. Nat. Gen. 20, 92-95.

Wang, X., Klevitsky, R., Huang, W., Glasford, J., Li, F., and Robbins, J. (2003). AlphaB-crystallin modulates protein aggregation of abnormal desmin. Circ. Res. 93, 998-1005.

Wang, X., and Robbins, J. (2006). Heart failure and protein quality control. Circ. Res. 99, 1315-1328.

Yang, H., and Hu, H.-Y. (2016). Sequestration of cellular interacting partners by protein aggregates: Implication in a loss-of-function pathology. FEBS J., ahead of print.

Yang, H., Li, J.-J., Liu, S., Zhao, J., Jiang, Y.-J., Song, A.-X., and Hu, H.-Y. (2014). Aggregation of polyglutamine-expanded ataxin-3 sequesters its specific interacting partners into inclusions: Implication in a loss-of-function pathology. Sci. Rep. 4, 6410.

Yusa, K. (2013). Seamless genome editing in human pluripotent stem cells using custom endonuclease–based gene targeting and the piggyBac transposon. Nat. Prot. 8, 2061-2078.

Yusa, K., Rashid, S.T., Strick-Marchand, H., Varela, I., Liu, P.-Q., Paschon, D.E., Miranda, E., Ordonez, A., Hannan, N.R.F., Rouhani, F.J., et al. (2011). Targeted gene correction of α-antitrypsin deficiency in induced pluripotent stem cells. Nature 478, 391-394.

CHAPTER 6

FUTURE DIRECTIONS FOR THE STUDY OF 343DELT HSPB5

Introduction

Myofibrillar myopathy describes a heterogeneous group of diseases resulting from malfunctioning muscle fibers, of which a subclass is caused by mutant protein chaperones. Multiple mutations in *HSPB5* (CRYAB or αB-crystallin) have been identified with both congenital-onset and adult-onset skeletal myopathy. HSPB5 is a small molecular-weight heat shock protein that functions as a chaperone for client substrates including desmin, titin, and actin. HSPB5 also impacts differentiation of skeletal muscle progenitor cells affecting proliferation, cell cycle exit, levels of the muscle-regulatory factor MyoD, and modulation of RNA-induced silencing complex (RISC) activity. A patient harboring the homozygous recessive, nonsense mutation, 343delT in *HSPB5* has been reported with symptoms and signs of severe congenital myopathy including extreme muscle stiffness and degeneration following normal development. The patient's muscle biopsy shows dense, irregular staining of 343delT consistent with aggregation observed in culture upon overexpression, which also induces a cellular stress response and stochastically incorporates the intermediate protein desmin. The patient's presentation also has similarities to the *HSPB5/*HSPB2 double knockout mouse, though the mouse seems to have less severe and later onset muscle deterioration. Therefore, the question as to whether this disease pathology results from loss of HSPB5 function and/or gain-of-toxic function of 343delT HSPB5 remains and whether this impact is seen in myogenic progenitor cells and/or differentiated myotubes. Clinical disease manifestation is likely multifactorial, stochastic, age-dependent, and perhaps tissue dependent.

This chapter outlines future directions for the study of 343delT including both *in vitro* human cell culture models and *in vivo* rat models to define loss and gain of function effects of the mutation and is written in the form of a proposal. It builds upon preliminary studies of 343delT presented in Chapter 3 and utilizes genome editing techniques outlined in Chapter 4. The underlying hypothesis being tested is that mutant chaperones result in myopathy not only due to a loss of function mechanism but that aggregation of the mutant protein itself exacerbates disease severity and progression and that principal defects in muscle progenitor cells contribute to the inability of damaged muscle to sufficiently repair itself. The future experiments presented in this chapter can be divided into the following two major aims as outlined in Figure 6.1:

Aim 1: Modeling disease-causing HSPB5 343delT-associated congenital myopathy in human iPSCs.

Human iPSCs will be used to model HSPB5 343delT congenital myopathy as well as knockout of HSPB5 *in vitro* through differentiation to skeletal myotubes (iSKMs).

Aim 1.1. Phenotypic analysis of iSKMs will be performed including examination of aggregation, sarcomere and cellular breakdown, titin disruption, as well as changes in gene expression. Exogenous stressors will be supplied to provoke phenotypes that may not be visible in 2D static cultures.

Aim 1.2. Skeletal muscle progenitor cells will be isolated and analyzed for defects in proliferation, cell cycle exit, differentiation, and gene expression with response to cellular injury *in vitro* and transplanted *in vivo*. Successful completion of this aim will provide a platform for the study of congenital myopathies *in vitro*.

Aim 2: Modeling disease-causing HSPB5 343delT-associated congenital myopathy using genetically engineered rats

To promote this research for translation into humans, genetically engineered rat models with knock-in of *HSPB5* 343delT will be generated. The extent of myopathy will be characterized

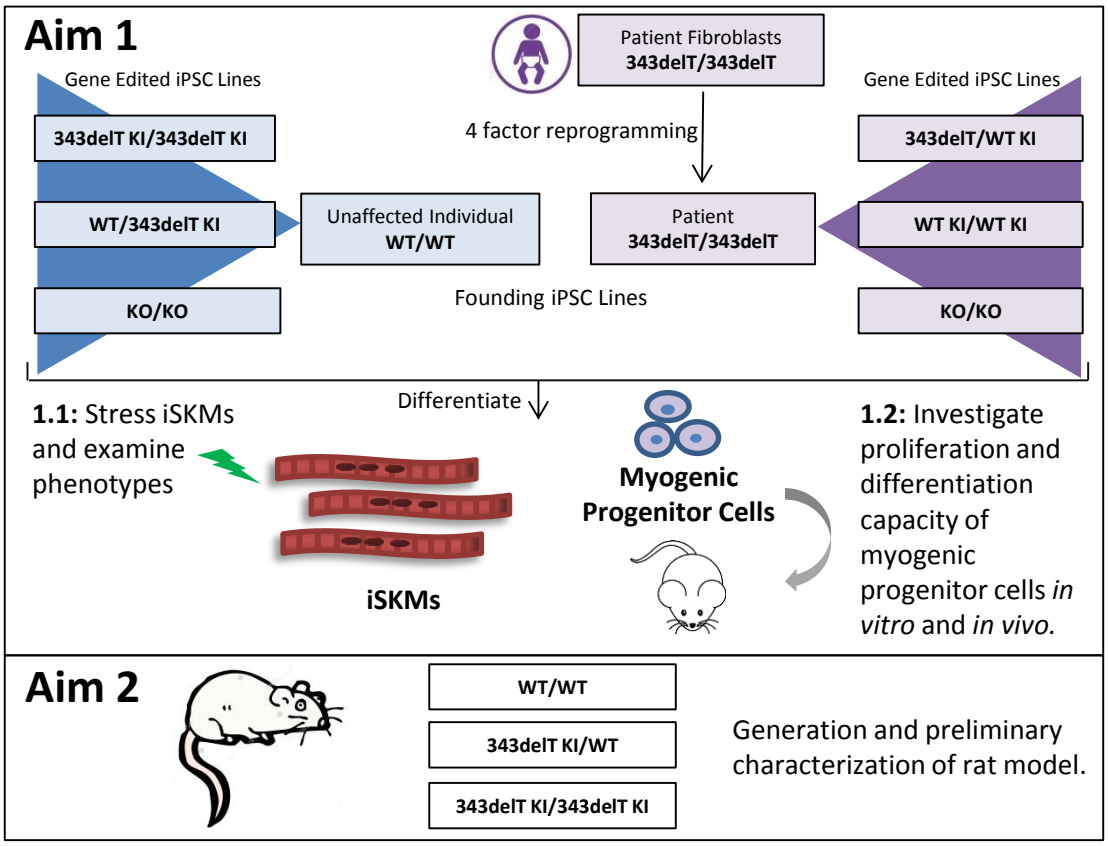

Figure 6.1 A schematic representation of aims for future directions. Aim 1 involves the study of 343delT disease pathogenesis using iPSCs derived from the patient and an unaffected individual. Founding iPSC lines will undergo genome editing generating two separate cohorts of isogenic cell lines for direct comparisons. iPSC-derived skeletal myotubes (iSKMs) and myogenic progenitor cells will be studied in subaims 1.1 and 1.2, respectively. Aim 2 incorporates the generation and characterization of *in vivo* knock-in rat models for 343delT.

in rats through histopathology, serum creatine kinase levels, and examination of muscle strength. Successful completion of this aim will provide a complementary system to the *in vitro* human iPSC model described in Aim1 with an *in vivo* model system in Aim 2, in which the defects in progenitor cells could be studied and disease treatments including gene and cell therapy could be tested.

Significance

Myofibrillar myopathy (MFM), or muscle weakness caused by malfunctioning muscle fibers, results from a disruption in sarcomere structure. Mutations in genes that are important in myofibrillar structure, including desmin, filamin-C, and myotilin, as well as mutations in genes encoding chaperones, including *HSPB5*, have been associated with MFM. Molecular chaperones are essential in the regulation of protein quality control, through binding of unfolded/misfolded proteins, allowing them the opportunity to refold or be marked for degradation rather than accumulate as potentially pathogenic aggregates. The small molecular-weight heat shock protein, HSPB5 (aka CRYAB or αB-crystallin), functions as a molecular chaperone and has genomic enhancer regions that allow for tissue-specific expression in the lens, heart, and skeletal muscle (Swamynathan and Piatigorsky, 2007). HSPB5 acts as a chaperone for the muscle contractile proteins desmin (Bennardini et al., 1992), titin (Golenhofen, 2002), and actin (Bennardini et al., 1992). Many different mutations in *HSPB5* have been linked to multisystem disorders including cataracts, cardiomyopathy, and myopathy (Sacconi et al., 2012). These different mutants have variable penetrance and expressivity, are dominant or recessive, exhibit tissue-specific effects, and many are aggregation prone. The well-studied, dominant R120G mutation (Vicart et al., 1998) promotes the aggregation of the intermediate filament protein desmin, among others, which contributes to the disease pathology (Perng et al., 2004). Whereas dominant mutations in *HSPB5* typically show progressive symptoms later in life (Sacconi et al., 2012; Vicart et al., 1998), recessive mutations such as 343delT (Forrest et al., 2011) and 60delC (Del Bigio et al., 2011)

result in early-onset, more severe conditions during infancy, termed congenital myopathy.

The Benjamin Laboratory has extensively characterized the biological and functional roles of mutant *HSPB5* in experimental animal models, including mice (Rajasekaran et al., 2007; Rajasekaran et al., 2008; Rajasekaran et al., 2011) and *Drosophila* (Xie et al., 2013), and *in vitro* cell culture models, including H9C2 cells and neonatal rat cardiomyocytes (Banerjee Mustafi et al., 2014; Zhang et al., 2010), as well as induced pluripotent stem cell (iPSC) models (Limphong et al., 2013; Mitzelfelt et al., 2016). Because the mechanisms of disease pathogenesis for mutant *HSPB5* congenital myopathy in humans are poorly understood, interest is focused on the human 343delT that results in the protein modification S115fs129X. This deletion causes a frameshift resulting in a large C-terminal deletion of HSPB5 (Forrest et al., 2011), removing a portion of the highly conserved α-crystallin domain and the C-terminus, critical for dimer stabilization (Hilton et al., 2013). An infant, female patient harboring this rare, homozygous recessive mutation born from unrelated, heterozygous parents presented initially at age 4 months following normal development with severe skeletal muscle stiffness, persistent creatine kinase elevation, and a muscle biopsy indicative of myofibrillar myopathy so severe that ventilation is required to sustain life (Forrest et al., 2011). The skeletal muscle biopsy shows dense, irregular staining of HSPB5 in the myofibers and western blot shows the presence of a truncated form of the protein (Forrest et al., 2011). Additionally, previous work has suggested a role for HSPB5 in skeletal muscle progenitor proliferation and differentiation (Neppl et al., 2014; Singh et al., 2010).

Mitzelfelt et al. demonstrated that the 343delT protein is extremely insoluble and likely unavailable to perform normal cellular functions (see Chapter 3) (Mitzelfelt et al., 2016). Whereas the autosomal recessive mutation manifests myopathy, both heterozygous nonconsanguineous parents are phenotypically normal for known signs and symptoms of disease (Forrest et al., 2011), suggesting that the patient's clinical presentation may be at least either partly due to loss of HSPB5 function or that genetic modifiers and other factors mitigate the disease. Such findings are reminiscent but not identical to the *HSPB5/HSPB2* double knockout

(DKO) mouse, which exhibits progressive muscle deterioration over time (Brady et al., 2001). The aggregation potential of 343delT in cell culture models (Mitzelfelt et al., 2016) and the patient muscle biopsy (Forrest et al., 2011) as well as 343delT's ability to coaggregate with desmin and induce a cellular stress response (Mitzelfelt et al., 2016) raise the intriguing possibility that 343delT may have some gain-of-toxic function effect causing symptoms observed in the patient to appear more severe compared with the DKO mouse.

Goals

This proposal aims to address the mechanisms for the relative loss and gain of function effects of 343delT in congenital myopathy. The proposed novel and innovative approaches for modeling 343delT-associated congenital myopathy using both *in vitro* (Aim 1) and *in vivo (*Aim 2) systems will provide a general platform for detailed mechanistic and functional studies. Modeling cell-autonomous disease using a patient's own iPSCs cells offers the potential for drug screening, possible cell-based therapies, or both. To mitigate the limitations of 2D culture, an *in vivo* rat model is both necessary and sufficient for disease recapitulation, required for testing future treatments.

Specific Aim 1: Modeling Disease-causing HSPB5 343delT-Associated Congenital Myopathy in Human iPSCs

Aim 1.1: iPSC model generation and phenotypic characterization

Rationale. This aim is high-risk since to date it has been difficult to model stress-dependent protein aggregation diseases in iPSCs. HSPB5 is expressed at high levels in mature muscle where it plays a key role as a chaperone for cytoskeletal and contractile proteins (Bennardini et al., 1992; Golenhofen, 2002). Loss of this chaperone function and/or the presence of the 343delT mutant form of HSPB5 may contribute to the severe, congenital myopathy observed in the patient (Forrest et al., 2011). In this aim, 343delT-induced myopathy will be modeled using iPSC-derived, multinucleated skeletal myotubes (iSKMs). 343delT HSPB5 cells

will be compared with HSPB5 knockout cells, to define phenotypes and determine whether phenotypes are due to loss or gain-of-toxic function of 343delT, providing insight into the requirement for HSPB5 in skeletal muscle maintenance. If successful, this model system will be highly useful for studying mechanisms driving MFM associated with chaperone dysfunction.

Methods. Genome engineering of mutant and control cell lines will be/has been performed using a novel gene editing strategy that markedly enhances one's ability to isolate modified clones, cotargeting with selection (CTS) (Chapter 4) (outlined in Figure 6.2). The CTS hypothesis is that selection for homology-directed repair (HDR)-competent cells through incorporation of a primary selectable event will enrich for an HDR-mediated modification at a second locus. Proposed iPSC lines are outlined in Figure 6.3, a majority of which were generated previously. One iPSC line derived from the female 343delT patient (Pt), previously generated by the Benjamin Laboratory (Mitzelfelt et al., 2016), and one iPSC line from an independent, unrelated, unaffected male, hB53 hiPS6 (Riedel et al., 2014) (unaffected- UA), will be used along with gene edited versions of all lines to generate 2 separate isogenic sets of cells lines that are WT, heterozygous and homozygous for 343delT. To generate knockout of *HSPB5*, two guide RNAs will be designed using ZiFiT Targeter Version 4.2 to target upstream of the transcriptional start site and within the 3' untranslated region. Guides will be transfected together so as to retrieve clones with the entire gene removed. This strategy to generate a complete knockout is proposed as opposed to targeted disruption early in the gene since even with very early truncations of HSPB5 (Del Bigio et al., 2011), protein is visible and may or may not impact disease. Per the CTS protocol, cells are transfected with components for targeting *AAVS1* and *HSPB5* simultaneously (Figure 6.2) and selected with puromycin for 10 days prior to manually picking and screening by Sanger sequencing of *HSPB5* (Figure 6.3). Confirmation of *HSPB5* deletion will be initially screened for with PCR and confirmed by Southern Blot followed by western blot to confirm loss of the protein. Many of the proposed iPSC lines have been previously generated with CTS and other published strategies (Mitzelfelt et al., 2016). Generated

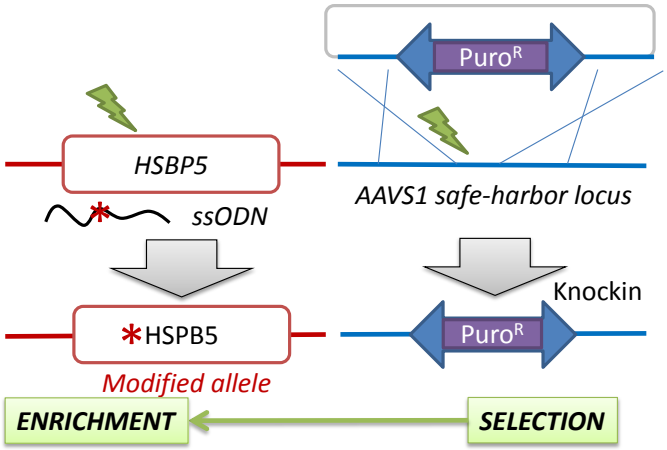

Figure 6.2: Cotargeting with selection (CTS) gene editing strategy (Chapter 4). Modification of the *AAVS1* and *HSPB5* loci will be performed simultaneously. The primary, selectable modification utilized is incorporation of a puromycin selection cassette (Puro^R) into the *AAVS1* safe-harbor locus using a commercially available system (Transposagen, SKU: AAVS-P-TALEN), while the secondary modification utilizes CRISPR/Cas9 along with a single strand oligonucleotide (ssODN) as a repair template to incorporate/correct *HSPB5* 343delT. Selection of the primary modification allows for enrichment of the secondary modification per the CTS hypothesis.

Heterozygous 343delT	Homozygous 343delT	WT	Knockout
Pt-het KI	**Pt-homo**	Pt-WT KI	Pt-KO
UA- het KI	UA-homo KI	**UA-WT**	UA-KO

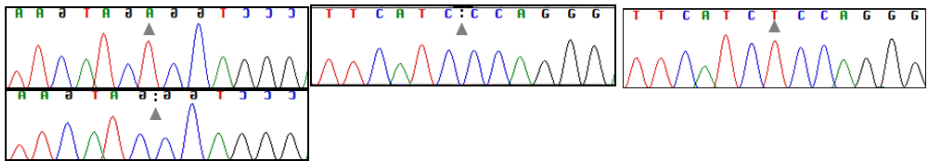

Figure 6.3: Proposed iPSC lines to use for Aim 1 studies. Patient-derived (Pt) - and unaffected (UA) cell lines already generated and others to be generated are labeled in black and red text, respectively. Bold indicates founding cell lines for which gene editing was/will be performed. KI (knockin) indicates cell lines made with genetic knockin of either the WT or 343delT. KO indicates homozygous knockout of *HSPB5*. Representative chromatograms shown below.

iPSC lines are characterized for pluripotency and screened for genomic stability prior to differentiation as described below (Mitzelfelt et al., 2016).

iPSCs will be differentiated to skeletal myotubes (iSKMs) as previously described (Mitzelfelt et al., 2016) using the EZ sphere protocol (Hosoyama et al., 2014). This differentiation approach generates both muscle progenitor cells as wells as multinucleated skeletal myotubes (iSKMs) (Figure 6.4). A range of phenotypic assays will be performed to fully characterize iSKMs. Initial assays will be performed in the cell lines derived from Pt-homo (i.e., homozygous mutant, heterozygous mutant, WT, and knockout) for optimization and assessment of differences to determine feasibility. Assays will then be repeated using the additional cell lines derived from UA-WT. In previously generated iSKMs (Pt-homo, Pt-het KI, Pt-WT KI, UA-homo KI), mutant protein (15kDa) is undetectable by either western blot or immunocytochemistry, while the WT protein (22kDa) is detected (Chapter 3, Figure 3.2) (Mitzelfelt et al., 2016). A series of detailed, mechanistic experiments shows that extreme insolubility of the mutant protein is the reason for lack of detection prompting the conclusion that insoluble 343delT would likely be unavailable to perform essential, normal functions of HSPB5 and therefore, loss of function is a factor likely contributing to disease (Chapter 3) (Mitzelfelt et al., 2016). In the patient biopsy, dense, irregular staining of 343delT is visible, suggesting that the presence of the mutant protein may contribute to disease. To this end, visible cytoplasmic aggregates containing the mutant protein that appear to stochastically incorporate desmin are visible upon overexpression of the mutant protein (Mitzelfelt et al., 2016). Aggregates also induce a cellular stress response (i.e., HSP70 induction), indicative of disruption of proteostasis (Mitzelfelt et al., 2016). Assays described in this proposal aim to determine the mutant protein's relative loss and gain-of-toxic function contribution to disease.

Mutant protein has proven undetectable at basal levels. Therefore, a series of experimental manipulations to invoke its detection will be employed providing a platform to study aggregation of the endogenous protein. Additionally, these stressors may evoke phenotypes

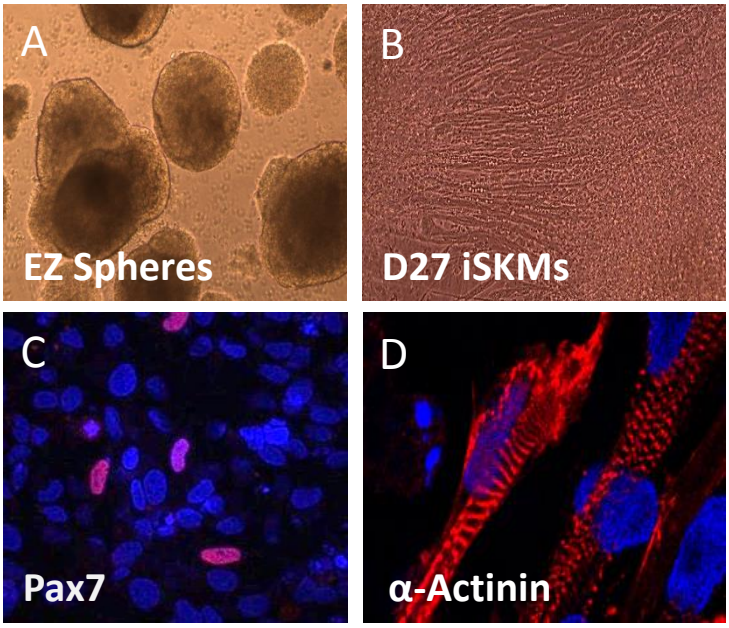

Figure 6.4: iPSC-derived myogenic cells generated with the EZ sphere protocol. A.) EZ spheres at 6 weeks of suspension culture. B.) iSKMs after 27 days of terminal dissociation. C.) Pax7 immunostaining showing the presence of myogenic progenitor cells in cultures after 4 days terminal differentiation. D.) α-actinin immunostaining in day 21 iSKMs. Immunostaining merged with DAPI.

resulting from loss of *HSPB5* function, which will be evident in *HSPB5* knockout cell lines. A suspected threshold exists with which the level of the mutant must surpass to reach detectable levels within cells, as with overexpression 343delT protein is detectable. We hypothesize that surpassing this threshold may trigger a cascade of events that results in the overall disruption of cellular proteostasis and contributes to muscle breakdown/dysfunction (please see Discussion in Chapter 5). The recently described CRISPR/Cas9 system with catalytically inactive Cas9 (dCas9) fused to transcriptional activators VP64-p65-Rta (VPR)(Chavez et al., 2015) along with guide RNA that recognize regions of the *HSPB5* proximal promoter/enhancer will be used to upregulate endogenous *HSPB5*. This system for upregulation of *HSPB5* has been validated in iPSC through qRT-PCR (Figure 6.5). Next steps are to validate protein level increases by western blot and to examine for the presence of aggregates with immunocytochemistry. iSKMs will be transfected at day 25 of differentiation (multinucleated iSKMs) using TransIT-LT1 transfection reagent (Mirus Bio) and examined 36-48 h later for expression of HSPB5 at the RNA (qRT-PCR) and protein (western blot and immunocytochemistry) levels. The presence/level of other meta-stable proteins within the cell may be required for nucleation of the aggregation process, as with stress, meta-stable proteins are prone to unfolding. Transfection of a desmin containing plasmid (Addgene plasmid #54059) and/or use the dCas9-VPR system with guide RNAs generated to bind to the *Desmin* promoter to upregulate the metastable protein desmin within iSKMs as a stress on proteostasis will also be performed. Additional stressors include rapid, electrical pacing performed as described previously (Riedel et al., 2014) and calcium overload using a calcium ionophore (Malinska et al., 2010; Verma et al., 2011). In this way endogenous aggregation of 343delT and its overall impact on cell structure and function will be examined.

Phenotypic analysis will be performed with and without stressors described above and includes (described in more details below) sarcomere breakdown, titin aggregation (stiffness), cellular breakdown, and changes in gene expression. Sarcomere breakdown will be scored by immunostaining cells with α-actinin as described previously (Hinson et al., 2015). Titin is a key

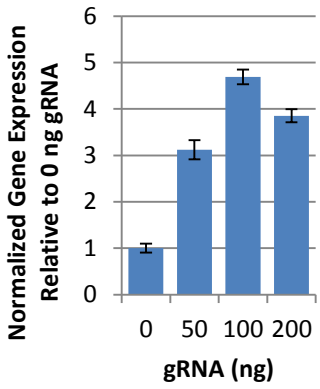

Figure 6.5: Upregulation of *HSPB5* with dCas9-VPR. Four guide RNAs (gRNA) recognizing the promoter region of *HSPB5* were pooled together and transfected in increasing amounts (0, 50, 100, 200 ng) with dCas9-VPR in iPSCs. Approximately 4-fold enhanced expression was observed, which is an underrepresentation of individual cell effects due to relatively low transfection efficiency.

elastic protein in muscle that contains spring-like immunoglobulin (Ig) domains, for which HSPB5 is a chaperone (Bullard et al., 2004; Golenhofen et al., 2002; Golenhofen et al., 2004), that unfold and allow contracted muscle to stretch (Minajeva et al., 2001; Rief, 1997). If left unchecked, the Ig domains can aggregate and result in muscle stiffness (Kotter et al., 2014). As congenital myopathy patients associated with recessive *HSPB5* mutations show profound muscle stiffness, titin will be analyzed through immunostaining and electron microscopy with immunogold labeling of titin and HSPB5. Enzyme-linked immunosorbent assay (ELISA) will be used to determine the level of human skeletal muscle α-actinin (kit from MyBioSource) in the cell culture media as a readout of cellular breakdown. Additionally, qRT-PCR on a panel of stress response genes will be performed to determine differences between cell lines. Overall, this phenotypic analysis in conjunction with the proposed stressors will likely evoke a pathological phenotype in iSKMs providing an *in vitro* disease model of congenital myopathy where histopathological abnormalities observed in the patient are the result of accumulated cellular stress.

Expected results and interpretation. It is expected that cell lines expressing 343delT may show a range of phenotypes indicating the "loss of function" effects of 343delT and others indicating "gain of function" effects of 343delT or partial 343delT function. Upregulation of *HSPB5* using the dCas9-VPR system is expected to result in detectable aggregates of 343delT that will be further analyzed in future experiments. Sarcomere breakdown, titin aggregation, and elevated levels of media α-actinin is expected in homozygous 343delT cells that is more severe than knockout cell lines, while heterozygous 343delT cells will likely behave similarly to WT. Global changes in gene expression of stress response genes are anticipated, as homeostasis is disrupted.

Possible pitfalls and alternative approaches. If the proposed stressors do not result in visible aggregation of 343delT, iSKMs can be transfected with a plasmid expressing the 343delT cDNA, described previously (Mitzelfelt et al., 2016), as a means to study aggregation. If

transfection efficiency is too low with TransIT-LT1 (Mirus Bio), viral vectors and viruses will be generated and used as an alternative approach. Additional aggregation prone proteins highly studied in neurodegenerative diseases, including tau and poly-glutamine (Guerreiro et al., 2015; Seidel et al., 2016), could be transfected into cells as well to stimulate aggregation. Aggregation of titin may require cellular stretch, in which case devices that incorporate static stretch could be employed (Nguyen et al., 2013).

Aim 1.2: Examine the impact of mutant HSPB5 on muscle progenitor cell proliferation and differentiation

Rationale. HSPB5 affects not only differentiated, mature muscle, but also plays a role in the muscle progenitor cell during differentiation (Singh et al., 2010). Proliferating myoblasts must turn off expression of the master regulatory transcription factor, MyoD, exit the cell cycle, turn on myogenin, and fuse to form multinucleated myotubes (Weintraub, 1993). When HSPB5 is overexpressed in C2C12 myoblasts, MyoD levels are lower in the myoblast and cell cycle exit is delayed, both negatively impacting differentiation to myotubes (Singh et al., 2010). DKO mice have a significantly reduced number of satellite cells in their skeletal muscle and a reduced ability to regenerate muscle following cardiotoxin-induced injury, indicating a potential role for HSPB5 in skeletal muscle regeneration (Neppl et al., 2014). Neppl and colleagues show that in the absence of HSPB5, Argonaute2, a key component of the RNA-induced silencing complex (RISC) has significantly reduced activity affecting the proliferation/differentiation capacity of skeletal muscle progenitor cells (Neppl et al., 2014). In this aim, myogenic progenitor cells will be isolated from early iSKM cultures and analyzed for proliferation and differentiation capacity *in vitro* and *in vivo* to determine relative impact of gain and loss of function. This analysis will evaluate the requirement for HSPB5 in skeletal muscle differentiation.

Methods. EZ sphere cultures will be generated as described in Aim 1.1 and muscle progenitor cells (Pax7 positive) will be isolated by fluorescence activated cell sorting (FACS)

with an antibody to the surface marker α7-integrin (Pawlikowski et al., 2009). α7-Integrin is also present on myotubes, but progenitors and myotubes can likely be differentiated by size and granularity (forward scatter and side scatter). Cells will be cultured *in vitro* stimulating spontaneous differentiation to myotubes with and without cardiotoxin (Demonbreun et al., 2010; Langone et al., 2014) to observe an injury response. Cell-cycle analysis will be performed by propidium iodide staining and visualized by flow cytometry on samples harvested at various time points to see if 343delT and/or *HSPB5* knockout cells exit from the cell cycle at different time points compared with control. Proliferative potential of progenitor cells will be measured by co-staining with Ki67 and MyoD followed by counting the number of double positive cells at different time points after sorting. MyoD mRNA and protein levels will be analyzed by qRT-PCR and western blot, respectively, to determine if temporal expression is altered. Immunocytochemistry costaining will be performed at different time points of differentiation with markers of progenitors, Pax7 and MyoD, or markers for more mature myotubes, α-actinin or myogenin, to characterize HSPB5 expression throughout the differentiation process.

In parallel, a less biased approach will be undertaken to determine differences in gene expression between 343delT, knockout, and control cells. To this end RNAseq and small RNA-seq, including microRNAs, will be performed on isolated progenitor cells cultured *in vitro* with and without cardiotoxin injury. Candidate factors of interest will be validated by qRT-PCR.

In vitro injury response of progenitor cells will likely not fully recapitulate *in vivo* conditions. For this reason, isolated muscle progenitor cells from 343delT, knockout and WT iPSC lines will be injected into the tibialis anterior muscles of NOD/SCID gamma-c (NSG) mice (Shultz et al., 2005), with cardiotoxin injury as previously described (Darabi et al., 2012). Two months after transplantation muscle sections will be harvested and evaluated for engraftment by immunostaining with pandystrophin and human-specific dystrophin antibodies as previously described (Darabi et al., 2012). The percentage of fibers expressing human dystrophin will be calculated and compared between lines.

Expected results and interpretation. *HSPB5* knockout progenitors are expected to exit the cell cycle at faster rates than controls, which would be shown by an increased number of knockout cells compared with control in the G0 state at earlier time points following sorting. Knockout cells may also show less Ki67-positive cells, indicating lower proliferative potential. MyoD levels may be altered in knockout cells compared to control. MyoD may turn on earlier or stay on longer due to the loss of function hypothesis, which would be consistent with the previous report showing delayed MyoD expression due to overexpression of HSPB5 (Singh et al., 2010). These results would indicate that loss of HSPB5 expression has an impact on proliferation and differentiation of myogenic progenitors to myotubes. Novel genes, including microRNAs whose expression is affected by loss of HSPB5 will be identified with the unbiased RNAseq. 343delT is expected to exhibit the same defects as knockout cells, which would indicate that this phenotype is likely due to loss of function effects of 343delT. Gain of function effects of 343delT due to aggregation are expected to manifest in mature muscle where expression levels of HSPB5 are higher, not necessarily in the progenitor cell state. With *in vivo* injection of human progenitor cells into mice, *HSPB5* knockout cells are expected to account for a lower percentage of regenerated muscle fibers as compared with control cells, indicative of decreased regenerative capacity in the absence of *HSPB5*. 343delT progenitor cells are predicted to behave similarly to knockout cells in this assay.

Possible pitfalls and alternative approaches. α7-Integrin may not be specific enough to identify the myogenic progenitor population of interest. Myomaker, a surface protein required for myoblast fusion, is another surface marker that could potentially be used to isolate progenitor cells (Millay et al., 2013). Additional surface markers could be used to deplete other cells in the culture. Alternatively, a lentivirus containing GFP driven by the Pax7 promoter could be used to make stable cell lines followed by differentiation and sorting for GFP-positive progenitor cells.

Aim 1: Future directions

Experiments proposed in this aim provide detailed phenotypic analysis of defects associated with 343delT in skeletal muscle. These studies lay the groundwork for future examination of protein aggregates through cell fractionation coupled with proteomics via mass spectrometry. Components lost from the cytoplasm into the aggregates could be identified and their rescue tested for amelioration of phenotypes. Additionally, factors that upregulate autophagy (Hochfeld et al., 2013) and compounds that induce activation of the master regulator of heat shock gene expression, HSF-1 (Calamini et al., 2012) could also be examined for their ability to mitigate aggregation and additional phenotypes. Future work may also focus on better defining mechanisms of action as well as defining tissue-specific effects. iPSCs can be readily differentiated into cardiomyocytes, which, as of now, in the patient appear to be asymptomatic for cardiac manifestations. These studies may elucidate why skeletal but not cardiac muscle is impacted and may be predictive of future cardiac involvement in the patient.

Specific Aim 2: Modeling Disease-causing HSPB5 343delT-Associated Congenital Myopathy Using Genetically Engineered Rats

Aim 2: *In vivo* rat model generation

Rationale. iPSC model system has its limitations for the study of HSPB5-associated myopathies (Limphong et al., 2013; Mitzelfelt et al., 2016). Establishment of critical models with translational relevance in humans is crucial to pursue mechanisms of disease pathogenesis (i.e., progenitor cell biology, mitochondrial biology, calcium homeostasis) that might impact treatment outcomes in affected patients. Specifically, proinflammatory and extracellular matrix pathways also contribute to muscle integrity and function in both health and disease. Accordingly, a rat model of *HSPB5* 343delT will complement the studies outlined in Aim 1 providing an *in vivo* model system. Genetically engineered rats are a larger rodent model, compared with mice, which will be able to follow the progression of early-onset myopathy and aggregate accumulation

during development and throughout the organism's lifespan. This advantage may also expose cardiac phenotypes not yet observed in the patient due to maturity, which has added benefit of potential preventative care. Finally, the use of a rat model allows for the opportunity to test methods of treatment for similarly affected patients. While preliminary work could be conducted in 343delT and control iSKMs, further testing in a whole model organism is an essential next step to validate any therapeutic intervention before clinical applications. This is an ambitious aim with considerable risk due to the inherent challenges of developing a transgenic rat model; however, the ability to study 343delT with an *in vivo* system will provide an invaluable tool to advance the understanding and treatment of MFM.

Methods. A rat strain containing the 343delT patient mutation will be produced by the transgenic core. Homozygous and heterozygous 343delT rats will be generated to model both the affected patient and the unaffected parents, respectively. Verification of the intended truncation of HSPB5 will be conducted using western blotting, qRT-PCR, and immunohistochemistry comparing with wildtype rats from the same genetic background. While there was no evidence of lethality observed in the DKO mouse (Brady et al., 2001), viability of the proposed strains will be assessed via surveying the genotypes of the neonate pups and determining the survival rate of each genotypes throughout the duration of the study.

Axial muscles surrounding the spine, the muscles of the forelimb, and the muscles of the hind limb of 343delT homozygous rats could exhibit the most severe phenotype (Brady et al., 2001) compared with either heterozygous 343delT or controls rats. The 343delT patient also demonstrates respiratory distress, thus, the diaphragm will be examined for evidence of myopathy (Forrest et al., 2011). Standard muscle fiber cross sectional size and fibrosis will be quantified and compared across all rat strains using H&E and trichrome staining as previously described (Brady et al., 2001). However, both electron microscopy and immunohistochemistry, including the more reliable Evans blue exclusion assay, will be used to evaluate myocyte damage and membrane integrity (Accornero et al., 2014; Heydemann et al., 2012) and to confirm western

blotting and immunofluorescence studies. Evidence of adverse outcomes will include quantitative biochemical analysis of skeletal muscle damage (e.g., creatine kinase MM, p62, desmin, and myotilin) (Goicoechea et al., 2008), aggregation (HSPB5 and desmin), apoptosis (Fas and p53), extracellular matrix proteins (e.g, MMP9) and fibrosis (e,g., hydroxyproline assay) observed between 343delT vs controls as previously described (Forrest et al., 2011; Lee et al., 2001). qRT-PCR will be performed to determine whether either increases or decreases of selected biomarkers are due to enhanced transcription or selective protein degradation. If time permits, preliminary studies will assess mitochondrial biogenesis such as PGC-1α content, cytochrome-c, ETC complexes I-V, citrate synthase, antioxidative pathways including SOD2, GPX and several markers of inflammation (NFkB) and immune cell infiltration (e.g., MPO staining, CD45) of homozygous 343delT compared with controls. Whole body strength will be determined by using a wire screen holding test as previously described (Carlson et al., 2010).

The 343delT patient exhibits severe muscle stiffness and weakness. Therefore, functional assessment of skeletal myopathy in all rat strains listed will be conducted in collaboration with Dr. Robert Fitts as previously described (Fitts et al., 2010). Briefly, bundles of fibers will be prepared from the primarily slow soleus and fast gastrocnemius muscles, the bundles chemically skinned, and stored at -20°C. On the day of an experiment, single fibers will be isolated, mounted between a force transducer and length motor, and sarcomere length set at 2.5 µ. Short, rapid length perturbations (0.05% fiber length at 1.5 KHz) will then be applied in relaxing (pCa 9.0) and activating (pCa 4.5) solution and fiber stiffness determined from the resulting change in force in response to the length step (Fitts et al., 2010). Passive fiber stiffness will be determined by measuring the length-tension relationship in relaxing solution at sarcomere lengths from 1.9 -3.1 µ. Following the stiffness measurements, fiber strength will be assessed by determining peak force, rate of tension development (dp/dt), velocity and power (Fitts et al., 2010).

Expected results and interpretation. Production of homozygous 343delT rat strains are expected to model phenotypes observed in the 343delT patient. Examination of the homozygous

343delT rat should reveal increased muscle degeneration when compared to the wildtype rats. Expected phenotypes include: aggregates containing HSPB5, alterations in muscle fiber size, increased fibrosis, elevated apoptosis, increased expression of myofibrillar degeneration markers, and ultrastructural evidence of degenerative changes. Functionally, the homozygous 343delT rats should demonstrate decreased muscle strength similar to the affected patient. In the 343delT fibers compared to control fibers, titin is expected to be altered to increase the passive tension (i.e., stiffness) but have less effect on stiffness measured in activated fibers as that reflects the number of active cross-bridges. Altered stiffness in activated fibers would suggest that either the cross-bridge number was altered and/or that other factors such as changes in myosin binding protein C altered stiffness. Additionally, the heterozygous 343delT rats are expected to have a phenotype similar to that of the wildtype rats, which would model the asymptomatic parents of the 343delT patient.

Possible pitfalls and alternative approaches. If the 343delT rats do not demonstrate degeneration of muscle cells, animals will be physically stressed to elucidate a phenotype. Exercise stress will be administered via swimming or treadmill exercise as previously described (Handschin et al., 2007; Samy et al., 2015). Increased evidence of muscle degradation is expected in response to physical stress.

Aim 2: Future directions

The generation of a 343delT rat would allow for significant studies investigating the role of HSPB5 in myogenic progenitor cells and potential treatments for MFM patients especially with early-onset and age-dependent damaged tissues. The 343delT model would be an invaluable tool to further study the role of HSPB5 in muscle development and regeneration. Moreover, a whole organism model of the 343delT patient would provide a platform to assess effective therapeutic interventions including drug testing and is a prerequisite for any future gene/cell-based therapies in humans.

Acknowledgements

I thank Dr. Kurt D. Kolander (Medical College of Wisconsin), Dr. Robert H. Fitts (Marquette University), and Dr. Ivor J. Benjamin (Medical College of Wisconsin) for their contribution in writing this Chapter.

References

Accornero, F., Kanisicak, O., Tjondrokoesoemo, A., Attia, A.C., McNally, E.M., and Molkentin, J.D. (2014). Myofiber-specific inhibition of TGFβ signaling protects skeletal muscle from injury and dystrophic disease in mice. Hum. Molecular Gen. 23, 6903-6915.

Banerjee Mustafi, S., Grose, J.H., Zhang, H., Pratt, G.W., Sadoshima, J., Christians, E.S., and Benjamin, I.J. (2014). Aggregate-prone R120GCRYAB triggers multifaceted modifications of the thioredoxin system. Antioxid. Redox Sign. 20, 2891-2906.

Bennardini, F., Wrzosek, A., and Chiesi, M. (1992). Alpha B-crystallin in cardiac tissue: Association with actin and desmin filaments. Circ. Res. 71, 288-294.

Brady, J.P., Garland, D.L., Green, D.E., Tamm, E.T., Giblin, F.J., and Wawrousek, E.F. (2001). aB-Crystallin in lens development and muscle integrity: A gene knockout approach. IOVS 42, 2924-2934.

Bullard, B., Ferguson, C., Minajeva, A., Leake, M.C., Gautel, M., Labeit, D., Ding, L., Labeit, S., Horwitz, J., Leonard, K.R., et al. (2004). Association of the chaperone alphaB-crystallin with titin in heart muscle. J. Biol. Chem. 279, 7917-7924.

Calamini, B., Silva, M.C., Madoux, F., Hutt, D.M., Khanna, S., Chalfant, M.A., Saldanha, S.A., Hodder, P., Tait, B.D., Garza, D., et al. (2012). Small-molecule proteostasis regulators for protein conformational diseases. Nat. Chem. Biol. 8, 185-196.

Carlson, C.G., Rutter, J., Bledsoe, C., Singh, R., Hoff, H., Bruemmer, K., Sesti, J., Gatti, F., Berge, J., and McCarthy, L. (2010). A simple protocol for assessing inter-trial and inter-examiner reliability for two noninvasive measures of limb muscle strength. J. Neuro. Meth. 186, 226-230.

Chavez, A., Scheiman, J., Vora, S., Pruitt, B.W., Tuttle, M., P R Iyer, E., Lin, S., Kiani, S., Guzman, C.D., Wiegand, D.J., et al. (2015). Highly efficient Cas9-mediated transcriptional programming. Nat. Meth. 12, 326-328.

Darabi, R., Arpke, R.W., Irion, S., Dimos, J.T., Grskovic, M., Kyba, M., and Perlingeiro, R.C. (2012). Human ES- and iPS-derived myogenic progenitors restore DYSTROPHIN and improve contractility upon transplantation in dystrophic mice. Cell Stem Cell 10, 610-619.

Del Bigio, M.R., Chudley, A.E., Sarnat, H.B., Campbell, C., Goobie, S., Chodirker, B.N., and Selcen, D. (2011). Infantile muscular dystrophy in Canadian aboriginals is an alphaB-crystallinopathy. Annals. of Neuro. 69, 866-871.

Demonbreun, A.R., Lapidos, K.A., Heretis, K., Levin, S., Dale, R., Pytel, P., Svensson, E.C., and

McNally, E.M. (2010). Myoferlin regulation by NFAT in muscle injury, regeneration and repair. J. Cell Sci. 123, 2413-2422.

Fitts, R.H., Trappe, S.W., Costill, D.L., Gallagher, P.M., Creer, A.C., Colloton, P.A., Peters, J.R., Romatowski, J.G., Bain, J.L., and Riley, D.A. (2010). Prolonged space flight-induced alterations in the structure and function of human skeletal muscle fibres. J. Phys. 588, 3567-3592.

Forrest, K.M., Al-Sarraj, S., Sewry, C., Buk, S., Tan, S.V., Pitt, M., Durward, A., McDougall, M., Irving, M., Hanna, M.G., et al. (2011). Infantile onset myofibrillar myopathy due to recessive CRYAB mutations. Neuromuscular Disord.: NMD 21, 37-40.

Goicoechea, M., Cía, F., San José, C., Asensio, A., Emparanza, J.I., Gil, A.G., de Cerain, A.L., Aldazabal, P., Azpitarte, M., Otaegui, D., et al. (2008). Minimizing creatine kinase variability in rats for neuromuscular research purposes. Lab. Animals 42, 19-25.

Golenhofen, N. (2002). Ischemia-induced association of the stress protein αB-crystallin with I-band portion of cardiac titin. J. Mol. and Cell. Cardiol. 34, 309-319.

Golenhofen, N., Arbeiter, A., Koob, R., and Drenckhahn, D. (2002). Ischemia-induced association of the stress protein alpha B-crystallin with I-band portion of cardiac titin. J. Mol. Cell. Cardiol. 34, 309-319.

Golenhofen, N., Perng, M.D., Quinlan, R.A., and Drenckhahn, D. (2004). Comparison of the small heat shock proteins alphaB-crystallin, MKBP, HSP25, HSP20, and cvHSP in heart and skeletal muscle. Histochem. Cell Biol. 122, 415-425.

Guerreiro, P.S., Gerhardt, E., Lopes da Fonseca, T., Bähr, M., Outeiro, T.F., and Eckermann, K. (2015). LRRK2 promotes tau accumulation, aggregation and release. Mol. Neurobiol., 1-12.

Handschin, C., Chin, S., Li, P., Liu, F., Maratos-Flier, E., LeBrasseur, N.K., Yan, Z., and Spiegelman, B.M. (2007). Skeletal muscle fiber-type switching, exercise intolerance, and myopathy in PGC-1α muscle-specific knock-out animals. J. Biol. Chem. 282, 30014-30021.

Heydemann, A., Swaggart, K.A., Kim, G.H., Holley-Cuthrell, J., Hadhazy, M., and McNally, E.M. (2012). The superhealing MRL background improves muscular dystrophy. Skeletal Muscle 2, 1-12.

Hilton, G.R., Hochberg, G.K.A., Laganowsky, A., McGinnigle, S.I., Baldwin, A.J., and Benesch, J.L.P. (2013). C-terminal interactions mediate the quaternary dynamics of αB-crystallin. Philos. T. R. Soc. B: 368, 20110405-20110405.

Hinson, J.T., Chopra, A., Nafissi, N., Polacheck, W.J., Benson, C.C., Swist, S., Gorham, J., Yang, L., Schafer, S., Sheng, C.C., et al. (2015). Titin mutations in iPS cells define sarcomere insufficiency as a cause of dilated cardiomyopathy. Science 349, 982-986.

Hochfeld, W.E., Lee, S., and Rubinsztein, D.C. (2013). Therapeutic induction of autophagy to modulate neurodegenerative disease progression. Acta Pharmacol. Sin 34, 600-604.

Hosoyama, T., McGivern, J.V., Van Dyke, J.M., Ebert, A.D., and Suzuki, M. (2014). Derivation of myogenic progenitors directly from human pluripotent stem cells using a sphere-based culture. Stem Cells Trans. Med.

Kotter, S., Unger, A., Hamdani, N., Lang, P., Vorgerd, M., Nagel-Steger, L., and Linke, W.A. (2014). Human myocytes are protected from titin aggregation-induced stiffening by small heat shock proteins. J. Cell Biol. 204, 187-202.

Langone, F., Cannata, S., Fuoco, C., Lettieri Barbato, D., Testa, S., Nardozza, A.P., Ciriolo, M.R., Castagnoli, L., Gargioli, C., and Cesareni, G. (2014). Metformin protects skeletal muscle from cardiotoxin induced degeneration. PloS One 9, e114018.

Lee, M.C., Lee, J.S., Lee, M.J., Lee, J.H., and Kim, H.I. (2001). Fas mediates apoptosis in steroid-induced myopathy of rats. Neuropath. Applied Neurobiol. 27, 396-402.

Limphong, P., Zhang, H., Christians, E., Liu, Q., Riedel, M., Ivey, K., Cheng, P., Mitzelfelt, K., Taylor, G., Winge, D., et al. (2013). Modeling human protein aggregation cardiomyopathy using murine induced pluripotent stem cells. Stem Cells Trans. Med. 2, 161-166.

Malinska, D., Kulawiak, B., Wrzosek, A., Kunz, W.S., and Szewczyk, A. (2010). The cytoprotective action of the potassium channel opener BMS-191095 in C2C12 myoblasts is related to the modulation of calcium homeostasis. Cell. Phys. Biochem. 26, 235-246.

Millay, D.P., O'Rourke, J.R., Sutherland, L.B., Bezprozvannaya, S., Shelton, J.M., Bassel-Duby, R., and Olson, E.N. (2013). Myomaker is a membrane activator of myoblast fusion and muscle formation. Nature 499, 301-305.

Minajeva, A., Kulke, M., Fernandez, J.M., and Linke, W.A. (2001). Unfolding of Titin domains explains the viscoelastic behavior of skeletal myofibrils. Biophys. J. 80, 1442-1451.

Mitzelfelt, K.A., Limphong, P., Choi, M.J., Kondrat, F.D.L., Lai, S., Kolander, K.D., Kwok, W.-M., Dai, Q., Grzybowski, M.N., Zhang, H., et al. (2016). Human 343delT *HSPB5* chaperone associated with early-onset skeletal myopathy causes defects in protein solubility. J. Biol. Chem. 291, 14939-14953.

Neppl, R.L., Kataoka, M., and Wang, D.Z. (2014). Crystallin-alphaB regulates skeletal muscle homeostasis via modulation of Argonaute2 activity. J. Biol. Chem. 289, 17240-17248.

Nguyen, M.-D., Tinney, J.P., Yuan, F., Roussel, T.J., El-Baz, A., Giridharan, G., Keller, B.B., and Sethu, P. (2013). Cardiac cell culture model as a left ventricle mimic for cardiac tissue generation. Anal. Chem. 85, 8773-8779.

Pawlikowski, B., Lee, L., Zuo, J., and Kramer, R.H. (2009). Analysis of human muscle stem cells reveals a differentiation-resistant progenitor cell population expressing Pax7 capable of self-renewal. Dev. Dyn.: Amer. Assoc. Anatomists 238, 138-149.

Perng, M.D., Wen, S.F., IJssel, P.v.d., Prescott, A.R., and Quinlan, R.A. (2004). Desmin aggregate formation by R120G alphaB-crystallin is caused by altered filament interactions and is dependent upon network status in cells. Mol. Biol. Cell 15, 2335-2346.

Rajasekaran, N.S., Connell, P., Christians, E.S., Yan, L.J., Taylor, R.P., Orosz, A., Zhang, X.Q., Stevenson, T.J., Peshock, R.M., Leopold, J.A., et al. (2007). Human alpha B-crystallin mutation causes oxido-reductive stress and protein aggregation cardiomyopathy in mice. Cell 130, 427-439.

Rajasekaran, N.S., Firpo, M.A., Milash, B.A., Weiss, R.B., and Benjamin, I.J. (2008). Global expression profiling identifies a novel biosignature for protein aggregation R120GCryAB cardiomyopathy in mice. Physiol. Gen. 35, 165–172.

Rajasekaran, N.S., Varadharaj, S., Khanderao, G.D., Davidson, C.J., Kannan, S., Firpo, M.A., Zweier, J.L., and Benjamin, I.J. (2011). Sustained activation of nuclear erythroid 2-related factor 2/antioxidant response element signaling promotes reductive stress in the human mutant protein aggregation cardiomyopathy in mice. Antioxid. Redox Sign. 14, 957-971.

Riedel, M., Jou, Chuanchau J., Lai, S., Lux, Robert L., Moreno, Alonso P., Spitzer, Kenneth W., Christians, E., Tristani-Firouzi, M., and Benjamin, Ivor J. (2014). Functional and pharmacological analysis of cardiomyocytes differentiated from human peripheral blood mononuclear-derived pluripotent stem cells. Stem Cell Rep. 3, 131-141.

Rief, M. (1997). Reversible unfolding of individual Titin immunoglobulin domains by AFM. Science 276, 1109-1112.

Sacconi, S., Feasson, L., Antoine, J.C., Pecheux, C., Bernard, R., Cobo, A.M., Casarin, A., Salviati, L., Desnuelle, C., and Urtizberea, A. (2012). A novel CRYAB mutation resulting in multisystemic disease. Neuromuscular Disord. NMD 22, 66-72.

Samy, D.M., Ismail, C.A., and Nassra, R.A. (2015). Circulating irisin concentrations in rat models of thyroid dysfunction — Effect of exercise. Metabolis. 64, 804-813.

Seidel, K., Siswanto, S., Fredrich, M., Bouzrou, M., Brunt, E.R., van Leeuwen, F.W., Kampinga, H.H., Korf, H.W., Rüb, U., and den Dunnen, W.F.A. (2016). Polyglutamine aggregation in Huntington's disease and spinocerebellar ataxia type 3: Similar mechanisms in aggregate formation. Neuropath. Appl. Neuro. 42, 153-166.

Shultz, L.D., Lyons, B.L., Burzenski, L.M., Gott, B., Chen, X., Chaleff, S., Kotb, M., Gillies, S.D., King, M., Mangada, J., et al. (2005). Human lymphoid and myeloid cell development in NOD/LtSz-scid IL2Rγnull mice engrafted with mobilized human hemopoietic stem cells. J. Immun. 174, 6477-6489.

Singh, B.N., Rao, K.S., and Rao Ch, M. (2010). Ubiquitin-proteasome-mediated degradation and synthesis of MyoD is modulated by alphaB-crystallin, a small heat shock protein, during muscle differentiation. Biochim. Biophys. Acta 1803, 288-299.

Swamynathan, S.K., and Piatigorsky, J. (2007). Regulation of the mouse αB-crystallin and MKBP/HspB2 promoter activities by shared and gene specific intergenic elements: the importance of context dependency. Int. J. Dev. Biol. 51, 689-700.

Verma, A., Bhatt, A.N., Farooque, A., Khanna, S., Singh, S., and Dwarakanath, B.S. (2011). Calcium ionophore A23187 reveals calcium related cellular stress as "I-Bodies": An old actor in a new role. Cell Calcium 50, 510-522.

Vicart, P., Caron, A., Guicheney, P., Li, Z., Prevost, M.-C., Faure, A., Chateau, D., Chapon, F., Tome, F., Dupret, J.-M., et al. (1998). A missense mutation in the αB-crystallin chaperone gene causes a desmin-related myopathy. Nat. Genetics 20, 92-95.

Weintraub, H. (1993). The MyoD family and myogenesis- redundancy, networks, and thresholds.

Cell 75, 1241-1244.

Xie, H.B., Cammarato, A., Rajasekaran, N.S., Zhang, H., Suggs, J.A., Lin, H.-C., Bernstein, S.I., Benjamin, I.J., and Golic, K.G. (2013). The NADPH Metabolic Network Regulates Human αB-crystallin Cardiomyopathy and Reductive Stress in *Drosophila melanogaster*. PLoS Gen. 9, e1003544.

Zhang, H., Rajasekaran, N.S., Orosz, A., Xiao, X., Rechsteiner, M., and Benjamin, I.J. (2010). Selective degradation of aggregate-prone CryAB mutants by HSPB1 is mediated by ubiquitin-proteasome pathways. J. Mol. Cell. Cardiol. 49, 918-930.

CHAPTER 7

EPILOGUE

Technological advances with stem cells and genome editing have revolutionized methods for studying human disease. This dissertation presented an example utilizing these techniques for the study of a mutant chaperone, *HSPB5* 343delT, and its association with myopathy. It also attempts to address a technical hurdle currently faced by the genome editing field- low editing efficiencies in iPSCs- through presentation of a novel genome editing strategy called cotargeting with selection (CTS). Altogether, this work is at the forefront of new technological capabilities that has and will no doubt continue to provide mechanistic insights into disease, generate platforms for drug screening, and, perhaps, translates into regenerative cell therapies in humans.